

UC Santa Cruz

UC Santa Cruz Electronic Theses and Dissertations

Title

Chemical Biology of Carbon Monoxide in Cancer: Insights into Molecular Mechanisms of Drug Resistance

Permalink

<https://escholarship.org/uc/item/1rw7r42v>

Author

Kawahara, Brian A

Publication Date

2020

Peer reviewed|Thesis/dissertation

UNIVERSITY OF CALIFORNIA

SANTA CRUZ

**CHEMICAL BIOLOGY OF CARBON MONOXIDE IN CANCER:
INSIGHTS INTO MOLECULAR MECHANISMS OF DRUG RESISTANCE**

A dissertation submitted in partial satisfaction
of the requirements for the degree of

DOCTOR OF PHILOSOPHY

In

CHEMISTRY

by

Brian Kawahara

December 2020

The Dissertation of Brian Kawahara is
approved:

Disting. Professor Pradip K. Mascharak,
Chair

Professor Theodore R. Holman

Professor Scott R. J. Oliver

Quentin Williams
Interim Vice Provost and Dean of Graduate Studies

Copyright © by
Brian Kawahara
2020

Table of contents

	Page
List of figures	viii
List of tables	xvi
Abstract	xvii
Acknowledgements	xix

Chapter 1. Introduction to therapeutic carbon monoxide

1.1 Current cancer therapy: expensive and minimally effective	1
1.2 Carbon monoxide, a gasotransmitter	3
1.3 The therapeutic potential of carbon monoxide	6
1.4 Carbon monoxide in cancer therapy; what are its targets?	7
1.5 Carbon monoxide, a chemosensitizing agent	11
1.6 Direction of research	15
1.7 References	17
1.8 Reprint of publication	24

Chapter 2. Carbon monoxide attenuates the antioxidant capacity of human breast cancer cells through inhibition of cystathionine β -synthase

2.1 Background	41
----------------------	----

2.2. CBS promotes an elevated antioxidant capacity in breast cancer cells	46
2.3 CBS expression positively correlates with Nrf2 and downstream antioxidant genes	49
2.4 Addition of H ₂ S and CTH to CBS-silenced breast cancer cells restores the antioxidant capacity	52
2.5 Overexpression of CBS in normal human breast cancer cells increases cellular antioxidant capacity	56
2.6 CO inhibits CBS and attenuates the antioxidant capacity in human breast cancer	58
2.7 CO sensitizes human breast cancer to doxorubicin and paclitaxel	60
2.8 Discussion	64
2.9 Materials and methods	69
2.10 References	78
2.11 Reprint of publication	85

Chapter 3. Co-treatment of carbon monoxide with cisplatin induces apoptosis in cisplatin-resistant ovarian cancer

3.1 Background	101
----------------------	-----

3.2 CO sensitizes cisplatin-resistant ovarian cancer cells to cisplatin	104
3.3 CBS is overexpressed in cisplatin-resistant cells	112
3.4 CBS is associated with a cisplatin-resistant phenotype	113
3.5 Silencing CBS expression sensitizes cisplatin-resistant ovarian cancer cells to cisplatin	117
3.6 Silencing CBS abates the molecular markers of cisplatin resistance in ovarian cancer cells	119
3.7 CO sensitizes cisplatin-resistant ovarian cancer cells to cisplatin	122
3.8 Discussion	125
3.9 Material and methods	130
3.10 References	137
3.11 Reprint of publication	143

**Chapter 4. Antigen-specific delivery of carbon monoxide through a new class of
antibody-drug conjugate**

4.1 Background	162
----------------------	-----

4.2 Synthesis of biotinylated, photo-activatable carbon monoxide-releasing molecule	164
4.3 Synthesis of streptavidin-conjugated antibody	170
4.4 Synthesis of antibody-photoCORM conjugate	172
4.5 Antigen-mediated delivery of carbon monoxide to ovarian cancer cells	176
4.6 Discussion	176
4.7 Materials and methods	184
4.8 References	194
4.9 Reprint of publication	198

Chapter 5. Carbon monoxide inhibits cytochrome P450 enzymes CYP3A4/2C8 in human breast cancer cells, increasing sensitivity to paclitaxel

5.1 Background	222
5.2 Expression and activity of CYP3A4 in breast cancer cells and tissues	225
5.3 CYP3A4 activity in human breast cancer cells in the presence of CO, delivered by photoCORM	226
5.4 Pharmacokinetics and pharmacodynamics of PTX in immortalized, human breast cancer cell cultures	228

5.5 Effect of CO on the pharmacokinetics of PTX and the effects in human breast cancer cells	233
5.6 Effects of chloramphenicol on CYP3A4/2C8-mediated metabolism of PTX in human breast cancer cells	238
5.7 CO and the pharmacokinetics of PTX in HepG2 cells	242
5.8 Discussion	244
5.9 Materials and methods	250
5.10 References	256

Chapter 6. Conclusion

6.1 Reimagining cancer therapy	263
6.2 Perspective of findings	265
6.3 Future directions	270
6.4 References	272

List of Figures

	Page
Figure 1.1	A carbon monoxide-based therapy to improve chemotherapeutic regimen efficacy 2
Figure 1.2	Levels and tolerances of CO 4
Figure 1.3	Gasotransmitters: endogenously produced, gaseous signaling molecules with essential roles in normal, physiological function 5
Figure 1.4	CO acts hormetically to reduce inflammation in normal cells and tissues 8
Figure 1.5	CO: potentially, an anti-cancer agent with high orthogonality to normal cells 9
Figure 1.6	Relationship between redox homeostasis and chemotherapeutic resistance in cancer 13
Figure 1.7	Proposed mechanisms of CO-mediated drug sensitization in cancer cells 16
Figure 2.1	Transmethylation, transsulfuration and glutathione biosynthesis pathways 43
Figure 2.2	photoCORM used in this study 45
Figure 2.3	Effects of silencing CBS on the antioxidant capacity, redox homeostasis and GSH homeostasis in human breast cancer cells 48

Figure 2.4	Transcriptional effect(s) of CBS-silencing on antioxidant response in human breast cancer cells	51
Figure 2.5	Effect(s) of H ₂ S and cystathionine treatment on redox homeostasis in CBS-silenced human breast cancer cells	53
Figure 2.6	Assessment of H ₂ S and cystathionine treatment to reverse transcriptional effects of silencing CBS in human breast cancer cells..	55
Figure 2.7	Effect(s) of CBS overexpression on the antioxidant capacity of normal human breast cells	57
Figure 2.8	Effect(s) of CO, delivered by visible light activation of 120 μM photoCORM, on the antioxidant capacity of human breast cancer cells	59
Figure 2.9	Assessment of the ability of CO to sensitize human breast cancer cells to Dox	61
Figure 2.10	Assessing any non-specific effects of the molecular scaffold of iCORM on cell viability and drug sensitization to Dox in human breast cancer cells	62
Figure 2.11	Assessment of CO co-treatment to sensitize human breast cancer cells to Dox and PTX	63
Figure 2.12	Determining any non-specific effects of the molecular scaffold of iCORM on cell viability and drug sensitization to PTX in human breast cancer cells	64

Figure 3.1	[Mn(CO) ₃ (phen)(PTA)]CF ₃ SO ₃ , photoactivatable CO-releasing molecule (photoCORM 1)	104
Figure 3.2	Comparison of dose-response to CO, delivered by photoCORM 1, on cell viability, comparing wild type and cisplatin-resistant variants of ovarian cancer cell lines	105
Figure 3.3	Assessing sensitivity to cisplatin of cisplatin-resistant and wild type variants of ovarian cancer cell lines	106
Figure 3.4	Cell viability assays and apoptotic signaling in cisplatin-resistant ovarian cancer cells co-treated with CO and cisplatin	107
Figure 3.5	Assessment of cytotoxicity and drug sensitizing effects of iCORM on cisplatin-resistant ovarian cancer cells	108
Figure 3.6	Cytotoxicity and drug sensitizing effects of iCORM on cisplatin-resistant ovarian cancer cells	109
Figure 3.7	Dose-response of cisplatin-resistant ovarian cancer cells to cisplatin in the presence of increasing concentrations of CO	110
Figure 3.8	NAC reverses the cytotoxic effects of combined CO-cisplatin treatment in cisplatin-resistant ovarian cancer cell lines	110
Figure 3.9	Effect of treatment of cisplatin-resistant ovarian cancer cell lines with NAC on markers of cisplatin resistance	111
Figure 3.10	Expression of transsulfuration pathway enzymes in wild type ovarian cancer cell lines and their cisplatin-resistant variants	113

Figure 3.11	Steady state levels of sulfur-containing peptides and proteins in cisplatin-resistant ovarian cancer cells compared to their cisplatin sensitive-derived cell lines	116
Figure 3.12	Western blot of xCT expression in whole cell lysates of wild type and cisplatin-resistant ovarian cancer cells	117
Figure 3.13	Effect of silencing CBS expression on the dose-response relationship between cisplatin and cell viability of cisplatin-resistant ovarian cancer cells	119
Figure 3.14	Sulfur homeostasis and molecular markers of resistance in cisplatin-resistant ovarian cancer cells exhibiting stable silencing of CBS compared to control transfected cells	121
Figure 3.15	Effects of stable silencing of CBS on xCT activities and expressions in cisplatin-resistant ovarian cancer cells	122
Figure 3.16	Effects of exogenous CO treatment on sulfur homeostasis in cisplatin-resistant ovarian cancer cells	124
Figure 4.1	Structure of biotinylated photoCORM (Complex 1)	164
Figure 4.2	Synthetic scheme for Complex 1: a biotinylated, photoCORM	165
Figure 4.3	Electrospray ionization mass spectrometry of Complex 1	165
Figure 4.4	¹ H NMR for Complex 1	166
Figure 4.4	Infrared (IR) spectrum of Complex 1	166
Figure 4.5	Electronic absorption spectrum of Complex 1 in 1X PBS	167

Figure 4.6	Electronic absorption spectrum of Complex 1 upon illumination with low power, broadband visible light.....	168
Figure 4.7	Myoglobin assay for CO release of Complex 1	169
Figure 4.8	Effect of treatment of ovarian cancer cell lines with indicated concentrations of Complex 1 upon illumination with visible light on cell viability, measured 24 h post-treatment in ovarian cancer cell lines	170
Figure 4.9	Complex 2: streptavidin-conjugated IgG.....	171
Figure 4.10	Synthesis and characterization of the Ab-photoCORM and proteomic analysis of Ab-photoCORM	172
Figure 4.11	Proteomic scores of the Ab-photoCORMs synthesized in this study	173
Figure 4.12	Detection of Complex 1 in tryptic digest of Ab-photoCORM	174
Figure 4.13	Myoglobin assay for light-triggered CO release from Ab-photoCORM..	175
Figure 4.14	Live-cell, immunosorbent assay scheme	177
Figure 4.15	Ab-photoCORMs deliver cytotoxic levels to ovarian cancer cell lines via immunosorbent assay	178
Figure 4.16	Cell viability of ovarian cancer cell lines OVCAR-5 and SKOV-3 treated with light-inactivated Complex 1 and Complex 1 in the dark to assess the cytotoxicity of the non-CO components of Complex 1 ...	179

Figure 4.17	Cell viability, as measured by reduction of MTT 24 h post-treatment, of OVCAR-5 and SKOV-3 treated with 2 $\mu\text{g}/\text{mL}$ Complex 2 and control antibodies	180
Figure 4.18	Calculations for estimation of molar release of CO from antibody-photoCORM conjugates	180
Figure 5.1	Expression and activity of CYP3A4 in human breast cancer cells and tissues	226
Figure 5.2	$[\text{Mn}(\text{CO})_3(\text{phen})(\text{PTA})]\text{CF}_3\text{SO}_3$ (photoCORM)	227
Figure 5.3	CYP3A4 activity in the presence of CO, delivered by photoCORM.....	228
Figure 5.4	Representative chromatograms of the measurement, by HPLC-MS of intracellular PTX and OH-PTX in PTX-treated human breast cancer cells	229
Figure 5.5	Standard curve of hydroxyl-paclitaxel prepared in cell lysate	230
Figure 5.6	Pharmacokinetics and pharmacodynamics of PTX in immortalized, human breast cancer cell cultures	232
Figure 5.7	Effects of CO on the pharmacokinetics of PTX and the effects in human breast cancer cells	234
Figure 5.8	Normalization to 0 μM PTX ($\log[0 \mu\text{M PTX}] \sim -7.8$) of cell viability curves of human breast cancer cell line MCF-7, presenting the dose-response of PTX on cell viability in the absence and presence of CO, delivered by 50/100 μM photoCORM	235

Figure 5.9	Effect of CO co-treatment on the dose-response of PTX on the cell viability of human breast cancer cell line MDA-MB-231	236
Figure 5.10	Cell viability of human breast cancer and human hepatocellular carcinoma cell lines in the presence of CO	237
Figure 5.11	Initial value-normalized dose-response curves to PTX on cell viability of human breast cancer cell line MDA-MB-231 in the absence and presence of CO, delivered by 50/100 photoCORM	238
Figure 5.12	Effects of small molecule, pharmacological inhibition of CYP3A4-mediated metabolism of PTX in human breast cancer cells	239
Figure 5.13	Initial value-normalized cell viability curves of the dose-response of PTX on cell viability of human breast cancer cell line MCF-7 in the absence and presence of 10/20 μ M CAM	240
Figure 5.14	Effect of CAM co-treatment on the dose-response of PTX on the cell viability of human breast cancer cell line MDA-MB-231	241
Figure 5.15	Initial value-normalized cell viability curves of human breast cancer cell line MDA-MB-231 of the dose-response of PTX on cell viability in the absence and presence of 10/20 μ M CAM	242
Figure 5.16	Effects of CO on the pharmacokinetics of PTX in human hepatocellular carcinoma cells	243
Figure 5.17	Initial condition-normalized cell viability curves of the response of human hepatocellular carcinoma cells to PTX in the absence and presence of CO delivered by 1 and 10 μ M photoCORM	244

Figure 6.1	Graphical summary of CO-mediated sensitization of cancer cells to chemotherapeutics	267
Figure 6.2	Graphical summary of CO-mediated inhibition of paclitaxel metabolism by CYP3A4/2C8	268
Figure 6.3	Steps towards realizing more effective chemotherapeutic regimens with CO	269
Figure 6.4	CO, a tool for studying drug resistance in cancer	270

List of Tables

	Page
Table 1.1	Putative and proposed molecular targets of CO 11
Table 2.1	Table of Content 41
Table 3.1	Table of Content101
Table 4.1	Table of Content162
Table 4.2	Family of antibody-photoCORM conjugates (Ab-photoCORMs) synthesized from commercial antibodies, recognizing indicated human cell surface antigens implicated in ovarian cancer176
Table 5.1	Table of Content222
Table 6.1	Graphical summary of CO-mediated inhibition of heme-containing enzymes towards sensitizing cancer cells to chemotherapeutics263

CHEMICAL BIOLOGY OF CARBON MONOXIDE IN CANCER: INSIGHTS INTO MOLECULAR MECHANISMS OF DRUG RESISTANCE

Brian Kawahara

Abstract

Cancer cells have the ability to develop resistance to traditional therapies, resulting in poor patient outcomes. The increasing prevalence of chemotherapeutic resistant cancers demands novel therapies that address this issue. One intriguing strategy is the recent development of carbon monoxide (CO) as a potential cancer therapeutic. CO is a gasotransmitter, an endogenously produced, diffusible, signaling molecule with essential roles in physiological processes, including resolving inflammation. Cancer, a disease characterized by chronic up-regulation of inflammatory processes, could be an intriguing therapeutic candidate for CO.

Preliminary studies have reported CO to be a chemosensitizing agent, but the mechanism(s) by which this effect occurs are largely unknown. If the therapeutic potential of CO is to be realized, understanding of the chemical biology of CO in the cancer cell is essential. Identified here are two targets of CO that mediate sensitization of cancer cells to standard chemotherapeutics, including doxorubicin, paclitaxel and cisplatin: cystathionine β -synthase (CBS) in breast and ovarian cancer cells and cytochrome P450 3A4/2C8 (CYP3A4/2C8) in breast cancer cells. In studying CO-mediated inhibition of these two enzymes, molecular mechanisms of

drug resistance, promoted and maintained by the enzymatic actions of CBS and CYP3A4/2C8, were revealed. Additionally, reported here is the synthesis of a novel class of CO-donating molecules, a CO-releasing molecule-conjugated to monoclonal antibodies, capable of delivering therapeutic levels of CO to a cancer target with antigen-specificity.

Collectively these results suggest co-administration of CO with existing cancer treatment regimens may ultimately improve clinical outcomes in cancer therapy.

Acknowledgments

All my gratitude must be directed to my research advisor and boss, Distinguished Professor Pradip K. Mascharak for mentoring me during my PhD career. He exercised a lot of trust in me by taking me, a molecular biologist, into his synthetic, inorganic chemistry lab. Our work together has been the most fun, rewarding, intellectually stimulating and greatest contribution I have made to the scientific community. It has been the highlight of my professional career to train under his guidance and mentorship. I cannot thank him enough for his time, effort and patience while training me. His character, vigor and integrity are of the highest level that I have seen in any person. I look forward to continued collaborations, as there are still so many meaningful, interesting scientific questions that arose during the execution of this thesis.

I am very thankful to Professors Ted Holman and Scott Oliver, who generously served on my thesis committee, guided me through the graduate program and always had my best interest in mind. Thank you for being patient and receptive to my molecular biology projects.

The contributions of Dr. Kym Francis Faull, Director of the Pasarow Mass Spectrometry Laboratory (PMSL) at UCLA, cannot be overstated. Without his generosity in time, money and facilities, the work comprised in this thesis would have been far lower impact and quality. As mass spectrometry, performed in his lab, was key to completing the studies reported in this thesis, I am extremely grateful to him and his mentorship. Gratitude must be expressed for Professor Julian Whitelegge,

whose expertise in whole-protein mass spectrometry and proteomics was key to completing the studies reported in Chapter 4. Special thanks must also be given to Dr. Carla Janzen, who generously offered her lab at UCLA for our group to conduct the numerous molecular biology experiments.

Without my previous working under the guidance of Dr. Suvajit Sen, I would have never been introduced to Dr. Mascharak. Training under Dr. Sen at UCLA during my formative years afforded me a solid foundation in independent research. I am grateful to Suvajit for his continued support and belief in my pursuit of a PhD, even if it was several years later than he would have wished for me.

My current and former lab mates were key to the synthetic chemistry performed in the completion of experiments in Chapter 4. Dr. Miguel Pinto and Jorge Martinez were my patient teachers of synthetic chemistry, to whom I owe the deepest gratitude. Deep appreciation must be expressed for Dr. Jorge Martinez, in providing our group a carbon monoxide-releasing molecule with a pyridine-4-aldehyde ligand, a key molecule that afforded the feasibility in synthesizing the “immunoCORM” synthesized in Chapter 4. Additionally, I must express immense gratitude to Alex Yoon of the PMSL, whose pioneering work developing the method to measure sulfur metabolism was key to completing the work reported in Chapters 2 and 3. It was also a professional pleasure being able to include Ariel Wen M.B.A. of UCLA in the work reported here. Her support in the statistical analyses of data from studies performed in Chapter 3 is gratefully acknowledged.

My lab mates, co-workers and friends in the Chemistry Department at UCSC and the PMSL at UCLA made coming into the lab always a joy. Dr. Brett Lomenick and Dr. Austin Quach, who had already earned their Ph.D.'s when I started graduate school, were always available to guide me through the process. Whitaker Cohn, and to a far greater extent, Lucy Gao of UCLA, were lab mates who made graduate school entertaining and lively like others had, yet gratuitously and shamelessly asked to be acknowledged in this thesis. Actually, they were indeed invaluable to the work reported in Chapter 4. I would thank them more, but they were co-authors on Chapter 4's associated publication, which is already a sufficient show of gratitude in most professional circles.

Dr. Randa Roland worked tirelessly as our TA boss to make sure that we were in the best position to succeed. My regret in graduate school was that I couldn't work for her more than I did. I'm thankful to her for making the most frustrating part of graduate school so much better. Her hard work is appreciated by all her TAs and me.

My parents provided far more emotional and material support these past four years than I deserved. I don't know how I can repay them, but I love them for it.

Graduate school was purported to be a lonely, frustrating, stressful, Dickensian experience. However, the sum of having mentors, bosses, lab mates, friends and family of the highest talent, character, generosity and integrity made graduate school the most fun and professionally meaningful experience I have done. I hope I returned the favor to them and helped everyone I could along the way.

Chapter 1

Introduction to therapeutic carbon monoxide

1.1. Current cancer therapy: expensive and minimally effective

The studies reported and discussed here, exploring the chemical biology of carbon monoxide (CO) in cancer, were performed, in part, to evaluate its therapeutic potential as a novel anti-cancer therapeutic. The suggestion of using a gaseous molecule of some infamy as a cancer therapy will be met with skepticism. After all, are not current chemotherapeutics more effective than they have ever been? With the advent of immunotherapies, monoclonal antibodies, antibody-drug conjugates, drugs that target the “undruggable” targets and therapies that target proteins with polymorphisms unique to an individual patient; why should we waste our time evaluating a carbon monoxide-based cancer therapy, a technology that is highly unconventional and fraught with technical challenges? Because the current system is broken.

The average anti-cancer drug costs \$1.2-1.8 billion per medicine to develop and is administered and billed to the patient at \$10,000 per month.¹ It targets proteins involved in cell growth, cell cycle and DNA repair processes.² They are often described as “targeted therapies” and/or molecules that drug the “undruggable” therapeutic targets in the cell like K-ras.³ These highly specific drugs, however, exert a strong evolutionary pressure on the tumor.² They either select for or elicit the development of subpopulations of drug resistant cancer cells that, through clonal

expansion, result in relapse, metastasis and poor patient outcomes (Figure 1.1, top). As a result, the typical anti-cancer drug, at tremendous financial cost, elicits a median improvement in progression-free survival of only 2.5 months.¹ Worse yet, it improves overall survival by only 2.1 months.¹ The current cancer treatment strategy is unimaginative and minimally effective, stifling innovation and creativity. A fresh approach to cancer therapy is needed.

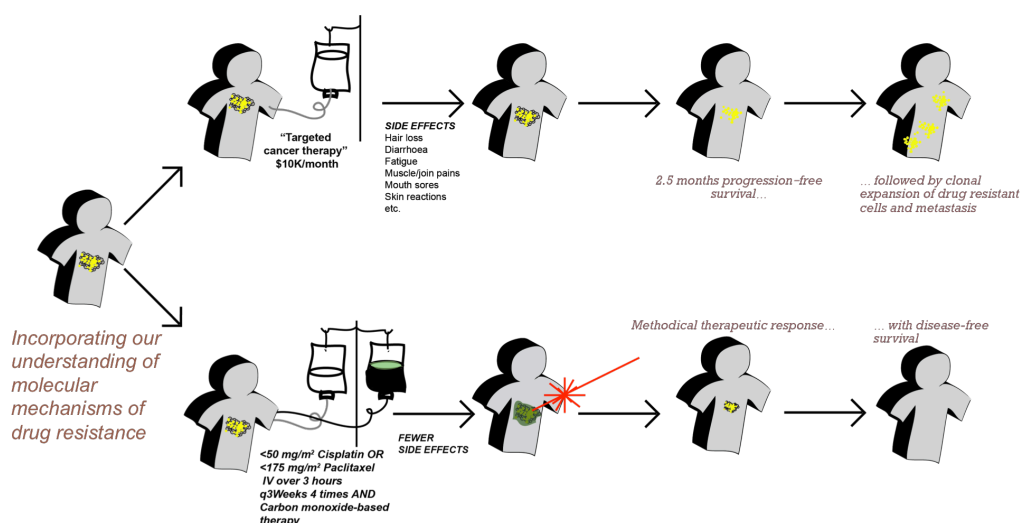


Figure 1.1. A carbon monoxide-based therapy to improve chemotherapeutic regimen efficacy. Schematic of comparing chemotherapeutic regimen scenarios using (top) targeted drug therapies versus (bottom) carbon monoxide-based therapies.

As will be explored in this thesis, a therapeutic strategy of targeting the cancer cellular processes involved in drug resistance itself will likely reinvigorate the field of cancer therapy. The use of a CO-based therapy that targets molecular mechanisms of drug resistance, with co-treatment with off patent/off-license drugs (e.g. paclitaxel, cisplatin) at lower doses than are currently indicated when these drugs are used alone,

could result in lower side effects, a methodical therapeutic response and a greater likelihood of disease-free survival for patients (Figure 1.1, bottom).

1.2 Carbon monoxide, a gasotransmitter

CO is a non-irritating, odorless, tasteless and colorless gas that most regard in the public's mind as the toxic byproduct of incomplete hydrocarbon combustion. Indeed, the mere mention of CO brings to mind, in the layperson, acute CO-poisoning. And while accidental deaths from CO poisonings result in ~438 deaths per year in the United States,⁴ it is interesting to mention that accidental overdoses of acetaminophen, an over-the-counter pain reliever and fever reducer broadly used and indicated to treat a number of medial conditions, results in more than deaths than CO, ~458 deaths per year.⁵ This is brought up not to dismiss the dangers of exogenous CO toxicity or question the merit of educating the public about the dangers of CO or acetaminophen poisoning, but rather emphasize a classic adage in pharmacology: "the dose makes the poison".

Acute toxicity from CO results from the binding of CO to hemoglobin, displacing molecular oxygen, to form carboxy-hemoglobin (CO-Hb).⁶ Life-threatening effects generally set in with >40% CO-Hb formation in the blood, though this threshold varies by age, pregnancy status and overall health. Some studies have found extremely high tolerance to CO, with lethal effects setting in at 50-70% CO-Hb.⁶ In fact, most healthy adults do not feel or experience any noticeable symptoms at

CO-Hb levels <20-33%. Together, these data lend to the conclusion that despite its infamy, CO is highly tolerated over a very broad range (Figure 1.2).

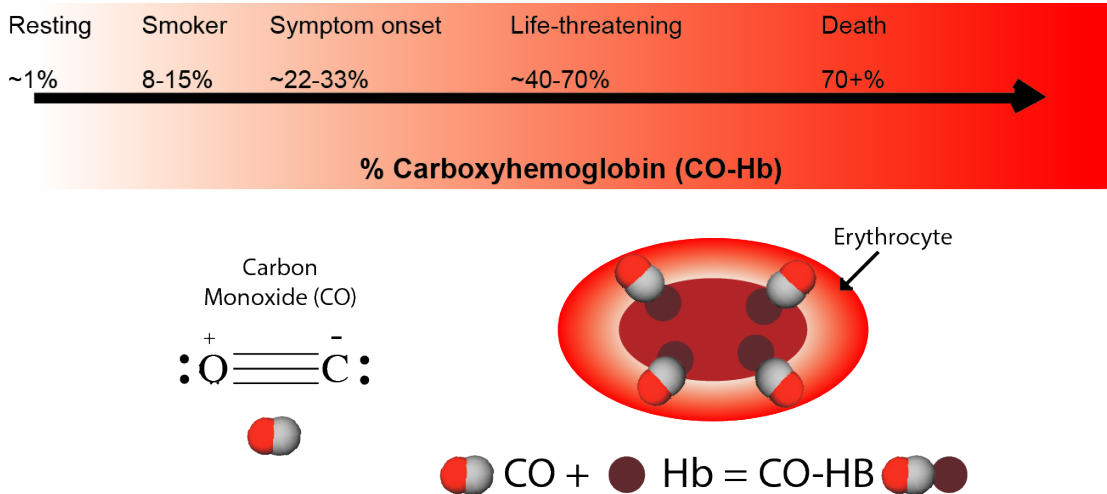


Figure 1.2. Levels and tolerances of carbon monoxide (CO). Formation of carboxyhemoglobin, in the human body.

Active smokers experience 8-15% CO-Hb and experience no immediate deleterious effects from CO. Perhaps most intriguing, ~1% CO-Hb is present in the blood of healthy, non-smoking adults in the absence of any environmental CO exposure, indicating a non-environmental source of CO. This observation precludes the fact that CO is not only tolerated over a wide range in human physiology, but is also endogenously produced by normal physiological processes.⁷

CO is, in fact, a gasotransmitter, an endogenously produced, gaseous signaling molecule that elicits a physiological response.^{8,9} Along with nitric oxide (NO) and hydrogen sulfide (H₂S), gasotransmitters have recently been shown to play roles in a wide array of chemistry in biological systems (Figure 1.3).¹⁰

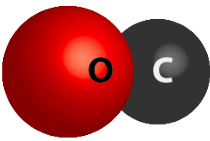
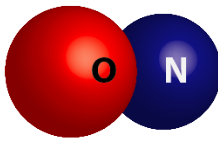
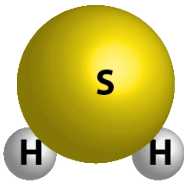
	Carbon monoxide (CO)	Nitric oxide (NO)	Hydrogen sulfide (H ₂ S)
			
Enzymatic production	HO-1 HO-2	nNOS eNOS iNOS	CBS CGL 3MPST
Notable physiological roles	resolving inflammation metabolism oxygen sensing	vasodilation metabolism apoptosis	redox homeostasis metabolism cytoprotection

Figure 1.3. Gasotransmitters: endogenously produced, gaseous signaling molecules with essential roles in normal, physiological function.

Endogenous production of CO, as a product of heme catabolism, has been known for over 70 years.^{11,12} This reaction is catalyzed by microsomal heme oxygenase (HO), an enzyme that exists in two isoforms namely, HO-1 (inducible) and HO-2 (constitutive).¹³ Catabolism of free heme is vital for maintaining cellular health and mitigating the toxic effects of heme-catalyzed oxidation reactions. Loss-of-function mutations in HO-1 are lethal, evidence of the importance of HO-1, and possibly CO, in human physiology.¹⁴ In the human body, ~16 μmol amounts of CO are generated collectively by HO-2 and HO-1.¹⁵ Constitutive HO-2 produces CO in the liver, testes, endothelial cells and the brain where it is reputed to play important roles in maintaining vascular tone.¹⁶ Nearly all tissues are capable of HO-1 induction,¹⁷ though its expression in Kupffer cells and anti-inflammatory/M2-polarized macrophages indicate an anti-inflammatory role for HO-1 and CO.¹⁸

1.3 The therapeutic potential of CO

Interest in CO as a therapeutic molecule has stemmed from its potential role in opposing and resolving inflammation. Many diseases are initiated by and/or characterized by inflammation,¹⁹ processes which CO could attenuate. Consequently, research during the past three decades has explored the potential of low doses of CO as therapeutic in a wide array of injury and disease models including wound healing, colitis, sepsis, cerebral malaria, diabetes, balloon angioplasty-induced stenosis, ileus/bowel immotility and organ transplantation.^{20,21} The observed salutary effects of CO in these disease/injury models may be partially explained by the ability of CO to increase intracellular levels of reactive oxygen species (ROS) in target cells, attenuate macrophage activation by cytokine and endotoxin, inhibit endothelial cell apoptosis, and prevent T-cell proliferation.²² In light of observations of the protective and anti-inflammatory effects of HO-1/2 and CO, recent efforts have been made to explore the possible therapeutic application of CO.

Therapeutic implications aside, the technological feat of delivering a diffusible, gaseous molecule to a therapeutic site at sufficient concentrations remains. Towards this end, extensive research and development has afforded novel delivery modes, including the design of CO-releasing molecules (CORMs).^{23,24} Although some progress along this line has been achieved in recent years,²⁰ therapeutic application of CO in a clinical setting is still in its infancy. Photoactivatable CO-releasing molecules (photoCORMs), small molecules capable of introducing CO to a

biological target with temporal and dose control, has been arguably the most important development in terms of being able to efficiently and consistently deliver CO.²⁵ Interesting photoCORM variants, including photoactivatable CO-releasing polymers (photoCORPs),²⁶ CO-releasing nanoparticles,²⁷ biomaterial embedded photoCORMs²⁸ and single photon-IR-activated photoCORMs²⁹ have further expanded the possible modes by which CO might delivered to a biological target. The Mascharak group's members have made great strides in developing photoCORMs with biological compatibility, sufficient water solubility and controlled release of CO has been instrumental in advancing the study of therapeutic CO. The next research goal would be to determine its therapeutic potential, evaluating the ability of CO to elicit a therapeutic effect in a cancer model and identify the mechanism(s) by which this occurs.

1.4 Carbon monoxide in cancer therapy; what are its targets?

CO has been shown to be effective in attenuating and resolving chronic inflammation, a process implicated in the initiation, progression, metastasis and development of drug resistance in cancer.³⁰ Consequently, numerous groups have initiated and published studies assessing the effect of CO on cancer cell proliferation and viability. CO has been reported to have anti-proliferative and apoptotic effects in certain cancer cell models, preliminary indication that CO could be a possible drug candidate against cancer.³¹

In normal cells and tissues, CO is believed to promiscuously interact with ferrous heme enzymes, decreasing the formation of ROS from inhibition of NADPH oxidase (NOX) and reactive nitrogen species from inhibition of endothelial nitric oxide synthase (eNOS), while concertedly inhibiting cytochrome c oxidase to uncouple oxidative phosphorylation, resulting in an increase in mitochondrial ROS.³² The net effect is an overall *increase* in intracellular ROS levels, which hormetically acts to increase the target cell's/tissue's antioxidant/cytoprotective responses to the mild CO-induced stress, ultimately decreasing inflammation (Figure 1.4).³²

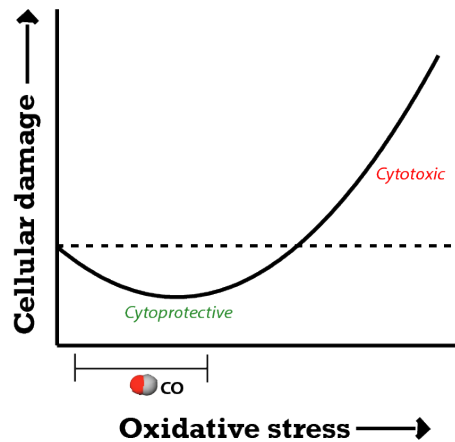


Figure 1.4. Carbon monoxide (CO) acts hormetically to reduce inflammation in normal cells and tissues.

In cancer cells, however, it is widely regarded that such an increase in intracellular ROS induced by CO would overload the cancer cells ability maintain redox homeostasis, as they exhibit unique redox status (vide infra, Figure 1.6) resulting in cell death (Figure 1.5).

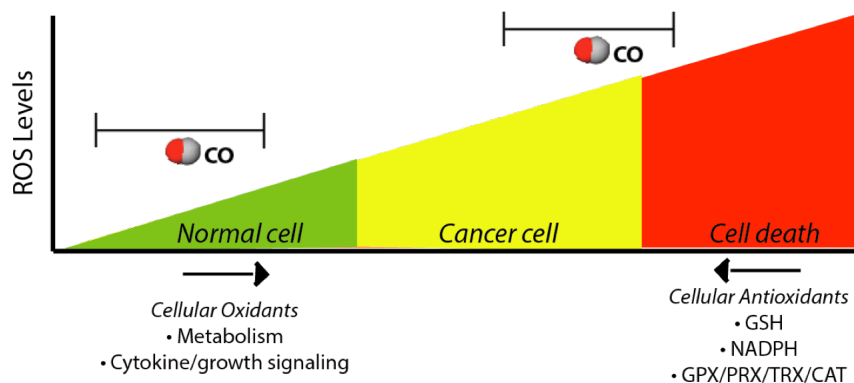


Figure 1.5. Carbon monoxide (CO): potentially, an anti-cancer agent with high orthogonality to normal cells.

In this way, CO could be a promising anti-cancer agent with high orthogonality to normal tissues. Interestingly, one study, prior to the initiation of the work in this thesis, reported that CO has a far more subtle and intriguing effect, not killing but *sensitizing* cancer cells to other chemotherapeutics,³³ a prelude to its potential application in a cancer therapy regimen.

However, as emphasized by Motterlini, the therapeutic potential of CO is hampered by our lack of detailed understanding of the *chemical biology* of CO in the cancer cell.²⁰ The molecular targets of CO in the cancer must be identified and validated if the therapeutic potential of CO is to be properly considered. Additionally, such research would afford deep insight, using synthetic molecules (i.e. photoCORMs and CO) to manipulate a biological system (a cancer cell) and achieve a greater understanding of the cellular processes driving drug resistance. The field of therapeutic CO has remained stagnant over the past decade by studies that report the design and application of novel CORMs and photoCORMs, but apply them to cancer

cell cultures in poorly designed studies without proper controls or mechanistic insight.³⁴⁻³⁹ Even higher order studies in animal models have shown cytotoxic effects of CO against cancer cells, but have not attempted to elucidate CO's mechanism(s) of action.⁴⁰ The sum of these published studies have created a false sense of progress. Without the necessary mechanistic studies, there is no legitimacy in claiming therapeutic potential of CO as a cancer therapy. Identification of cancer-specific targets and eliciting of cancer-specific effects by CO are necessary to substantiate the claim that CO is a potential anti-cancer therapy.

Otterbein and others have reported that CO targets cytochrome c oxidase in the mitochondria to increase generation of reactive oxygen species (ROS).^{33,41} While cytochrome c oxidase is likely *a* target of CO, it seems unlikely that cytochrome c oxidase is the *major* mediator of CO's effects in the cell, considering the 10-fold greater affinity of cytochrome c oxidase for oxygen (O₂) compared to CO.⁴² Furthermore, in the mitochondria, heme a₃, the target of CO in cytochrome c oxidase, exists primarily, 94%, in the ferric, Fe³⁺ oxidation state and is only transiently, ~6%, in the Fe²⁺ state.⁴³ As CO is only a weak Lewis base, it has preferential affinity for Fe²⁺ heme and low affinity for Fe³⁺ heme,⁴⁴ making it unlikely that CO's effects in the cancer cell are largely mediated by cytochrome c oxidase. Despite this, little effort has been made to identify the other, and likely more consequential, targets of CO in the cancer cell.

Slow progress in identifying the therapeutic targets of CO in the cancer cell is surprising, as the chemistry of CO is well characterized, making the endeavor

relatively straightforward. As a weak Lewis base, the reactions of CO with cellular components are essentially exclusive to ferrous (Fe^{2+}) heme-containing enzymes.⁴⁵ At the time of this thesis, fourteen molecular targets of CO have been either confirmed or purported, all ferrous heme-containing enzymes (Table 1).⁴⁶⁻⁵⁹ CO must be acting largely through these known binding partners, though the expression in and importance to the cancer cell must be elucidated as well.

BK_{Ca} channel	(Hou, Heimemann & Hoshi 2009)	Myoglobin	(George & Stratmann 1952)
Cystathionine β-synthase	(Taoka, West & Banerjee 1999)	NADPH oxidase	(Nisimoto, Otsukamurakami & Iwata 1994)
Cytochrome c oxidase	(Wever et al. 1977)	Neuroglobin	(Fago et al. 2004)
cytochrome c*	(Kapetanaki et al. 2009)	Neuronal nitric oxide synthase	(Tetreau et al. 1999)
Cytochrome P450s	(Omura & Sato 1962)	Neuronal PAS domain protein 2	(Dioum et al. 2002)
Fibrinogen	(Cohen et al. 2011)	Progesterone receptor membrane associated component 1	(Kabe et al. 2016)
Hemoglobin	(Bernard 1857)	Soluble guanylyl cyclase	(Sharma & Magde 1999)

*in presence of cardiolipin

Table 1.1. Putative and proposed molecular targets of CO.

1.5 Carbon monoxide, a chemosensitizing agent

In collaboration with the University of California Los Angeles, our group obtained a panel of human breast cancer cell lines, including MCF-7, MDA-MB-468 and Hs 578T in 2016. The Mascharak lab had previously reported the ability of CO to induce cell death in human breast cancer cell line MDA-MB-231,³⁷ which led us to predict similar results in the newly obtained cell lines. To our surprise, none of the cell lines exhibited significant restrictions in cell growth or viability (data not shown). However, Wegiel et al. previously reported that exogenously applied CO not only

elicited cell death and growth arrest, but also sensitized those cells to the chemotherapeutic doxorubicin.³³ In light of their observations, we hypothesized that CO may not be restricting growth and viability per se, but perhaps disrupting cellular processes in the cancer cell that could render them more sensitive to chemotherapeutics. If CO does disrupt these cellular processes; it could prove to be a novel cancer therapeutic to target drug resistance in cancer.

Drug resistance is a major impediment to the management of cancer.^{60,61} Accumulating evidence suggests that the unique metabolic profile found in cancer cells is integral for imparting a drug resistant phenotype. Hallmarks of cancer cellular biology such as altered glucose metabolism, peroxisome activity, ROS-generating enzyme activity, increased protein folding, mitochondrial dysfunction and enhanced growth/inflammatory pathway activity alter the redox balance in cancer cells, generating higher levels of ROS and inducing chronic oxidative stress (Figure 1.6).⁶²

While high oxidative stress is acutely cytotoxic, the low and chronic oxidative stress within cancer cells hormetically enhances antioxidant metabolic pathways and production of antioxidants.⁶³ The sum total cellular antioxidant responses in the cancer cell are qualitatively referred to as the total antioxidant capacity of the cell, the ability of the cell to cope with acute oxidative stress. There is substantial evidence of the pro-tumorigenic role for antioxidants, including the master regulator of anti-oxidative responses nuclear factor (erythroid-derived 2)-like 2 (Nrf2), antioxidant enzymes and cellular antioxidants such as NADPH, cysteine and glutathione (GSH).⁶³

Cancer cells maintaining an elevated antioxidant capacity acquire resistance to future, acute stressors, including that induced by chemotherapeutic agents (Figure 1.6).⁶³

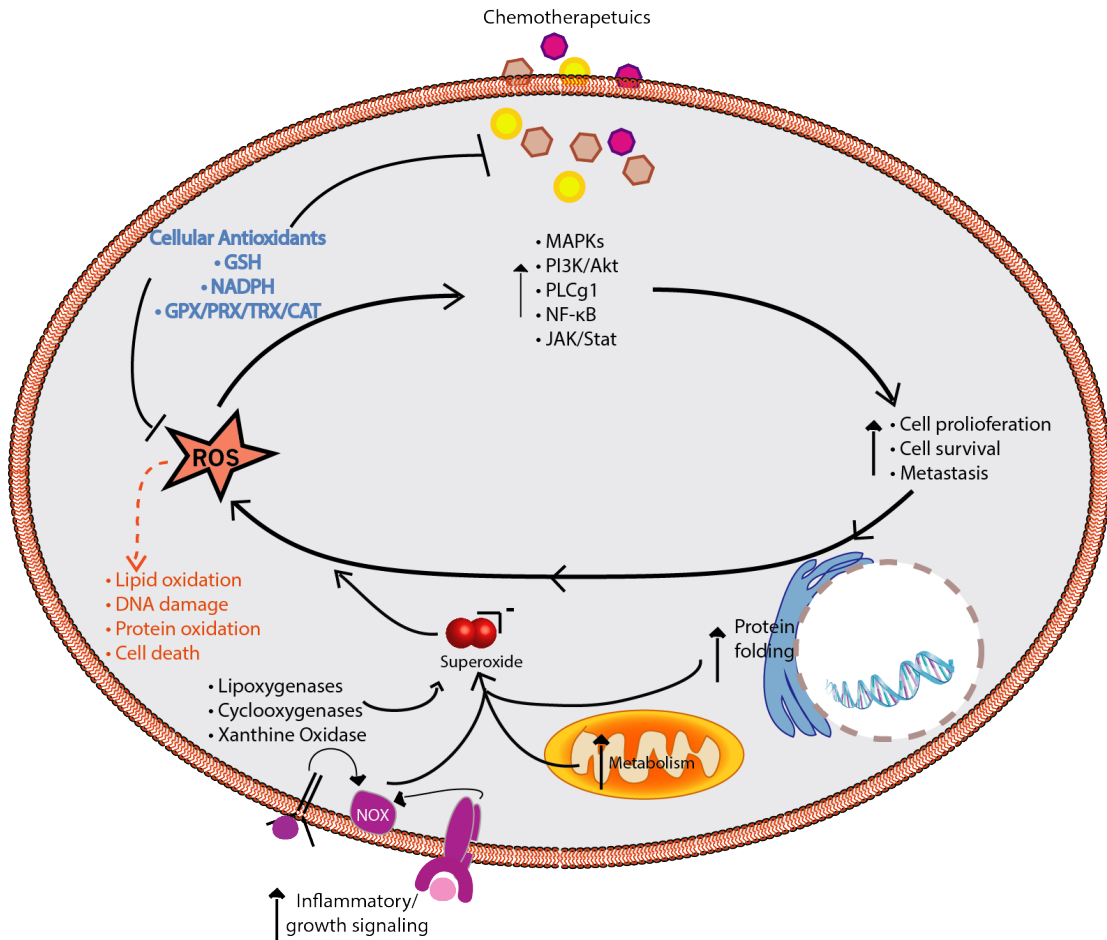


Figure 1.6. Relationship between redox homeostasis and chemotherapeutic resistance in the cancer cell. Abbreviations: catalase (CAT), glutathione (GSH), glutathione peroxidase (GPX), Janus kinase (JAK), mitogen-activated protein kinase (MAPK), NADPH oxidase (NOX), nuclear factor kappa-light-chain-enhancer of activated B cells (NF-κB), peroxiredoxin (PRX), phosphoinositide 3-kinase (PI3K), mammalian target of rapamycin (mTOR), Phospholipase C, gamma 1 (PLCg1), reactive oxygen species (ROS), signal transducer and activator of transcription proteins (Stat), thioredoxin (TRX).

Many chemotherapeutics (e.g. vinca alkaloids, taxanes, anthracyclines and platinum-based drugs) and non-chemical therapies (e.g. radiation) directly generate excessive

ROS in cancer cells, inducing apoptosis by interfering with processes including cell cycle progression and DNA stability.⁶⁴ In most cases, the anti-neoplastic drug effects are indirectly mediated by ROS which eventually bring about the apoptotic death of the cancer cell. Elevated antioxidant processes in cancer, therefore, directly impart drug resistance against chemotherapeutics.⁶⁰⁻⁶³ Furthermore, thiol-containing antioxidants and peptides, GSH and metallothionein, are known to bind and inactivate chemotherapeutics.⁶⁵ As a consequence, selective suppression of the antioxidant capacity of cancer cells by inhibiting antioxidant pathways could mitigate the incidence and intensity of therapeutic resistance and poor prognosis.

CO has been reported to increase ROS levels in cancer cells. Previous studies have hypothesized that this is to CO-mediated inhibition of cytochrome c oxidase which results in an increase in the rate of mitochondrial ROS production, resulting in increased steady-state levels of intracellular ROS.⁴¹ However, as discussed earlier (vide supra) the low of CO for cytochrome c oxidase casts substantial doubt over this proposed mechanism.⁴²⁻⁴⁴ Furthermore, a hallmark of cancer growth is mitochondrial dysfunction and suppression of oxidative phosphorylation.⁶⁵ The conspicuousness of mitochondrial deficits in cancer further suggest that the mitochondria are not the sole target and effector of CO. The mitochondria may certainly be *one* of the targets of CO because of the diffusible nature and promiscuous affinity for ferrous heme-containing enzymes,⁴⁵ though because of its low affinity towards cytochrome c oxidase and lack of mitochondrial integrity in the cancer cell,^{42-44, 66} it appears likely induction of ROS by CO is substantially mediated by other cellular targets.

1.6 Direction of Research

An alternative explanation is that CO may be inhibiting antioxidant processes in the cell, decreasing steady-state levels of cellular antioxidants, perturbing the balance between the generation and neutralization of intracellular ROS, resulting in increased steady state levels of ROS (Figure 1.7). As discussed earlier, cancer cells specifically up-regulate antioxidant processes to control and maintain elevated levels of intracellular ROS.⁶³ These antioxidant processes may be fundamentally regulated by heme-containing enzymes that are sensitive to disruption by CO. Heme uptake and biosynthesis is significantly higher in malignant tissues versus normal tissues, where it is believed to maintain cancer processes including enhancing cellular metabolism.⁶⁷ This up-regulation also disrupts tumor suppressors and provide the necessary co-factor for heme-containing enzymes known to play a role in cancer, including myoglobin, tryptophan 2,3-dioxygenase, indoleamine-2,3-dioxygenase 1 and 2, mitochondrial cytochromes, cyclooxygenases and cytochrome P450s.⁶⁸ The broad requirements of the cancer cell for the heme co-factor suggest that heme-containing enzymes may be therapeutic targets in cancer. The broad sensitivity of ferrous heme-containing enzymes to CO makes CO an intriguing tool with strong indications for therapeutic potential. Inhibition of heme-containing enzymes responsible for maintaining elevated antioxidant levels in the cancer cell could sensitize those cells to chemotherapeutics.

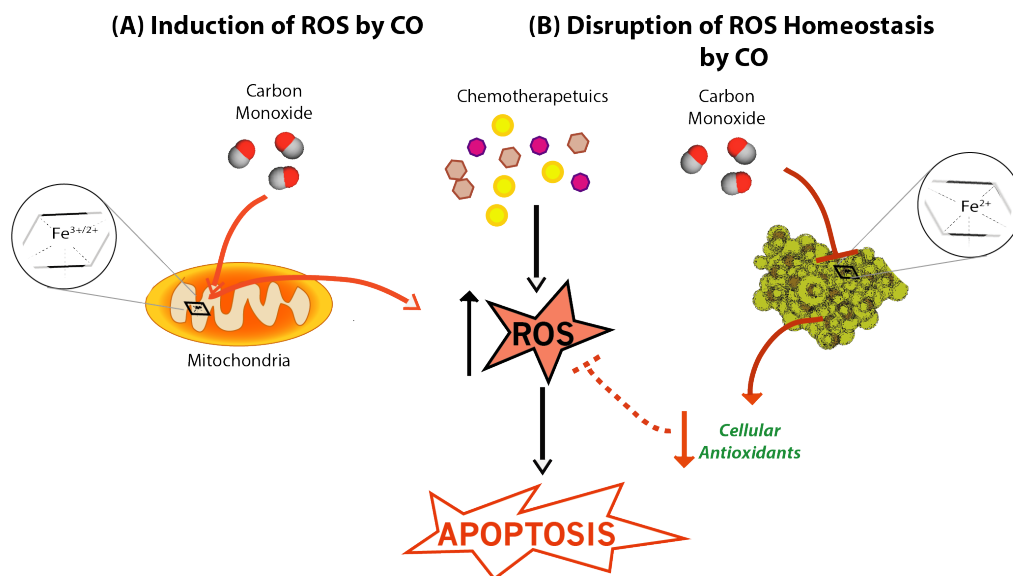


Figure 1.7. Proposed mechanisms of carbon monoxide (CO)-mediated drug sensitization in cancer cells. (A) CO enhances mitochondrial reactive oxygen species (ROS) production to induce elevated levels of intracellular ROS. (B) CO, through ferrous heme-containing enzymes, inhibits antioxidant processes which decrease cellular antioxidant levels, disrupting ROS homeostasis to raise intracellular ROS levels.

If incorporation of CO into existing chemotherapeutic regimens could indeed improve drug efficacy, health outcomes could dramatically improve. This hypothesis has prompted us to undertake research efforts to explore the effects of CO co-administration with conventional chemotherapeutics on human cancer models and in this account we provide strong evidence that CO mitigates drug resistance in refractory cancer cells through alteration of cellular antioxidant capacity. Because of the specific chemical nature of CO, we further hypothesized the importance of ferrous-heme containing enzymes in imparting drug resistance in the cancer cell (Figure 1.7).

1.7 References

1. Fojo, T.; Mailankody, S.; Lo, A., Unintended Consequences of Expensive Cancer Therapeutics-The Pursuit of Marginal Indications and a Me-Too Mentality That Stifles Innovation and Creativity The John Conley Lecture. *Jama Otolaryngology-Head & Neck Surgery* **2014**, *140* (12), 1225-1236.
2. Friedman, R., Drug resistance in cancer: molecular evolution and compensatory proliferation. *Oncotarget* **2016**, *7* (11), 11746-11755.
3. McCormick, F., KRAS as a Therapeutic Target. *Clinical Cancer Research*. **2015**, *21*(8), 1797-1801.
4. Sircar, K.; Clower, J.; Shin, M. K.; Bailey, C.; King, M.; Yip, F. Carbon monoxide poisoning deaths in the United States, 1999 to 2012. *American Journal of Emergency Medicine* **2015**, *33*, 1140-1145.
5. Lee, W. M. Acetaminophen and the US Acute Liver Failure Study Group: Lowering the risks of hepatic failure. *Hepatology* **2004**, *40*, 6-9.
6. Olson, K.; Smollin, C., Carbon monoxide poisoning (acute). *BMJ Clinical Evidence* **2008**, *2008*.
7. Coburn, R. F., The measurement of endogenous carbon monoxide production. *Journal of Applied Physiology* **2012**, *112* (11), 1949-1955.
8. Marks, G. S.; Brien, J. F.; Nakatsu, K.; McLaughlin, B. E., Does carbon-monoxide have a physiological-function. *Trends in Pharmacological Sciences* **1991**, *12* (5), 185-188.
9. Kim, H. P.; Ryter, S. W.; Choi, A. M. K., CO as a cellular signaling molecule. *Annual Review of Pharmacology and Toxicology* **2006**, *46*, 411-449.
10. Yang, G. D.; Sener, A.; Ji, Y.; Pei, Y. X.; Pluth, M. D., Gasotransmitters in biology and medicine: molecular mechanisms and drug targets. *Oxidative Medicine and Cellular Longevity* **2016**, *2016*.
11. Tenhunen, R.; Marver, H. S.; Schmid, R., Enzymatic conversion of heme to bilirubin by microsomal heme oxygenase. *Proceedings of the National Academy of Sciences of the United States of America* **1968**, *61* (2), 748-&.

12. Tenhunen, R.; Marver, H. S.; Schmid, R., Microsomal heme oxygenase – characterization of enzyme. *Journal of Biological Chemistry* **1969**, *244* (23), 6388-&.
13. Kikuchi, G.; Yoshida, T.; Noguchi, M., Heme oxygenase and heme degradation. *Biochemical and Biophysical Research Communications* **2005**, *338* (1), 558-567.
14. Yachie, A.; Niida, Y.; Wada, T.; Igarashi, N.; Kaneda, H.; Toma, T.; Ohta, K.; Kasahara, Y.; Koizumi, S. Oxidative stress causes enhanced endothelial cell injury in human heme oxygenase-1 deficiency. *Journal of Clinical Investigation* **1999**, *103*, 129-135.
15. Stocker, R.; Perrella, M. A., Heme oxygenase-1 - A novel drug target for atherosclerotic diseases? *Circulation* **2006**, *114* (20), 2178-2189.
16. Munoz-Sanchez, J.; Chanez-Cardenas, M. E., A review on hemeoxygenase-2: focus on cellular protection and oxygen response. *Oxidative Medicine and Cellular Longevity* **2014**.
17. Waza, A. A.; Hamid, Z.; Ali, S.; Bhat, S. A.; Bhat, M. A., A review on heme oxygenase-1 induction: is it a necessary evil. *Inflammation Research* **2018**, *67* (7), 579-588.
18. Naito, Y.; Takagi, T.; Higashimura, Y., Heme oxygenase-1 and anti-inflammatory M2 macrophages. *Archives of Biochemistry and Biophysics* **2014**, *564*, 83-88.
19. Hunter, P., The inflammation theory of disease - The growing realization that chronic inflammation is crucial in many diseases opens new avenues for treatment. *Embo Reports* **2012**, *13* (11), 968-970.
20. Motterlini, R.; Otterbein, L. E., The therapeutic potential of carbon monoxide. *Nature Reviews Drug Discovery* **2010**, *9* (9), 728-U24.
21. Motterlini, R.; Foresti, R., Biological signaling by carbon monoxide and carbon monoxide-releasing molecules. *American Journal of Physiology-Cell Physiology* **2017**, *312* (3), C302-C313.

22. Motterlini, R.; Haas, B.; Foresti, R., Emerging concepts on the anti-inflammatory actions of carbon monoxide-releasing molecules (CO-RMs). *Medical Gas Research* **2012**, *2* (1), 28.
23. Zobi, F., CO and CO-releasing molecules in medicinal chemistry. *Future Medicinal Chemistry* **2013**, *5* (2), 175-188.
24. Schatzschneider, U., Novel lead structures and activation mechanisms for CO-releasing molecules (CORMs). *British Journal of Pharmacology* **2015**, *172* (6), 1638-1650.
25. Chakraborty, I.; Carrington, S. J.; Mascharak, P. K., Design strategies to improve the sensitivity of photoactive metal carbonyl complexes (photocorms) to visible light and their potential as CO-Donors to biological targets. *Accounts of Chemical Research* **2014**, *47* (8), 2603-2611.
26. Pinto, M. N.; Chakraborty, I.; Sandoval, C.; Mascharak, P. K., Eradication of HT-29 colorectal adenocarcinoma cells by controlled photorelease of CO from a CO-releasing polymer (photoCORP-1) triggered by visible light through an optical fiber-based device. *Journal of Controlled Release* **2017**, *264*, 192-202.
27. Chakraborty, I.; Carrington, S. J.; Hauser, J.; Oliver, S. R. J.; Mascharak, P. K., Rapid eradication of human breast cancer cells through trackable light-triggered CO delivery by mesoporous silica nanoparticles packed with a designed photoCORM. *Chemistry of Materials* **2015**, *27* (24), 8387-8397.
28. Chakraborty, I.; Jimenez, J.; Mascharak, P. K., CO-Induced apoptotic death of colorectal cancer cells by a luminescent photoCORM grafted on biocompatible carboxymethyl chitosan. *Chemical Communications* **2017**, *53* (40), 5519-5522.
29. Stenger-Smith, J.; Chakraborty, I.; Quattara, R.; Sameera, W.M.C.; Rue, K.; Mascharak, P.K., CO release from Mn(I)-based photoCORMs with Single Photons in the Phototherapeutic Region. *Chemical Communications* [submitted November 10, 2020].
30. Coussens, L. M.; Werb, Z., Inflammation and cancer. *Nature* **2002**, *420* (6917), 860-867.

31. Kourti, M.; Jiang, W. G.; Cai, J., Aspects of carbon monoxide in form of co-releasing molecules used in cancer treatment: More light on the way. *Oxidative Medicine and Cellular Longevity* **2017**.
32. Choi, Y. K.; Por, E. D.; Kwon, Y. G.; Kim, Y. M., Regulation of ROS Production and Vascular Function by Carbon Monoxide. *Oxidative Medicine and Cellular Longevity* **2012**, 2012.
33. Wegiel, B.; Gallo, D.; Csizmadia, E.; Harris, C.; Belcher, J.; Vercellotti, G. M.; Penacho, N.; Seth, P.; Sukhatme, V.; Ahmed, A.; Pandolfi, P. P.; Helczynski, L.; Bjartell, A.; Persson, J. L.; Otterbein, L. E., Carbon monoxide expedites metabolic exhaustion to inhibit tumor growth. *Cancer Research* **2013**, 73 (23), 7009-7021.
34. Niesel, J.; Pinto, A.; N'Dongo, H. W. P.; Merz, K.; Ott, I.; Gust, R.; Schatzschneider, U., Photoinduced CO release, cellular uptake and cytotoxicity of a tris(pyrazolyl) methane (tpm) manganese tricarbonyl complex. *Chemical Communications* **2008**, (15), 1798-1800.
35. Jackson, C. S.; Schmitt, S.; Dou, Q. P.; Kodanko, J. J., Synthesis, characterization, and reactivity of the stable iron carbonyl complex Fe(CO)(N4Py) (ClO4)(2): Photoactivated carbon monoxide release, growth inhibitory activity, and peptide ligation. *Inorganic Chemistry* **2011**, 50 (12), 5336-5338.
36. Carrington, S. J.; Chakraborty, I.; Mascharak, P. K., Rapid CO release from a Mn(I) carbonyl complex derived from azopyridine upon exposure to visible light and its phototoxicity toward malignant cells. *Chemical Communications* **2013**, 49 (96), 11254-11256.
37. Carrington, S. J.; Chakraborty, I.; Bernard, J. M. L.; Mascharak, P. K., Synthesis and characterization of a "turn-on" photoCORM for trackable CO delivery to biological targets. *Acs Medicinal Chemistry Letters* **2014**, 5 (12), 1324-1328.
38. Vitek, L.; Gbelcova, H.; Muchova, L.; Vanova, K.; Zelenka, J.; Konickova, R.; Suk, J.; Zadinova, M.; Knejzlik, Z.; Ahmad, S.; Fujisawa, T.; Ahmed, A.; Ruml,

- T., Antiproliferative effects of carbon monoxide on pancreatic cancer. *Digestive and Liver Disease* **2014**, *46* (4), 369-375.
39. Carrington, S. J.; Chakraborty, I.; Bernard, J. M. L.; Mascharak, P. K., A theranostic two-tone luminescent photoCORM derived from Re(I) and (2-Pyridyl)-benzothiazole: Trackable co delivery to malignant cells. *Inorganic Chemistry* **2016**, *55* (16), 7852-7858.
40. Allanson, M.; Reeve, V. E., Carbon monoxide signalling reduces photocarcinogenesis in the hairless mouse. *Cancer Immunology Immunotherapy* **2007**, *56* (11), 1807-1815.
41. Zuckerbraun, B. S.; Chin, B. Y.; Bilban, M.; d'Avila, J. C.; Rao, J.; Billiar, T. R.; Otterbein, L. E., Carbon monoxide signals via inhibition of cytochrome c oxidase and generation of mitochondrial reactive oxygen species. *FASEB Journal* **2007**, *21* (4), 1099-1106.
42. Weber, R. E.; Vinogradov, S. N., Nonvertebrate hemoglobins: Functions and molecular adaptations. *Physiological Reviews* **2001**, *81* (2), 569-628.
43. Vilhjalmsdottir, J.; Gennis, R. B.; Brzezinski, P. The electron distribution in the "activated" state of cytochrome c oxidase. *Scientific Reports* **2018**, *8*.
44. Li, J. F.; Noll, B. C.; Schulz, C. E.; Scheidt, W. R. Comparison of Cyanide and Carbon Monoxide as Ligands in Iron(II) Porphyrinates. *Angewandte Chemie-International Edition* **2009**, *48*, 5010-5013.
45. Piantadosi, C. A., Biological chemistry of carbon monoxide. *Antioxidants & Redox Signaling* **2002**, *4* (2), 259-270.
46. Bernard, C., Leçons sur les effets des substances toxiques et médicamenteuses. Baillière et Fils: Paris, France, 1857.
47. George, P.; Stratmann, C. J., The oxidation of myoglobin to methmyoglobin by oxygen. .1. *Biochemical Journal* **1952**, *51* (1), 103-108.
48. Omura, T.; Sato, R., A new cytochrome in liver microsomes. *Journal of Biological Chemistry* **1962**, *237* (4), 1375-&.

49. Wever, R.; Vandrooge, J. H.; Muijsers, A. O.; Bakker, E. P.; Vangelder, B. F., Binding of carbon-monoxide to cytochrome-c oxidase. *European Journal of Biochemistry* **1977**, *73* (1), 149-154.
50. Nisimoto, Y.; Otsukamurakami, H.; Iwata, S., NADPH-cytochrome-c reductase from human neutrophil membranes – purification, characterization and localization. *Biochemical Journal* **1994**, *297*, 585-593.
51. Taoka, S.; West, M.; Banerjee, R., Characterization of the heme and pyridoxal phosphate cofactors of human cystathionine beta-synthase reveals nonequivalent active sites. *Biochemistry* **1999**, *38* (9), 2738-2744.
52. Sharma, V. S.; Magde, D., Activation of soluble guanylate cyclase by carbon monoxide and nitric oxide: A mechanistic model. *Methods-a Companion to Methods in Enzymology* **1999**, *19* (4), 494-505.
53. Tetreau, C.; Tourbez, M.; Gorren, A.; Mayer, B.; Lavalette, D., Dynamics of carbon monoxide binding with neuronal nitric oxide synthase. *Biochemistry* **1999**, *38* (22), 7210-7218.
54. Dioum, E. M.; Rutter, J.; Tuckerman, J. R.; Gonzalez, G.; Gilles-Gonzalez, M. A.; McKnight, S. L., NPAS2: A gas-responsive transcription factor. *Science* **2002**, *298* (5602), 2385-2387.
55. Fago, A.; Hundahl, C.; Dewilde, S.; Gilany, K.; Moens, L.; Weber, R. E., Allosteric regulation and temperature dependence of oxygen binding in human neuroglobin and cytoglobin - Molecular mechanisms and physiological significance. *Journal of Biological Chemistry* **2004**, *279* (43), 44417-44426.
56. Hou, S. W.; Heinemann, S. H.; Hoshi, T., Modulation of BKCa channel gating by endogenous signaling molecules. *Physiology* **2009**, *24* (1), 26-35.
57. Kapetanaki, S. M.; Silkstone, G.; Husu, I.; Liebl, U.; Wilson, M. T.; Vos, M. H., Interaction of carbon monoxide with the apoptosis-inducing cytochrome c-cardiolipin complex. *Biochemistry* **2009**, *48* (7), 1613-1619.
58. Cohen, J. B.; Persaud, J. M.; Malayaman, S. N.; Nielsen, V. G., Carbon monoxide releasing molecule-2 enhances coagulation and attenuates fibrinolysis by two

- mechanisms: insights gained with colloid dilution. *Blood Coagulation & Fibrinolysis* **2011**, *22* (1), 60-66.
59. Kabe, Y.; Yamamoto, T.; Kajimura, M.; Sugiura, Y.; Koike, I.; Ohmura, M.; Nakamura, T.; Tokumoto, Y.; Tsugawa, H.; Handa, H.; Kobayashi, T.; MakotoSuematsu, A., Cystathionine beta-synthase and PGRMC1 as CO sensors. *Free Radical Biology and Medicine* **2016**, *99*, 333-344.
60. Lippert, T. H.; Ruoff, H.-J.; Volm, M., Intrinsic and acquired drug resistance in malignant tumors. *Arzneimittel-Forschung-Drug Research* **2008**, *58* (6), 261-264.
61. Housman, G.; Byler, S.; Heerboth, S.; Lapinska, K.; Longacre, M.; Snyder, N.; Sarkar, S., Drug Resistance in Cancer: An Overview. *Cancers* **2014**, *6* (3), 1769-1792.
62. Grek, C. L.; Tew, K. D., Redox metabolism and malignancy. *Current Opinion in Pharmacology* **2010**, *10* (4), 362-368.
63. Hawk, M. A.; McCallister, C.; Schafer, Z. T., Antioxidant activity during tumor progression: A necessity for the survival of cancer Cells? *Cancers* **2016**, *8* (10).
64. Yokoyama, C.; Sueyoshi, Y.; Ema, M.; Mori, Y.; Takaishi, K.; Hisatomi, H., Induction of oxidative stress by anticancer drugs in the presence and absence of cells. *Oncology Letters* **2017**, *14* (5), 6066-6070.
65. Galluzzi, L.; Senovilla, L.; Vitale, I.; Michels, J.; Martins, I.; Kepp, O.; Castedo, M.; Kroemer, G., Molecular mechanisms of cisplatin resistance. *Oncogene* **2012**, *31* (15), 1869-1883.
66. Solaini, G.; Sgarbi, G.; Baracca, A., Oxidative phosphorylation in cancer cells. *Biochimica Et Biophysica Acta-Bioenergetics* **2011**, *1807* (6), 534-542.
67. Navone, N. M.; Polo, C. F.; Frisardi, A. L.; Andrade, N. E.; Batlle, A. M. D., Heme-biosynthesis in human breast-cancer mimetic invitro studies and some heme enzymatic-activity. *International Journal of Biochemistry* **1990**, *22* (12), 1407-1411.
68. Fiorito, V.; Chiabrando, D.; Petrillo, S.; Bertino, F.; Tolosano, E., The Multifaceted Role of Heme in Cancer. *Frontiers in Oncology* **2020**, *9*.

1.8 Reprint of publication



Future Science Ltd. - License Terms and Conditions

This is a License Agreement between Brian Kawahara, University of California Santa Cruz ("You") and Future Science Ltd. ("Publisher") provided by Copyright Clearance Center ("CCC"). The license consists of your order details, the terms and conditions provided by Future Science Ltd., and the CCC terms and conditions.

All payments must be made in full to CCC.

Order Date	24-Nov-2020	Type of Use	Republish in a thesis/dissertation
Order license ID	1079746-1	Publisher Portion	Future Science Ltd Chapter/article
ISSN	1756-8927		

LICENSED CONTENT

Publication Title	Future medicinal chemistry	Publication Type	e-Journal
Article Title	Reaction of carbon monoxide with cystathionine β -synthase: implications on drug efficacies in cancer chemotherapy.	Start Page	325
		End Page	337
		Issue	4
		Volume	12
Date	12/31/2008		
Language	English		
Country	United Kingdom of Great Britain and Northern Ireland		
Rightsholder	Future Science Ltd.		

REQUEST DETAILS

Portion Type	Chapter/article	Rights Requested	Main product
Page range(s)	325-337	Distribution	United States
Total number of pages	12	Translation	Original language of publication
Format (select all that apply)	Print, Electronic	Copies for the disabled?	No
Who will republish the content?	Academic institution	Minor editing privileges?	No
Duration of Use	Life of current edition	Incidental promotional use?	No
Lifetime Unit Quantity	Up to 499	Currency	USD

NEW WORK DETAILS

Title	CHEMICAL BIOLOGY OF CARBON MONOXIDE IN CANCER: INSIGHTS INTO MOLECULAR MECHANISMS OF DRUG RESISTANCE	Institution name	University of California Santa Cruz
Instructor name	Brian Kawahara	Expected presentation date	2020-12-11

ADDITIONAL DETAILS

Order reference number	N/A	The requesting person / organization to appear on the license	Brian Kawahara, University of California Santa Cruz
-------------------------------	-----	--	---

REUSE CONTENT DETAILS

Title, description or numeric reference of the portion(s)	Reaction of carbon monoxide with cystathionine β -synthase: implications on drug efficacies in cancer chemotherapy	Title of the article/chapter the portion is from	Reaction of carbon monoxide with cystathionine β -synthase: implications on drug efficacies in cancer chemotherapy.
Editor of portion(s)	Mascharak, Pradip K; Sen, Suvajit; Kawahara, Brian	Author of portion(s)	Mascharak, Pradip K; Sen, Suvajit; Kawahara, Brian
Volume of serial or monograph	12	Issue, if republishing an article from a serial	4
Page or page range of portion	325-337	Publication date of portion	2020-02-06

CCC Reproduction Terms and Conditions

1. **Description of Service; Defined Terms.** This Reproduction License enables the User to obtain licenses for republication of one or more copyrighted works as described in detail on the relevant Order Confirmation (the "Work(s)"). Copyright Clearance Center, Inc. ("CCC") grants licenses through the Service on behalf of the rightsholder identified on the Order Confirmation (the "Rightsholder"). "Reproduction", as used herein, generally means the inclusion of a Work, in whole or in part, in a new work or works, also as described on the Order Confirmation. "User", as used herein, means the person or entity making such reproduction.
2. The terms set forth in the relevant Order Confirmation, and any terms set by the Rightsholder with respect to a particular Work, govern the terms of use of Works in connection with the Service. By using the Service, the person transacting for a reproduction license on behalf of the User represents and warrants that he/she/it (a) has been duly authorized by the User to accept, and hereby does accept, all such terms and conditions on behalf of User, and (b) shall inform User of all such terms and conditions. In the event such person is a "freelancer" or other third party independent of User and CCC, such party shall be deemed jointly a "User" for purposes of these terms and conditions. In any event, User shall be deemed to have accepted and agreed to all such terms and conditions if User republishes the Work in any fashion.
3. **Scope of License; Limitations and Obligations**
 - 3.1. All Works and all rights therein, including copyright rights, remain the sole and exclusive property of the Rightsholder. The license created by the exchange of an Order Confirmation (and/or any invoice) and payment by User of the full amount set forth on that document includes only those rights expressly set forth in the Order Confirmation and in these terms and conditions, and conveys no other rights in the Work(s) to User. All rights not expressly granted are hereby reserved.

- 3.2. **General Payment Terms.** You may pay by credit card or through an account with us payable at the end of the month, if you and we agree that you may establish a standing account with CCC, then the following terms apply. Remit Payment to Copyright Clearance Center, 29118 Network Place, Chicago, IL 60673-1291. Payments Due. Invoices are payable upon their delivery to you (or upon our notice to you that they are available to you for downloading). After 30 days, outstanding amounts will be subject to a service charge of 1-1/2% per month or, if less, the maximum rate allowed by applicable law. Unless otherwise specifically set forth in the Order Confirmation or in a separate written agreement signed by CCC, invoices are due and payable on "net 30" terms. While User may exercise the rights licensed immediately upon issuance of the Order Confirmation, the license is automatically revoked and is null and void, as if it had never been issued, if complete payment for the license is not received on a timely basis either from User directly or through a payment agent, such as a credit card company.
- 3.3. Unless otherwise provided in the Order Confirmation, any grant of rights to User (i) is "one-time" (including the editions and product family specified in the license), (ii) is non-exclusive and non-transferable and (iii) is subject to any and all limitations and restrictions (such as, but not limited to, limitations on duration of use or circulation) included in the Order Confirmation or invoice and/or in these terms and conditions. Upon completion of the licensed use, User shall either secure a new permission for further use of the Work(s) or immediately cease any new use of the Work(s) and shall render inaccessible (such as by deleting or by removing or severing links or other locators) any further copies of the Work (except for copies printed on paper in accordance with this license and still in User's stock at the end of such period).
- 3.4. In the event that the material for which a republication license is sought includes third party materials (such as photographs, illustrations, graphs, inserts and similar materials) which are identified in such material as having been used by permission, User is responsible for identifying, and seeking separate licenses (under this Service or otherwise) for, any of such third party materials; without a separate license, such third party materials may not be used.
- 3.5. Use of proper copyright notice for a Work is required as a condition of any license granted under the Service. Unless otherwise provided in the Order Confirmation, a proper copyright notice will read substantially as follows: "Republished with permission of [Rightsholder's name], from [Work's title, author, volume, edition number and year of copyright]; permission conveyed through Copyright Clearance Center, Inc." Such notice must be provided in a reasonably legible font size and must be placed either immediately adjacent to the Work as used (for example, as part of a by-line or footnote but not as a separate electronic link) or in the place where substantially all other credits or notices for the new work containing the republished Work are located. Failure to include the required notice results in loss to the Rightsholder and CCC, and the User shall be liable to pay liquidated damages for each such failure equal to twice the use fee specified in the Order Confirmation, in addition to the use fee itself and any other fees and charges specified.
- 3.6. User may only make alterations to the Work if and as expressly set forth in the Order Confirmation. No Work may be used in any way that is defamatory, violates the rights of third parties (including such third parties' rights of copyright, privacy, publicity, or other tangible or intangible property), or is otherwise illegal, sexually explicit or obscene. In addition, User may not conjoin a Work with any other material that may result in damage to the reputation of the Rightsholder. User agrees to inform CCC if it becomes aware of any infringement of any rights in a Work and to cooperate with any reasonable request of CCC or the Rightsholder in connection therewith.
4. **Indemnity.** User hereby indemnifies and agrees to defend the Rightsholder and CCC, and their respective employees and directors, against all claims, liability, damages, costs and expenses, including legal fees and expenses, arising out of any use of a Work beyond the scope of the rights granted herein, or any use of a Work which has been altered in any unauthorized way by User, including claims of defamation or infringement of rights of copyright, publicity, privacy or other tangible or intangible property.
5. **Limitation of Liability.** UNDER NO CIRCUMSTANCES WILL CCC OR THE RIGHTSHOLDER BE LIABLE FOR ANY DIRECT, INDIRECT, CONSEQUENTIAL OR INCIDENTAL DAMAGES (INCLUDING WITHOUT LIMITATION DAMAGES FOR LOSS OF BUSINESS PROFITS OR INFORMATION, OR FOR BUSINESS INTERRUPTION) ARISING OUT OF THE USE OR INABILITY

TO USE A WORK, EVEN IF ONE OF THEM HAS BEEN ADVISED OF THE POSSIBILITY OF SUCH DAMAGES. In any event, the total liability of the Rightsholder and CCC (including their respective employees and directors) shall not exceed the total amount actually paid by User for this license. User assumes full liability for the actions and omissions of its principals, employees, agents, affiliates, successors and assigns.

6. Limited Warranties. THE WORK(S) AND RIGHT(S) ARE PROVIDED "AS IS". CCC HAS THE RIGHT TO GRANT TO USER THE RIGHTS GRANTED IN THE ORDER CONFIRMATION DOCUMENT. CCC AND THE RIGHTSHOLDER DISCLAIM ALL OTHER WARRANTIES RELATING TO THE WORK(S) AND RIGHT(S), EITHER EXPRESS OR IMPLIED, INCLUDING WITHOUT LIMITATION IMPLIED WARRANTIES OF MERCHANTABILITY OR FITNESS FOR A PARTICULAR PURPOSE. ADDITIONAL RIGHTS MAY BE REQUIRED TO USE ILLUSTRATIONS, GRAPHS, PHOTOGRAPHS, ABSTRACTS, INSERTS OR OTHER PORTIONS OF THE WORK (AS OPPOSED TO THE ENTIRE WORK) IN A MANNER CONTEMPLATED BY USER; USER UNDERSTANDS AND AGREES THAT NEITHER CCC NOR THE RIGHTSHOLDER MAY HAVE SUCH ADDITIONAL RIGHTS TO GRANT.
7. Effect of Breach. Any failure by User to pay any amount when due, or any use by User of a Work beyond the scope of the license set forth in the Order Confirmation and/or these terms and conditions, shall be a material breach of the license created by the Order Confirmation and these terms and conditions. Any breach not cured within 30 days of written notice thereof shall result in immediate termination of such license without further notice. Any unauthorized (but licensable) use of a Work that is terminated immediately upon notice thereof may be liquidated by payment of the Rightsholder's ordinary license price therefor; any unauthorized (and unlicensable) use that is not terminated immediately for any reason (including, for example, because materials containing the Work cannot reasonably be recalled) will be subject to all remedies available at law or in equity, but in no event to a payment of less than three times the Rightsholder's ordinary license price for the most closely analogous licensable use plus Rightsholder's and/or CCC's costs and expenses incurred in collecting such payment.
8. Miscellaneous.
 - 8.1. User acknowledges that CCC may, from time to time, make changes or additions to the Service or to these terms and conditions, and CCC reserves the right to send notice to the User by electronic mail or otherwise for the purposes of notifying User of such changes or additions; provided that any such changes or additions shall not apply to permissions already secured and paid for.
 - 8.2. Use of User-related information collected through the Service is governed by CCC's privacy policy, available online here <https://marketplace.copyright.com/rs-ui-web/mp/privacy-policy>
 - 8.3. The licensing transaction described in the Order Confirmation is personal to User. Therefore, User may not assign or transfer to any other person (whether a natural person or an organization of any kind) the license created by the Order Confirmation and these terms and conditions or any rights granted hereunder, provided, however, that User may assign such license in its entirety on written notice to CCC in the event of a transfer of all or substantially all of User's rights in the new material which includes the Work(s) licensed under this Service.
 - 8.4. No amendment or waiver of any terms is binding unless set forth in writing and signed by the parties. The Rightsholder and CCC hereby object to any terms contained in any writing prepared by the User or its principals, employees, agents or affiliates and purporting to govern or otherwise relate to the licensing transaction described in the Order Confirmation, which terms are in any way inconsistent with any terms set forth in the Order Confirmation and/or in these terms and conditions or CCC's standard operating procedures, whether such writing is prepared prior to, simultaneously with or subsequent to the Order Confirmation, and whether such writing appears on a copy of the Order Confirmation or in a separate instrument.
 - 8.5. The licensing transaction described in the Order Confirmation document shall be governed by and construed under the law of the State of New York, USA, without regard to the principles thereof of conflicts of law. Any case, controversy, suit, action, or proceeding arising out of, in connection with, or related to such licensing transaction shall be brought, at CCC's sole discretion, in any federal or state court located in the County of New York, State of New York, USA, or in any federal or state court whose geographical jurisdiction covers the location of the Rightsholder set forth in the Order Confirmation. The parties expressly submit to the personal jurisdiction and venue of each such federal or state court. If you have any comments or questions about the Service or Copyright Clearance Center, please contact us at 978-750-8400 or send an e-mail to support@copyright.com.

Reaction of carbon monoxide with cystathionine β -synthase: implications on drug efficacies in cancer chemotherapy

Brian Kawahara¹, Suvajit Sen² & Pradip K Mascharak^{*,1} 

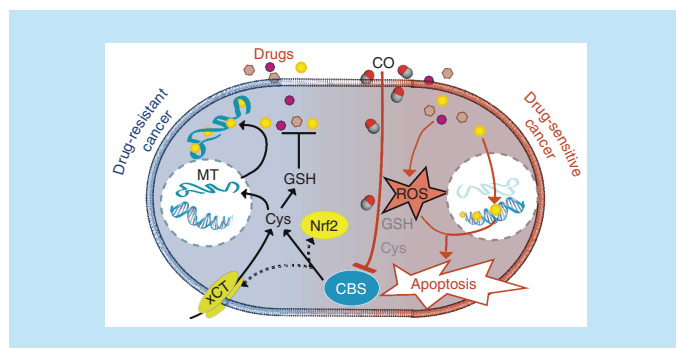
¹Department of Chemistry & Biochemistry University of California, Santa Cruz, CA 95060, USA

²Department of Obstetrics & Gynecology, David Geffen School of Medicine University of California, Los Angeles, CA 90095, USA

*Author for correspondence: Tel.: +831 459 4251; pradip@ucsc.edu

Photo-activatable carbon monoxide (CO)-releasing molecules (photoCORMs), have recently provided help to identify the salutary effects of CO in human pathophysiology. Among them notable is the ability of CO to sensitize chemotherapeutic-resistant cancer cells. Findings from our group have shown CO to mitigate drug resistance in certain cancer cells by the inhibition of cystathionine β -synthase (CBS), a key regulator of redox homeostasis in the cell. Diminution of the antioxidant capacity of cancer cells leads to sensitization to reactive oxygen species-producing drugs like doxorubicin and paclitaxel upon cotreatment with CO as well as in mitigating the drug effects of cisplatin. We hypothesize that the development of CO delivery techniques for coadministration with existing cancer treatment regimens may ultimately improve clinical outcomes in cancer therapy.

Graphical abstract:



First draft submitted: 10 September 2019; Accepted for publication: 8 November 2019; Published online: 7 February 2020

Keywords: antioxidant capacity • breast cancer • carbon monoxide • chemotherapy • cystathionine β -synthase • drug resistance • glutathione • ovarian cancer • photoCORM • reactive oxygen species

Carbon monoxide (CO), an endogenously produced gaseous molecule, has been recognized as a gasotransmitter, that elicits biological responses in mammalian pathophysiology [1,2]. Along with nitric oxide and hydrogen sulfide (H₂S), gasotransmitters have recently been shown to play roles in a wide array of chemistry in biological systems. Unlike nitric oxide, a radical species, and H₂S, a weak acid and reducing agent, CO is relatively inert. This weak Lewis base interacts with transition metal centers in low oxidation states. In human cells and tissues, CO reacts almost exclusively with 5-coordinate ferrous heme cofactors [3].

**newlands
press**

Historically CO is noted for its generation from incomplete hydrocarbon combustion and toxicity arising from its binding to hemoglobin, the oxygen carrier in mammals. However, endogenous production of CO as a product of heme catabolism has been known for over 70 years. This reaction is catalyzed by microsomal heme oxygenase (HO), an enzyme that exists in two isoforms namely, HO-1 (inducible) and HO-2 (constitutive) [4]. Catabolism of free heme is vital for maintaining cellular health and mitigating the toxic effects of heme-catalyzed oxidation reactions. Indeed, loss-of-function mutations in HO-1 are lethal. In the human body, micromolar amounts of CO are generated collectively by HO-1 and HO-2. Nearly all tissues are capable of HO-1 induction, though its expression in Kupffer cells and anti-inflammatory/M2-polarized macrophages suggest a role for CO in modulating immune response and inflammation. Constitutive HO-2 produces CO in the liver, testes, endothelial cells and the brain where it is reputed to play important roles in maintaining vascular tone.

Research during the past three decades has explored the potential of low doses (10–100 ppm) of CO as a therapeutic in a wide array of injury and disease models including wound healing, colitis, sepsis, cerebral malaria, diabetes, balloon angioplasty-induced stenosis, ileus/bowel immotility and organ transplantation [5,6]. The observed salutary effects of CO in these disease/injury models may be partially explained by the ability of CO to modulate intracellular levels of reactive oxygen species (ROS) in target cells, attenuate macrophage activation by cytokine and endotoxin, inhibit endothelial cell apoptosis and prevent T-cell proliferation [6]. In addition, CO has been shown to be effective in attenuating and resolving chronic inflammation, a process implicated in many diseases including cancer [7]. Upregulated and chronic inflammation is implicated as a key factor in the initiation and progression, metastatic spread and the development of therapeutic resistance in cancer [8]. In light of observations of the protective and anti-inflammatory effects of HO-1/2 and CO, recent efforts have been made to explore the possible therapeutic application of CO in cancer models.

CO in cancer therapy

Work from our group and others have provided evidence for the therapeutic potential of exogenous CO in cancer cell models in recent years [9–15]. However, the delivery of CO to malignant targets require novel delivery approaches using either CO gas or CO-releasing molecules (CORMs) [16,17]. Although some progress along this line has been achieved in recent years [5,9,11,18], therapeutic application of CO in a clinical setting is still in its infancy. Fortunately, the CORMs have provided crucial help in exploring, among others, the physiological processes that lead tumorigenic initiation, progression and ultimate management of cancer. The pathology of cancer often poses challenges arising from therapeutic drug resistance and the role of CO in mitigating such processes could be quite interesting. In this context, CO has been shown to sensitize cells to chemotherapeutics in cancer models [15]. If incorporation of CO into existing chemotherapeutic regimens could indeed improve drug efficacy, health outcomes may improve significantly. This hypothesis has prompted us to undertake research efforts to explore the effects of CO coadministration with conventional chemotherapeutics on human cancer models.

Antioxidant capacity in chemoresistant cancer

Drug resistance remains as the main impediment to the management of cancer [19,20]. Accumulating evidence suggests that the unique metabolic profile found in cancer cells is integral for imparting a drug resistant phenotype. Hallmarks of cancer cellular biology such as altered glucose metabolism, peroxisome activity, mitochondrial dysfunction and enhanced growth/signaling pathway activity alter the redox balance in cancer cells, generating higher levels of ROS and inducing chronic oxidative stress [21].

While high oxidative stress is acutely cytotoxic, the low and chronic oxidative stress within cancer cells homeostatically enhances antioxidant metabolic pathways and production of antioxidants. Total cellular antioxidants are qualitatively referred to as the total antioxidant capacity of the cell, the ability of the cell to cope with oxidative stress. There is substantial evidence of the protumorigenic role for antioxidants, including the master regulator of anti-oxidative responses nuclear factor (erythroid-derived 2)-like 2 (Nrf2), antioxidant enzymes and cellular antioxidants such as nicotinamide adenine dinucleotide phosphate (NADPH), cysteine and glutathione (GSH) [22]. Cancer cells maintaining an elevated antioxidant capacity acquire resistance to future, acute stressors, including that induced by chemotherapeutic agents [19]. Many chemotherapeutics (e.g., vinca alkaloids, taxanes, anthracyclines and platinum-based drugs) and nonchemical therapies (e.g., radiation) directly generate excessive ROS in cancer cells, inducing apoptosis by interfering with processes including cell-cycle progression and DNA stability [23]. In most cases, the antineoplastic drug effects are indirectly mediated by ROS which eventually bring about the apoptotic death of the cancer cell. Furthermore, thiol-containing antioxidants and peptides, GSH and metallothionein,

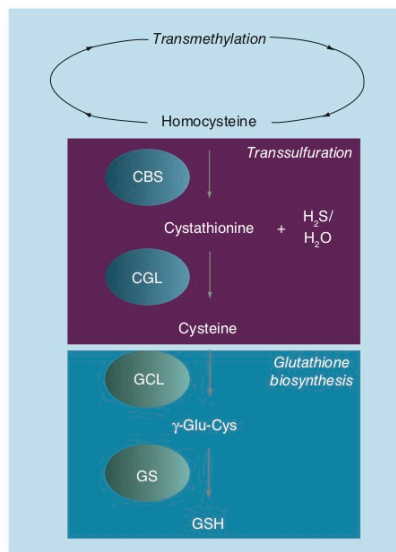


Figure 1. Scheme of transsulfuration and glutathione biosynthesis pathways.
 CBS: Cystathionine β -synthase; CGL: Cystathionine γ -lyase; GCL: Glutamate-cysteine ligase; GS: Glutathione synthase; GSH: Glutathione.

are known to bind and inactivate chemotherapeutics [24]. As a consequence, selective suppression of the antioxidant capacity of cancer cells by inhibiting antioxidant pathways could mitigate the incidence and intensity of therapeutic resistance and associated poor prognosis.

The chemosensitizing effects of CO observed in prostate cancer cells by Otterbein and coworkers, indicate that one mechanism by which CO exerts its salutary effect(s) is through 'metabolic exhaustion' a depletion of intracellular ATP combined with increased mitochondrial oxygen consumption and decreased glycolytic activity [15], which in turn has been recently reported to decrease drug efflux by ATP-binding cassette transporters [25]. Kaczara *et al.* have provided evidence that this occurs via uncoupling of mitochondrial respiration [26], though the nature of mitochondrial uncoupling by CO is unclear and somewhat controversial. Mechanisms involving direct/indirect interactions of CO with ion channels have also been proposed [27], though CO exerting its salutary effect(s) by 'metabolic exhaustion' most possibly occurs by binding to enzymes involved in energy metabolism [28,29]. CO has several demonstrated direct biological targets [3], though consensus over those that are therapeutically relevant is lacking. The elevated levels of ROS in cancer cells strongly suggest that interaction of CO with enzymes involved in maintaining their antioxidant capacity could be another important target of CO leading to drug sensitization. Therefore, we have focused on cystathionine β -synthase (CBS) as a potential target of CO in moderating the overall redox environment in cancer cells and alleviating drug resistance.

CBS

CBS, a heme-containing enzyme, catalyzes the first step of the transsulfuration pathway: the condensation of homocysteine with either serine or cysteine to generate cystathionine (CTH) and water or H_2S , respectively (Figure 1) [30]. CTH is further catabolized into cysteine, catalyzed by CTH γ -lyase, the second enzyme of the transsulfuration pathway. In tissues where demand for GSH is high, including the liver and pancreas, CBS and the transsulfuration pathway provide a significant source of cysteine for GSH biosynthesis [31]. Alternatively, homocysteine can be diverted from the transsulfuration pathway and be recycled into methionine, catalyzed by the enzyme methionine synthase, a cobalamin-containing enzyme. Interestingly, methionine synthase, unlike CBS, is prone to oxidative inactivation, suggesting a prominent role for CBS in regulating methylation and transsulfuration in the cell, especially under oxidative conditions [32].

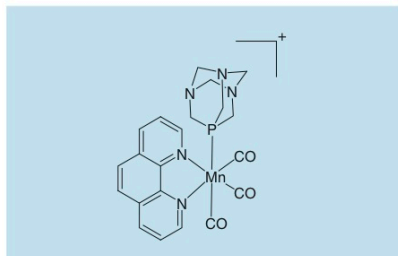


Figure 2. Structure of the cation of the photoCORM used in our study: $[\text{Mn}(\text{CO})_3(\text{phen})(\text{PTA})]\text{CF}_3\text{SO}_3$.

GSH levels have been shown to be elevated in tumor tissues from patients with head and neck, lung, breast and ovarian cancers compared with corresponding nonmalignant tissues [22]. GSH and other antioxidants have been shown to play a key role in protecting cancer cells from a wide range of anticancer therapies, with elevated levels predictive of drug resistance and therapeutic failure. Inhibition of CBS in cancer cells exhibiting overexpression could reduce GSH levels, perturbing the balance between the generation and quenching of ROS, inducing oxidative stress and abating the drug resistant phenotype.

Inhibition of CBS by CO

CBS is unique in that it is the only pyridoxal phosphate-dependent enzyme that also contains a prosthetic heme, which renders CBS sensitive to CO. CO has a high affinity for ferrous heme in CBS [30]. The binding of CO to CBS is kinetically slow, 0.0166 s^{-1} , as CO binds via displacement of Cys52 from the iron center. The displaced thiolate on Cys52 is stabilized by Arg266, the likely mechanism by which CO inactivates CBS. Physiological levels of CO are sufficient to inhibit CBS activity, $K_i = 3 \mu\text{M}$.

Is CBS a therapeutically relevant target of CO in cancer cells?

Substantial evidence supports the therapeutic relevance of CBS as a cancer-specific target. Previous studies have utilized RNA interference and pharmacological inhibitors to reveal the oncogenic and cytoprotective effects of CBS in ovarian, colon and breast cancers [32]. Recently, our group has found that CO, delivered from biologically compatible, photo-activatable CO-releasing molecules (photoCORMs) can induce apoptotic death in human breast and colon cancer cells [9–13]. This finding prompted us to the second phase of the project where we sought to find out the target(s) of CO in cancer cells that leads to apoptosis and whether CO binding to such targets could sensitize them to conventional chemotherapeutics. Because diminution of the antioxidant capacity could lead to drug sensitization, we hypothesized that CBS is one of the main effectors of CO-mediated sensitization of cancer cells to chemotherapeutics. We therefore selected human breast and ovarian cancer cells, two disease models where CBS is overexpressed and correlate with tumor grade, to study the drug sensitizing effects of CO.

Effects of CO in human breast cancer cells

The pathology atlas of human cancer transcriptome [33] revealed that despite absence in normal breast cells, CBS is expressed in transformed breast cancer cells to a moderate extent. This fact allowed us to study the effects of CO on CBS in a cancer cell model. The photoCORM used in our study was $[\text{Mn}(\text{CO})_3(\text{phen})(\text{PTA})]\text{CF}_3\text{SO}_3$, a water-soluble CORM that releases CO upon exposure to visible light (Figure 2) [10]. This CO donor allowed us to deliver CO to biological targets under the control of visible light, when desired.

In previously published work from our group, we employed a set of three human breast cancer cell lines representing both estrogen/progesterone receptor-positive cell line MCF-7 and triple negative breast cancer cell lines MDA-MB-468 and Hs 578T to demonstrate the general applicability of our observations [34]. Quite in agreement with our hypothesis light-triggered CO delivery from $120 \mu\text{M}$ photoCORM to these cancer cells inhibited CBS enzyme activity, as measured by decreases in steady state levels of CTH (Figure 3) [34]. Incidentally, CTH and H_2S , enzymatic products of CBS, themselves promote endoplasmic reticulum homeostasis and positively regulate Nrf2 [35–37]. Through this H_2S -Nrf2 axis, CBS promotes expression of GSH biosynthesis enzymes, as well as glucose-6-phosphate dehydrogenase, the rate-limiting enzyme in the pentose phosphate pathway,

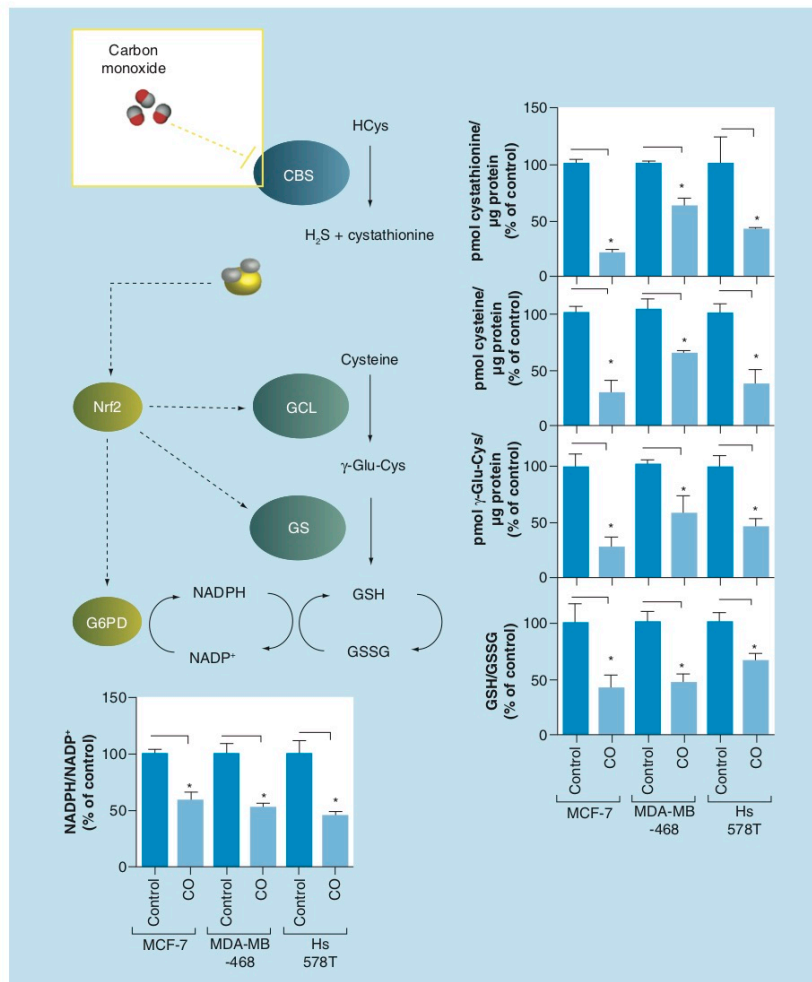


Figure 3. Effect of carbon monoxide on steady state levels of transsulfuration/glutathione biosynthesis metabolites, as measured by liquid chromatography-mass spectrometry, and NADPH/NADP⁺ in human breast cancer cells. CO inhibits CBS mediated production of cystathionine and H₂S, downregulating Nrf2. Downregulation of Nrf2, in turn, attenuates expression of GCL, GS and G6PD, antioxidant genes downstream involved in GSH biosynthesis/regeneration of GSH from GSSG. Data representative of at least n = 3 individual experiments; *p < 0.05. CBS: Cystathionine β -synthase; CO: Carbon monoxide; GS: Glutathione synthase; GSH: Glutathione; GSSG: Glutathione disulfide; H₂S: Hydrogen sulfide; Nrf2: Nuclear factor (erythroid-derived 2)-like 2; GCL: Glutamate-cysteine ligase; G6PD: Glucose 6-phosphate dehydrogenase.

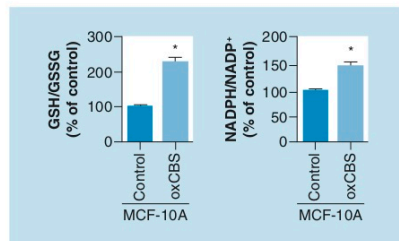


Figure 4. Overexpression of cystathionine β -synthase in normal human breast cell line MCF-10A enhances the antioxidant capacity, as measured by the increase in ratios of NADPH/NADP⁺ and GSH/GSSG.

Data representative of at least $n = 3$ individual experiments; * $p < 0.05$. CBS: Cystathionine β -synthase; GSH: Glutathione; GSSG: Glutathione disulfide.

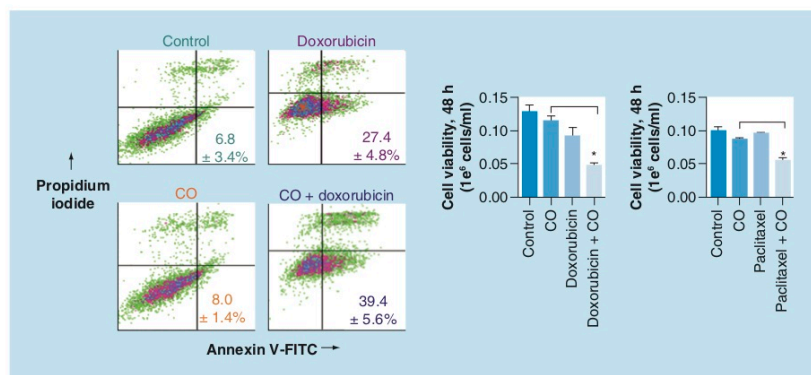


Figure 5. Annexin V-FITC/propidium iodide staining and cell viability by trypan blue exclusion, demonstrating cotreatment with exogenous carbon monoxide sensitizes human breast cancer cell line MCF-7 to conventional chemotherapeutics, doxorubicin and paclitaxel.

Data representative of at least $n = 3$ individual experiments; * $p < 0.05$. CO: Carbon monoxide.

whose activity promotes production of NADPH (Figure 3), the reducing equivalent required for regeneration of GSH from glutathione disulfide (GSSG). In our previously published experiments [34], inhibition of CBS by CO led to a decreased NADPH/NADP⁺ and GSH/GSSG ratios indicating a reduction in the antioxidant capacity in all three breast cancer cells (Figure 3).

Also, treatments with the slow H₂S-releasing drug (p-methoxyphenyl)morpholino-phosphinodithioic acid (GY 4137) and CTH were able to restore the elevated antioxidant capacity of cancer cell line MCF-7, showing that inhibition of CBS by CO was indeed responsible for the observed lowering of NADPH/NADP⁺ and GSH/GSSG ratios [34]. To further confirm the role of CBS in these measurements, we checked whether expression of CBS activity in a CBS-free cell model could increase the NADPH/NADP⁺ and GSH/GSSG ratios through H₂S-mediated stabilization of Nrf2. In this attempt, we overexpressed CBS in the normal human breast cell line MCF-10A (normally lacking CBS expression/activity) and observed increased ratios of these redox pairs (Figure 4) [34]. Together these findings published from our group confirm that CBS is an important player in maintaining an elevated antioxidant capacity in human breast cancer cells [34].

Finally, we wanted to check whether CBS inhibition by CO, and the subsequent lowering of the antioxidant capacity of the cancer cells, sensitizes them toward chemotherapeutics. In such attempt, we pretreated MCF-7 cells with CO (delivered from the photoCORM) for 30 min followed by addition of doxorubicin. The results from cell viability assays 48 h post-treatment clearly showed that pretreatment of the cells with CO significantly enhanced the cytotoxic effects of doxorubicin compared with doxorubicin treatment alone (Figure 5) [34]. Similar results were obtained with paclitaxel as the chemotherapeutic (Figure 5) [34]. In conclusion, our results from this previous study

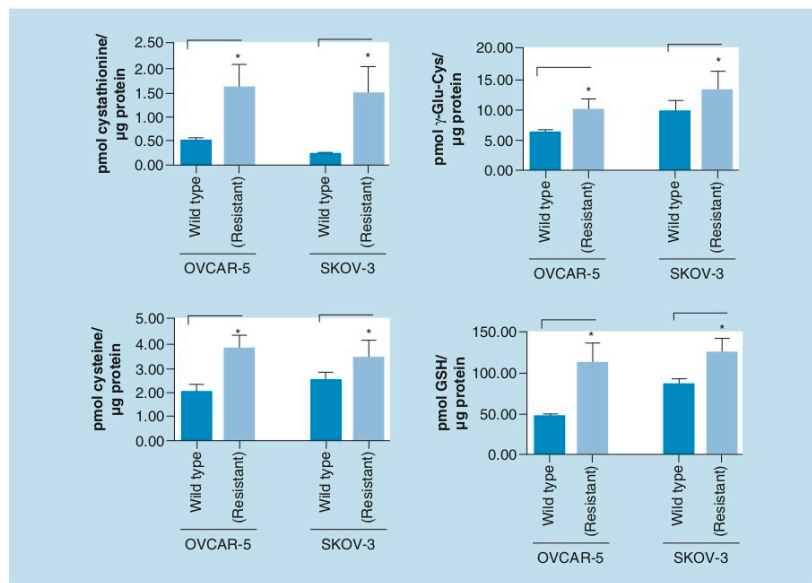


Figure 6. Steady state levels of transsulfuration/glutathione biosynthesis metabolites in cisplatin-resistant ovarian cancer cell lines compared with respective parent cell lines OVCAR-5 and SKOV-3. Cisplatin-resistant ovarian cancer cells exhibit elevated levels of transsulfuration pathway metabolites (cystathionine and cysteine) and glutathione biosynthesis pathway metabolites (γ -Glu-Cys and glutathione). Data representative of at least $n = 3$ individual experiments; * $p < 0.05$.

strongly suggest that CO has the ability to lower the antioxidant capacity of breast cancer cells by inhibition of CBS, and consequently sensitize the cells to chemotherapeutics such as doxorubicin and paclitaxel [34].

Effects of CO in human ovarian cancer cells

In neoplasms of the ovaries, CBS expression correlates with carcinogenesis and tumor grade; we therefore hypothesized that CO could inhibit CBS in an ovarian cancer model. Recent work published by our group, involving careful screening of the human ovarian cancer cells OVCAR-5 and SKOV-3 and their cisplatin-resistant variants, revealed that the expression of the transsulfuration pathway enzymes CBS and cystathionine γ -lyase in the cisplatin-resistant cell lines are both profoundly higher compared with the parent cell lines [38]. This important finding suggested a direct role for CBS and the transsulfuration pathway in imparting cisplatin-resistance. One largely elucidated mechanism of cisplatin resistance is the binding and inactivation of cisplatin by cellular thiols GSH and metallothionein, both of which are highly dependent on the bioavailability of cysteine (a product of CBS activity) [39]. In initial measurements the cisplatin-resistant ovarian cancer cells, as expected, exhibited nearly twofold higher steady state levels of the transsulfuration metabolites (CTH and cysteine), GSH and its biosynthesis metabolite γ -Glu-Cys (Figure 6), and the expression of metallothionein compared with the cisplatin-sensitive variants [38].

Furthermore, N-acetyl-cysteine, a bioavailable cysteine donor, further increased the levels of both GSH and metallothionein in these cells [38]. It is important to note that GSH and metallothionein are the two clinically relevant markers and predictors of cisplatin resistance in ovarian cancer patients [39]. Treatment of the cisplatin-resistant ovarian cancer cells with CO attenuated all the steady state levels of these CBS-derived products (Figure 7). Also, the effect of CO was mimicked by lentiviral-mediated silencing of CBS in these cisplatin-resistant cells, supporting the hypothesis that CO-derived attenuation of the metabolite levels was mediated by CBS [38].

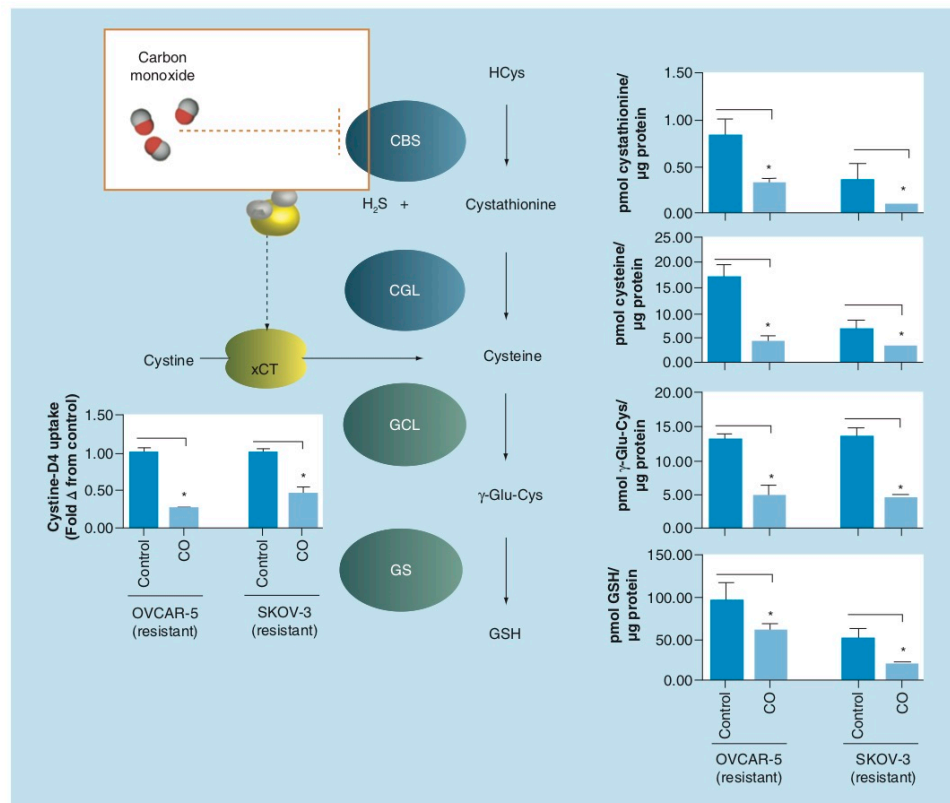


Figure 7. Effect of carbon monoxide on transsulfuration/glutathione biosynthesis pathway metabolites, assayed by liquid chromatography-mass spectrometry, in cisplatin-resistant ovarian cancer cell lines, 24 h post-treatment. CO inhibits cystathionine β -synthase, decreasing cystine uptake via the xCT and lowering steady state levels of cystathionine, the substrate for cystathionine γ -lyase. Consequently, CO decreases intracellular cysteine levels to inhibit glutathione biosynthesis as measured by steady state levels of γ -Glu-Cys and GSH, products of GCL and GS, respectively. Data representative of at least $n = 3$ individual experiments; * $p < 0.05$. CBS: Cystathionine β -synthase; CO: Carbon monoxide; GCL: Glutamate-cysteine ligase; GS: Glutathione synthase; GSH: Glutathione; H₂S: Hydrogen sulfide; xCT: Glutamate-cystine antiporter.

In addition to the transsulfuration pathway, H₂S generated by CBS has been shown to increase the activity of the cystine-glutamate antiporter xCT which imports, from the extracellular milieu, a significant portion of cystine into cancer cells that is converted into cysteine. This cysteine is also utilized in the synthesis of GSH and metallothionein [40]. In our experiment, the cisplatin-resistant ovarian cancer cells exhibited nearly twofold increase in the uptake of cystine-D₄ (compared with the cisplatin-sensitive cells) in cell culture conditions, as indicated by the intracellular cysteine-D₂ concentrations within the cancer cells (Figure 8) [38]. CO treatment of the same cells led to a significant drop in the concentration of cysteine-D₂ showing that inhibition of CBS by CO (with concomitant decrease in H₂S) downregulates the activity of the xCT antiporter (Figure 3).

Figure 8. Glutamate–cystine antiporter activity assayed by extracellular D4-cystine uptake and determined by relative steady state levels of intracellular D2-cysteine in cisplatin-resistant and wild-type ovarian cancer cell lines OVCAR-5 and SKOV-3. Cisplatin-resistant ovarian cancer cells exhibit significantly greater uptake of extracellular D4-cystine compared with their wild-type counterparts. Data representative of at least $n = 3$ individual experiments; * $p < 0.05$. xCT: Glutamate–cystine antiporter.

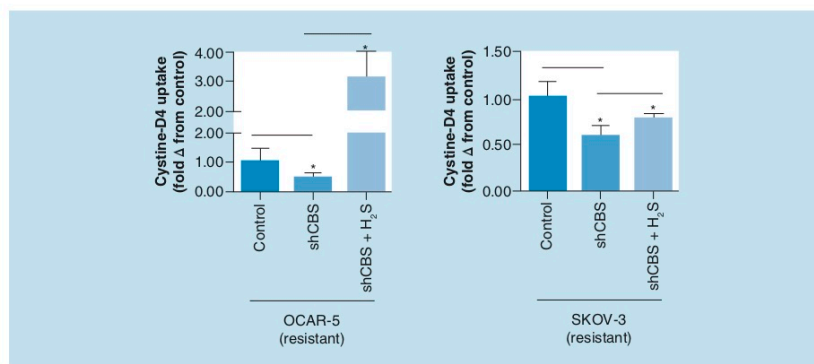
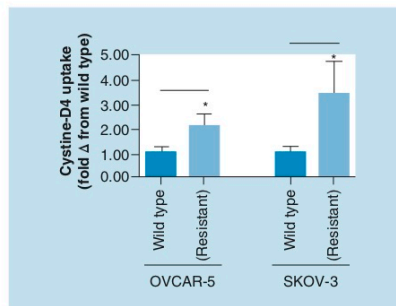


Figure 9. Relative glutamate–cystine antiporter activity assayed by extracellular D4-cystine uptake, determined by steady state levels of intracellular D2-cysteine in cisplatin-resistant ovarian cancer cell lines silenced for cystathionine β -synthase and treated with H₂S for 24 h. Silencing CBS expression decreases D4-cystine uptake, which is mitigated by the donation of extracellular H₂S. Data representative of at least $n = 3$ individual experiments; * $p < 0.05$. CBS: Cystathionine β -synthase, xCT: Glutamate–cystine antiporter, H₂S: Hydrogen sulfide.

Addition of H₂S by the use of the slow H₂S-releasing drug GYY 4137 enhanced the cystine-D4 uptake, an observation that further confirms the role of CBS in positively regulating the activity of the xCT antiporter (Figure 9) [38].

Finally, we tested the hypothesis that CO does sensitize the cisplatin-resistant ovarian cancer cells and makes them susceptible to cisplatin. Indeed, when the cisplatin-resistant ovarian cancer cells were cotreated with cisplatin and CO, we observed a much higher extent of apoptotic cell death of cells compared with cells that were treated only with cisplatin (Figure 10) [38]. Together, these results published by our group elucidate a distinct role for CBS in imparting cisplatin resistance and provide preliminary evidence for CO as a novel adjuvant therapeutic for ovarian cancer [38].

Future perspective

Breast cancer is the leading cancer diagnosed in women and the second leading cause of cancer-related death in women. It is estimated that one in eight women will be diagnosed with breast cancer in their lifetime and over 40,000 women deaths will occur each year due to lack of or poor response to treatment [41]. Incidentally, chemotherapeutic drug resistance is a major impediment to effective treatment of breast cancer. The cancer cells often acquire resistance to cisplatin, paclitaxel and doxorubicin, and leads to poor clinical outcomes. Because

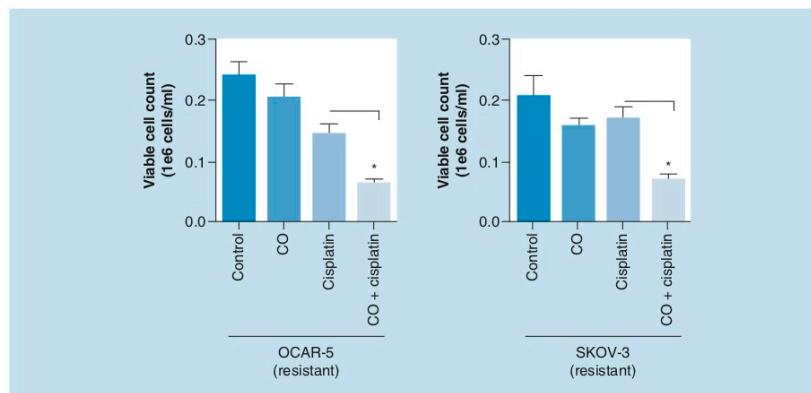


Figure 10. Trypan blue exclusion cell viability assay of cisplatin-resistant ovarian cancer cells 24 h post-treatment with carbon monoxide, cisplatin or coadministration of carbon monoxide and cisplatin. Cells cotreated with CO and cisplatin exhibit greater cell death compared with cells treated with cisplatin alone. Data representative of at least n = 3 individual experiments; *p < 0.05. CO: Carbon monoxide.

elevated levels of ROS and alteration of redox balance are common hallmarks of cancer progression and drug resistance [42], we focused on CBS, an enzyme intimately involved with redox homeostasis [35]. Although role of CBS in cancer has been examined to find out the role of H₂S in the pathophysiology of cancer [43], we focused on the interactions of CO with CBS and the utility of this gasotransmitter in cancer therapy. In particular, we are interested in the role of CBS in promoting an elevated antioxidant capacity and drug resistance. Our results, described above, strongly suggest that CBS inhibition by CO could be one effective strategy for enhancing the efficacy of drugs such as doxorubicin and paclitaxel which exert their tumoricidal effect(s) via induction of ROS [44,45].

Clinically cisplatin is the standard of care for the management of human ovarian cancer [46]. Unfortunately, the majority of patients develop resistance to cisplatin and succumb to the disease. Our results indicate that modulation of CBS activity in ovarian cancer cells might provide a strategy for mitigating drug-resistance observed frequently with ovarian cancer patients. While our work focused on the effects of CO-mediated inhibition of CBS on the transsulfuration pathway, notable work by Suematsu and coworkers has focused on the transmethylation pathway [47]. In this work, stress-induced CO production in human leukemia cell line U937 suppressed CBS activity, in contrast to our studies in breast and ovarian cancer models, to promote generation of cellular antioxidants via decreased phosphofructokinase/fructose bisphosphatase type-3 methylation. This resulted in a shift in glucose biotransformation toward the pentose phosphate pathway, promoting generation of cellular reductants to impart resistance to chemotherapeutics [47]. The paradoxical effect(s) of CO-mediated inhibition of CBS in leukemia [47] versus breast/ovarian cancer tissues [34,38] highlight the context-dependent role of CBS in tumor growth and progression, a concept strongly emphasized in a recent review on the role of CBS in different human cancers [48]. It is very apparent that CBS has a functional role in chemotherapeutic resistance and together, these findings suggest that CO, a relatively unreactive gaseous molecule once thought of as a toxic byproduct of heme catabolism, exerts profound biological effects in cancer cells. It is quite possible that smart CO delivery to cancer cells could sensitize them to conventional chemotherapeutics and mitigate the grim statistics of cancer-related death arising from drug resistance.

A close scrutiny of the literature reveals that most antitumor therapeutics are aimed at proteins that drive cancer proliferation. Blocking of such pathways almost always triggers the evolution of escape routes or alternative pathways to meet the continuous demand for proliferation in cancer cells [49]. However little is known about whether cancer cells are equally efficient in adapting alternative routes when it comes to the inhibition of 'cancer maintenance/homeostatic' functionalities. Redox homeostasis is one such function and the CBS-CO inhibitory

axis essentially perturbs this crucial pathway. Because upregulation of antioxidant capacity in adaptation of intrinsic oxidative stress in cancer cells often leads to drug resistance, disruption of the homeostatic rather than proliferative potential of the cancer cells through inhibition of the redox regulatory effects of CBS by CO might be an effective strategy to eliminate these cells [50]. The results of our studies on CBS inhibition by CO in relation to cancer pathogenesis and therapeutic resistance, presented here, support another perspective to the therapeutic potential of CO.

Executive summary

- Carbon monoxide (CO) has recently been identified as a gasotransmitter, a diffusible molecule that plays many roles in physiological processes.
- Concomitant development of improved CO donor molecules, including photo-activatable CO-releasing molecules (photoCORMs), has been helpful in identifying the beneficial effects of CO in human pathophysiology.
- Elucidation of these effects has strengthened the potential for CO-based therapeutics. Detailed studies in cell culture and animal models have also demonstrated promise for the development of CO-based cancer therapies, notably the ability of CO to sensitize chemotherapeutic-resistant cancer cells.
- Chemoresistance is one of the leading causes of therapeutic failure and poor clinical outcomes in cancer. This perspective summarizes the findings on the ability of CO to mitigate drug resistance in certain cancer cells through inhibition of cystathionine β -synthase (CBS), a key regulator of redox homeostasis in the cell.
- In human breast cancer cells, the heme-containing enzyme CBS maintains the antioxidant capacity by maintaining increased ratios of reduced/oxidized glutathione (GSH/GSSG), reduced/oxidized NADPH (NADPH/NADP⁺) compared with normal breast cells lacking CBS. Inhibition of CBS by CO (delivered from a photoCORM) lowers these antioxidant ratios considerably. Because H₂S, a product of CBS activity, positively regulates Nrf2, inhibition of CBS by CO downregulates enzymes regulated by Nrf2, including those involved in GSH biosynthesis and the pentose phosphate pathway. Genetic silencing of CBS mimics the effect of CO treatment in these same cells. Overexpression of CBS and addition of H₂S reverse such diminution of the levels of the antioxidants. Collectively, diminution of the antioxidant capacity of human breast cancers leads to sensitization to reactive oxygen species producing drugs like doxorubicin and paclitaxel upon cotreatment with CO.
- In human ovarian malignancy, CBS is overexpressed only in those ovarian cancer cells resistant to cisplatin. CO treatment of these cells results in reduction of intracellular cysteine, GSH and nuclear metallothionein expression; features implicated in mitigating the drug effects of cisplatin. Cell viability studies clearly demonstrate sensitization of human ovarian cancer cells to cisplatin upon cotreatment with CO, indicating the role of CBS in the emergence of drug resistance in ovarian cancer cells.
- Collectively the results suggest that improved delivery techniques for coadministration of CO with existing cancer chemotherapeutics could improve clinical outcomes in cancer therapy.

Financial & competing interests disclosure

Financial support from the NSF grant DMR-1409335 and the Cancer Research Coordinating Committee (UC) grant CTR-19-580346 is gratefully acknowledged. Research in UCLA was supported by the NIH U01 grant HD087221. The authors have no other relevant affiliations or financial involvement with any organization or entity with a financial interest in or financial conflict with the subject matter or materials discussed in the manuscript apart from those disclosed.

No writing assistance was utilized in the production of this manuscript.

References

Papers of special note have been highlighted as: • of interest; •• of considerable interest

1. Wang R (Ed.). Evolution of gasotransmitter biology and medicine. In: *Signal transduction and the gasotransmitters. NO, CO and H₂S in biology and medicine*. Humana Press, NJ, USA, 3–32 (2004).
2. Kim HP, Ryter SW, Choi AMK. CO as a cellular signaling molecule. *Ann. Rev. Pharmacol. Toxicol.* 46, 411–449 (2006).
3. Motterlini R, Foresti R. Biological signaling by carbon monoxide and carbon monoxide-releasing molecules. *Am. J. Physiol.-Cell Physiol.* 312(3), C302–C313 (2017).
4. Kikuchi G, Yoshida T, Noguchi M. Heme oxygenase and heme degradation. *Biochem. Biophys. Res. Commun.* 338(1), 558–567 (2005).
5. Motterlini R, Otterbein LE. The therapeutic potential of carbon monoxide. *Nat. Rev. Drug Discov.* 9(9), 728–743 (2010).
6. Motterlini R, Haas B, Foresti R. Emerging concepts on the anti-inflammatory actions of carbon monoxide-releasing molecules (CO-RMs). *Med. Gas Res.* 2(1), 28 (2012).
7. Coussens LM, Werb Z. Inflammation and cancer. *Nature* 420(6917), 860–867 (2002).

8. Raposo TP, Beirao BCB, Pang LY, Queiroga FL, Argyle DJ. Inflammation and cancer: till death tears them apart. *Vet. J.* 205(2), 161–174 (2015).
9. Chakraborty I, Jimenez J, Mascharak PK. CO-induced apoptotic death of colorectal cancer cells by a luminescent photoCORM grafted on biocompatible carboxymethyl chitosan. *Chem. Commun.* 53(40), 5519–5522 (2017).
10. Chakraborty I, Carrington SJ, Roseman G, Mascharak PK. Synthesis, structures, and CO release capacity of a family of water-soluble photoCORMs: assessment of the biocompatibility and their phototoxicity toward human breast cancer cells. *Inorg. Chem.* 56(3), 1534–1545 (2017).
11. Chakraborty I, Carrington SJ, Hauser J, Oliver SRJ, Mascharak PK. Rapid eradication of human breast cancer cells through trackable light-triggered CO delivery by mesoporous silica nanoparticles packed with a designed photoCORM. *ACS Chem. Mater.* 27(24), 8387–8397 (2015).
12. Chakraborty I, Carrington SJ, Mascharak PK. Design strategies to improve the sensitivity of photoactive metal carbonyl complexes (photoCORMs) to visible light and their potential as CO-donors to biological targets. *Acc. Chem. Res.* 47(8), 2603–2611 (2014).
13. Carrington SJ, Chakraborty I, Mascharak PK. Rapid CO release from a Mn(I) carbonyl complex derived from azopyridine upon exposure to visible light and its phototoxicity toward malignant cells. *Chem. Commun.* 49(96), 11254–11256 (2013).
14. Kourti M, Jiang WG, Cai J. Aspects of carbon monoxide in form of CO-releasing molecules used in cancer treatment: more light on the way. *Oxid. Med. Cell. Longev.* 2017, 9326454 (2017).
15. Wegiel B, Gallo D, Cszimadia E *et al.* Carbon monoxide expedites metabolic exhaustion to inhibit tumor growth. *Cancer Res.* 73(23), 7009–7021 (2013).
16. Zobi F. CO and CO-releasing molecules in medicinal chemistry. *Future Med. Chem.* 5(2), 175–188 (2013).
17. Schatzschneider U. Novel lead structures and activation mechanisms for CO-releasing molecules (CORMs). *Br. J. Pharmacol.* 172(6), 1638–1650 (2015).
18. Pinto MN, Chakraborty I, Sandoval C, Mascharak PK. Eradication of HT-29 colorectal adenocarcinoma cells by controlled photorelease of CO from a CO-releasing polymer (photoCORP-1) triggered by visible light through an optical fiber-based device. *J. Control. Rel.* 264, 192–202 (2017).
19. Housman G, Byler S, Heerboth S *et al.* Drug resistance in cancer: an overview. *Cancers* 6(3), 1769–1792 (2014).
20. Lippert TH, Ruoff H-J, Volm M. Intrinsic and acquired drug resistance in malignant tumors. *Arzneimittelforschung* 58(6), 261–264 (2008).
21. Grek CL, Tew KD. Redox metabolism and malignancy. *Curr. Opin. Pharmacol.* 10(4), 362–368 (2010).
22. Hawk MA, McCallister C, Schafer ZT. Antioxidant activity during tumor progression: a necessity for the survival of cancer cells? *Cancers* 8(10), 92 (2016).
- **Discusses the protumorigenic role of antioxidant activity in facilitating tumor progression.**
23. Yokoyama C, Sueyoshi Y, Ema M, Mori Y, Takaishi K, Hisatomi H. Induction of oxidative stress by anticancer drugs in the presence and absence of cells. *Oncol. Lett.* 14(5), 6066–6070 (2017).
24. Galluzzi L, Senovilla L, Vitale I *et al.* Molecular mechanisms of cisplatin resistance. *Oncogene* 31(15), 1869–1883 (2012).
25. Li YJ, Dang JJ, Liang QJ, Yin LC. Thermal-responsive carbon monoxide (CO) delivery expedites metabolic exhaustion of cancer cells toward reversal of chemotherapy resistance. *ACS Cent. Sci.* 5(6), 1044–1058 (2019).
26. Kaczara P, Motterlini R, Rosen GM *et al.* Carbon monoxide released by CORM-401 uncouples mitochondrial respiration and inhibits glycolysis in endothelial cells: a role for mitoBK(Ca) channels. *Biochim. Biophys. Acta* 1847(10), 1297–1309 (2015).
27. Wilkinson WJ, Kemp PJ. Carbon monoxide: an emerging regulator of ion channels. *J. Physiol.* 589(13), 3055–3062 (2011).
28. Lo Iacono L, Boczkowski J, Zini R *et al.* A carbon monoxide-releasing molecule (CORM-3) uncouples mitochondrial respiration and modulates the production of reactive oxygen species. *Free Radic. Biol. Med.* 50(11), 1556–1564 (2011).
29. Long R, Salouage I, Berdeux A, Motterlini R, Morin D. CORM-3, a water soluble CO-releasing molecule, uncouples mitochondrial respiration via interaction with the phosphate carrier. *BBA-Bioenergetics* 1837(1), 201–209 (2014).
30. Banerjee R, Zou CG. Redox regulation and reaction mechanism of human cystathionine-beta-synthase: a PLP-dependent hemesensor protein. *Arch. Biochem. Biophys.* 433(1), 144–156 (2005).
- **Summarizes the work of Banerjee and coworkers identifying cystathionine β-synthase (CBS) as a direct binding partner of carbon monoxide (CO) and subsequent inhibition of the enzyme activity.**
31. Belalcázar AD, Ball JG, Frost LM, Valentovic MA, Wilkinson J. Transsulfuration Is a significant source of sulfur for glutathione production in human mammary epithelial cells. *ISRN Biochem.* 2013, 637897 (2014).
32. Zhu HR, Blake S, Chan KT, Pearson RB, Kang J. Cystathionine beta-synthase in physiology and cancer. *Biomed. Res. Int.* doi:10.1155/2018/3205125 (2018).
33. Uhlen M, Zhang C, Lee S *et al.* A pathology atlas of the human cancer transcriptome. *Science* 357(6352), pii: ean2507 (2017).

34. Kawahara B, Moller T, Hu-Moore K *et al.* Attenuation of antioxidant capacity in human breast cancer cells by carbon monoxide through inhibition of cystathionine β -synthase activity: implications in chemotherapeutic drug sensitivity. *J. Med. Chem.* 60(19), 8000–8010 (2017).
- **Findings from this study connected the chemosensitizing effects of CO with modulation of cancer cellular antioxidants via modulation of CBS activity in three breast cancer cell lines.**
35. Sen S, Kawahara B, Gupta D *et al.* Role of cystathionine beta-synthase in human breast cancer. *Free Radic. Biol. Med.* 86, 228–238 (2015).
36. Sen S, Kawahara B, Mahata SK *et al.* Cystathionine: a novel oncometabolite in human breast cancer. *Arch. Biochem. Biophys.* 604, 95–102 (2016).
37. Hourihan JM, Kenna JG, Hayes JD. The gasotransmitter hydrogen sulfide induces Nrf2-target genes by inactivating the keep1 ubiquitin ligase substrate adaptor through formation of a disulfide bond between cys-226 and cys-613. *Antioxid. Redox Signal.* 19(5), 465–481 (2013).
38. Kawahara B, Ramadoss S, Chaudhuri G, Janzen C, Sen S, Mascharak PK. Carbon monoxide sensitizes cisplatin-resistant ovarian cancer cell lines toward cisplatin via attenuation of levels of glutathione and nuclear metallothionein. *J. Inorg. Biochem.* 191, 29–39 (2019).
- **Establishes that CO sensitizes cisplatin-resistant ovarian cancer cells through attenuation of biomarkers of cisplatin-resistance (glutathione, metallothionein) via inhibition of CBS.**
39. Galluzzi L, Senovilla L, Vitale I *et al.* Molecular mechanisms of cisplatin resistance. *Oncogene* 31(15), 1869–1883 (2012).
40. Verschoor ML, Singh G. Ets-1 regulates intracellular glutathione levels: key target for resistant ovarian cancer. *Mol. Cancer* 12(1), 138 (2013).
41. National Breast Cancer Foundation I. Breast cancer facts 2015 (2016) www.nationalbreastcancer.org/breast-cancer-facts
42. Kumari S, Badana AK, Mohan GM, Shailender G, Malla R. Reactive oxygen species: a key constituent in cancer survival. *Biomark. Insights* 13, DOI: 10.1177/1177271918755391 (2018).
43. Hellmich MR, Szabo C. Hydrogen sulfide and cancer. *Handb. Exp. Pharmacol.* 230, 233–241 (2015).
44. Ramanathan B, Jan KY, Chen CH, Hour TC, Yu HJ, Pu YS. Resistance to paclitaxel is proportional to cellular total antioxidant capacity. *Cancer Res.* 65(18), 8455–8460 (2005).
45. Yokoyama C, Sueyoshi Y, Ema M, Mori Y, Takaishi K, Hisatomi H. Induction of oxidative stress by anticancer drugs in the presence and absence of cells. *Oncol. Lett.* 14(5), 6066–6070 (2017).
46. Matsuo K, Lin YG, Roman LD, Sood AK. Overcoming platinum resistance in ovarian carcinoma. *Expert Opin. Investig. Drugs* 19(11), 1339–1354 (2010).
47. Yamamoto T, Takano N, Ishiwata K *et al.* Reduced methylation of PFKFB3 in cancer cells shunts glucose towards the pentose phosphate pathway. *Nat. Commun.* 5, doi:10.1038/ncomms4480 (2014).
48. Zhu HR, Blake S, Chan KT, Pearson RB, Kang J. Cystathionine beta-synthase in physiology and cancer. *Biomed. Res. Int.* 2018, 3205125 (2018).
49. Frantz S. Drug approval triggers debate on future direction for cancer treatments. *Nat. Rev. Drug Discov.* 5(2), 91–91 (2006).
- **Highlights the unmet need to specifically identify and understand which cellular processes impart chemotherapeutic resistance; therapeutic CO may fill this unmet need.**
50. Trachootham D, Alexandre J, Huang P. Targeting cancer cells by ROS-mediated mechanisms: a radical therapeutic approach? *Nat. Rev. Drug Discov.* 8(7), 579–591 (2009).
- **Proposes pharmacological oxidative insult could selectively kill cancer cells; CO may be an ideal candidate to treat cancer by this approach.**

Chapter 2

Carbon monoxide attenuates the antioxidant capacity of human breast cancer cells through inhibition of cystathionine β -synthase

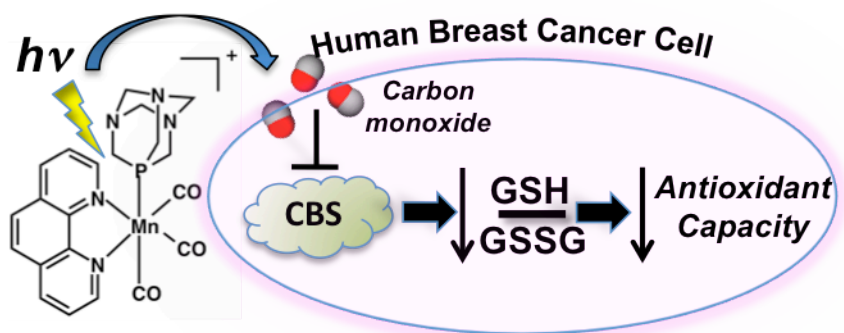


Table 2.1 Table of Content

2.1 Background

Drug resistance remains as the main impediment to the management of cancer.^{1,2} Accumulating evidence suggests that the unique metabolic profile found in cancer cells is integral for imparting a drug resistant phenotype. Hallmarks of cancer cellular biology such as altered glucose metabolism, peroxisome activity, mitochondrial dysfunction and enhanced growth/signaling pathway activity alter the redox balance in cancer cells, generating higher levels of ROS and inducing chronic oxidative stress.³ While high oxidative stress is acutely cytotoxic, the low and chronic oxidative stress within cancer cells hormetically enhances antioxidant metabolic pathways and production of antioxidants. Total cellular antioxidants are qualitatively referred to as the total antioxidant capacity of the cell, the ability of the cell to cope with acute

oxidative stress. There is substantial evidence of the pro-tumorigenic role for antioxidants, including the master regulator of anti-oxidative responses nuclear factor (erythroid-derived 2)-like 2 (Nrf2), antioxidant enzymes and cellular antioxidants such as NADPH, cysteine and glutathione (GSH).⁴ Cancer cells maintaining an elevated antioxidant capacity acquire resistance to future, acute stressors, including that induced by chemotherapeutic agents.⁵ Many chemotherapeutics (e.g. vinca alkaloids, taxanes, anthracyclines and platinum-based drugs) and non-chemical therapies (e.g. radiation) directly generate excessive ROS in cancer cells, inducing apoptosis by interfering with processes including cell cycle progression and DNA stability.⁶ In fact, all anti-neoplastic drug effects are mediated by ROS as apoptosis is mediated by ROS induction.^{4,7,8} As a consequence, selective suppression of the antioxidant capacity of cancer cells by inhibiting antioxidant pathways could mitigate the incidence and intensity of therapeutic resistance and poor prognosis.

In tissues where demand for GSH and antioxidants is high, including the liver and pancreas, the enzymatic action of cystathionine β -synthase (CBS) and the transsulfuration pathway provide a significant source of cysteine for GSH biosynthesis.⁹ The transsulfuration pathway serves a major source of intracellular cysteine for GSH biosynthesis, a conduit for cysteine salvaged from homocysteine/methionine and the transmethylation pathway (Figure 2.1). The first and rate-limiting step in the pathway is catalyzed by CBS, a heme-containing enzyme. CBS catalyzes the condensation of homocysteine and either serine or cysteine to produce cystathionine (CTH) and H₂O or H₂S respectively. The second step in the

pathway is catalyzed by cystathionine γ -lyase (CGL), in which a second condensation reaction between CTH and H_2O occurs, producing cysteine, α -keto butyrate, and NH_3 . Cysteine can be utilized by γ -glutamyl-cysteine synthetase (GCS) to produce γ -glutamylcysteine (γ -Glu-Cys), which is subsequently combined with glycine by glutathione synthase (GS) to form GSH.^{10,11} Alternatively, homocysteine can be diverted from the transsulfuration pathway and be recycled into methionine, catalyzed by the enzyme methionine synthase, a cobalamin-containing enzyme. Interestingly, methionine synthase, unlike CBS, is prone to oxidative inactivation, suggesting a prominent role for CBS in regulating methylation and transsulfuration in the cell, especially under oxidative conditions.¹²

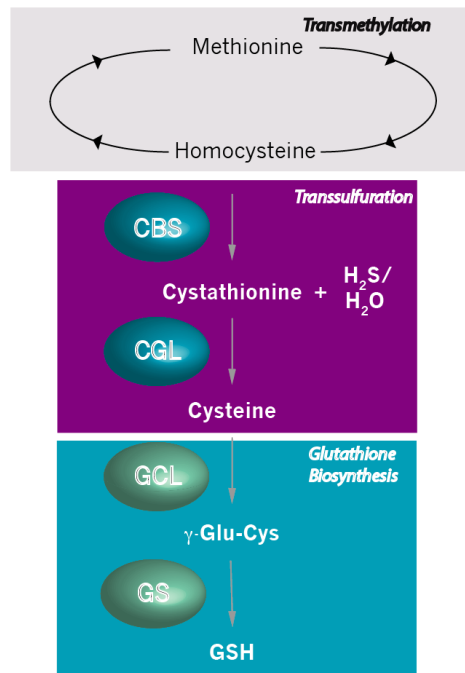


Figure 2.1. Transmethylation, transsulfuration and glutathione biosynthesis pathways.

GSH levels have been shown to be elevated in malignant tissues from patients with head and neck, lung, breast and ovarian cancers compared to corresponding non-malignant tissues.⁴ GSH and other antioxidants have been shown to play a key role in protecting cancer cells from a wide range of anti-cancer therapies, with elevated levels predictive of drug resistance and therapeutic failure. Inhibition of CBS in cancer cells exhibiting overexpression could reduce GSH levels, perturbing the balance between the generation and quenching of ROS, inducing oxidative stress and abating the drug resistant phenotype.

CBS is the only pyridoxal phosphate-dependent enzyme that also contains a prosthetic heme, which renders the enzyme redox sensitive. This prosthetic heme group also renders CBS sensitive to CO. CO has a high affinity for ferrous heme in CBS, though the binding of CO to CBS is kinetically slow, 0.0166 s^{-1} , as CO binds via displacement of Cys52 from the iron center.¹³ The displaced thiolate on Cys52 is stabilized by Arg266, the likely mechanism by which CO inactivates CBS. Physiological levels of CO are sufficient to inhibit CBS activity, $K_i = 3 \text{ }\mu\text{M}$.

Substantial evidence supports the therapeutic relevance of CBS as a cancer-specific target. Previous studies have utilized RNA interference (RNAi) and pharmacological inhibitors to reveal the oncogenic and cytoprotective effects of CBS in ovarian, colon and breast cancers.¹⁴ Malignant breast tissues overexpress CBS, but lack the expression of CGL, though CBS nevertheless plays a key role in breast cancer health and proliferation.^{15,16}

The Mascharak group, and others, has found CO, delivered from biologically compatible, photo-activated CO-releasing molecules (photoCORMs) to induce apoptotic cell death in human cancer cell models,^{17,18} though mechanistic studies have not been performed. CO is known to elevate ROS levels within the cancer cell,¹⁹ but the mediating target(s) of CO have not been convincingly studied. This knowledge gap prompted this chapter's work, where we sought to find out if CBS was a target CO in breast cancer cells and whether CO-mediated inhibition CBS could sensitize those cells to conventional chemotherapeutics. Because diminution of the antioxidant capacity likely leads to drug sensitization,²⁰ we hypothesized that CBS was one main effectors of CO-mediated sensitization of cancer cells to chemotherapeutics. We selected human breast cancer as the model to study the drug sensitizing effects of CO, delivered by photoCORM (Figure 2.2), as CBS is overexpressed in and correlates with breast tumor grade.¹⁵

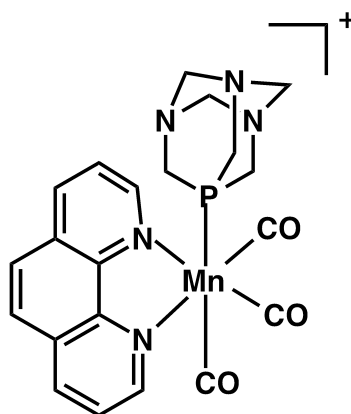


Figure 2.2. photoactivatable CO-releasing molecule (photoCORM) used in this study. $[\text{Mn}(\text{CO})_3(\text{phen})(\text{PTA})]\text{CF}_3\text{SO}_3$ where phen is 1,10-phenanthroline, PTA is 1,3,5-Triaza-7-phosphaadamantane and CF_3SO_3 is trifluoromethylsulfonate. Protons and CF_3SO_3 counterion have been omitted for clarity.

2.2 CBS promotes an elevated antioxidant capacity in breast cancer cells

We first assessed the dependency, if any, of intracellular GSH/GSSG in three human breast cancer cell lines on the presence of CBS expression and activity. Lentiviral-mediated silencing of CBS in MCF-7, MDA-MB-468 and Hs 578T afforded three derivative cell lines (shCBS) that exhibited decreased CBS protein expression (Figure 2.3A) and activity (Figure 2.3B) compared to lentiviral control-treated derivative cell lines (scram). Despite there being no direct metabolic connection between CBS activity and GSH biosynthesis, CBS-silenced cells were observed to have ~2-fold lower intracellular GSH/GSSG ratios compared to respective scrambled controls, indicative of increased, mild oxidative stress (Figure 2.3G).^{21,22} GSH/GSSG is an important redox buffer for the cell, resisting acute changes in the generation and scavenging of ROS.⁵ Along with decreased GSH/GSSG, intracellular ROS levels in CBS-silenced cell lines were ~50% higher than the corresponding control-silenced cell lines (Figure 2.3H).

The ratio of GSH/GSSG inside the cell is dependent upon two processes: the de novo synthesis of GSH and the regeneration of 2 GSH from the enzymatic reduction of GSSG.⁵ GSH biosynthesis occurs through the action of the transsulfuration pathway, while the reduction of GSSG occurs through the enzymatic action of glutathione reductase and requires the reducing co-factor NADPH.

Concentrations of transsulfuration pathway metabolites in CBS-silenced cells and control-silenced cells were measured and compared to determine whether the

CBS expression and activity affected the de novo biosynthesis of GSH in human breast cancer. Steady-state levels of cysteine, γ -Glu-Cys and GSH were all significantly lower in CBS-silenced cells versus control-silenced cells, evidence that CBS was a significant and positive regulator of GSH biosynthesis in human breast cancer cells (Figure 2.3C-E).

Next, the role of CBS, if any, in the regeneration of GSH from GSSG was assessed. The two-electron reduction of GSSG into 2 GSH by glutathione reductase (GSR) is dependent on the reducing potential of NADPH, which in turn is itself oxidized to NADP^+ .¹² NADP^+ is regenerated back to NADPH through a coupled redox reaction with glucose-6-phosphate, which is catalyzed by glucose 6-phosphate dehydrogenase (G6PD).²³ Like GSH/GSSG, $\text{NADPH}/\text{NADP}^+$ can be considered a redox buffer, whose ratio is tightly regulated by the cell to balance intracellular ROS levels. The supply of NADPH is the limiting factor in the activity of GR,²⁴ therefore $\text{NADPH}/\text{NADP}^+$ is a measure of the cells ability to generate GSH from GSSG. NADPH assay measurements indicated that $\text{NADPH}/\text{NADP}^+$ ratios in CBS-silenced human breast cancer cell lines were significantly lower compared to corresponding control-silenced cells, suggesting that CBS also maintained elevated GSH levels through the maintenance of elevated $\text{NADPH}/\text{NADP}^+$ (Figure 2.3F).

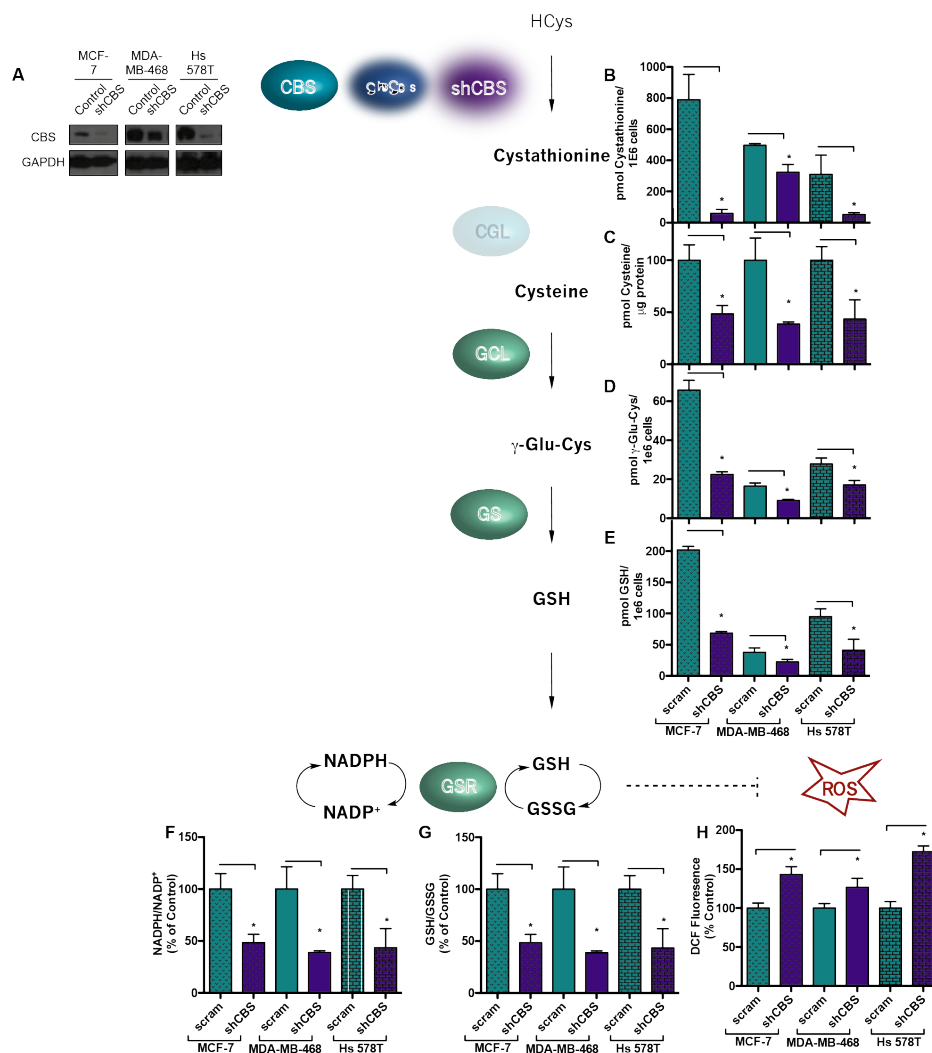


Figure 2.3. Effects of silencing CBS on the antioxidant capacity, redox homeostasis and GSH homeostasis in human breast cancer cells. (A) Western blot analysis of whole cell lysates for CBS expression in CBS-silenced (shCBS) and control shRNA (scram) human breast cancer cells. GAPDH probed for loading control. Effects of CBS knockdown in human breast cancer cells on intracellular, steady state levels of (B) cystathionine, (C) cysteine, (D) γ -Glu-cys and (E) GSH, measured by HPLC-MS. (F) Percent change in ratios of NADPH/NADP⁺ and (G) GSH/GSSG ratios in CBS-silenced human breast cancer cells. (H) Effect of CBS-silencing on relative intracellular ROS levels, determined by DCF fluorescence and analyzed by flow cytometry. Data and blots representative of n=3 independent experiments. (* p \leq 0.05) Abbreviations: cystathionine β -synthase (CBS), cystathionine γ -lyase (CGL), glutamate-cysteine ligase (GCL), glutathione synthase (GS), nicotinamide adenine dinucleotide phosphate (NADPH), glutathione (GSH), glutathione reductase (GSR) high performance liquid chromatography-mass spectrometry (HPLC-MS), reactive oxygen species (ROS), 2', 7'-dichlorofluorescein (DCF).

2.3 CBS expression positively correlates with Nrf2 and downstream antioxidant genes

Having found that CBS expression/activity in human breast cancer cells is highly correlated to an elevated antioxidant capacity, evidenced by increased GSH/GSSG and NADPH/NADP⁺ ratios in (Figure 2.3F-G), we sought to elucidate the underlying mechanisms. This effort was of particular intrigue because of the lack of direct connection between CBS and GSH biosynthesis, due to a truncated transsulfuration pathway.¹⁵

This apparent indirect up-regulation of both de novo GSH synthesis and regeneration of GSH from GSSG by CBS in human breast cancer led us to believe that CBS was working through a transcription factor, as activated transcription factors possess the ability to regulate multiple downstream processes through transcriptional regulation of multiple genes. RT-qPCR experiments revealed that Nrf2 mRNA expression was ~2-fold lower in CBS-silenced cells compared to control-silenced cells (Figure 2.4A). Nrf2, a key transcriptional regulator of cellular response to oxidants, regulates the expression of several genes related to both GSH biosynthesis and regeneration of GSH from GSSG.^{25,26} In addition to Nrf2, CBS-silenced cells exhibited decreased expressions of glutamate-cysteine ligase (GCL) (Figure 2.4B), the rate-limiting transsulfuration pathway enzyme, G6PD (Figure 2.4C), the rate-limiting enzyme of the pentose phosphate pathway, and GSR (Figure 2.4D).

The promotion of an elevated antioxidant capacity in human breast cancer cells by CBS appeared to be substantially mediated by Nrf2, though with the data in hand, such an observation was merely correlative. Off target, non-sequence specific effects, including unintended mRNA gene silencing due to non-specific binding, Toll-like receptors (TLRs) activation by shRNA and cytotoxicity due to saturation of the endogenous miRNA pathway are well documented and in some cases, have been responsible for misattributed effectiveness of RNAi therapies.²⁷ Additional experiments were necessary to control for the possibility that Nrf2, and genes downstream of it, were not altered in CBS-silenced cell lines due to non-sequencing specific effects.

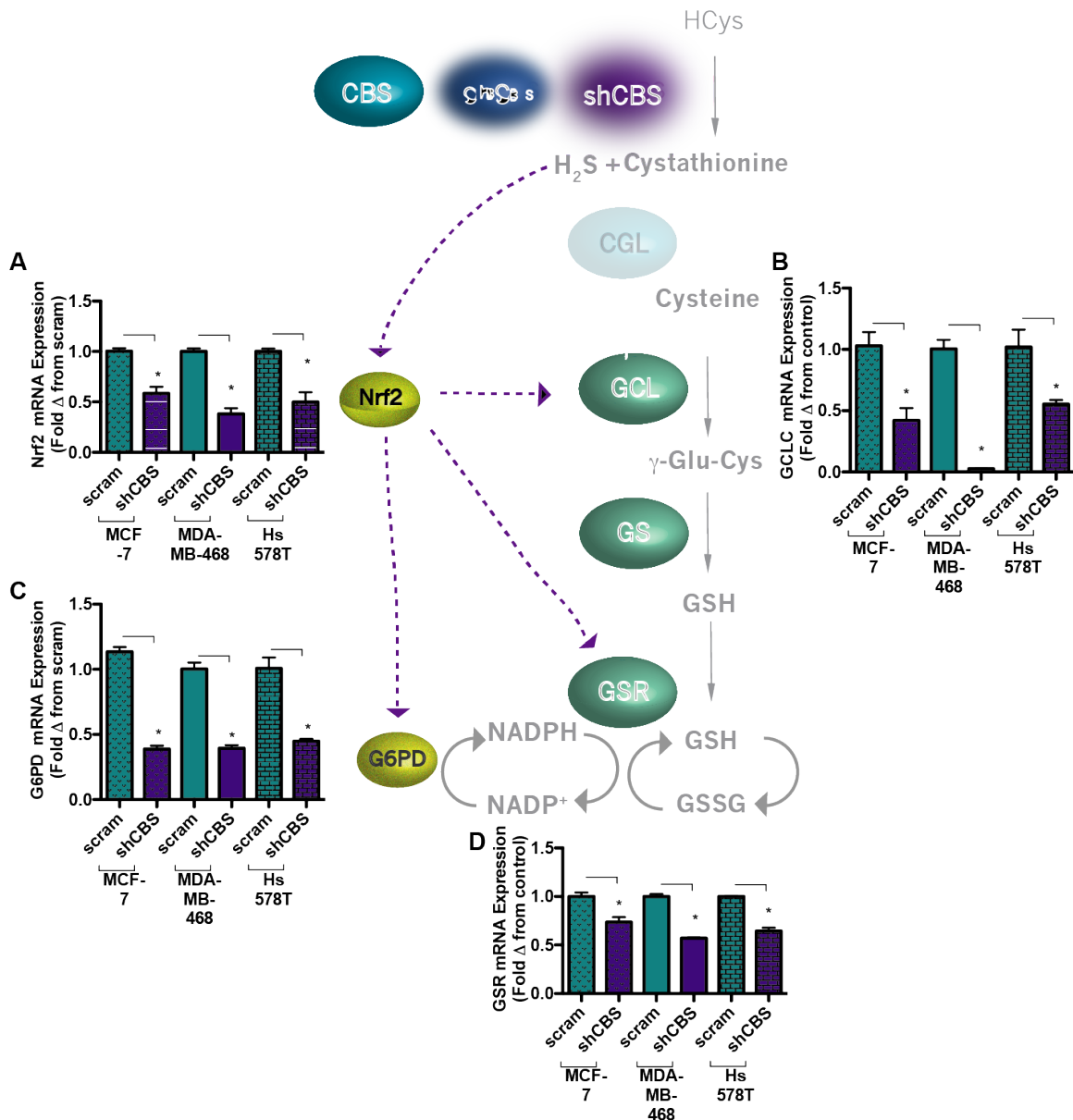


Figure 2.4. Transcriptional effect(s) of CBS-silencing on antioxidant response in human breast cancer cells. (A) RT-qPCR data showing the expression of Nrf2 in CBS-silenced cells (shCBS) compared to control shRNA-transfected cells (scram). Relative mRNA expression levels of antioxidant response genes regulated by Nrf2: (B) GCLC, (C) G6PD and (D) GSR. Data representative of n=3 independent experiments. (* p<0.05) Abbreviations: cystathionine β-synthase (CBS), nuclear factor erythroid 2-related factor 2 (Nrf2), glutamate-cysteine ligase catalytic subunit (GCLC), glucose 6-phosphate dehydrogenase (G6PD), glutathione reductase (GSR).

2.4 Addition of H₂S and CTH to CBS-silenced breast cancer cells restores the antioxidant capacity

To address these shortcomings and establish a causative, rather than correlative, relationship between genetic silencing of CBS and antioxidant capacity, we assessed whether H₂S and CTH, products of CBS enzymatic activity, could partially restore the antioxidant capacity in CBS-silenced human breast cancer line MCF-7. This could be considered a functional CBS knock-in, whereby the specificity of CBS activity towards promoting an elevated antioxidant capacity in human breast cancer cells could be established. To MCF-7(shCBS), extracellular H₂S, delivered by slow H₂S-releaser GYY 4137, and CTH were added. 24 h post-treatment, the antioxidant capacity of the cells, indicated by GSH/GSSG and NADPH/NADP⁺, was largely restored to levels similar to control-silenced MCF-7 cells, MCF-7(scram) (Figure 2.5B, C). The restored antioxidant capacity in H₂S/CTH-treated MCF-7(shCBS) was co-observed with a decrease in intracellular ROS levels (Figure 2.5D). A significant increase in steady state levels of GSH, upon treatment of MCF-7(shCBS) cells with H₂S/CTH, was also observed (Figure 2.5A), reinforcing the action of CBS towards promoting an elevated antioxidant level in human breast cancer cells through positive regulation of intracellular GSH levels.

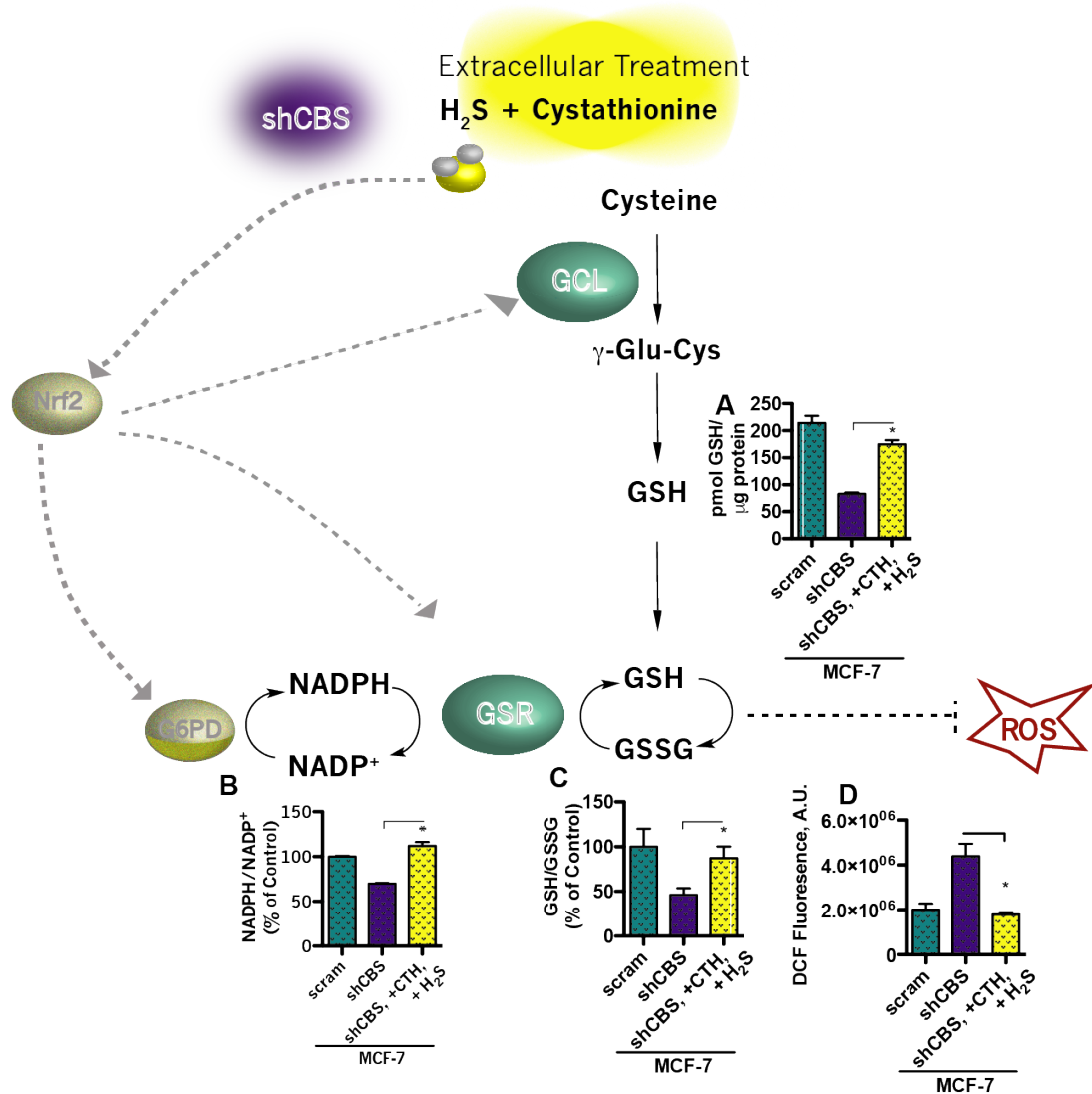


Figure 2.5 Effect(s) of H_2S and cystathionine treatment on redox homeostasis in CBS-silenced human breast cancer cells. (A) Steady state levels of intracellular GSH in CBS-silenced MCF-7 cells, MCF-7(shCBS), upon treatment with H_2S , delivered from 40 μ M GYY 4137, and 100 μ M cystathionine for 24 h. (B) Cytosolic NADPH/NADP⁺ and (C) GSH/GSSG ratios in MCF-7(shCBS) cells treated with H_2S /CTH. (D) Intracellular ROS levels of MCF-7(shCBS) cells treated with H_2S /CTH, determined by DCF fluorescence and analyzed by flow cytometry. Data representative of n=3 independent experiments. (* $p \leq 0.05$) Abbreviations: cystathionine β -synthase (CBS), nicotinamide adenine dinucleotide phosphate (NADPH), glutathione (GSH), reactive oxygen species (ROS), 2', 7'-dichlorofluorescein (DCF).

Mechanistically, these CBS knock-in experiments indicated that CBS up-regulated both de novo GSH biosynthesis and the regeneration of GSH from GSSG through Nrf2. Treatment of MCF-7(shCBS) cells with H₂S and CTH resulted in significantly increased expression of Nrf2 (Figure 2.6A). Such an observation is partially corroborated by previous studies, which demonstrate the ability of H₂S to stabilize Nrf2 through persulfidation of cysteine-rich regulatory protein, Keap1.²⁸ Functional CBS knock-in, in MCF-7(shCBS) cells, significantly increased expressions of the rate-limiting enzyme in GSH biosynthesis, GCL(Figure 2.6B), and the two key enzymes that regenerate GSH from GSSG, GSR and G6PD (Figure 2.6B, C). Knocking-in CBS activity, by extracellular treatment with H₂S and CTH, largely reversed the attenuation of the antioxidant capacity that had resulted from lentiviral silencing of CBS in MCF-7(shCBS), providing clear evidence for the direct actions of CBS towards promoting an elevated antioxidant capacity in human breast cancer.

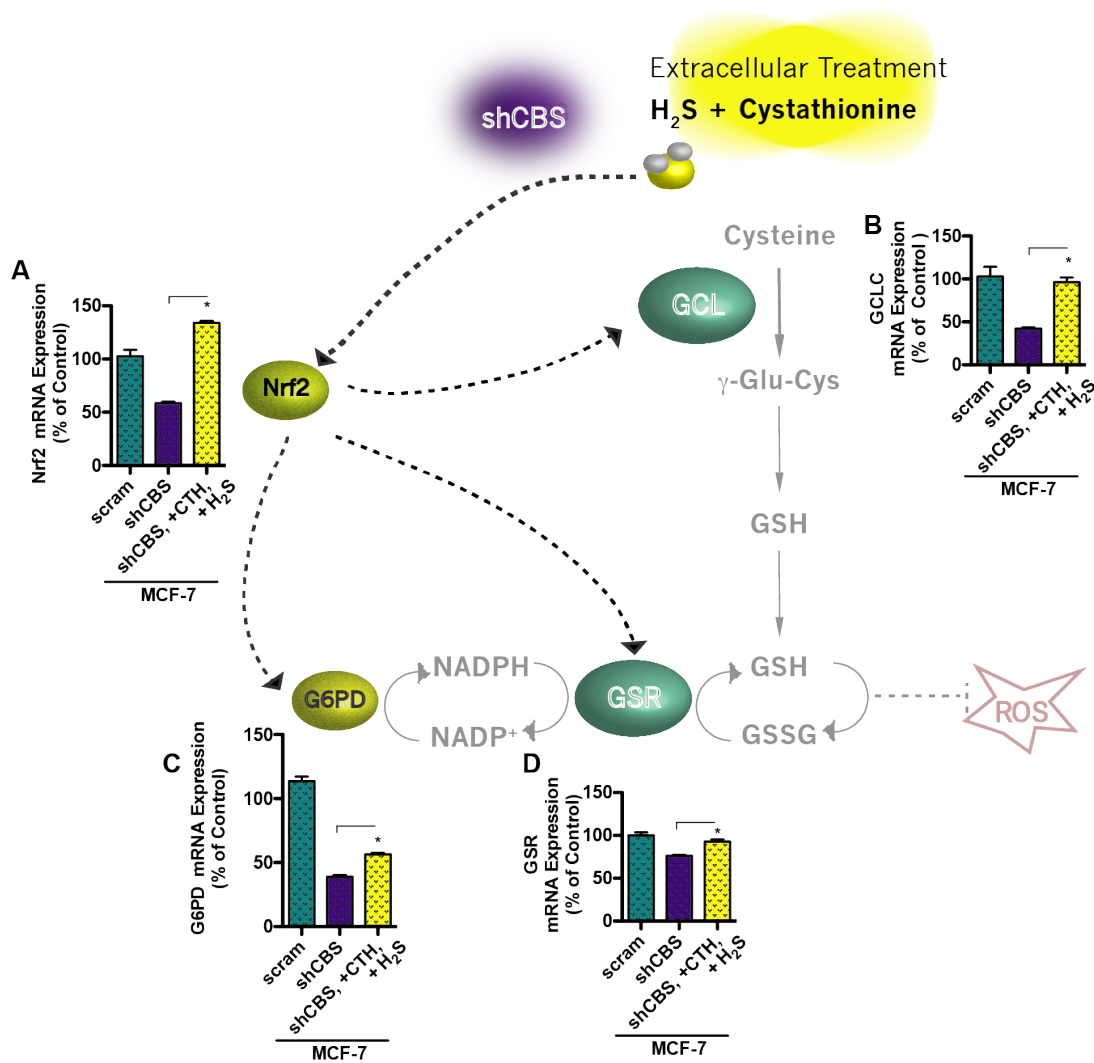


Figure 2.6 Assessment of H₂S and cystathionine treatment to reverse transcriptional effects of silencing CBS in human breast cancer cells. (A) RT-qPCR data showing relative change in Nrf2 expression resulting from treatment of CBS-silenced cells with H₂S, delivered by 40 μM GYY 4137, and 100 μM cystathionine for 24 h. RT-qPCR data showing the effects of 24 h H₂S/cystathionine treatment of CBS-silenced breast cancer cells on transcription levels of (B) GLCL, (C) G6PD and (D) GSR. Data representative of n=3 independent experiments. (*p≤0.05) Abbreviations: cystathionine β-synthase (CBS), nuclear factor erythroid 2-related factor 2 (Nrf2), glutamate-cysteine ligase catalytic subunit (GCLC), glucose 6-phosphate dehydrogenase (G6PD), glutathione reductase (GSR).

2.5 Overexpression of CBS in normal human breast cells increases cellular antioxidant capacity

The expression and activity of CBS in breast cancer cells up-regulated transcriptional and metabolic processes that promoted an increased antioxidant capacity (Figure 2.3-6). However, we further wanted to understand the extent to which CBS alone promotes the antioxidant capacity of human breast cancer cells, or if cancer-specific cellular conditions are required for its action. Unlike in malignant breast tissues and cells, in normal breast cells and tissues, including normal breast cell line MCF-10A, CBS is nearly undetectable by western analysis of whole cell lysates (Figure 2.7A). Knock-in of *CBS* into MCF-10A cells was achieved using adenoviral transduction of the *CBS* gene, with *GFP* gene transduction used as a control, MCF-10A(oxNull). Successful transduction of *CBS* into MCF-10A cells, MCF-10A(oxCBS), compared to MCF-10A(oxNull) was confirmed by western analysis (Figure 2.7A). Intracellular levels of CTH, the gene specific product of CBS, was >10-fold higher upon transduction of *CBS* (Figure 2.7B). This enhanced activity was associated with an increase in the antioxidant capacity of the cell, as measured by GSH/GSSG (Figure 2.7F), as well as increased steady state levels of GSH (Figure 2.7E) and its metabolic precursors, cysteine (Figure 2.7C) and γ -Glu-Cys (Figure 2.7D), suggesting up-regulation of the GSH biosynthesis pathway. Furthermore, overexpression of CBS increased the capacity of MCF-10A to regenerate GSH from GSSG, indicated by increased NADPH/NADP⁺ (Figure 2.7G).

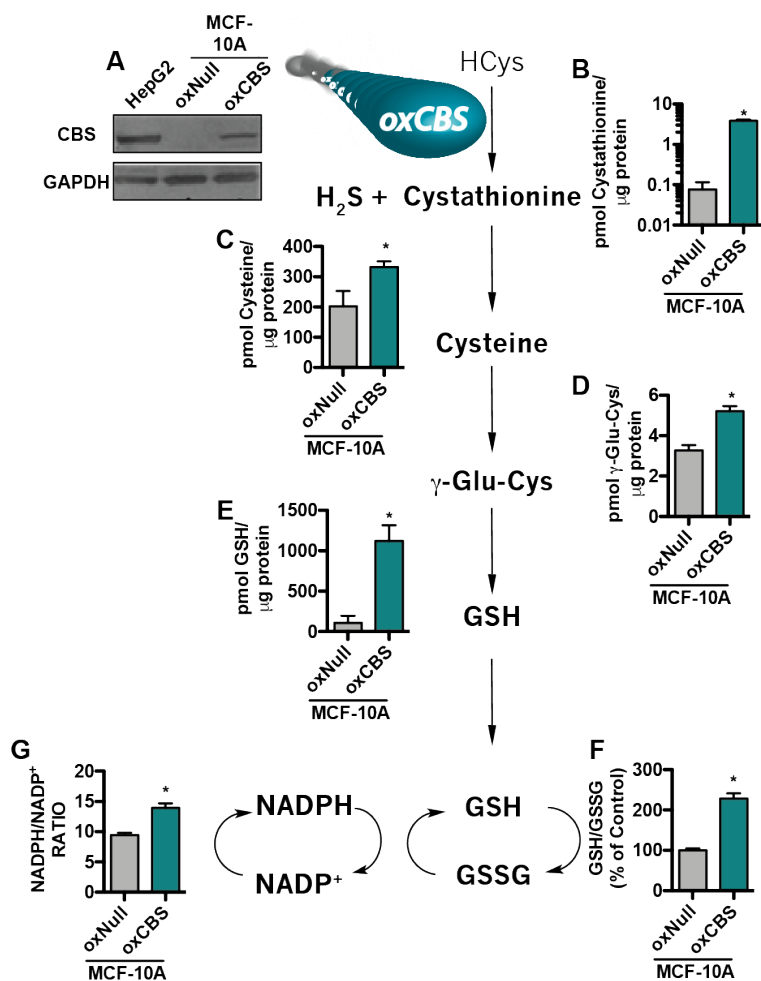


Figure 2.7 Effect(s) of CBS overexpression on the antioxidant capacity of normal human breast cells. (A) Western blot analysis for CBS expression in whole cell lysates of normal human breast cell line MCF-10A transduced with CBS-overexpression (oxCBS) or transduction control (oxNull). GAPDH expression was used as loading control, and HepG2 whole cell lysate was used a positive control for CBS expression. Effect of CBS overexpression on intracellular, steady state levels of transsulfuration metabolites (B) cystathionine, (C) cysteine and GSH biosynthesis metabolites (D) γ -Glu-Cys, (E) GSH performed by HPLC-MS and normalized to total protein. (F) Intracellular GSH/GSSG and (G) NADPH/NADP⁺ ratios in normal breast cells overexpressing CBS. Blots and data representative of n-3 independent experiments. (* $p \leq 0.05$) Abbreviations: cystathionine β -synthase (CBS), nicotinamide adenine dinucleotide phosphate (NADPH), glutathione (GSH).

2.6 CO inhibits CBS and attenuates the antioxidant capacity in human breast cancer

Having discovered strong evidence to the role of CBS in promoting and maintaining an elevated antioxidant capacity, we sought to determine whether CO, a known inhibitor of CBS, could exert a meaningful, therapeutic response in human breast cancer cells. Light-triggered delivery of CO from 120 μ M photoCORM to cell lines MCF-7, MDA-MB-468 and Hs 578T significantly inhibited CBS activity (Figure 2.8A). In a similar manner to CBS-silencing, CO-mediated inhibition decreased the antioxidant capacity, indicated by a decrease in GSH/GSSG, in all three human breast cancer cell lines (Figure 2.8F), as well as increased intracellular ROS levels (Figure 2.8G). Steady state levels of GSH, as well as the metabolic intermediates of GSH biosynthesis, were significantly lower in CO-treated cells, demonstrating the ability of CO to inhibit GSH biosynthesis in human breast cancer cells (Figure 2.8B-D). Additionally, CO-treatment resulted in a decrease in NADPH/NADP⁺ (Figure 2.8E).

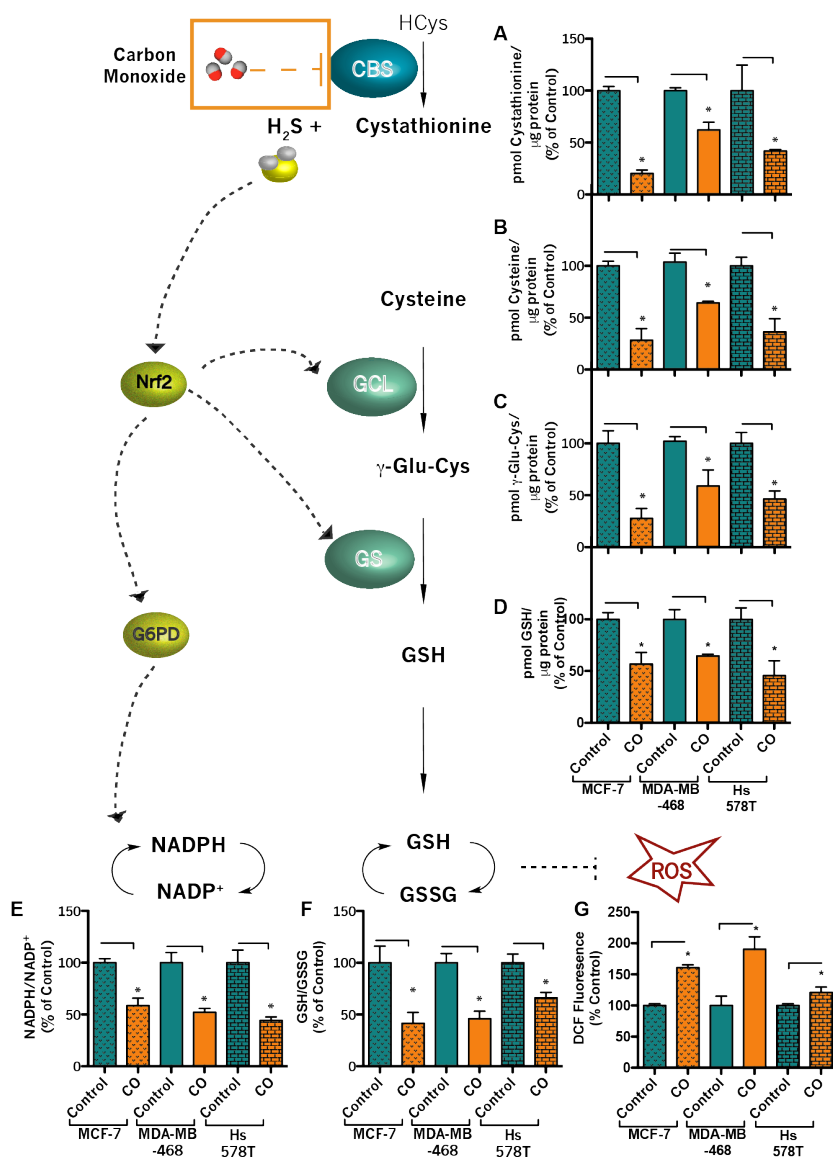


Figure 2.8. Effect(s) of CO, delivered by visible light activation of 120 μM photoCORM, on the antioxidant capacity of human breast cancer cells. Effect of CO treatment on intracellular, steady state levels of (A) cystathionine, (B) cysteine, (C) γ -Glu-Cys and (D) GSH in human breast cancer cells, measured by HPLC-MS. (E) Intracellular ratios of (E) NADPH/NADP⁺ and (F) GSH/GSSG in breast cancer cells treated with CO. (G) Effect of CO treatment on intracellular ROS levels of human breast cancer cells, determined by DCF fluorescence and analyzed by flow cytometry. Data representative of n=3 independent experiments. (* $p \leq 0.05$) Abbreviations: carbon monoxide (CO), photoactivatable CO-releasing molecule (photoCORM), high performance liquid chromatography-mass spectrometry (HPLC-MS), nicotinamide adenine dinucleotide phosphate (NADPH), glutathione (GSH), reactive oxygen species (ROS), 2', 7'-dichlorofluorescein (DCF).

2.7. CO sensitizes human breast cancer to doxorubicin and paclitaxel

To explore this therapeutic potential of CO, we designed an experiment that involved pre-treatment of MCF-7 cells with 120 μ M photoCORM and light-triggered release of CO, followed 30 min by treatment with doxorubicin. If the combination of CO and doxorubicin were to induce greater cell death than the sum of either treatment alone, this would be strong evidence that CO could sensitize human breast cancer cells to chemotherapeutics. Assessment of apoptosis and cell viability 48 h post-treatment revealed that together, CO and doxorubicin induced greater cell death than the sum of either treatment alone, or control cells (Figure 2.9).

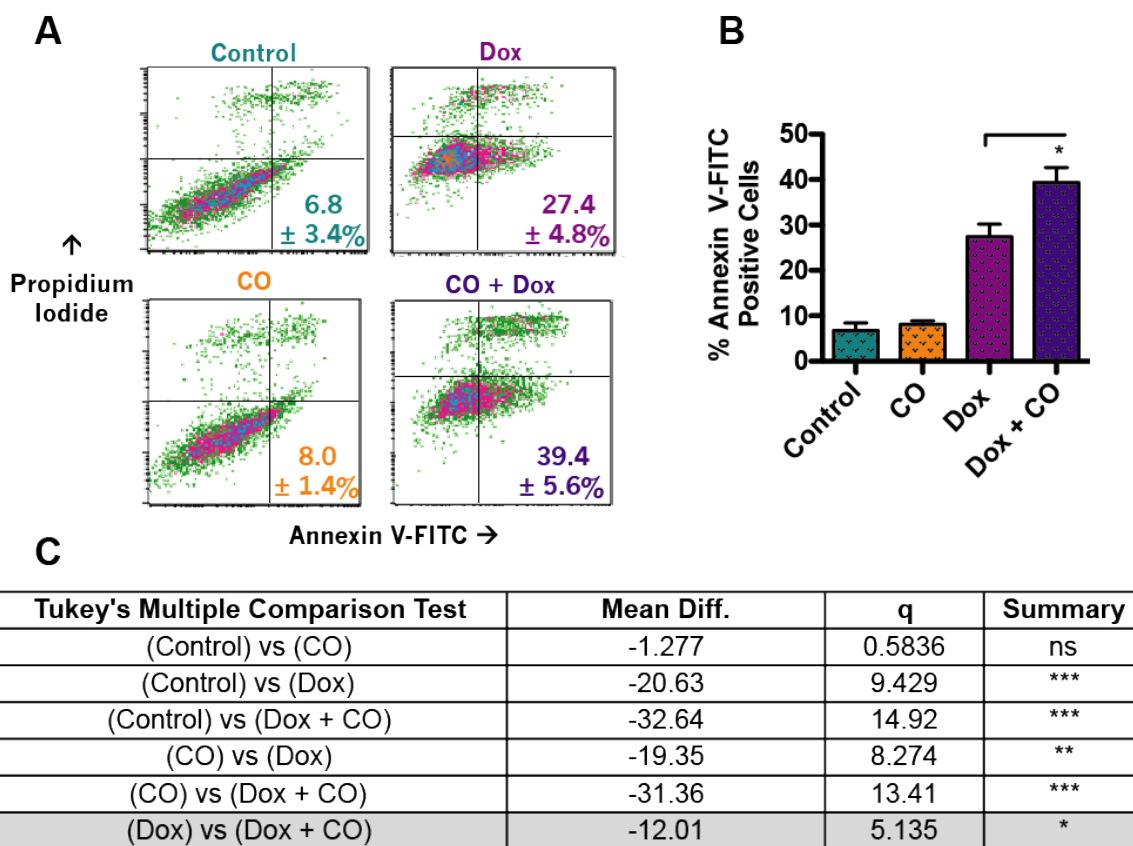
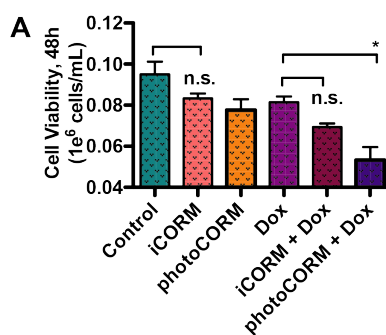


Figure 2.9 Assessment of the ability of CO to sensitize human breast cancer cells to Dox. (A) Representative plots of apoptosis assay by Annexin/propidium iodide staining and flow cytometry analysis of MCF-7 cells treated for 24 h with CO, delivered by 120 μ M photoCORM 1, 1 μ M Dox or both. (B) Graphical summary of $n=3$ independent apoptosis assays. (C) Results of Tukey's test for post-hoc analysis of CO, Dox, and CO + Dox treatment of MCF-7 cells. (* $p \leq 0.05$, ** $p \leq 0.01$, *** $p \leq 0.001$) Abbreviations: carbon monoxide (CO), doxorubicin (Dox), photoactivatable CO-releasing molecule (photoCORM).

Certain CORMs have been reported to exhibit significant cytotoxicity independent of CO, highlighting the possible non-specific toxicities of transition metal-based CORMs.²⁹ However, control experiments, utilizing photo-inactivated photoCORM (iCORM) as a control for the non-CO molecular scaffolding, did not sensitize human breast cancer cells to doxorubicin, indicating the specificity of CO as the chemosensitizing agent for doxorubicin (Figure 2.10).



B

Tukey's Multiple Comparison Test	Mean Diff.	q	P < 0.05?	Summary
Control vs iCORM	0.01167	2.096	No	ns
Control vs photoCORM	0.01733	3.814	No	ns
Control vs Dox	0.0135	2.657	No	ns
Control vs (iCORM + Dox)	0.02567	4.612	Yes	*
Control vs (photoCORM + Dox)	0.04167	7.486	Yes	***
photoCORM vs Dox	-0.0038	0.7545	No	ns
photoCORM vs (iCORM + Dox)	0.00833	1.497	No	ns
photoCORM vs (photoCORM + Dox)	0.02433	4.372	No	ns

Tukey's Multiple Comparison Test	Mean Diff.	q	P < 0.05?	Summary
Dox vs (iCORM + Dox)	0.01217	2.024	No	ns
Dox vs (photoCORM + Dox)	0.02817	4.685	Yes	*
(iCORM + Dox) vs (photoCORM + Dox)	0.016	2.49	No	ns
iCORM vs photoCORM	0.00567	1.018	No	ns
iCORM vs Dox	0.00183	0.305	No	ns
iCORM vs (iCORM + Dox)	0.014	2.178	No	ns
iCORM vs (photoCORM + Dox)	0.03	4.668	Yes	*

Figure 2.10. Assessing any non-specific effects of the molecular scaffold of iCORM on cell viability and drug sensitization to Dox in human breast cancer cells. (A) Live cell count, by trypan blue exclusion, 48 h post-treatment of MCF-7 cells treated with 120 μ M iCORM, 120 μ M photoCORM and/or 1 μ M Dox. (B) Results of Tukey's test for post-hoc analysis of MCF-7 cells treated with iCORM, photoCORM and/or Dox. Data representative of n=3 independent experiments. (* $p \leq 0.05$, ** $p \leq 0.01$, *** $p \leq 0.001$). Abbreviations: inactivated carbon monoxide-releasing molecule (iCORM), photoactivatable carbon monoxide-releasing molecule (photoCORM), doxorubicin (Dox).

While these findings demonstrated the ability of CO to sensitize human breast cancer cells to doxorubicin, it was noted in peer review of the limited scope of such findings. After all, the primary mechanism of action of doxorubicin is as a DNA interchelator, with its ability to induce ROS generation a secondary mechanism of action.³⁰ If our claims, that CO acted by attenuation of the antioxidant capacity of the cancer cell, such drug sensitization by CO would also be observed with other chemotherapeutics. We addressed this criticism by assessing the ability of CO to sensitize MCF-7 cells to another chemotherapeutic, paclitaxel, and assessed cell viability 48 h post-treatment

by trypan blue exclusion. In a similar manner, cells co-treated with CO and either paclitaxel or doxorubicin exhibited significantly lower cell viability compared to paclitaxel and doxorubicin treatments alone (Figure 2.11).

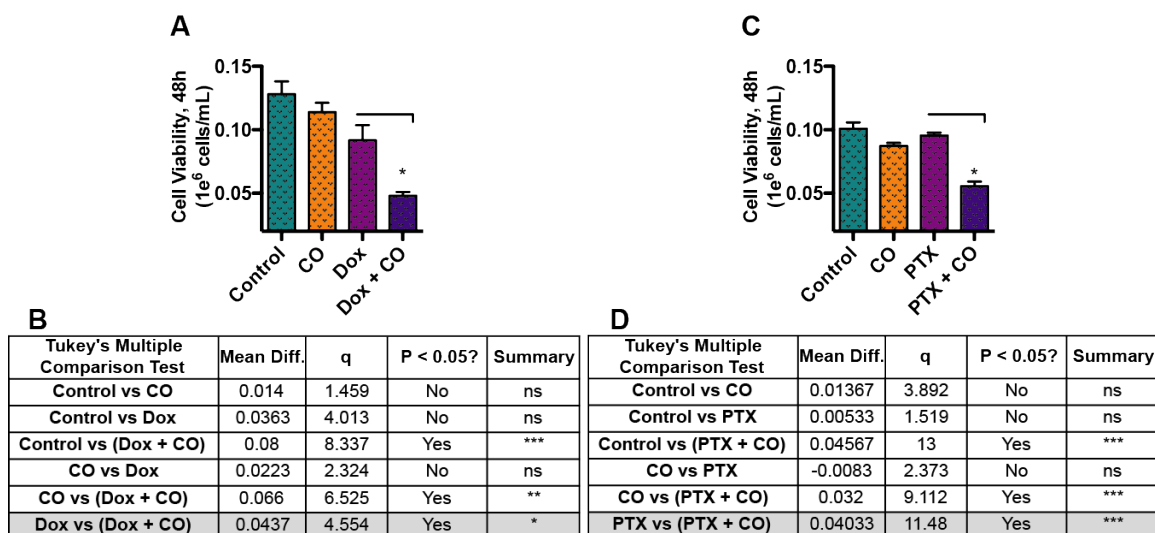
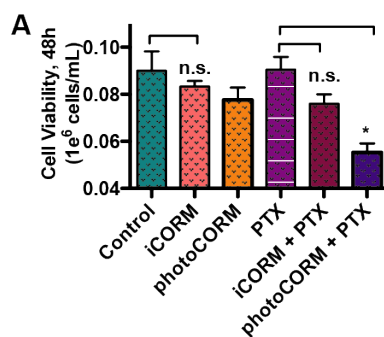


Figure 2.11. Assessment of CO co-treatment to sensitize human breast cancer cells to Dox and PTX. (A) Live cell count by trypan blue exclusion of MCF-7 cells treated with CO, delivered by 120 μ M photoCORM 1, 1 μ M Dox or both, 48 h post-treatment. (B) Results of Tukey's test for post-hoc analysis of MCF-7 cells treated with CO, Dox or both. (C) Live cell count by trypan blue exclusion of MCF-7 cells treated with CO, 20 nM PTX or both, 48 h post-treatment. (D) Results of Tukey's test for post-hoc analysis of MCF-7 cells treated with CO, PTX or both. Data representative of n=3 independent experiments. (* $p \leq 0.05$, ** $p \leq 0.01$, *** $p \leq 0.001$). Abbreviations: carbon monoxide (CO), doxorubicin (Dox), paclitaxel (PTX).

Control experiments utilizing iCORM also did not sensitize human breast cancer cells to paclitaxel, indicating the specificity of CO as the chemosensitizing agent for paclitaxel (Figure 2.12).



B

Tukey's Multiple Comparison Test	Mean Diff.	q	P < 0.05?	Summary
Control vs iCORM	0.00667	1.07	No	ns
Control vs photoCORM	0.01233	2.342	No	ns
Control vs PTX	-0.0005	0.0867	No	ns
Control vs (iCORM + PTX)	0.014	1.982	No	ns
Control vs (photoCORM + PTX)	0.03467	5.564	Yes	*
photoCORM vs PTX	-0.0128	2.437	No	ns
photoCORM vs (iCORM + PTX)	0.00167	0.2502	No	ns
photoCORM vs (photoCORM + PTX)	0.02233	3.872	No	ns
PTX vs (photoCORM + PTX)	0.03517	5.644	Yes	*
iCORM + PTX vs (photoCORM + PTX)	0.02067	2.775	No	ns
PTX vs (iCORM + PTX)	0.0145	2.052	No	ns
iCORM vs photoCORM	0.00567	0.9823	No	ns
iCORM vs PTX	-0.0072	1.15	No	ns
iCORM vs (iCORM + PTX)	0.00733	0.9847	No	ns
iCORM vs (photoCORM + PTX)	0.028	4.204	No	ns

Figure 2.12. Determining any non-specific effects of the molecular scaffold of iCORM on cell viability and drug sensitization to PTX in human breast cancer cells. (A) Live cell count, by trypan blue exclusion, 48 h post-treatment of MCF-7 cells treated with 120 μ M iCORM, 120 μ M photoCORM and/or 1 μ M PTX. (B) Results of Tukey's test for post-hoc analysis of MCF-7 cells treated with iCORM, photoCORM and/or PTX. Data representative of n=3 independent experiments. (* $p \leq 0.05$, ** $p \leq 0.01$, *** $p \leq 0.001$). Abbreviations: inactivated carbon monoxide-releasing molecule (iCORM), photoactivatable carbon monoxide-releasing molecule (photoCORM), paclitaxel (PTX).

2.8 Discussion

The enhanced antioxidant capacity of breast cancer cells is a significant feature in breast cancer therapy. Resistance to anti-cancer drugs remains a significant impediment to successful chemotherapy in human breast cancer management.^{4,5,31-34} Numerous anti-cancer drugs elicit their tumor eliminating effects via the induction of ROS in cancer cells.^{4,7,8} Cancer cells, however, exhibit an increased antioxidant

capacity by maintaining an elevated battery of antioxidant metabolites and enzymes, that ultimately imparts chemotherapeutic drug resistance.³⁵⁻³⁸ The intracellular antioxidant capacity is dependent on the contribution of redox couples, which are pairs of reduced/oxidized species that can either donate or accept reducing equivalents.^{39,40} GSH/GSSG is one of the most important redox couples in the cell, as it is 500 to 1000-fold more abundant than other redox couples.¹² NADPH, a ubiquitous intracellular metabolite and product of the pentose phosphate pathway, supplies reducing equivalents to GSSG to regenerate GSH. Hence, both the GSH/GSSG and NADPH/NADP⁺ ratios are used as indicators of the intracellular antioxidative capacity and increased GSH/GSSG and NADPH/NADP⁺ ratios have been individually shown to be associated with chemotherapeutic resistance in human breast cancer.^{39,41,42}

In human breast cancer, elevated GSH levels are a key marker for greater invasiveness, chemotherapeutic resistance and poor patient outcomes.⁴² In this chapter, we established a clear connection between CBS and elevated GSH levels in human breast cancer cells, this despite a truncated transsulfuration pathway.¹⁵ In fact, the truncation is significant enough to increase levels of CTH in human breast cancer to the extent that it could be considered an oncometabolite, a biomarker specific to breast cancer.¹⁶ H₂S levels are significantly higher in human breast cancer cells as well, which has previously been reported by Sen, et al. to impart cytoprotection to reactive aldehydes and maintain organelle integrity.¹⁵ However, the relationship between CBS and GSH, if any, had remained unclear until this study.

In this study, the GSH/GSSG ratio and total GSH in human breast cancer cells depended on CBS expression and activity in both estrogen receptor positive and estrogen receptor negative breast cancer cells: MCF-7, MDA-MB-468, and Hs 578T (Fig 2.3E, G). As GSH is the most abundant antioxidant cofactor in the cell,^{28,40} silencing CBS and the resulting decrease in the GSH/GSSG ratio was expected to be accompanied increased intracellular ROS. Indeed, silencing of CBS increased ROS levels in human breast cancer cells (Figure 2.3H). The GSH/GSSG ratio is mainly dependent on the *de novo* synthesis of GSH, which in turn is dependent upon the availability of cysteine.^{21,39} Despite the lack of a direct link between CTH and cysteine in human breast cancer cells, silencing of CBS led to depletion of internal cysteine levels (Figure 2.3C). Cysteine is either synthesized inside the cell by the transsulfuration pathway, which is truncated in human breast cancer, or uptaken by specialized transporters, including the glutamate-cystine antiporter (xCT).⁴³ Since human breast cancer cells are compromised in their ability to synthesize endogenous cysteine,¹⁵ its uptake is likely the main source of cysteine. In support of this notion, xCT is the main source of cysteine in human breast cancer cells.⁴⁴⁻⁴⁶ Our current findings suggest that CBS positively regulated xCT activity. This is consistent with previous findings that H₂S, a metabolic product of CBS, enhances xCT activity.^{44,47}

In addition to the *de novo* synthesis of GSH, GSH can also be regenerated from GSSG via reduction by NADPH.²¹ We observed that CBS silencing in human breast cancer cells resulted in a significant decrease in the NADPH/NADP⁺ ratio versus scrambled controls (Figure 2.3F). One of the most important sources of

NADPH production in the cell is the pentose phosphate pathway.²³ G6PD is the rate limiting enzyme in this pathway, which produces NADPH. NADPH donates electrons to GSSG to generate two GSH, a redox reaction catalyzed by the enzyme GSR.²¹ G6PD, GSR and GCLC together are known to be regulated by Nrf2, the most important regulator of antioxidant genes within the cell.⁴⁸ Our results indicated that Nrf2 gene expression was directly correlated to CBS expression in human breast cancer cells since CBS-silenced breast cancer cells had significantly lower Nrf2 mRNA expressions versus scrambled controls (Figure 2.4A). This observation is consistent with previous studies that have shown H₂S and Nrf2 to be positively associated with each other.^{49,50} As CBS silencing resulted in decreased Nrf2 expression, one would expect CBS-silencing to correlate to down-regulation of those genes regulated by Nrf2. Indeed, our data revealed that GCLC, G6PD and GSR gene expression decreased upon silencing of CBS in human breast cancer cells with respect to scrambled controls (Figure 2.4B-3D). These findings indicate that CBS is an upstream regulator of Nrf2. Inhibition of CBS activity may be a promising therapeutic target to, via Nrf2, inhibit GSH biosynthesis in human breast cancer.

Inhibition of GSH biosynthesis with BSO, an inhibitor of GCL, has had notable failures in pre-clinical and clinical studies due to very poor pharmacokinetic properties.⁵¹ This failure has necessitated the search for alternative inhibitors and/or targets. Towards that end, efforts have been made to determine the feasibility and efficacy of inhibiting Nrf2 signaling. In addition to GSH biosynthesis, active Nrf2 is known to positively regulate numerous cancer hallmarks, including metabolism,

cancer stem cell characteristics, tumor aggressiveness, invasion, and metastasis formation.⁵² Nrf2 may be an ideal therapeutic target for inhibiting GSH biosynthesis and towards this end, natural product inhibitors of Nrf2 and genetic silencing of Keap1 and Nrf2 have been suggested as agents to increase cancer cell sensitivity to chemotherapeutic drugs, though druggable members of the Nrf2 pathway have yet to be identified.⁵² Findings in the present study indicate CBS may be a promising target of the Nrf2 pathway that is also breast cancer-specific. However, systemic administration of pharmacological inhibitors of CBS, non-specific PLP analogues, are not ideal as CBS expression is high in other non-malignant tissues like the liver and brain.¹⁴ Furthermore, the effect of Nrf2 activation is highly context-specific, where it has been shown to promote positive or negative health outcomes in the management of cancer.⁵² This fact highlights the need for localized inhibition of CBS and the Nrf2 pathway, a challenge well suited to localized and controllable delivery of CO to a therapeutic site.

Our data show that CO inhibited CBS in human breast cancer cells (Figure 2.8A) and decreased the antioxidant capacities in both estrogen receptor positive and negative human breast cancer cells alike (Figure 2.8E, F). Our findings are consistent with previous data that have shown CO to inhibit both isolated CBS^{53,54} and CBS in certain tissue types.^{55,56} CBS appears to be an ideal target for CO in the context of breast cancer therapy in that it is overexpressed in cancer cells versus normal cells,¹⁵ and is responsive to CO-mediated inhibition (Figure 2.8).

The antioxidant capacity of breast cancer cells is an important feature with regard to cancer therapy, as numerous anticancer drugs and radiation therapies work by increasing ROS in cancer cells.^{7,57} For these therapies, high GSH levels, increased GSH/GSSG ratios and increased antioxidant capacity are markers for chemotherapeutic/radiation resistance.^{35,58} We have shown a clear connection between CBS activity and maintaining elevated GSH levels in breast cancer cells. Inhibition of CBS by CO, delivered by photoCORM, could be an affective approach towards decreasing therapeutic resistance of breast cancer cells. Herein we provide strong preliminary evidence supporting this claim, as CO was able to sensitize human breast cancer cells to both doxorubicin and paclitaxel (Figure 2,9, 2.11).

CO, in pharmacology, is a standard tool, used to reveal heme-enzyme involvement in drug metabolism and other metabolic processes. In a similar manner, we have used CO, delivered by photoCORM, to reveal the involvement of the heme-containing enzyme CBS in the processes of cancer pathogenesis and therapeutic resistance. Furthermore, we have revealed the possibility of CBS inhibition as a therapeutic strategy and largely elucidated the mechanism by which inhibition of CBS would improve the response of human breast cancer cells to doxorubicin and paclitaxel.

2.9 Materials and methods

Materials and reagents

photoCORM was synthesized by following the published procedure and analyzed to confirm purity before application.¹³ Protease inhibitor cocktail (P8340), puromycin

(P8833), and all other chemicals were purchased from Sigma-Aldrich (St. Louis, MO) unless stated otherwise. The primary antibodies namely, anti-CBS (sc-133208) and anti-GAPDH (sc-47724) were procured from Santa Cruz Biotechnology (Santa Cruz, CA).

Cell culture and treatments

MCF-7, MDA-MB-468, Hs 578T and MCF-10A were obtained from American Type Culture Collection (Manassas, VA). MDA-MB-468 and Hs 578T cells were grown in 1x DMEM supplemented with 10 mM HEPES buffer, 1x antibiotic-antimycotic and 10% fetal bovine serum (FBS). MCF-7 cells were grown in 1x DMEM supplemented with 1 µg/mL insulin, 1mM sodium pyruvate, 1x antibiotic-antimycotic and 10% FBS. MCF-10A cells were grown in 50/50 DMEM/F12 supplemented with 20 ng/mL epidermal growth factor, 0.5 mg/mL hydrocortisone, 100 ng/mL cholera toxin, 10 µg/mL insulin, 1x Pen/Strep and 5% horse serum. Cells were passaged no more than 10 times post-procurement from the supplier, and their genetic characteristics were tested regularly. Additionally, the absence of mycoplasma was determined regularly with a MycoAlert mycoplasma detection kit (LT07-318) from Lonza (Basel, Switzerland). All treatments, including exogenous addition of 100 µM CTH and 40 µM GYY 4137, concentrations similar to those used in previous studies^{7,8}, were performed under serum-free conditions unless otherwise noted.

Generation of stable cell lines

Stable cell lines, silenced for CBS were generated for MCF-7, MDA-MB-468 and Hs578T human breast cancer cells with short hairpin RNA (shRNA) using lentiviral particles obtained from Santa Cruz Biotechnology (Santa Cruz, CA). CBS-silenced cell lines were transfected with lentiviral particles containing three to five lentiviral plasmids, each encoding for a 19-25 nucleotide shRNA complimentary to CBS mRNA (sc-60335-V) to knockdown CBS gene expression. Stable, control cell lines were transfected with lentiviral particles containing a plasmid encoding for a scrambled shRNA sequence (sc-108080) that does not lead to the specific degradation of any specific mRNA. Cells were selected with 1 µg/mL puromycin until resistant colonies were identified and propagated. MCF-7, MDA-MB- 468 and Hs 578T cells that survived puromycin selection after transfection with shRNA were annotated as MCF-7(scram)/MCF-7(shCBS), MDA-MB-468(scram)/MDA-MB-468(shCBS) and Hs 578T(scram)/Hs 578 T(shCBS) for scrambled controls and CBS-silenced cells, respectively.

Measurement of metabolites via high pressure, liquid chromatography-mass spectrometry

GSH, GSSG, γ -Glu-Cys, cysteine and CTH were quantified via high pressure, liquid chromatography-mass spectrometry (HPLC-MS) as described.^{7,8} 5×10^6 cells were lysed via three freeze/thaw cycles in 200 µL of 10 mM N-ethylmaleimide (NEM) + 10 mM ammonium acetate, pH 7.4. After lysis, methanol (800 µL) was added and the samples were vortexed. Following centrifugation (16,000 x g, 5 min) of samples,

supernatants were transferred to microcentrifuge tubes and dried by vacuum centrifugation. 100 μL methanol was added to the dried samples and then dried under a stream of nitrogen. Benzene (100 μL) was added and the samples were dried under a stream of nitrogen. Next, each sample was treated with 100 μL of 3N methanolic HCl for 60 min, 60°C. Then, the samples were dried under a nitrogen stream. All samples were finally dissolved in 100 μL H₂O and centrifuged at 16,000 x g for 5 min. The supernatants were transferred to liquid chromatography (LC) injector vials. 8 μL aliquots of the solutions were injected onto a Kinetex XB-C18, 100 x 2.1 mm, 1.7- μm particle size, 100Å pore diameter, reverse phase column from Phenomenex (Torrance, CA). The column was equilibrated with 85% 0.1 mM perfluorooctanoic acid in water (eluant A) and 15% 0.1 mM perfluorooctanoic acid in acetonitrile (eluant B) and eluted at 100 $\mu\text{L}/\text{min}$ with increasing concentration of eluant B (min/% B: 0/15, 5/15, 35/50, 33/ 15, 45/15). The eluant was directed to an Agilent Jet Stream electrospray ionization (ESI) source connected to a triple quadrupole mass spectrometer (Agilent 6460) operating in the positive ion tandem mass spectrometric multiple reaction-monitoring (MRM) mode. The intensities of the CTH parent to fragment transition (461 \rightarrow 318, rt 27.88 min), cysteine-NEM conjugate (261 \rightarrow 244, rt 24.06 min), GSH-NEM conjugate (461 \rightarrow 318, rt 26.06 min), GSSG (669 \rightarrow 383, rt 28.18 min) and γ -Glu-Cys-NEM conjugate (404 \rightarrow 244, rt 26.59 min) parent to fragment transitions were recorded using previously optimized settings. With each independent experiment, standards were prepared containing known concentrations of CTH (0, 20, 40, 40, 80, 160 pmol), cysteine (0, 10, 20, 40, 80 pmol), GSH (0,100, 200, 400, 800

pmol), GSSG (0, 25, 50, 100, 200 pmol) and γ -Glu-Cys (0, 100, 200, 400, 800 pmol). The peak areas of the standards of CTH, cysteine, GSH, GSSG and γ -Glu-Cys were used to construct calibration curves. The amount of CTH, cysteine, GSH, GSSG and γ -Glu-Cys in each biological sample was calculated by interpolation from the curves.

Detection of Reactive Oxygen Species

Relative, intracellular reactive oxygen species (ROS) was determined with 2',7'-dichlorodihydrofluorescein diacetate (hereafter: DCFDA). Cells were treated with 50 μ M DCFDA for 30 min at 37 °C. Cells were washed twice with phosphate-buffered saline (PBS) + 0.5% FBS, then analyzed by flow cytometry using a C6 Flow Cytometer and CFlow software from Becton Dickinson Biosciences (Franklin Lakes, NJ).

NADPH/NADP⁺ Assay

Intracellular nucleotides NADPH and NADP⁺ were measured using the NADP/NADPH Assay Kit (ab65349), which was procured from Abcam (Cambridge, MA).

RNA purification and reverse transcriptase-qualitative PCR

Total RNA was extracted using the Rneasy Mini Kit (#74106) obtained from Qiagen (Valencia, CA). RNA concentrations were measured using a NanoDrop 2000 c spectrophotometer (Nanodrop: Wilmington, DE). First strand cDNA synthesis was performed using the iScript cDNA synthesis kit from Bio-Rad (Hercules, CA).

Relative levels of mRNA were assayed for the following genes: β -actin, nuclear factor erythroid 2-related factor 2 (Nrf2), glucose 6-phosphate dehydrogenase (G6PD), the catalytic subunit of γ -glutamylcysteine synthetase (GCLC) and glutathione reductase (GSR). The primer sequences used were as follows: β -Actin (forward: 5'-ATTGGCAATGAGCGGTTC-3', reverse: 5'-GGATGCCACAGGACTCCAT-3'), Nrf2 (forward: 5'-GAGAGCCCAGTCTTCATTGC-3', reverse: 5'-TGCTCAATGTCCTGTTGCAT-3'), G6PD (forward: 5'-ATCGACCACTACCTGGGCAA-3', reverse: 5'-TTCTGCATCACGTCCCGGA-3'), GCLC (forward: 5'-AGTTCAATACAGTTGAGG-3', reverse: 5'-TACTGATCCTATAGTTAT-3') and GSR (forward: 5'-TTGGTAACTGCGTGATACATCGGG-3', reverse: 5'-AACATCCCAACT GTGGTCTTCAGC-3'). Qualitative PCR (qPCR) was performed on the ABI (Applied Biosystems) 7900 HT Thermal cycler in standard mode using SYBR Green (Life Technologies: Carlsbad, CA) for 40 cycles. Each reaction was run in triplicate in three independent experiments. Relative mRNA expression values were calculated using the $2^{\Delta\Delta Ct}$ method.

Overexpression of CBS

Human CBS overexpression plasmids (Ad-h-CBS, # ADV-204180) and the corresponding control plasmids (Ad-CMV-null, # 1300), packaged in adenovirus, were obtained from Vector Biolabs (Malvern, PA). Briefly, MCF-10A cells were seeded into 100 mm dishes and grown to ~95% confluency and then infected with the

CBS overexpression or control viral stocks of 10^5 - 10^6 PFU/mL. After 24 h, the cells were washed, fresh medium was added, and the cells were used for subsequent experiments including HPLC-MS, NADP⁺/NADPH assaying and western blot analysis.

Western blot analysis

Whole cell lysates were prepared from cells after various treatments in lysis buffer containing 50 mM Hepes (pH 7.5), 1 mM DTT, 150 mM NaCl, 1 mM EDTA, 0.1% Tween 20, 10% glycerol, 10 mM β -glycerophosphate, 1 mM NaF, 0.1 mM orthovanadate, 10 mg/mL leupeptin, 10 mg/mL aprotinin, and 0.1 mM phenylmethylsulfonyl fluoride (PMSF). The soluble cell lysate protein concentrations were quantified by Bradford assay. 20 μ g cell lysate from each sample was separated on a 10% SDS-PAGE gel and transferred to polyvinylidene difluoride (PVDF) membranes. Membrane blocking was done with 5% nonfat dried milk and incubated overnight at 4°C. Primary (1:1000 dilution) and horse radish peroxidase (HRP)-conjugated secondary (1:10,000 dilution) antibody incubations were done at 4°C overnight and 1 h at room temperature, respectively. Immunofluorescent signals were detected using Pierce™ ECL Plus Western Blotting Substrate (#32132) from ThermoFisher Scientific (Waltham, MA).

Light-activated photoCORM treatment

Cells were treated with 120 μ M photoCORM in serum-free conditions as previously described.¹⁸ 10^6 cells were placed in 100 mm tissue culture dishes and allowed to

seed overnight. The next day, cells were treated with 120 μM photoCORM in the dark. For experimental (i.e. CO-treated) samples, cells were exposed to visible light for 30 min at room temperature, then allowed to incubate at $37^\circ\text{C} + 5\% \text{CO}_2$ for 1 h. Next, the media was aspirated, and the cells were washed three times with 1x PBS, followed by the addition of serum-containing media. The cells were then allowed to incubate at $37^\circ\text{C} + 5\% \text{CO}_2$ for 6 h and finally assayed for GSH and GSH metabolites by HPLC-MS and ROS by DCFDA fluorescence. For control samples, cells were handled exactly the same as experimental samples, but not exposed to light.

Doxorubicin and photoCORM treatments

For assaying the chemosensitizing effects of CO, cells were pre-treated with 120 μM photoCORM as mentioned above with the exception of the addition of serum-free media after CO-treatment. Following this, either 1 μM doxorubicin or vehicle control (dimethyl sulfoxide, DMSO) was added to respective tissue culture dishes. Cells were allowed to incubate at $37^\circ\text{C} + 5\% \text{CO}_2$ for 24 h, after which cells were assayed for viability and apoptosis.

Cell viability assay

A Vi-Cell XR cell viability analyzer from Beckman Coulter (Brea, CA) was used to determine cell viability by the trypan blue exclusion method. The number of viable cells, 24 hours post-treatment, was determined in triplicate. Data represents mean \pm SEM of three independent experiments.

Detection of apoptosis

Apoptosis/necrosis of doxorubicin and photoCORM-treated cells was determined with a FITC Annexin V Apoptosis Detection Kit I, containing Annexin V-FITC and propidium iodide (BD Pharmingen, #556570). After doxorubicin/photoCORM treatment, cells were harvested and counted. 10^6 cell aliquots were washed twice with cold, 1x PBS and re-suspended in 100 μ L of 1x Annexin V Binding Buffer. The cells were transferred to 5-mL culture tubes and stained with 5 μ L Annexin V-FITC and 5 μ L of propidium iodide. Cells were incubated for 15 min at room temperature in the dark, then 400 μ L of 1x Annexin V Binding Buffer was added to the samples and the cells were analyzed with a BD FACScanTM flow cytometer from Becton Dickinson Biosciences. Data were acquired and analyzed using BD CellQuestTM software.

Statistical analysis

Data are presented as means +/- SEM. Statistical comparison between two groups was performed using a Student's t-test. Statistical comparisons between more than two groups were performed using ANOVA with post-hoc Tukey's test. P values less than 0.05 were considered statistically significant (* $p < 0.05$).

2.10 References

1. Housman, G.; Byler, S.; Heerboth, S.; Lapinska, K.; Longacre, M.; Snyder, N.; Sarkar, S., Drug resistance in cancer: An overview. *Cancers* **2014**, *6* (3), 1769-1792.
2. Lippert, T. H.; Ruoff, H.-J.; Volm, M., Intrinsic and acquired drug resistance in malignant tumors. *Arzneimittel-Forschung-Drug Research* **2008**, *58* (6), 261-264.
3. Grek, C. L.; Tew, K. D., Redox metabolism and malignancy. *Current Opinion in Pharmacology* **2010**, *10* (4), 362-368.
4. Conklin, K. A., Chemotherapy-associated oxidative stress: impact on chemotherapeutic effectiveness. *Integrative Cancer Therapies* **2004**, *3* (4), 294-300.
5. Hayes, J. D.; McLellan, L. I., Glutathione and glutathione-dependent enzymes represent a co-ordinately regulated defense against oxidative stress. *Free Radical Research* **1999**, *31* (4), 273-300.
6. Barrera, G., Oxidative stress and lipid peroxidation products in cancer progression and therapy. *ISRN Oncology*, **2012**; *2012*, 21.
7. Kaufmann, S. H.; Earnshaw, W. C., Induction of apoptosis by cancer chemotherapy. *Experimental Cell Research* **2000**, *256* (1), 42-49.
8. Berndtsson, M.; Hagg, M.; Panaretakis, T.; Havelka, A. M.; Shoshan, M. C.; Linder, S., Acute apoptosis by cisplatin requires induction of reactive oxygen species but is not associated with damage to nuclear DNA. *International Journal of Cancer* **2007**, *120* (1), 175-180.
9. Anderson, M. E., Glutathione: an overview of biosynthesis and modulation. *Chemico-Biological Interactions* **1998**, *112*, 1-14.
10. Mosharov, E.; Cranford, M. R.; Banerjee, R., The quantitatively important relationship between homocysteine metabolism and glutathione synthesis by the transsulfuration pathway and its regulation by redox changes. *Biochemistry* **2000**, *39* (42), 13005-13011.

11. Finkelstein, J. D., The metabolism of homocysteine: pathways and regulation. *European Journal of Pediatrics* **1998**, *157*, S40-S44.
12. Schafer, F. Q.; Buettner, G. R., Redox environment of the cell as viewed through the redox state of the glutathione disulfide/glutathione couple. *Free Radical Biology and Medicine* **2001**, *30* (11), 1191-1212.
13. Puranik, M.; Weeks, C. L.; Lahaye, D.; Kabil, O.; Taoka, S.; Nielsen, S. B.; Groves, J. T.; Banerjee, R.; Spiro, T. G., Dynamics of carbon monoxide binding to cystathionine beta-synthase. *Journal of Biological Chemistry* **2006**, *281* (19), 13433-13438.
14. Zhu, H. R.; Blake, S.; Chan, K. T.; Pearson, R. B.; Kang, J., Cystathionine beta-synthase in physiology and cancer. *Biomed Research International* **2018**.
15. Sen, S.; Kawahara, B.; Gupta, D.; Tsai, R.; Khachatryan, M.; Roy-Chowdhuri, S.; Bose, S.; Yoon, A.; Faull, K.; Farias-Eisner, R.; Chaudhuri, G., Role of cystathionine beta-synthase in human breast cancer. *Free Radical Biology and Medicine* **2015**, *86*, 228-238.
16. Sen, S.; Kawahara, B.; Mahata, S. K.; Tsai, R.; Yoon, A.; Hwang, L.; Hu-Moore, K.; Villanueva, C.; Vajihuddin, A.; Parameshwar, P.; You, M.; Bhaskar, D. L.; Gomez, O.; Faull, K. F.; Farias-Eisner, R.; Chaudhuri, G., Cystathionine: A novel oncometabolite in human breast cancer. *Archives of Biochemistry and Biophysics* **2016**, *604*, 95-102.
17. Chakraborty, I.; Carrington, S. J.; Hauser, J.; Oliver, S. R. J.; Mascharak, P. K., Rapid Eradication of Human Breast Cancer Cells through Trackable Light-Triggered CO Delivery by Mesoporous Silica Nanoparticles Packed with a Designed photoCORM. *Chemistry of Materials* **2015**, *27* (24), 8387-8397.
18. Chakraborty, I.; Carrington, S. J.; Roseman, G.; Mascharak, P. K., Synthesis, Structures, and CO Release Capacity of a Family of Water-Soluble PhotoCORMs: Assessment of the biocompatibility and their phototoxicity toward human breast cancer cells. *Inorganic Chemistry* **2017**, *56* (3), 1534-1545.

19. Zuckerbraun, B. S.; Chin, B. Y.; Bilban, M.; d'Avila, J. C.; Rao, J.; Billiar, T. R.; Otterbein, L. E., Carbon monoxide signals via inhibition of cytochrome c oxidase and generation of mitochondrial reactive oxygen species. *Faseb Journal* **2007**, *21* (4), 1099-1106.
20. Hawkes, N., Drug resistance: the next target for cancer treatment. *Bmj-British Medical Journal* **2019**, 365.
21. Lu, S. C., Regulation of glutathione synthesis. *Molecular Aspects of Medicine* **2009**, *30* (1-2), 42-59.
22. Meister, A., Glutathione metabolism and its selective modification. *Journal of Biological Chemistry* **1988**, *263* (33), 17205-17208.
23. Ramos-Martinez, J. I., The regulation of the pentose phosphate pathway: Remember Krebs. *Archives of Biochemistry and Biophysics* **2017**, *614*, 50-52.
24. Fabregat, I.; Vitorica, J.; Satrustegui, J.; Machado, A., The pentose-phosphate cycle is regulated by NADPH NADP ratio in rat-liver. *Archives of Biochemistry and Biophysics* **1985**, *236* (1), 110-118.
25. Mitsuishi, Y.; Taguchi, K.; Kawatani, Y.; Shibata, T.; Nukiwa, T.; Aburatani, H.; Yamamoto, M.; Motohashi, H., Nrf2 redirects glucose and glutamine into anabolic pathways in metabolic reprogramming. *Cancer Cell* **2012**, *22* (1), 66-79.
26. Mitsuishi, Y.; Taguchi, K.; Yamamoto, M.; Motohashi, H., Nrf2 activates the pentose phosphate pathway and glutamine consumption in proliferating cells. *International Journal of Molecular Medicine* **2011**, *28*, S16-S16.
27. Mansoori, B.; Mohammadi, A.; Jang, S. S.; Baradaran, B., Mechanisms of immune system activation in mammals by small interfering RNA (siRNA). *Artificial Cells Nanomedicine and Biotechnology* **2016**, *44* (7), 1589-1596.
28. Taguchi, K.; Motohashi, H.; Yamamoto, M., Molecular mechanisms of the Keap1-Nrf2 pathway in stress response and cancer evolution. *Genes to Cells* **2011**, *16* (2), 123-140.

29. Winburn, I. C.; Gunatunga, K.; McKernan, R. D.; Walker, R. J.; Sammut, I. A.; Harrison, J. C., cell damage following carbon monoxide releasing molecule exposure: Implications for therapeutic applications. *Basic & Clinical Pharmacology & Toxicology* **2012**, *111* (1), 31-41.
30. Hortobagyi, G. N., Anthracyclines in the treatment of cancer - An overview. *Drugs* **1997**, *54*, 1-7.
31. Wang, X. J.; Sun, Z.; Villeneuve, N. F.; Zhang, S.; Zhao, F.; Li, Y. J.; Chen, W. M.; Yi, X. F.; Zheng, W. X.; Wondrak, G. T.; Wong, P. K.; Zhang, D. D., Nrf2 enhances resistance of cancer cells to chemotherapeutic drugs, the dark side of Nrf2. *Carcinogenesis* **2008**, *29* (6), 1235-1243.
32. Pelicano, H.; Carney, D.; Huang, P., ROS stress in cancer cells and therapeutic implications. *Drug Resistance Updates* **2004**, *7* (2), 97-110.
33. Ramanathan, B.; Jan, K. Y.; Chen, C. H.; Hour, T. C.; Yu, H. J.; Pu, Y. S., Resistance to paclitaxel is proportional to cellular total antioxidant capacity. *Cancer Research* **2005**, *65* (18), 8455-8460.
34. Hecht, F.; Pessoa, C. F.; Gentile, L. B.; Rosenthal, D.; Carvalho, D. P.; Fortunato, R. S., The role of oxidative stress on breast cancer development and therapy. *Tumor Biology* **2016**, *37* (4), 4281-4291.
35. Tai, D. J.; Jin, W. S.; Wui, C. S.; Si, H. W.; Cao, X. D.; Guo, A. J.; Chang, J. C., Changes in intracellular redox status influence multidrug resistance in gastric adenocarcinoma cells. *Experimental and Therapeutic Medicine* **2012**, *4* (2), 291-296.
36. Diehn, M.; Cho, R. W.; Lobo, N. A.; Kalisky, T.; Dorie, M. J.; Kulp, A. N.; Qian, D. L.; Lam, J. S.; Ailles, L. E.; Wong, M. Z.; Joshua, B.; Kaplan, M. J.; Wapnir, I.; Dirbas, F. M.; Somlo, G.; Garberoglio, C.; Paz, B.; Shen, J.; Lau, S. K.; Quake, S. R.; Brown, J. M.; Weissman, I. L.; Clarke, M. F., Association of reactive oxygen species levels and radioresistance in cancer stem cells. *Nature* **2009**, *458* (7239), 780-U123.

37. Scarbrough, P. M.; Mapuskar, K. A.; Mattson, D. M.; Gius, D.; Watson, W. H.; Spitz, D. R., Simultaneous inhibition of glutathione- and thioredoxin-dependent metabolism is necessary to potentiate 17AAG-induced cancer cell killing via oxidative stress. *Free Radical Biology and Medicine* **2012**, *52* (2), 436-443.
38. Backos, D. S.; Franklin, C. C.; Reigan, P., The role of glutathione in brain tumor drug resistance. *Biochemical Pharmacology* **2012**, *83* (8), 1005-1012.
39. Gorrini, C.; Harris, I. S.; Mak, T. W., Modulation of oxidative stress as an anticancer strategy. *Nature Reviews Drug Discovery* **2013**, *12* (12), 931-947.
40. Meister, A., Glutathione deficiency produced by inhibition of its synthesis, and its reversal – applications in research and therapy. *Pharmacology & Therapeutics* **1991**, *51* (2), 155-194.
41. Lewandowicz, G. M.; Britt, P.; Elgie, A. W.; Williamson, C. J.; Coley, H. M.; Hall, A. G.; Sargent, J. M., Cellular glutathione content, in vitro chemoresponse, and the effect of BSO modulation in samples derived from patients with advanced ovarian cancer. *Gynecologic Oncology* **2002**, *85* (2), 298-304.
42. Gamcsik, M. P.; Kasibhatla, M. S.; Teeter, S. D.; Colvin, O. M., Glutathione levels in human tumors. *Biomarkers* **2012**, *17* (8), 671-691.
43. Sato, H.; Tamba, M.; Ishii, T.; Bannai, S., Cloning and expression of a plasma membrane cystine/glutamate exchange transporter composed of two distinct proteins. *Journal of Biological Chemistry* **1999**, *274* (17), 11455-11458.
44. Habib, E.; Linher-Melville, K.; Lin, H. X.; Singh, G., Expression of xCT and activity of system X-c(-) are regulated by NRF2 in human breast cancer cells in response to oxidative stress. *Redox Biology* **2015**, *5*, 33-42.
45. Timmerman, L. A.; Holton, T.; Yuneva, M.; Louie, R. J.; Padro, M.; Daemen, A.; Hu, M.; Chan, D. A.; Ethier, S. P.; van 't Veer, L. J.; Polyak, K.; McCormick, F.; Gray, J. W., Glutamine sensitivity analysis identifies the xCT antiporter as a common triple-negative breast tumor therapeutic target. *Cancer Cell* **2013**, *24* (4), 450-465.

46. Ishimoto, T.; Nagano, O.; Yae, T.; Tamada, M.; Motohara, T.; Oshima, H.; Oshima, M.; Ikeda, T.; Asaba, R.; Yagi, H.; Masuko, T.; Shimizu, T.; Ishikawa, T.; Kai, K.; Takahashi, E.; Imamura, Y.; Baba, Y.; Ohmura, M.; Suematsu, M.; Baba, H.; Saya, H., CD44 variant regulates redox status in cancer cells by stabilizing the xCT subunit of system xc(-) and thereby promotes tumor growth. *Cancer Cell* **2011**, *19* (3), 387-400.
47. Majid, A. S. A.; Majid, A.; Yin, Z. Q.; Ji, D., Slow regulated release of H₂S inhibits oxidative stress induced cell death by influencing certain key signaling molecules. *Neurochemical Research* **2013**, *38* (7), 1375-1393.
48. Sporn, M. B.; Liby, K. T., NRF2 and cancer: the good, the bad and the importance of context. *Nature Reviews Cancer* **2012**, *12* (8), 564-571.
49. Hourihan, J. M.; Kenna, J. G.; Hayes, J. D., The gasotransmitter hydrogen sulfide induces Nrf2-target genes by inactivating the Keap1 ubiquitin ligase substrate adaptor through formation of a disulfide bond between Cys-226 and Cys-613. *Antioxidants & Redox Signaling* **2013**, *19* (5), 465-481.
50. Islam, K. N.; Polhemus, D. J.; Donnarumma, E.; Brewster, L. P.; Lefer, D. J., Hydrogen Sulfide Levels and Nuclear Factor-Erythroid 2-Related Factor 2 (NRF2) activity are attenuated in the setting of critical limb ischemia (CLI). *Journal of the American Heart Association* **2015**, *4* (5).
51. Smith, A. C.; Liao, J. T. F.; Page, J. G.; Wientjes, M. G.; Grieshaber, C. K., Pharmacokinetics of buthionine sulfoximine (NSC-326231) and its effect on melphalan-induced toxicity in mice. *Cancer Research* **1989**, *49* (19), 5385-5391.
52. Smolkova, K.; Miko, E.; Kovacs, T.; Leguina-Ruzzi, A.; Sipos, A.; Bai, P., Nuclear Factor Erythroid 2-Related Factor 2 in regulating cancer metabolism. *Antioxidants & Redox Signaling* **2020**, *33* (13), 966-997.
53. Kabil, O.; Weeks, C. L.; Carballal, S.; Gherasim, C.; Alvarez, B.; Spiro, T. G.; Banerjee, R., Reversible heme-dependent regulation of human cystathionine beta-synthase by a flavoprotein oxidoreductase. *Biochemistry* **2011**, *50* (39), 8261-8263.

54. Taoka, S.; West, M.; Banerjee, R., Characterization of the heme and pyridoxal phosphate cofactors of human cystathionine beta-synthase reveals nonequivalent active sites. *Biochemistry* **1999**, *38* (9), 2738-2744.
55. Shintani, T.; Iwabuchi, T.; Soga, T.; Kato, Y.; Yamamoto, T.; Takano, N.; Hishiki, T.; Ueno, Y.; Ikeda, S.; Sakuragawa, T.; Ishikawa, K.; Goda, N.; Kitagawa, Y.; Kajjimura, M.; Matsumoto, K.; Suematsu, M., Cystathionine beta-synthase as a carbon monoxide-sensitive regulator of bile excretion. *Hepatology* **2009**, *49* (1), 141-150.
56. Yamamoto, T.; Takano, N.; Ishiwata, K.; Suematsu, M., Carbon monoxide stimulates global protein methylation via its inhibitory action on cystathionine beta-synthase. *Journal of Clinical Biochemistry and Nutrition* **2011**, *48* (1), 96-100.
57. Dioum, E. M.; Rutter, J.; Tuckerman, J. R.; Gonzalez, G.; Gilles-Gonzalez, M. A.; McKnight, S. L., NPAS2: A gas-responsive transcription factor. *Science* **2002**, *298* (5602), 2385-2387.
58. Ryu, C. S.; Kwak, H. C.; Lee, J. Y.; Oh, S. J.; Phuong, N. T.; Kang, K. W.; Kim, S. K., Elevation of cysteine consumption in tamoxifen-resistant MCF-7 cells. *Biochemical Pharmacology* **2013**, *85* (2), 197-206.

2.11 Reprint of publication

Reprinted with permission from [Kawahara, B.; Moller, T.; Hu-Moore, K.; Carrington, S.; Faull, K. F.; Sen, S.; Mascharak, P. K., Attenuation of antioxidant capacity in human breast cancer cells by carbon monoxide through inhibition of cystathionine β -synthase activity: implications in chemotherapeutic drug sensitivity. *Journal of Medicinal Chemistry* **2017**, *60* (19), 8000-8010.]. **Copyright [2017] American Chemical Society.**

Rightslink® by Copyright Clearance Center



RightsLink®



Home



Help



Email Support



Brian Kawahara ▾

Attenuation of Antioxidant Capacity in Human Breast Cancer Cells by Carbon Monoxide through Inhibition of Cystathionine β -Synthase Activity: Implications in Chemotherapeutic Drug Sensitivity



Author: Brian Kawahara, Travis Moller, Kayla Hu-Moore, et al

Publication: Journal of Medicinal Chemistry

Publisher: American Chemical Society

Date: Oct 1, 2017

Copyright © 2017, American Chemical Society

PERMISSION/LICENSE IS GRANTED FOR YOUR ORDER AT NO CHARGE

This type of permission/license, instead of the standard Terms & Conditions, is sent to you because no fee is being charged for your order. Please note the following:

- Permission is granted for your request in both print and electronic formats, and translations.
- If figures and/or tables were requested, they may be adapted or used in part.
- Please print this page for your records and send a copy of it to your publisher/graduate school.
- Appropriate credit for the requested material should be given as follows: "Reprinted (adapted) with permission from (COMPLETE REFERENCE CITATION). Copyright (YEAR) American Chemical Society." Insert appropriate information in place of the capitalized words.
- One-time permission is granted only for the use specified in your request. No additional uses are granted (such as derivative works or other editions). For any other uses, please submit a new request.

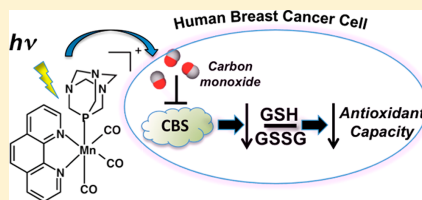
[BACK](#)

[CLOSE WINDOW](#)

Attenuation of Antioxidant Capacity in Human Breast Cancer Cells by Carbon Monoxide through Inhibition of Cystathionine β -Synthase Activity: Implications in Chemotherapeutic Drug SensitivityBrian Kawahara,[†] Travis Moller,[§] Kayla Hu-Moore,[‡] Samantha Carrington,[†] Kym F. Faull,[§] Suvajit Sen,^{*,‡} and Pradip K. Mascharak^{*,†}[†]Department of Chemistry and Biochemistry, University of California, Santa Cruz, California 95064, United States[‡]Department of Obstetrics and Gynecology, David Geffen School of Medicine at University of California, Los Angeles, Los Angeles, California 90095, United States[§]Semel Institute for Neuroscience and Human Behavior, University of California at Los Angeles, Los Angeles, California 90095, United States

Supporting Information

ABSTRACT: Drug resistance is a major impediment to effective treatment of breast cancer. Compared to normal cells, cancer cells have an increased antioxidant potential due to an increased ratio of reduced to oxidized glutathione (GSH/GSSG). This is known to confer therapeutic resistance. Here, we have identified a mechanism, unique to breast cancer cells, whereby cystathionine β -synthase (CBS) promotes elevated GSH/GSSG. Lentiviral silencing of CBS in human breast cancer cells attenuated GSH/GSSG, total GSH, nuclear factor erythroid 2-related factor 2 (Nrf2), and processes downstream of Nrf2 that promote GSH synthesis and regeneration of GSH from GSSG. Carbon monoxide (CO) reduced GSH/GSSG in three breast cancer cell lines by inhibiting CBS. Furthermore, CO sensitized breast cancer cells to doxorubicin. These results provide insight into mechanism(s) by which CBS increases the antioxidant potential and the ability for CO to inhibit CBS activity to alter redox homeostasis in breast cancer, increasing sensitivity to a chemotherapeutic.



INTRODUCTION

The transsulfuration pathway (TSP) is a metabolic pathway that is active in liver, kidney, and brain tissues, converting endogenous homocysteine to cysteine with the intermediate formation of cystathionine (CTH) and hydrogen sulfide (H_2S).^{1,2} The pathway comprises two successive steps: (i) homocysteine + serine/cysteine \rightarrow CTH + $\text{H}_2\text{O}/\text{H}_2\text{S}$ (catalyzed by cystathionine β -synthase, CBS) and (ii) CTH + $\text{H}_2\text{O} \rightarrow$ cysteine + α -ketobutyrate + NH_3 (catalyzed by cystathionine γ -lyase, CGL) (Figure 1A). Cysteine, produced in step (ii), can be utilized by γ -glutamylcysteine synthetase to produce γ -glutamylcysteine (γ -Glu-Cys), which is subsequently combined with glycine by glutathione synthase to form glutathione (GSH).^{1,2} Cysteine can also be imported from the extracellular environment via transporters, including the cystine/glutamate antiporter (xCT).³ Nonetheless, the TSP is a significant source of cysteine for GSH synthesis, especially under conditions of increased oxidative stress.^{1,2} During oxidative stress, GSH can cycle between the thiol-reduced and disulfide-oxidized (GSSG) forms, reducing cellular oxidants in the process.⁴ GSSG is reduced back to GSH by utilizing electrons from nicotinamide adenosine dinucleotide phosphate (NADPH), a coupled oxidation–reduction that is catalyzed by

glutathione reductase (GSR).⁴ Of the known cellular redox couples, GSH/GSSG is the most abundant and ubiquitous.⁵ GSH is essential for cell survival and for maintaining redox homeostasis.⁶ Therefore, the GSH/GSSG ratio is frequently used as a surrogate measure of intracellular antioxidant capacity and overall cellular redox homeostasis.^{4–6}

We have previously reported that the TSP appears to be absent in normal breast tissues: they express neither CBS nor CGL at significant levels⁷ (compare panels A and B in Figure 1). In contrast, human breast cancer (HBC) tissues, which possess a significantly increased ROS level compared to normal breast tissues, exhibit a *truncated form* of the TSP: HBC tissues overexpress CBS, the enzyme that catalyzes the condensation of homocysteine and cysteine to form CTH + H_2S , but they lack the expression of CGL (compare panels A and C in Figure 1).^{7,8} Consequently, CTH, synthesized by CBS in the truncated TSP in HBC, does not get metabolized into cysteine. Thus, the truncated TSP lacks a direct link to the formation of GSH. Despite this, we now report here that the ratio of GSH/GSSG in HBC cells is significantly dependent on the presence of CBS,

Received: April 3, 2017

Published: September 6, 2017

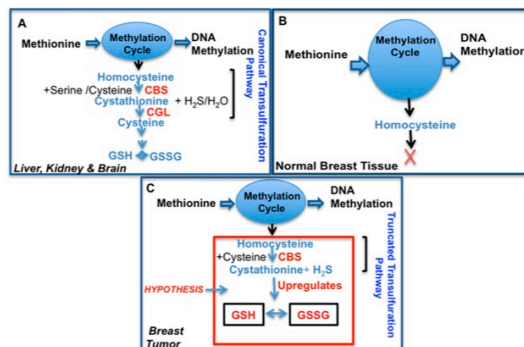


Figure 1. TSP as it exists in various tissues. (A) Canonical TSP in normal tissues such as the liver, kidney, and brain. (B) Absent TSP in normal breast tissue. (C) Truncated TSP in human breast tumor tissues, which is distinct from that in normal breast tissues.

and we have investigated possible mechanism(s) by which CBS regulates redox homeostasis.

Carbon monoxide (CO) inhibits the activity of isolated and purified CBS with a K_i of 5.6 μM .^{9,10} Endogenous CO has been shown to inhibit CBS in lymphocytes, colon, kidney, and mouse liver/brain.^{11,12} Recent research in this laboratory has established that CO photoreleased from designed photoactive CO-releasing molecules (photoCORMs) leads to dose-dependent eradication of cultured human breast, colon, and cervical cancer cells.^{13–16} However, the therapeutic implications of the inhibition of CBS by appropriate photoCORMs as the CO donor in the context of HBC has not been investigated. In breast cancer therapy and management, overcoming chemotherapeutic drug resistance is a major challenge.^{17–22} One of the main mechanism(s) by which chemotherapeutics eliminate cancer cells is by the enhancement of endogenous ROS.^{22,23} In this regard, it is also known that the increased antioxidative potential of cancer cells, specifically GSH concentrations, plays a major role in the manifestation of drug resistance.^{24,25} In this article, we show that light-induced CO release, utilizing $[\text{Mn}(\text{CO})_3(\text{phen})(\text{PTA})]\text{CF}_3\text{SO}_3$ (abbreviated $[\text{Mn}(\text{CO})_3]$ hereafter) as the photoCORM (Scheme 1), can perturb the redox homeostasis of breast cancer cells via the inhibition of endogenous CBS. The complete control of CO delivery through exposure to visible light is the principal reason for the choice of $[\text{Mn}(\text{CO})_3]$ as the CO donor in this study. We further

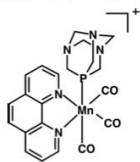
demonstrate that CO-mediated inhibition of CBS in breast cancer cells increases their chemosensitivity.

RESULTS

Lentiviral-Mediated Silencing of CBS Decreases the GSH/GSSG Ratio and Attenuates GSH Biosynthesis and Regeneration in Human Breast Cancer Cells. We first assessed the dependency of the GSH/GSSG ratio in HBC cells on the presence of CBS. Stable, lentiviral-mediated silencing of CBS in human breast cancer cell lines MCF-7, MDA-MB-468, and Hs 578T resulted in a ~2-fold decrease in their GSH/GSSG ratios versus scrambled controls (Figure 2A). A decrease in the ratio of GSH/GSSG is indicative of increased oxidative stress.^{4,6} To this end, we observed that a decrease in the GSH/GSSG ratio upon the silencing of CBS was associated with a significant increase in the steady-state levels of ROS, evidenced by an increase in DCFDA fluorescence (Figure 2B). The *de novo* synthesis of GSH is an important determinant of the GSH/GSSG ratio.^{4,26} Therefore, we looked at the total amount of intracellular GSH in CBS-silenced HBC cells versus those transfected with lentiviral controls. Total GSH (GSH + 2 × GSSG) was significantly lower in MCF7shCBS, 468shCBS, and Hs shCBS versus MCF7scram, 468scram, and Hs scram, respectively (Figure 2C). We next investigated the processes involved in GSH synthesis, including the rate-limiting step of GSH synthesis: the ATP-dependent condensation of glutamate and cysteine, catalyzed by γ -glutamylcysteine synthetase⁵ to form γ -Glu-Cys. In this regard, we observed that silencing CBS led to a significant decrease in the intracellular levels of γ -Glu-Cys (Figure 2D).

Furthermore, silencing CBS was also associated with a decrease in the steady-state levels of endogenous cysteine (Figure 2E), the rate-limiting substrate in the synthesis of GSH.²⁶ GSH cycles between its thiol-reduced state and the disulfide-oxidized form (GSSG), reducing cellular oxidants in this process.²⁷ GSSG is restored back to GSH by utilizing electrons from NADPH, which concomitantly is converted to NADP^+ .²⁷ Toward this, we observed that silencing of CBS in HBC cells also resulted in a decrease in the intracellular ratio of $\text{NADPH}/\text{NADP}^+$ (Figure 2F).

Scheme 1. $[\text{Mn}(\text{CO})_3(\text{phen})(\text{PTA})]\text{CF}_3\text{SO}_3^+$



⁴Phen is 1,10-phenanthroline, PTA is 1,3,5-triaza-7-phosphaadamantane, and CF_3SO_3 is trifluoromethylsulfonate. Protons and CF_3SO_3 counterion have been omitted for clarity.

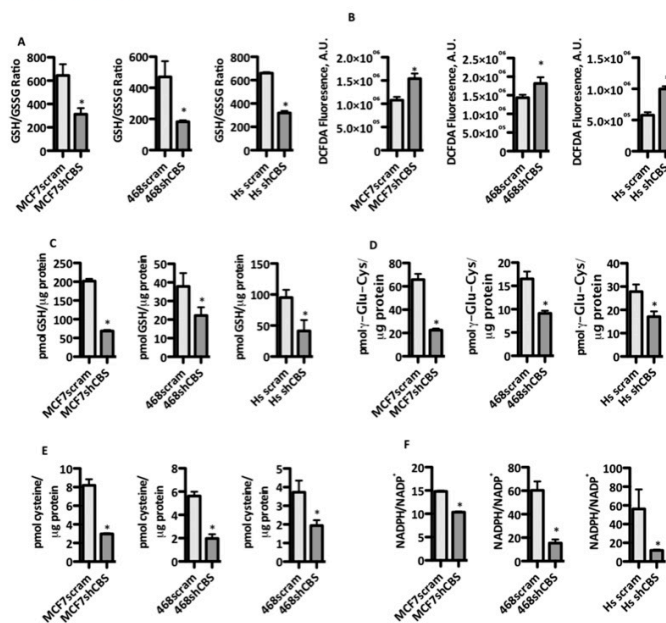


Figure 2. CBS silencing leads to a decrease in the GSH/GSSG ratio in a panel of breast cancer cell lines. (A) GSH/GSSG ratios in human breast cancer cells transfected with shRNA against CBS (shCBS) versus respective controls transfected with random, scrambled shRNA (scram). GSH and GSSG were assayed by HPLC-MS. (B) Intracellular ROS levels, as detected by DCFDA fluorescence, in CBS-silenced cells versus scrambled controls. (C–E) Effect of CBS silencing in HBC cells on the steady-state levels of total GSH, γ -Glu-Cys, and cysteine, as measured by HPLC-MS. (F) NADPH/NADP⁺ ratio in HBC cell lines upon silencing CBS versus respective scrambled controls. Data are representative of $n = 3$ independent experiments (* $p < 0.05$).

Silencing CBS Expression in Human Breast Cancer Cells Results in a Decrease in Nrf2 and Downstream Antioxidant mRNA Gene Expression. To further elucidate the underlying mechanism(s) by which CBS controls the GSH/GSSG ratio in HBC, we investigated whether CBS regulated Nrf2, the master regulator of antioxidant genes.²⁸ Among these antioxidant genes are included those involved in GSH synthesis and the regeneration of reduced GSH from GSSG.^{29,30} RT-qPCR experiments revealed that silencing CBS in human breast cancer cells significantly reduced Nrf2 mRNA expression compared to scrambled controls (Figure 3A). We also observed that silencing CBS decreased mRNA expression levels of GCLC (≥ 1.8 -fold), G6PD (≥ 2.2 -fold), and GSR (≥ 1.4 fold) (Figure 3B–D). These genes are involved in GSH synthesis (GCLC) and GSH regeneration (G6PD and GSR).²⁶

Addition of H₂S and CTH, Metabolic Products of CBS Enzymatic Activity, Partially Reverses Some of the Effects of CBS Silencing in HBC Cells. We assessed whether H₂S and CTH, the products of CBS catalytic activity, could reverse some of the effects of CBS silencing in HBC cells. We exogenously added GYY 4137 (a slow releaser of H₂S) and CTH to MCF7shCBS cells and observed a significant attenuation in the decrease of the GSH/GSSG ratio (Figure 4A). This attenuation in the GSH/GSSG ratio was correlated

with a decrease in ROS levels, as evidenced by DCFDA fluorescence (Figure 4B). We also observed an increase of total intracellular GSH in MCF7shCBS cells upon addition of CTH and H₂S to levels nearly as high as those in MCF7scram cells (Figure 4C). Additionally, exogenous addition of CTH and H₂S to MCF7shCBS cells resulted in attenuation of the decrease in Nrf2 mRNA expression and some of its associated downstream genes: GCLC, G6PD, and GSR (Figure 4D). In addition, we also observed attenuation of the decrease in the NADPH/NADP⁺ ratio (Figure 4E).

Overexpression of CBS in a Normal Breast Cell Line, MCF-10A, Results in an Increase in the GSH/GSSG Ratio. We further confirmed the CBS-mediated upregulation of GSH/GSSG in normal breast cells, which do not normally express significant levels of CBS.⁷ We used an adenoviral system to establish cell lines of MCF-10A that transiently overexpressed either the CBS gene (10AoxCBS) or GFP as a control (oxNull). SDS-PAGE and western analysis of whole cell lysates confirmed the overexpression of CBS in 10AoxCBS versus 10AoxNull cells. To confirm the bioactivity of the overexpressed CBS, we measured intracellular CTH levels with the aid of HPLC-MS. 10AoxCBS cells exhibited ~ 40 -fold more intracellular CTH versus 10AoxNull (Figure 5A). After validating both the overexpression and increased activity of

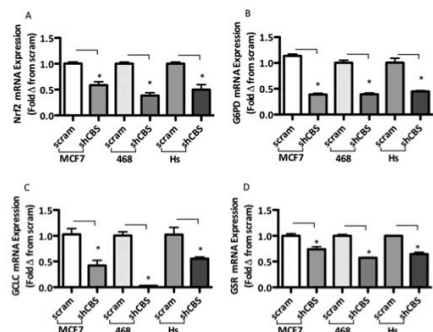


Figure 3. Silencing CBS in human breast cancer cells decreases mRNA expression of genes that promote GSH biosynthesis and regeneration. (A–D) Reverse transcriptase-quantitative PCR of Nrf2, G6PD, GCLC, and GSR mRNA of three HBC cell lines transfected with shRNA against CBS (shCBS) versus each cell line's respective controls transfected with random, scrambled shRNA (scram). Data are representative of at least $n = 3$ experiments ($*p < 0.05$).

CBS, we measured the GSH/GSSG ratio by HPLC-MS. We observed that overexpression of CBS indeed increased the GSH/GSSG ratio in 10AoxCBS versus 10AoxNull cells (Figure 5B). To confirm whether CBS was regulating either the biosynthesis of GSH and/or its regeneration from GSSG, we measured steady-state levels of total GSH and some of its precursor metabolites. Overexpression of CBS in normal breast cells resulted in significant increases in steady-state levels of total GSH, γ -Glu-Cys, and cysteine (Figure 5C–E). These results firmly established a role for CBS in promoting the biosynthesis of GSH. Lastly, we wanted to validate whether CBS overexpression promoted the regeneration of GSH from GSSG, having previously observed that CBS silencing inhibited some of these processes. Our data did reveal that 10AoxCBS cells exhibited a significantly higher NADPH/NADP⁺ ratio versus 10AoxNull cells (Figure 5F).

Exogenous CO Inhibits Bioactivity of CBS and Reduces Antioxidant Capacity of Breast Cancer Cells.

Having shown a role for CBS in maintaining increased antioxidant capacity in HBC cells, we hypothesized that CO could inhibit CBS and perturb redox homeostasis. Using an appropriate photoCORM as a CO-delivery system previously described,¹⁵ we treated cells with extracellular CO and monitored its effects on CBS bioactivity and subsequent effects on the GSH/GSSG ratio and redox state of the cell. First, we wanted confirm that CO could inhibit CBS bioactivity in breast cancer cells. In three breast cancer cell lines (MCF-7, MDA-MB-468, and Hs 578T) we did observe a significant decrease in steady-state levels of intracellular CTH (Figure 6A). These data validated our hypothesis that exogenous CO could inhibit CBS bioactivity. Next, we wanted to confirm that the inhibition of CBS by CO would reduce the GSH/GSSG ratio in HBC. In a similar manner to the effects of CBS silencing we previously observed, CO treatments resulted in significant decreases in the GSH/GSSG ratio in breast cancer cells (Figure 6B). This was also associated with increased ROS levels compared to control treatments (Figure 6C). To briefly confirm the mechanism of the decrease in antioxidant capacity by CO in breast cancer

cells, we measured steady-state levels of total GSH, γ -Glu-Cys, and cysteine, and we found that CO-treated cells contained significantly lower levels of total GSH, γ -Glu-Cys, and cysteine when compared to their respective controls (Figure 6D–F).

CO Increases the Sensitivity of Breast Cancer Cells to DOX. An increased antioxidant capacity and an enhanced GSH/GSSG ratio protect cancer cells from apoptosis.⁵ Furthermore, increased intracellular GSH and other antioxidants are critical toward promoting drug resistance against therapeutics that induce ROS in cancer cells.³¹ Our data so far suggest that CBS maintains the antioxidative capacity in HBC cells. We next hypothesized that CO, an inhibitor of CBS, could downregulate the antioxidant capacity of HBC cells and therefore increase their sensitivity toward a chemotherapeutic drug.

The anthracycline DOX is a chemotherapeutic drug that is cytotoxic via the generation of extremely high ROS levels.²² Viable cell counts, as determined by trypan blue exclusion, revealed that cells exposed to both [Mn(CO)₃] and DOX exhibited significantly lower cell viability than those cells treated with DOX alone (Figure 7A). To confirm that the lowered cell viability in DOX + [Mn(CO)₃] treated cells was indeed due to increased apoptosis, we performed flow cytometry to quantify Annexin V-FITC/PI double stained cells. Our data revealed that MCF-7 HBC cells, treated with both [Mn(CO)₃] and DOX, exhibited an ~37% increase in apoptosis versus those treated with DOX alone (Figure 7B,C). In order to check whether the increased ROS level contributes to heightening the sensitivity to DOX, we attenuated the levels of ROS in MCF-7 cells with the aid of PEG-CAT (mixture of poly(ethylene glycol) and catalase) and examined the extent of cell viability. In such experiments, the cell viability was significantly increased, indicating that in the presence of PEG-CAT, the combined ability of DOX + [Mn(CO)₃] to lower cell viability is significantly reduced (Supporting Information, Figure S1). This observation confirms that by interfering with the generation of ROS one can reduce the sensitization effect of [Mn(CO)₃] toward DOX in cancer cells. The observation also provides strong support to our hypothesis that the interaction of CO with CBS and the resulting increase in ROS are indeed the reason for the sensitization effects of the CO donor toward DOX.

DISCUSSION

Resistance to anticancer drugs remains a significant impediment to successful chemotherapy in HBC management.^{17–22} Numerous anticancer drugs elicit their tumor eliminating effects via the induction of ROS in cancer cells.^{22,32,33} Cancer cells, however, exhibit an increased antioxidative potential by maintaining an elevated battery of antioxidant metabolites and enzymes, which ultimately imparts chemotherapeutic drug resistance.^{25,31,34,35} The intracellular antioxidant capacity is dependent on the contribution of redox couples, which are pairs of reduced/oxidized species that can either donate or accept reducing equivalents.^{5,6} GSH/GSSG is one of the most important redox couples in the cell, as it is 500–1000-fold more abundant than other redox couples.²⁷ NADPH, a ubiquitous intracellular metabolite and product of the pentose phosphate pathway, supplies reducing equivalents to GSSG to regenerate GSH. Hence, both the GSH/GSSG and NADPH/NADP⁺ ratios are used as indicators of the intracellular antioxidative capacity, and increased GSH/GSSG and NADPH/NADP⁺

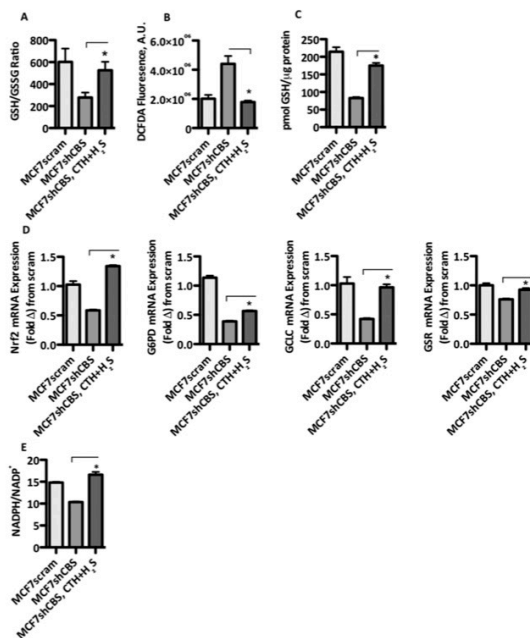


Figure 4. Exogenous addition of CTH and H₂S partially reverses some of the effects of CBS silencing in human breast cancer cells. CTH (100 μM) and GYY 4137 (40 μM) were added exogenously to serum-free media and allowed to incubate for 24 h. MCF7scram and MCF7shCBS cell lines were assayed alongside CTH/H₂S-treated MCF7shCBS cells for comparison purposes. (A) GSH/GSSG ratio in MCF7shCBS cells upon addition of CTH and H₂S. (B) Effect of exogenous addition of CTH and H₂S on intracellular ROS as measured by DCFDA fluorescence. (C) Total intracellular GSH in MCF7shCBS upon addition of CTH and H₂S. (D) Reverse transcriptase-quantitative PCR of Nrf2, G6PD, GCLC, and GSR mRNA. (E) Effect of extracellular treatment of MCF7shCBS with CTH and H₂S on the intracellular NADPH/NADP⁺ ratio. Data are representative of *n* = 3 independent experiments (**p* < 0.05).

ratios have been individually shown to be associated with chemotherapeutic resistance in HBC.^{5,36,37}

It is known that lowering the antioxidative capacity of cancer cells increases cellular sensitivity to chemotherapeutics.^{25,35} Therefore, this also allows for the use of decreased doses of chemotoxic drugs, thereby lowering detrimental side effects.^{17–21} However, drugs that would compromise the antioxidative capacities in cancer cells will do so in the surrounding normal cells as well, causing an increase in the incidences of adverse side effects.^{38,39} The reason for this is that these drugs will target antioxidative mechanism(s) that are common to both normal and cancer cells. Therefore, there is an unmet need to identify cancer-specific antioxidative pathways that could then be therapeutically targeted to increase the sensitivity of only cancer cells to relevant chemotherapeutics.

Along this line, the results of this investigation reveal that CBS, previously reported to be specifically expressed in HBC tissues and not in normal breast tissues,⁷ positively regulates the GSH/GSSG ratio in HBC cells. HBC exhibits a truncated version of the TSP, in which CBS catalyzes the conversion of homocysteine to CTH, but CTH is not converted into cysteine due to the absence of CGL (the enzyme that converts CTH

into cysteine).⁷ Despite such absence, our data strongly indicate that the GSH/GSSG ratio and GSH biosynthesis in HBC cells depend on CBS in both estrogen receptor positive and estrogen receptor negative breast cancer cells: MCF-7, MDA-MB-468, and Hs 578T (Figure 2A). As GSH is the most abundant antioxidant cofactor in the cell,^{29,30} silencing CBS and the resulting decrease in the GSH/GSSG ratio is expected to be accompanied by an increase in ROS. Indeed, we observed that silencing CBS resulted in an increase in ROS levels in at least three HBC cell lines (Figure 2B). The GSH/GSSG ratio in HBC cells is mainly dependent on the biosynthesis of GSH[†] from its constitutive amino acids glutamate, cysteine, and glycine.^{4,30} The rate-limiting step in GSH synthesis is the formation of γ-Glu-Cys from cysteine and glutamate, catalyzed by the enzyme CGL.³⁰ Upon silencing CBS, we observed a decrease in steady-state levels of both GSH and γ-Glu-Cys in HBC cells (Figure 2C,D).

With regards to the synthesis of γ-Glu-Cys, the rate-limiting step of GSH synthesis, the intracellular availability of cysteine is critical, as it is the rate-limiting substrate.² Our data indicate that silencing CBS results in a decrease in steady-state levels of intracellular cysteine. This is an interesting observation because

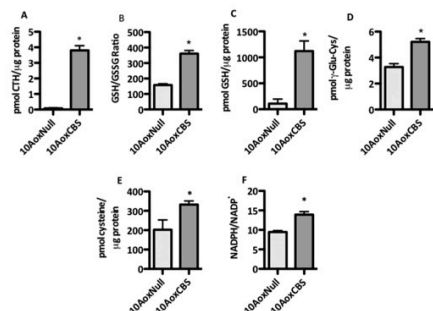


Figure 5. Overexpression of CBS in normal breast cell line MCF-10A increases the GSH/GSSG ratio. An adenoviral transduction system was used to establish a normal breast cell line that transiently overexpressed CBS enzyme (10AoxCBS). MCF-10A cells transduced with adenoviral particles containing the open reading frame for GFP were used as a transduction control (10AoxNull). Measurement of GSH metabolites was assayed by HPLC-MS. (A) Intracellular CTH levels in MCF-10A cells transiently overexpressing CBS (10AoxCBS) versus GFP control (10AoxNull) cells. (B) GSH/GSSG ratio in 10AoxCBS versus 10AoxNull control cells. (C–E) Effect of transient overexpression of CBS in MCF-10A cells on intracellular GSH, γ -Glu-Cys, and cysteine levels, as measured by HPLC-MS. (F) NADPH/NADP⁺ ratio upon overexpression of CBS in MCF-10A cells versus adenoviral control. Data are representative of $n = 3$ independent experiments ($*p < 0.05$).

despite the lack of a direct link between CTH and cysteine in HBC cells, silencing CBS led to depletion of internal cysteine levels (Figure 2E). Cysteine is either synthesized inside the cell by the TSP or taken up by specialized transporters, including xCT.³ Since HBC cells are compromised in their ability to synthesize endogenous cysteine (Figure 1C), its uptake is the main source of cysteine. Toward this, it is known that xCT is the main source of cysteine in HBC cells.^{40–42} Our current findings suggest that CBS positively regulates xCT activity. This is consistent with previous findings that H₂S, a metabolic product of CBS, enhances xCT activity.^{40,43}

In addition to the *de novo* synthesis of GSH, GSH can also be regenerated from GSSG via reduction by NADPH.⁴ In the present study, we observed that CBS silencing in HBC cells results in a significant decrease in the NADPH/NADP⁺ ratio versus scrambled controls (Figure 2F). One of the most important sources of NADPH production in the cell is the pentose phosphate pathway.⁴⁴ G6PD is the rate-limiting enzyme in this pathway, which produces NADPH. NADPH donates electrons to GSSG to generate two GSH, a redox reaction catalyzed by the enzyme GSR.⁴ G6PD, GSR, and GCLC together are known to be regulated by Nrf2, the most important regulator of antioxidant genes within the cell.²⁸ Our results indicated that Nrf2 gene expression is directly correlated to CBS expression in HBC cells since CBS-silenced breast cancer cells had significantly lower Nrf2 mRNA expression versus scrambled controls (Figure 3A). This observation is consistent with previous studies that have shown H₂S and Nrf2 to be positively associated with each other.^{45,46} As CBS silencing resulted in decreased Nrf2 expression, one would expect CBS silencing to correlate to downregulation of those

genes regulated by Nrf2. Indeed, our data revealed that GCLC, G6PD, and GSR gene expression decreases upon silencing of CBS in human breast cancer cells with respect to scrambled controls (Figure 3B–D). However, H₂S and CTH could also regulate γ -Glu-Cys synthetase/GCLC and GSR at the transcriptional and/or translational level. Further studies into this mechanism are warranted.

Once we established correlations between CBS and increased antioxidant capacity in HBC cells, we wanted to determine whether the enzymatic activity of CBS was indeed promoting the enhanced antioxidant capacity observed in cancer cells. Along this line, exogenous addition of H₂S and CTH to MCF7/shCBS cells resulted in a partial attenuation of the decrease in the GSH/GSSG ratio, intracellular ROS, and total GSH (Figure 4A–C). We hypothesize that this observation could be due in part to the positive relationship between H₂S and Nrf2^{45,46} that we discussed previously. Our findings are consistent with this inference since exogenous addition of H₂S and CTH resulted in a significant increase in Nrf2 mRNA expression, which in turn elicited increase in the antioxidant capacity as demonstrated by the upregulation of GCLC, G6PD, GSR, and NADPH/NADP⁺ ratio (Figure 4D,E).

In addition to the observation that H₂S and CTH reverse the downregulation of the GSH/GSSG caused by lentiviral-mediated silencing of CBS in HBC cells (Figure 4A), we found that CBS overexpression in MCF-10A could upregulate the GSH/GSSG ratio (Figure 5B). CBS expression also correlated with increases in steady-state levels of total GSH and its rate-determining intermediates γ -Glu-Cys and cysteine (Figure 5C–E).²⁴ With strong indications that CBS expression is directly connected to maintaining an increased GSH/GSSG ratio, we then assessed whether CO delivery by a novel photoCORM could inhibit CBS in HBC cells. Our data show that CO did inhibit CBS in HBC cells, decreasing the bioactivity of CBS (Figure 6A) as well as reducing the GSH/GSSG and NADPH/NADP⁺ ratios significantly in both estrogen receptor positive and estrogen receptor negative HBC cells alike (Figure 6B,C). Our findings are consistent with previous data that have shown CO to inhibit both isolated CBS^{9,10} and CBS in certain tissue types.^{11,12} CBS appears to be an ideal target for CO in the context of breast cancer therapy in that it is overexpressed in cancer cells versus normal cells,⁷ plays an important role in breast cancer cell cytoprotection,^{7,8} and has been shown in this study to promote antioxidant potential.

The antioxidant capacity of breast cancer cells is an important feature with regard to cancer therapy, as numerous anticancer drugs and radiation therapies work by increasing ROS in cancer cells.^{32,47} For these therapies, high GSH levels, increased GSH/GSSG ratios, and increased antioxidant capacity are markers for chemotherapeutic/radiation resistance.^{24,25} We have shown a clear connection between CBS activity and maintaining elevated GSH levels in breast cancer cells. On the basis of these results, we hypothesized that inhibition of CBS via CO delivery by photoCORMs, such as [Mn(CO)₃]₂, could be an affective approach toward decreasing therapeutic resistance of breast cancer cells. Herein, we provide strong preliminary evidence supporting this claim, as breast cancer cells treated with CO and DOX exhibited a ~43% increase in apoptosis versus those cells treated with DOX alone (Figure 7A–C). This is consistent with previous studies that have shown similar sensitizing effects from both endogenous and exogenous sources of CO.^{48–50} Incidentally, control

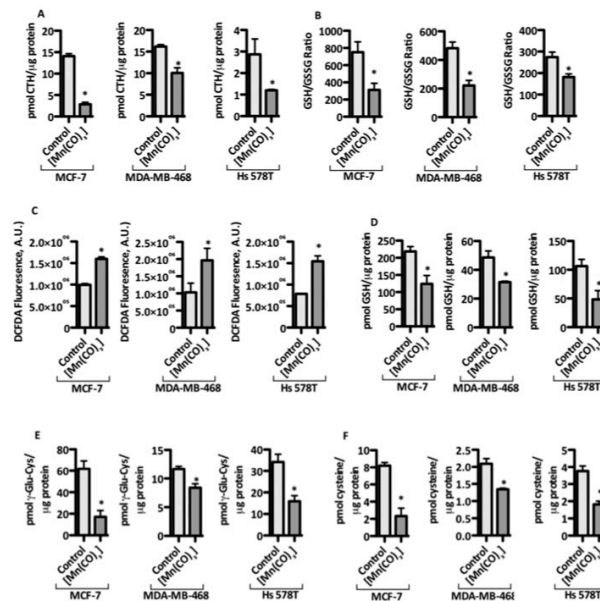


Figure 6. CO, delivered by photoCORM [$\text{Mn}(\text{CO})_3$], inhibits CBS activity and lowers the GSH/GSSG ratio in human breast cancer cells. Control cells were handled identically to CO treated-cells, but they were not exposed to visible light. (A) Effect of CO treatment on intracellular ROS, as measured by DCFDA fluorescence, in three human breast cancer cell lines: MCF-7, MDA-MB-468, and Hs 578T. (B) GSH/GSSG ratio in three breast cancer cell lines upon treatment with CO. (C) Intracellular ROS, measured by DCFDA fluorescence, in CO-treated breast cancer cells versus control cells. (D–F) Steady-state levels of intracellular GSH, γ -Glu-Cys, and cysteine in three human breast cancer cell lines exposed to CO versus respective controls. Data represents $n = 3$ independent experiments ($*p < 0.05$).

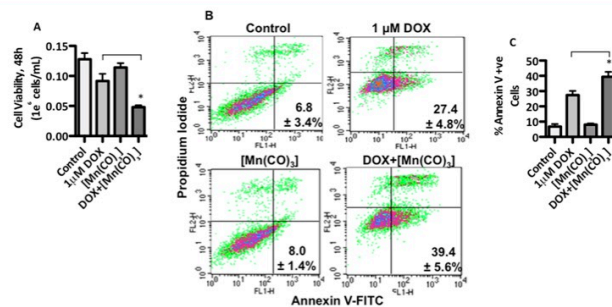


Figure 7. CO sensitizes MCF-7 breast cancer cells to DOX. (A) Viable cell count of MCF-7 cells 48 h after pretreatment with 121 μM [$\text{Mn}(\text{CO})_3$] \pm visible light followed by treatment with either 1 μM DOX or the appropriate vehicle control. (B, C) Representative plots and graphical representation of Annexin V-FITC/propidium iodide staining of cells 48 h after pretreatment with \pm CO followed by treatment with either 1 μM DOX or the appropriate vehicle control, as measured by flow cytometry. Data represents $n = 3$ independent experiments ($*p < 0.05$).

experiments in our laboratory demonstrated that Mn^{2+} ions themselves (concentration = 120 μM) and CO-spent iCORM (concentration = 120 μM) did not sensitize the breast cancer cells (Figure S2). Also, a similar enhancement of sensitivity of

breast cancer cells has been noted with [$\text{Mn}(\text{CO})_3$] + Paclitaxel (Figure S3), indicating that the mechanism of action of CO could be a more general effect and not specific or limited to DOX. Recently, we incorporated similar photoCORMs in

mesoporous Al-MCM-41 (silica-based) nanoparticles that get readily internalized by HBC cells and cause their dose-dependent eradication upon illumination.⁵¹ We anticipate that selective accumulation of such nanoparticle-photoCORM composites within tumors, followed by illumination (through fiberoptics), could circumvent therapeutic resistance often encountered in breast cancer therapy.

CONCLUSIONS

While it has been suggested that induction of oxidative stress could target cancer cells specifically,⁵ further studies into cancer cell metabolism will help to identify and define therapies that are more effective, have fewer side effects, utilize lower concentrations of drugs/radiation, and minimize drug resistance. The results from this study contribute to the groundwork by which CORMs may be utilized for the treatment of cancer. Our data provide needed insight into the metabolic profile of antioxidative potential and redox homeostasis in breast cancer cells. We have also shown that CBS expression and its enzymatic activity are important for maintaining an increased GSH/GSSG ratio and a robust antioxidative capacity. Furthermore, a photoCORM can inhibit CBS activity and perturb the redox environment in breast cancer cells to the point of increasing sensitivity to the chemotherapeutic DOX. It is therefore evident that CO could be employed in adjuvant therapy of breast cancer to circumvent drug resistant and that smart applications of photoCORMs could provide controlled doses of CO to achieve such a goal.

EXPERIMENTAL SECTION

Materials and Reagents. $[\text{Mn}(\text{CO})_5]$ was synthesized by following a published procedure and analyzed to confirm purity before application.¹³ Protease inhibitor cocktail (P8340), puromycin (P8833), and all other chemicals were purchased from Sigma-Aldrich (St. Louis, MO) unless otherwise stated. The primary antibodies, namely, anti-CBS (sc-133208) and anti-GAPDH (sc-47724), were procured from Santa Cruz Biotechnology (Santa Cruz, CA).

Cell Culture and Treatments. MCF-7, MDA-MB-468, Hs 578T, and MCF-10A were obtained from American Type Culture Collection (Manassas, VA). MDA-MB-468 and Hs 578T cells were grown in 1× DMEM supplemented with 10 mM HEPES buffer, 1× antibiotic-antimycotic, and 10% fetal bovine serum (FBS). MCF-7 cells were grown in 1× DMEM supplemented with 1 $\mu\text{g}/\text{mL}$ insulin, 1 mM sodium pyruvate, 1× antibiotic-antimycotic, and 10% FBS. MCF-10A cells were grown in 50/50 DMEM/F12 supplemented with 20 ng/mL epidermal growth factor, 0.5 mg/mL hydrocortisone, 100 ng/mL cholera toxin, 10 $\mu\text{g}/\text{mL}$ insulin, 1× Pen/Strep, and 5% horse serum. Cells were passaged no more than 10 times postprocurement from the supplier, and their genetic characteristics were tested regularly. Additionally, the absence of mycoplasma was determined regularly with a MycoAlert mycoplasma detection kit (LT07-318) from Lonza (Basel, Switzerland). All treatments, including exogenous addition of 100 μM CTH and 40 μM GY 4137, concentrations similar to those used in previous studies,^{7,8} were performed under serum-free conditions unless otherwise noted.

Generation of Stable Cell Lines. Stable cell lines in which CBS was silenced were generated for MCF-7, MDA-MB-468, and Hs578T HBC cells with short hairpin RNA (shRNA) using lentiviral particles obtained from Santa Cruz Biotechnology (Santa Cruz, CA). CBS-silenced cell lines were transfected with lentiviral particles containing three to five lentiviral plasmids, each encoding a 19–25 nucleotide shRNA complementary to CBS mRNA (sc-60335-V) to knockdown CBS gene expression. Stable control cell lines were transfected with lentiviral particles containing a plasmid encoding a scrambled shRNA sequence (sc-108080) that does not lead to the specific degradation of any specific mRNA. Cells were selected with 1 $\mu\text{g}/\text{mL}$ puromycin until

resistant colonies were identified and propagated. MCF-7, MDA-MB-468, and Hs 578T cells that survived puromycin selection after transfection with shRNA were annotated as MCF7scram/MCF7shCBS, 468scram/468shCBS, and Hs scram/Hs shCBS for scrambled controls and CBS-silenced cells, respectively.

Measurement of Metabolites via High Performance Liquid Chromatography–Mass Spectrometry. GSH, GSSG, γ -Glu-Cys, cysteine, and CTH were quantified via high performance liquid chromatography–mass spectrometry (HPLC-MS) as described.^{7,8} Cells (5×10^6) were lysed via three freeze/thaw cycles in 200 μL of 10 mM *N*-ethylmaleimide (NEM) + 10 mM ammonium acetate, pH 7.4. After lysis, methanol (800 μL) was added and the samples were vortexed. Following centrifugation (16000g, 5 min) of the samples, supernatants were transferred to microcentrifuge tubes and dried by vacuum centrifugation. Methanol (100 μL) was added to the dried samples, and they were dried under a stream of nitrogen. Benzene (100 μL) was added, and the samples were dried under a stream of nitrogen. Next, each sample was treated with 100 μL of 3 *N* methanolic HCl for 60 min at 60 °C. Then, the samples were dried under a nitrogen stream. All samples were finally dissolved in 100 μL of H_2O and centrifuged at 16000g for 5 min. The supernatants were transferred to liquid chromatography (LC) injector vials. Aliquots (8 μL) of the solutions were injected onto a Kinetex XB-C18, 100 \times 2.1 mm, 1.7 μm particle size, 100 Å pore diameter, reverse phase column from Phenomenex (Torrance, CA). The column was equilibrated with 85% 0.1 mM perfluorooctanoic acid in water (eluant A) and 15% 0.1 mM perfluorooctanoic acid in acetonitrile (eluant B) and eluted at 100 $\mu\text{L}/\text{min}$ with increasing concentration of eluant B (min/% B: 0/15, 5/15, 35/50, 33/15, 45/15). The eluant was directed to an Agilent Jet Stream electrospray ionization (ESI) source connected to a triple quadrupole mass spectrometer (Agilent 6460) operating in the positive ion tandem mass spectrometric multiple reaction-monitoring (MRM) mode. The intensities of the CTH (461 \rightarrow 318, t_{R} 27.88 min), cysteine-NEM conjugate (261 \rightarrow 244, t_{R} 24.06 min), GSH-NEM conjugate (461 \rightarrow 318, t_{R} 26.06 min), GSSG (669 \rightarrow 383, t_{R} 28.18 min), and γ -Glu-Cys-NEM conjugate (404 \rightarrow 244, t_{R} 26.59 min) parent to fragment transitions were recorded using previously optimized settings. With each independent experiment, standards were prepared containing known concentrations of CTH (0, 20, 40, 40, 80, 160 pmol), cysteine (0, 10, 20, 40, 80 pmol), GSH (0, 100, 200, 400, 800 pmol), GSSG (0, 25, 50, 100, 200 pmol), and γ -Glu-Cys (0, 100, 200, 400, 800 pmol). The peak areas of the standards of CTH, cysteine, GSH, GSSG, and γ -Glu-Cys were used to construct calibration curves. The amount of CTH, cysteine, GSH, GSSG, and γ -Glu-Cys in each biological sample was calculated by interpolation from the curves.

Detection of Reactive Oxygen Species. The intracellular concentration of ROS was determined with 2',7'-dichlorodihydrofluorescein diacetate (hereafter, DCFDA). Cells were treated with 50 μM DCFDA for 30 min at 37 °C. Cells were washed twice with phosphate-buffered saline (PBS) + 0.5% FBS and then analyzed by flow cytometry using a C6 flow cytometer and CFlow software from Becton Dickinson Biosciences (Franklin Lakes, NJ).

NADPH/NADP⁺ Assay. Intracellular nucleotides NADPH and NADP⁺ were measured using the NADP/NADPH assay kit (ab65349), which was procured from Abcam (Cambridge, MA).

RNA Purification and Reverse Transcriptase-Quantitative PCR. Total RNA was extracted using the RNeasy mini kit (no. 74106) obtained from Qiagen (Valencia, CA). RNA concentrations were measured using a NanoDrop 2000c spectrophotometer (Nanodrop, Wilmington, DE). First-strand cDNA synthesis was performed using the iScript cDNA synthesis kit from Bio-Rad (Hercules, CA). Relative levels of mRNA were assayed for the following genes: β -actin, nuclear factor erythroid 2-related factor 2 (Nrf2), glucose 6-phosphate dehydrogenase (G6PD), the catalytic subunit of γ -glutamylcysteine synthetase (GCLC), and glutathione reductase (GSR). The primer sequences used were as follows: β -actin (forward: 5'-ATTGGCAATG-AGCGGTTCC-3', reverse: 5'-GGATGCCACAGGACTCCATC-3'), Nrf2 (forward: 5'-GAGAGCCAGTCTTCATTGC-3', reverse: 5'-TGCTCAATGTCCTGTTGCAT-3'), G6PD (forward: 5'-ATCGA-

CCACTACCTGGGCAA-3', reverse: 5'-TTCTGCATCAGTCC-CGGA-3'), CGLC (forward: 5'-AGTTCAATACAGTTGAGG-3', reverse: 5'-TACTGATCCTATAGTTAT-3') and GSR (forward: 5'-TTGTAAGTGGCGTGATACATCGGG-3', reverse: 5'-AACAT-CCCAACTGTGGTCTTCAGC-3'). Quantitative PCR (qPCR) was performed on an ABI (Applied Biosystems) 7900 HT thermal cycler in standard mode using SYBR Green (Life Technologies, Carlsbad, CA) for 40 cycles. Each reaction was run in triplicate in three independent experiments. Relative mRNA expression values were calculated using the $2^{-\Delta\Delta C_T}$ method.

Overexpression of CBS. Human CBS overexpression plasmids (Ad-h-CBS, no. ADV-204180) and the corresponding control plasmids (Ad-CMV-null, no. 1300), packaged in adenovirus, were obtained from Vector Biolabs (Malvern, PA). Briefly, MCF-10A cells were seeded into 100 mm dishes, grown to ~95% confluence, and then infected with the CBS overexpression or control viral stocks of 10^5 – 10^6 PFU/mL. After 24 h, the cells were washed, fresh medium was added, and the cells were used for subsequent experiments including HPLC-MS, NADP⁺/NADPH assays, and western blot analysis.

Western Blot Analysis. Whole cell lysates were prepared from cells after various treatments in lysis buffer containing 50 mM Hepes (pH 7.5), 1 mM DTT, 150 mM NaCl, 1 mM EDTA, 0.1% Tween 20, 10% glycerol, 10 mM β -glycerophosphate, 1 mM NaF, 0.1 mM orthovanadate, 10 mg/mL leupeptin, 10 mg/mL aprotinin, and 0.1 mM phenylmethylsulfonyl fluoride (PMSF). The soluble cell lysate protein concentrations were quantified by Bradford assay. Cell lysate (20 μ g) from each sample was separated on a 10% SDS-PAGE gel and transferred to poly(vinylidene difluoride) (PVDF) membranes. Membrane blocking was done with 5% nonfat dried milk and incubated overnight at 4 °C. Primary (1:1000 dilution) and horse radish peroxidase (HRP)-conjugated secondary (1:10000 dilution) antibody incubations were done at 4 °C overnight and 1 h at room temperature, respectively. Immunofluorescent signals were detected using Pierce ECL Plus western blotting substrate (no. 32132) from ThermoFisher Scientific (Waltham, MA).

Light-Activated [Mn(CO)₃] Treatment. Cells were treated with 120 μ M [Mn(CO)₃] under serum-free conditions as previously described.¹³ One million cells were placed in 100 mm tissue culture dishes and allowed to seed overnight. The next day, cells were treated with 120 μ M [Mn(CO)₃] in the dark. For experimental (i.e., CO-treated) samples, cells were exposed to visible light for 30 min at room temperature and then allowed to incubate at 37 °C + 5% CO₂ for 1 h. Next, the media was aspirated, and the cells were washed three times with 1× PBS, followed by the addition of serum-containing media. The cells were then allowed to incubate at 37 °C + 5% CO₂ for 6 h and finally assayed for GSH and GSH metabolites by HPLC-MS and for ROS by DCFDA fluorescence. For control samples, cells were handled exactly the same as experimental samples, but they were not exposed to light.

DOX and [Mn(CO)₃] Treatments. For assaying the chemosensitizing effects of CO, cells were pretreated with 120 μ M [Mn(CO)₃] as mentioned above with the exception of the addition of serum-free media after CO treatment. Following this, either 1 μ M DOX or vehicle control (dimethyl sulfoxide, DMSO) was added to respective tissue culture dishes. Cells were allowed to incubate at 37 °C + 5% CO₂ for 24 h, after which cells were assayed for viability and apoptosis.

Cell Viability Assay. A Vi-Cell XR cell viability analyzer from Beckman Coulter (Brea, CA) was used to determine cell viability by the trypan blue exclusion method. The number of viable cells, 24 h post-treatment, was determined in triplicate. Data represents the mean \pm SEM of three independent experiments.

Detection of Apoptosis. Apoptosis/necrosis of DOX and [Mn(CO)₃]-treated cells was determined with a FITC Annexin V-apoptosis detection kit I, containing Annexin V-FITC and propidium iodide (BD Pharmingen, no. 556570). After DOX/[Mn(CO)₃] treatment, cells were harvested and counted. Aliquots of one million cells were washed twice with cold 1× PBS and resuspended in 100 μ L of 1× Annexin V binding buffer. The cells were transferred to 5 mL

culture tubes and stained with 5 μ L Annexin V-FITC and 5 μ L of propidium iodide. Cells were incubated for 15 min at room temperature in the dark; then, 400 μ L of 1× Annexin V binding buffer was added to the samples, and the cells were analyzed with a BD FACScan flow cytometer (Becton Dickinson Biosciences). Data were acquired and analyzed using BD CellQuest software.

Statistical Analysis. Data are presented as the mean \pm SEM. Statistical comparison between two groups was performed using Student's *t* test. Statistical comparisons between more than two groups were performed using ANOVA with posthoc Tukey's test. *P* values less than 0.05 were considered statistically significant (**p* < 0.05).

■ ASSOCIATED CONTENT

Supporting Information

The Supporting Information is available free of charge on the ACS Publications website at DOI: 10.1021/acs.jmedchem.7b00476.

Cell viability studies demonstrating the attenuation of the ability of DOX + [Mn(CO)₃] to induce cell death via interfering with the ROS levels with the aid of PEG-CAT (Figure S1), the inability of Mn²⁺ and iCORM to sensitize MCF-7 cells toward DOX (Figure S2), and the ability of [Mn(CO)₃] to sensitize MCF-7 cells toward Paclitaxel (Figure S3) (PDF)

■ AUTHOR INFORMATION

Corresponding Authors

*(S.S.) E-mail: ssen@mednet.ucla.edu. Phone: (310) 825-8022.

*(P.K.M.) E-mail: pradip@ucsc.edu. Phone: (831) 423-7125.

ORCID

Pradip K. Mascharak: 0000-0002-7044-944X

Notes

The authors declare no competing financial interest.

■ ACKNOWLEDGMENTS

Financial support from the NSF (grant DMR-1409335 to P.K.M.) and funding from the Department of Obstetrics and Gynecology, David Geffen School of Medicine at UCLA, are gratefully acknowledged.

■ ABBREVIATIONS USED

HBC, human breast cancer; [Mn(CO)₃], Mn(CO)₃(phen)-(PTA)]CF₃SO₃; photoCORM, photoactive CO-releasing molecule; TSP, transsulfuration pathway

■ REFERENCES

- (1) Mosharov, E.; Cranford, M. R.; Banerjee, R. The quantitatively important relationship between homocysteine metabolism and glutathione synthesis by the transsulfuration pathway and its regulation by redox changes. *Biochemistry* **2000**, *39*, 13005–13011.
- (2) Finkelstein, J. D. The metabolism of homocysteine: pathways and regulation. *Eur. J. Pediatr.* **1998**, *157*, S40–S44.
- (3) Sato, H.; Tamba, M.; Ishii, T.; Bannai, S. Cloning and expression of a plasma membrane cystine/glutamate exchange transporter composed of two distinct proteins. *J. Biol. Chem.* **1999**, *274*, 11455–11458.
- (4) Lu, S. C. Regulation of glutathione synthesis. *Mol. Aspects Med.* **2009**, *30*, 42–59.
- (5) Gorrini, C.; Harris, I. S.; Mak, T. W. Modulation of oxidative stress as an anticancer strategy. *Nat. Rev. Drug Discovery* **2013**, *12*, 931–947.
- (6) Meister, A. Glutathione deficiency produced by inhibition of its synthesis, and its reversal-applications in research and therapy. *Pharmacol. Ther.* **1991**, *51*, 155–194.

- (7) Sen, S.; Kawahara, B.; Gupta, D.; Tsai, R.; Khachatryan, M.; Roy-Chowdhuri, S.; Bose, S.; Yoon, A.; Faull, K.; Farias-Eisner, R.; Chaudhuri, G. Role of cystathionine beta-synthase in human breast cancer. *Free Radical Biol. Med.* **2015**, *86*, 228–238.
- (8) Sen, S.; Kawahara, B.; Mahata, S. K.; Tsai, R.; Yoon, A.; Hwang, L.; Hu-Moore, K.; Villanueva, C.; Vajihuddin, A.; Parameshwar, P.; You, M.; Bhaskar, D. L.; Gomez, O.; Faull, K. F.; Farias-Eisner, R.; Chaudhuri, G. Cystathionine: A novel oncometabolite in human breast cancer. *Arch. Biochem. Biophys.* **2016**, *604*, 95–102.
- (9) Kabil, O.; Weeks, C. L.; Carballal, S.; Gherasim, C.; Alvarez, B.; Spiro, T. G.; Banerjee, R. Reversible Heme-dependent regulation of human cystathionine beta-synthase by a flavoprotein oxidoreductase. *Biochemistry* **2011**, *50*, 8261–8263.
- (10) Taoka, S.; West, M.; Banerjee, R. Characterization of the heme and pyridoxal phosphate cofactors of human cystathionine beta-synthase reveals nonequivalent active sites. *Biochemistry* **1999**, *38*, 2738–2744.
- (11) Yamamoto, T.; Takano, N.; Ishiwata, K.; Ohmura, M.; Nagahata, Y.; Matsuura, T.; Kamata, A.; Sakamoto, K.; Nakanishi, T.; Kubo, A.; Hishiki, T.; Suematsu, M. Reduced methylation of PFKFB3 in cancer cells shunts glucose toward the pentose phosphate pathway. *Nat. Commun.* **2014**, *5*, 3480.
- (12) Shintani, T.; Iwabuchi, T.; Soga, T.; Kato, Y.; Yamamoto, T.; Takano, N.; Hishiki, T.; Ueno, Y.; Ikeda, S.; Sakuragawa, T.; Ishikawa, K.; Goda, N.; Kitagawa, Y.; Kajimura, M.; Matsumoto, K.; Suematsu, M. Cystathionine beta-synthase as a carbon monoxide-sensitive regulator of bile excretion. *Hepatology* **2009**, *49*, 141–150.
- (13) Chakraborty, I.; Carrington, S. J.; Roseman, G.; Mascharak, P. K. Synthesis, structures, and CO release capacity of a family of water-soluble photoCORMs: Assessment of the biocompatibility and their phototoxicity toward human breast cancer cells. *Inorg. Chem.* **2017**, *56*, 1534–1545.
- (14) Carrington, S. J.; Chakraborty, I.; Bernard, J. M. L.; Mascharak, P. K. A theranostic two-tone luminescent photoCORM derived from Re(I) and (2-Pyridyl)-benzothiazole: Trackable CO delivery to malignant cells. *Inorg. Chem.* **2016**, *55*, 7852–7858.
- (15) Carrington, S. J.; Chakraborty, I.; Bernard, J. M. L.; Mascharak, P. K. Synthesis and characterization of a "turn-on" photoCORM for trackable CO delivery to biological targets. *ACS Med. Chem. Lett.* **2014**, *5*, 1324–1328.
- (16) Carrington, S. J.; Chakraborty, I.; Mascharak, P. K. Rapid CO release from a Mn(I) carbonyl complex derived from azopyridine upon exposure to visible light and its phototoxicity toward malignant cells. *Chem. Commun.* **2013**, *49*, 11254–11256.
- (17) Wang, X. J.; Sun, Z.; Villeneuve, N. F.; Zhang, S.; Zhao, F.; Li, Y. J.; Chen, W. M.; Yi, X. F.; Zheng, W. X.; Wondrak, G. T.; Wong, P. K.; Zhang, D. D. Nrf2 enhances resistance of cancer cells to chemotherapeutic drugs, the dark side of Nrf2. *Carcinogenesis* **2008**, *29*, 1235–1243.
- (18) Pelicano, H.; Carney, D.; Huang, P. ROS stress in cancer cells and therapeutic implications. *Drug Resist. Updates* **2004**, *7*, 97–110.
- (19) Hayes, J. D.; McLellan, L. I. Glutathione and glutathione-dependent enzymes represent a co-ordinately regulated defense against oxidative stress. *Free Radical Res.* **1999**, *31*, 273–300.
- (20) Ramanathan, B.; Jan, K. Y.; Chen, C. H.; Hour, T. C.; Yu, H. J.; Pu, Y. S. Resistance to paclitaxel is proportional to cellular total antioxidant capacity. *Cancer Res.* **2005**, *65*, 8455–8460.
- (21) Hecht, F.; Pessoa, C. F.; Gentile, L. B.; Rosenthal, D.; Carvalho, D. P.; Fortunato, R. S. The role of oxidative stress on breast cancer development and therapy. *Tumor Biol.* **2016**, *37*, 4281–4291.
- (22) Conklin, K. A. Chemotherapy-associated oxidative stress: Impact on chemotherapeutic effectiveness. *Integr. Cancer Ther.* **2004**, *3*, 294–300.
- (23) Barrera, G. Oxidative stress and lipid peroxidation products in cancer progression and therapy. *ISRN Oncol.* **2012**, *2012*, 137289.
- (24) Ryu, C. S.; Kwak, H. C.; Lee, J. Y.; Oh, S. J.; Phueng, N. T.; Kang, K. W.; Kim, S. K. Elevation of cysteine consumption in tamoxifen-resistant MCF-7 cells. *Biochem. Pharmacol.* **2013**, *85*, 197–206.
- (25) Tai, D. J.; Jin, W. S.; Wu, C. S.; Si, H. W.; Cao, X. D.; Guo, A. J.; Chang, J. C. Changes in intracellular redox status influence multidrug resistance in gastric adenocarcinoma cells. *Exp. Ther. Med.* **2012**, *4*, 291–296.
- (26) Anderson, M. E. Glutathione: an overview of biosynthesis and modulation. *Chem.-Biol. Interact.* **1998**, *111–112*, 1–14.
- (27) Schafer, F. Q.; Buettner, G. R. Redox environment of the cell as viewed through the redox state of the glutathione disulfide/glutathione couple. *Free Radical Biol. Med.* **2001**, *30*, 1191–1212.
- (28) Sporn, M. B.; Liby, K. T. NRF2 and cancer: the good, the bad and the importance of context. *Nat. Rev. Cancer* **2012**, *12*, 564–571.
- (29) Taguchi, K.; Motohashi, H.; Yamamoto, M. Molecular mechanisms of the Keap1-Nrf2 pathway in stress response and cancer evolution. *Genes Cells* **2011**, *16*, 123–140.
- (30) Meister, A. Glutathione metabolism and its selective modification. *J. Biol. Chem.* **1988**, *263*, 17205–17208.
- (31) Diehn, M.; Cho, R. W.; Lobo, N. A.; Kalisky, T.; Dorie, M. J.; Kulp, A. N.; Qian, D. L.; Lam, J. S.; Ailles, L. E.; Wong, M. Z.; Joshua, B.; Kaplan, M. J.; Wapnir, I.; Dirbas, F. M.; Somlo, G.; Garberoglio, C.; Paz, B.; Shen, J.; Lau, S. K.; Quake, S. R.; Brown, J. M.; Weissman, I. L.; Clarke, M. F. Association of reactive oxygen species levels and radioresistance in cancer stem cells. *Nature* **2009**, *458*, 780–U123.
- (32) Kaufmann, S. H.; Earnshaw, W. C. Induction of apoptosis by cancer chemotherapy. *Exp. Cell Res.* **2000**, *256*, 42–49.
- (33) Berndtsson, M.; Hagg, M.; Panaretakis, T.; Havelka, A. M.; Shoshan, M. C.; Linder, S. Acute apoptosis by cisplatin requires induction of reactive oxygen species but is not associated with damage to nuclear DNA. *Int. J. Cancer* **2007**, *120*, 175–180.
- (34) Scarbrough, P. M.; Mapuskar, K. A.; Mattson, D. M.; Gius, D.; Watson, W. H.; Spitz, D. R. Simultaneous inhibition of glutathione- and thioredoxin-dependent metabolism is necessary to potentiate 17AAG-induced cancer cell killing via oxidative stress. *Free Radical Biol. Med.* **2012**, *52*, 436–443.
- (35) Backos, D. S.; Franklin, C. C.; Reigan, P. The role of glutathione in brain tumor drug resistance. *Biochem. Pharmacol.* **2012**, *83*, 1005–1012.
- (36) Lewandowicz, G. M.; Britt, P.; Elgie, A. W.; Williamson, C. J.; Coley, H. M.; Hall, A. G.; Sargent, J. M. Cellular glutathione content, in vitro chemoresistance, and the effect of BSO modulation in samples derived from patients with advanced ovarian cancer. *Gynecol. Oncol.* **2002**, *85*, 298–304.
- (37) Gamcsik, M. P.; Kasibhata, M. S.; Teeter, S. D.; Colvin, O. M. Glutathione levels in human tumors. *Biomarkers* **2012**, *17*, 671–691.
- (38) Trachootham, D.; Zhou, Y.; Zhang, H.; Demizu, Y.; Chen, Z.; Pelicano, H.; Chiao, P. J.; Achanta, G.; Arlinghaus, R. B.; Liu, J. S.; Huang, P. Selective killing of oncogenically transformed cells through a ROS-mediated mechanism by beta-phenylethyl isothiocyanate. *Cancer Cell* **2006**, *10*, 241–252.
- (39) Montero, A. J.; Diaz-Montero, C. M.; Deutsch, Y. E.; Hurler, J.; Koniaris, L. G.; Rumboldt, T.; Yasir, S.; Jorda, M.; Garret-Mayer, E.; Avisar, E.; Slingerland, J.; Silva, O.; Welsh, C.; Schuhwerk, K.; Seo, P.; Pegram, M. D.; Gluck, S. Phase 2 study of neoadjuvant treatment with NOV-002 in combination with doxorubicin and cyclophosphamide followed by docetaxel in patients with HER-2 negative clinical stage II-IIIc breast cancer. *Breast Cancer Res. Treat.* **2012**, *132*, 215–223.
- (40) Habib, E.; Linher-Melville, K.; Lin, H. X.; Singh, G. Expression of xCT and activity of system X-c(-) are regulated by NRF2 in human breast cancer cells in response to oxidative stress. *Redox Biol.* **2015**, *5*, 33–42.
- (41) Timmerman, L. A.; Holton, T.; Yuneva, M.; Louie, R. J.; Padro, M.; Daemen, A.; Hu, M.; Chan, D. A.; Ethier, S. P.; van 't Veer, L. J.; Polyak, K.; McCormick, F.; Gray, J. W. Glutamine sensitivity analysis identifies the xCT antiporter as a common triple-negative breast tumor therapeutic target. *Cancer Cell* **2013**, *24*, 450–465.
- (42) Ishimoto, T.; Nagano, O.; Yae, T.; Tamada, M.; Motohara, T.; Oshima, H.; Oshima, M.; Ikeda, T.; Asaba, R.; Yagi, H.; Masuko, T.; Shimizu, T.; Ishikawa, T.; Kai, K.; Takahashi, E.; Imamura, Y.; Baba, Y.; Ohmura, M.; Suematsu, M.; Baba, H.; Saya, H. CD44 Variant regulates redox status in cancer cells by stabilizing the xCT subunit of

system xc⁻ and thereby promotes tumor growth. *Cancer Cell* **2011**, *19*, 387–400.

(43) Majid, A. S. A.; Majid, A.; Yin, Z. Q.; Ji, D. Slow regulated release of H₂S inhibits oxidative stress induced cell death by influencing certain key signaling molecules. *Neurochem. Res.* **2013**, *38*, 1375–1393.

(44) Ramos-Martinez, J. I. The regulation of the pentose phosphate pathway: Remember Krebs. *Arch. Biochem. Biophys.* **2017**, *614*, 50–52.

(45) Hourihan, J. M.; Kenna, J. G.; Hayes, J. D. The gasotransmitter hydrogen sulfide induces Nrf2-target genes by inactivating the Keap1 ubiquitin ligase substrate adaptor through formation of a disulfide bond between Cys-226 and Cys-613. *Antioxid. Redox Signaling* **2013**, *19*, 465–481.

(46) Islam, K. N.; Polhemus, D. J.; Donnarumma, E.; Brewster, L. P.; Lefer, D. J. Hydrogen sulfide levels and nuclear factor-erythroid 2-related factor 2 (NRF2) activity are attenuated in the setting of critical limb ischemia (CLI). *J. Am. Heart Assoc.* **2015**, *4*, e001986.

(47) Dioum, E. M.; Rutter, J.; Tuckerman, J. R.; Gonzalez, G.; Gilles-Gonzalez, M. A.; McKnight, S. L. NPAS2: A gas-responsive transcription factor. *Science* **2002**, *298*, 2385–2387.

(48) Wegiel, B.; Gallo, D.; Csizmadia, E.; Harris, C.; Belcher, J.; Vercellotti, G. M.; Penacho, N.; Seth, P.; Sukhatme, V.; Ahmed, A.; Pandolfi, P. P.; Helczynski, L.; Bjartell, A.; Persson, J. L.; Otterbein, L. E. Carbon monoxide expedites metabolic exhaustion to inhibit tumor growth. *Cancer Res.* **2013**, *73*, 7009–7021.

(49) Vitek, L.; Gbelcova, H.; Muchova, L.; Vanova, K.; Zelenka, J.; Konickova, R.; Suk, J.; Zadinova, M.; Knejzlik, Z.; Ahmad, S.; Fujisawa, T.; Ahmed, A.; Ruml, T. Antiproliferative effects of carbon monoxide on pancreatic cancer. *Dig. Liver Dis.* **2014**, *46*, 369–375.

(50) Song, R. P.; Zhou, Z. H.; Kim, P. K. M.; Shapiro, R. A.; Liu, F.; Ferran, C.; Choi, A. M. K.; Otterbein, L. E. Carbon monoxide promotes Fas/CD95-induced apoptosis in Jurkat cells. *J. Biol. Chem.* **2004**, *279*, 44327–44334.

(51) Chakraborty, I.; Carrington, S. J.; Hauser, J.; Oliver, S. R. J.; Mascharak, P. K. Rapid eradication of human breast cancer cells through trackable light-triggered CO delivery by mesoporous silica nanoparticles packed with a designed photoCORM. *Chem. Mater.* **2015**, *27*, 8387–8397.

Supplementary Material

for

**Attenuation of Antioxidant Capacity in Human Breast Cancer Cells by Carbon Monoxide Through
Inhibition of Cystathionine β -synthase Activity: Implications in Chemotherapeutic Drug Sensitivity**

Brian Kawahara[†], Travis Moller[§], Kayla Hu-Moore[¶], Samantha Carrington[†], Kym F. Faull[§], Suvajit Sen^{*¶} and
Pradip K. Mascharak^{*†}

[†]Department of Chemistry and Biochemistry, University of California, Santa Cruz, CA 95064

*[¶]Contribution from Department of Obstetrics and Gynecology, David Geffen School of Medicine at University
of California, Los Angeles, Los Angeles, CA 90095*

*[§]Semel Institute for Neuroscience and Human Behavior, University of California at Los Angeles, Los Angeles,
CA 90095, USA*

List of Contents

Fig S1. Interference with generation of reactive oxygen species (ROS) attenuates ability of 120 μM $[\text{Mn}(\text{CO})_3]$ to sensitize breast cancer cells to DOX.

Fig S2. Mn^{2+} and inactivated $[\text{Mn}(\text{CO})_3]$ (iCORM) do not sensitize MCF-7 breast cancer cells to DOX.

Fig S3. CO sensitizes MCF-7 breast cancer cells to paclitaxel, another chemotherapeutic.

S2

=

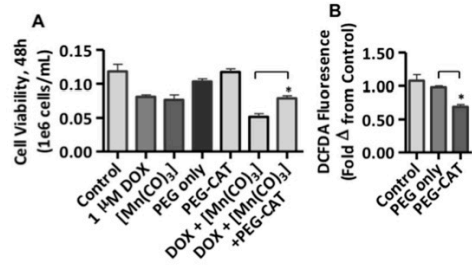


Fig S1. Interference with generation of reactive oxygen species (ROS) attenuates ability of 120 μ M [Mn(CO)₃] to sensitize breast cancer cells to DOX. (A) Viable cell count of MCF-7 cells 48h after pre-treatment with: 120 μ M [Mn(CO)₃] +/- visible light, polyethylene glycol only (PEG, 0.5 mg/mL) or 500U/mL catalase-polyethylene glycol (PEG-CAT). Subsequently, cells were treated with either 1 μ M DOX or appropriate vehicle control. (B) Intracellular ROS, measured by DCFDA fluorescence, in PEG-CAT-treated MCF-7 cells versus untreated and PEG-only controls. Data represent n=3 independent experiments. (*p<0.05)

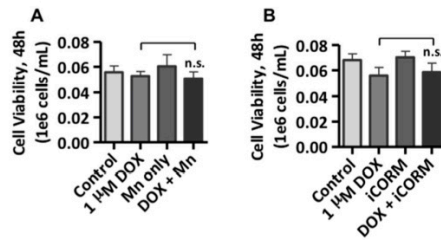


Fig S2. Mn²⁺ and inactivated [Mn(CO)₃] (iCORM) do not sensitize MCF-7 breast cancer cells to DOX. (A) Viable cell count of MCF-7 cells 48h after pre-treatment with 120 μ M MnCl₂, then treatment with either 1 μ M DOX or appropriate vehicle control. (B) Viable cell count of MCF-7 cells 48h after pre-treatment with 120 μ M iCORM, then treatment with either 1 μ M DOX or appropriate vehicle control. Data represent n = 3 independent experiments. (*p < 0.05)

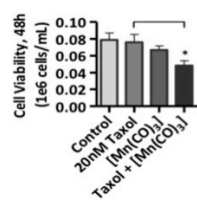


Fig S3. CO sensitizes MCF-7 breast cancer cells to paclitaxel, another chemotherapeutic. Viable cell count of MCF-7 cells 48h after pre-treatment with 120 µM [Mn(CO)₃]⁺ +/- visible light, then treatment with either 20 nM paclitaxel (Taxol) or vehicle control. Data represent n=3 independent experiments. (*p<0.05)

Chapter 3

Co-treatment of carbon monoxide with cisplatin induces apoptosis in cisplatin-resistant ovarian cancer

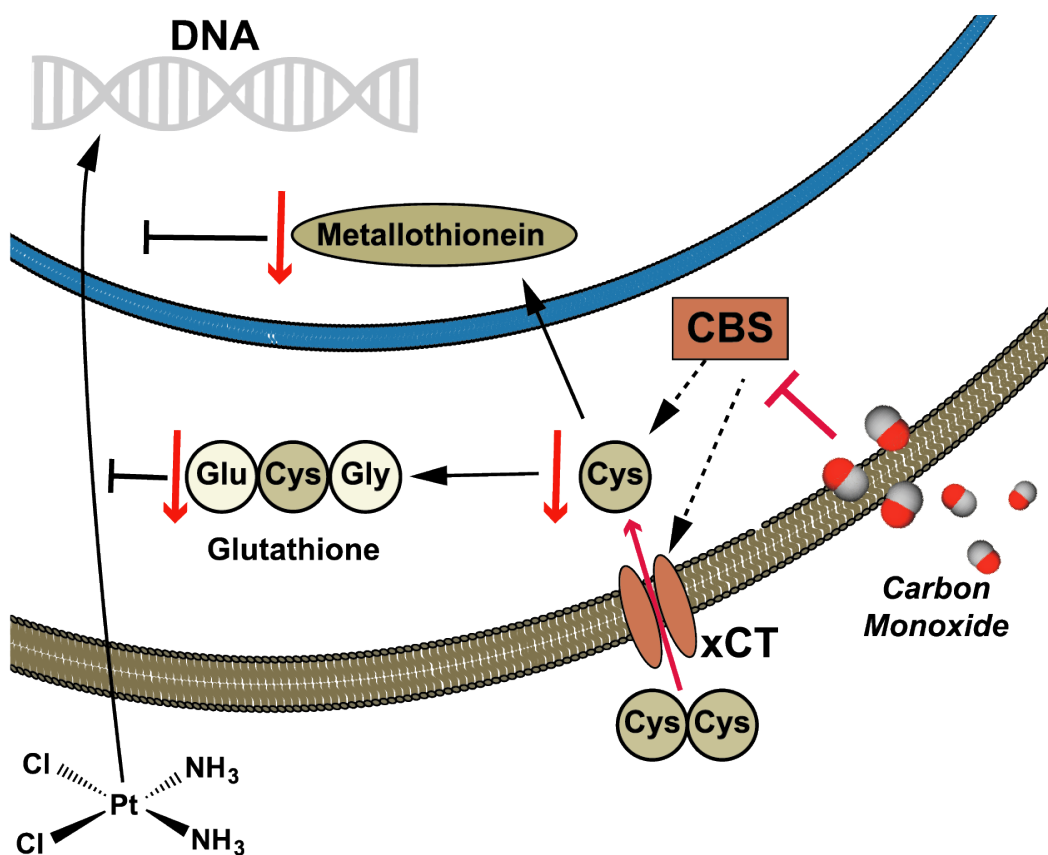


Table 3.1 Table of Content

3.1 Background

In chapter 2, we reported and discussed the therapeutic implications of carbon monoxide (CO) as a chemosensitizing agent against human breast cancer cells. Our findings revealed that cystathionine β-synthase (CBS) is sensitive to inhibition by

carbon monoxide (CO) in breast cancer. As a follow-up study, we assessed the effects of CO on another cancer cell model, ovarian cancer.

Though only the fifth most prevalent, ovarian cancer is the most lethal gynecological cancer in the United States.¹ The overall 5-year survival rate for advanced ovarian cancer patients is only ~40% and has not changed significantly for the past 20 years.² The current standard of care includes cytoreductive surgery and combination platinum/taxane chemotherapy.³ However, ~ 90% of ovarian cancer deaths are caused by chemotherapeutic resistance, which ultimately leads to metastasis.⁴ Clearly there is an unmet need for treatment modalities to mitigate chemotherapeutic resistance.

Cisplatin is one of the most widely used and effective anti-cancer drugs. In addition to ovarian cancer, it is the standard of care for other solid cancers of the head and neck, bowel and colon, cervix and lung. By localizing to the nucleus and binding to DNA, cisplatin gives rise to intrastrand DNA adducts and triggers G2 cell cycle arrest and subsequent apoptosis. The effectiveness of cisplatin, however, is limited by the high incidences of drug resistance.^{5,6} In the cases of colorectal, lung and prostate cancers, intrinsic resistance is common.⁵ In ovarian cancer, however, resistance is mainly acquired after initial treatment and response to cisplatin therapy.⁶ Understanding the cellular changes that occur in the development of cisplatin resistance will help in developing more effective means of circumventing cisplatin resistance in ovarian cancer.

Exogenous carbon monoxide (CO) has recently been shown to decrease chemotherapeutic resistance and proliferation in various cancer cell types.⁷⁻⁹ Our group has recently reported that CO increased the sensitivity of human breast cancer cells to doxorubicin mediated cell death by >40% via the inhibition of endogenous cystathionine β -synthase (CBS) enzymatic activity.¹⁰ CBS is overexpressed selectively in human breast cancer tissues and not in normal human breast tissues making it a potential therapeutic target.¹¹ Interestingly, CBS is overexpressed in only a few other neoplasms, one of which is ovarian cancer, where CBS has been implicated in resistance to cisplatin.¹² However, the mitigation of chemotherapeutic drug resistance, using a pharmacological inhibitor of CBS has not yet been demonstrated in ovarian cancer cells. This study for the first time assessed the pharmacological inhibition of CBS by a light-induced CO delivery modality to counter chemotherapeutic drug resistance in human ovarian cancer cells. The results underscore the important role of the transsulfuration pathway in the development of chemotherapeutic drug resistance in ovarian cancer.

The noxious nature of gaseous CO often poses challenging delivery issues in hospital settings. To avoid this problem, a designed metal carbonyl complex namely $[\text{Mn}(\text{CO})_3(\text{phen})(\text{PTA})]\text{CF}_3\text{SO}_3$ (phen = 1,10-phenanthroline; PTA = 1,3,5-triza-7-phosphaadamantane; abbreviated “photoCORM 1” hereafter) has been employed as the exogenous CO source in this study (Figure 3.1). This designed manganese carbonyl complex is water-soluble and rapidly releases CO only when exposed to low-power (10 mW/cm^2) broadband visible light. This photoactive CO-releasing

molecule (photoCORM) has been a convenient source of CO in delivery under controlled conditions.^{10,13}

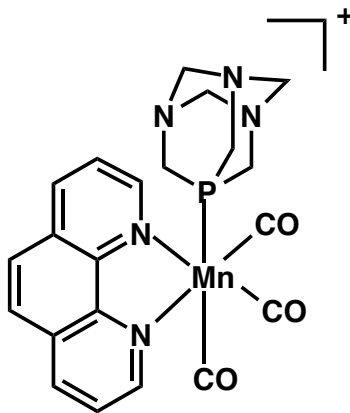


Figure 3.1. $[\text{Mn}(\text{CO})_3(\text{phen})(\text{PTA})]\text{CF}_3\text{SO}_3$, photoactivatable CO-releasing molecule (photoCORM **1**).

3.2 CO sensitizes cisplatin-resistant ovarian cancer cells to cisplatin

Previous studies have demonstrated the ability of CO to sensitize cancer cells to chemotherapeutics,^{7,9,10} though cisplatin resistance and ovarian cancer had yet to be addressed. In this study, we wanted to assess the ability of CO, delivered by 30 μM photoCORM, to enhance the sensitivity of cisplatin-resistant ovarian cancer cells to cisplatin. 30 μM of photoCORM **1** was used in this study because high concentrations of CO, higher than that delivered from >30 μM photoCORM **1**, were cytotoxic to the cells used in this study (Figure 3.2). Therefore, 30 μM photoCORM **1** was the ideal concentration to elucidate the mechanism of action(s) by which CO might sensitize cisplatin-resistant ovarian cancer cells to cisplatin.

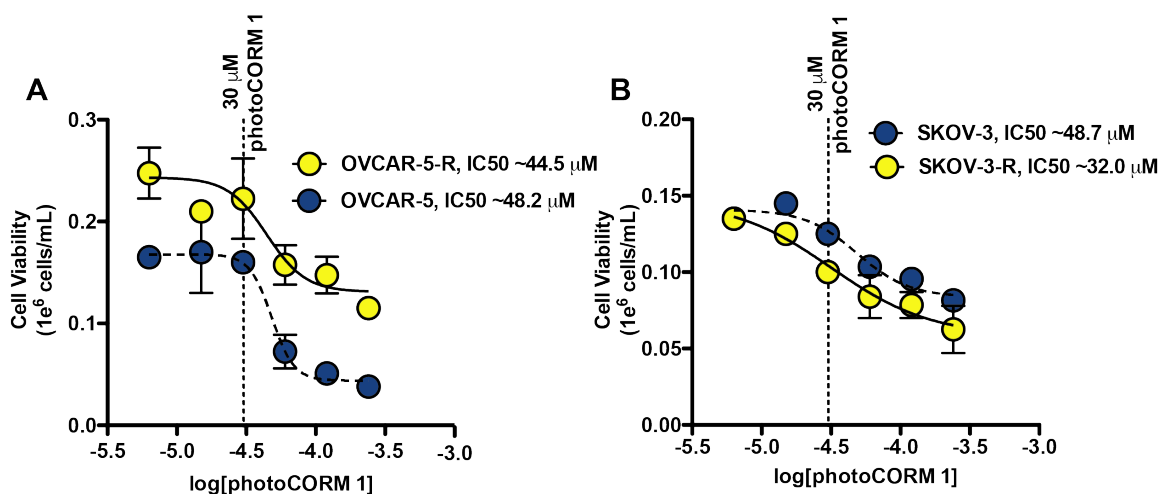


Figure 3.2. Comparison of dose-response to CO, delivered by photoCORM 1, on cell viability, comparing wild type and cisplatin-resistant variants of ovarian cancer cell lines. (A) OVCAR-5 and (B) SKOV-3. Cells were treated with 0-240 μM photoCORM 1 for 24 h prior to trypan blue cell viability assays. Log(dose)-response curves were fit to the data by nonlinear regression to calculate approximate IC₅₀ values. Data representative of n=3 independent experiments. Abbreviations: carbon monoxide (CO), photoactivatable CO-releasing molecule (photoCORM).

Cisplatin-resistant versions of ovarian cancer cell lines OVCAR-5 and SKOV-3 (OVCAR-5-R and SKOV-3-R respectively) were assessed for their resistance to therapeutically relevant concentrations of cisplatin compared with their respective parent cancer cell lines, OVCAR-5 and SKOV-3. Dose-response experiments revealed that OVCAR-5-R and SKOV-3-R exhibited greater cisplatin resistance, >2-fold increased ED₅₀ values for cisplatin, compared with OVCAR-5 and SKOV-3 respectively (Figure 3.3).

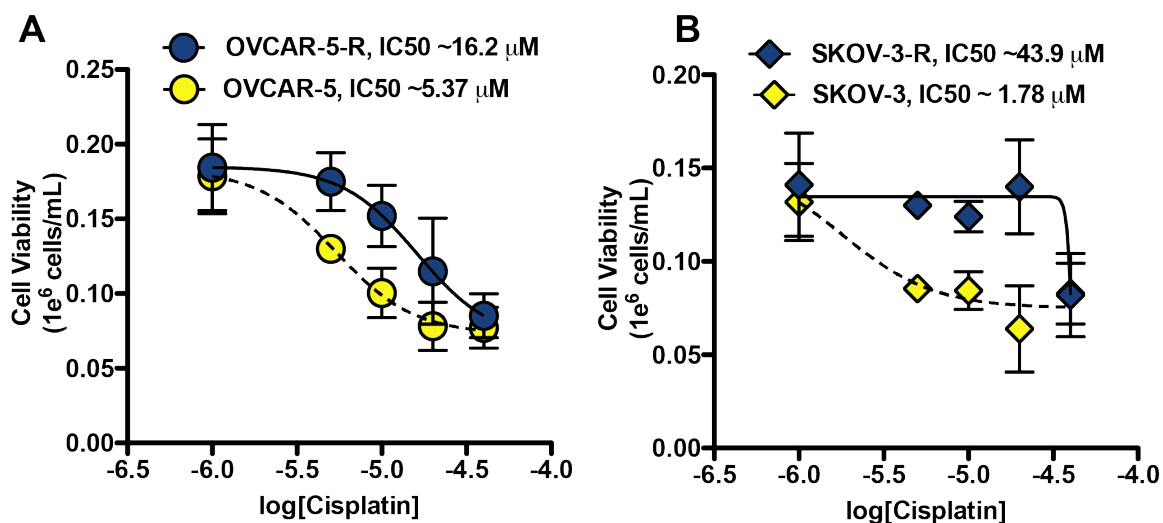


Figure 3.3. Assessing sensitivity to cisplatin of cisplatin-resistant and wild type variants of ovarian cancer cell lines. (A) Cell viabilities of OVCAR-5 and its cisplatin-resistant variant, OVCAR-5-R. (B) Cell viabilities of SKOV-3 and its cisplatin-resistant variant, SKOV-3-R. Cells were treated with 0-40 μM cisplatin for 24 h prior to cell viability measurements performed by trypan blue exclusion. Log(dose)-response curves were fit to the data by nonlinear regression to calculate IC₅₀ values. Data representative of n=3 independent experiments.

Since CO has been shown to sensitize certain cancer cells to chemotherapeutics, we wanted to assess whether CO, delivered from a photoCORM **1**, could attenuate drug resistance for platinum-based chemotherapies in an ovarian cancer model. CO, delivered by 30 μM photoCORM **1**, was assessed for the ability to increase the cell growth inhibition and apoptotic response of cisplatin-resistant cell lines OVCAR-5-R and SKOV-3-R to 20 μM cisplatin. CO significantly enhanced the sensitivity of cisplatin-resistant ovarian cancer cells to cisplatin compared to cisplatin treatment alone (Figure 3.4A-D). OVCAR-5-R and SKOV-3-R treated with cisplatin alone exhibited ~40% and ~29% decreases in cell viability, which was enhanced >2-fold in both cell lines by CO, (Figure 3.4A, C). The reduction in cell viability correlated

with increased PARP-1 cleavage in CO + cisplatin treated cells compared with cisplatin treatment alone, indicating increased apoptotic induction with CO-cisplatin co-treatment (Figure 3.4E).

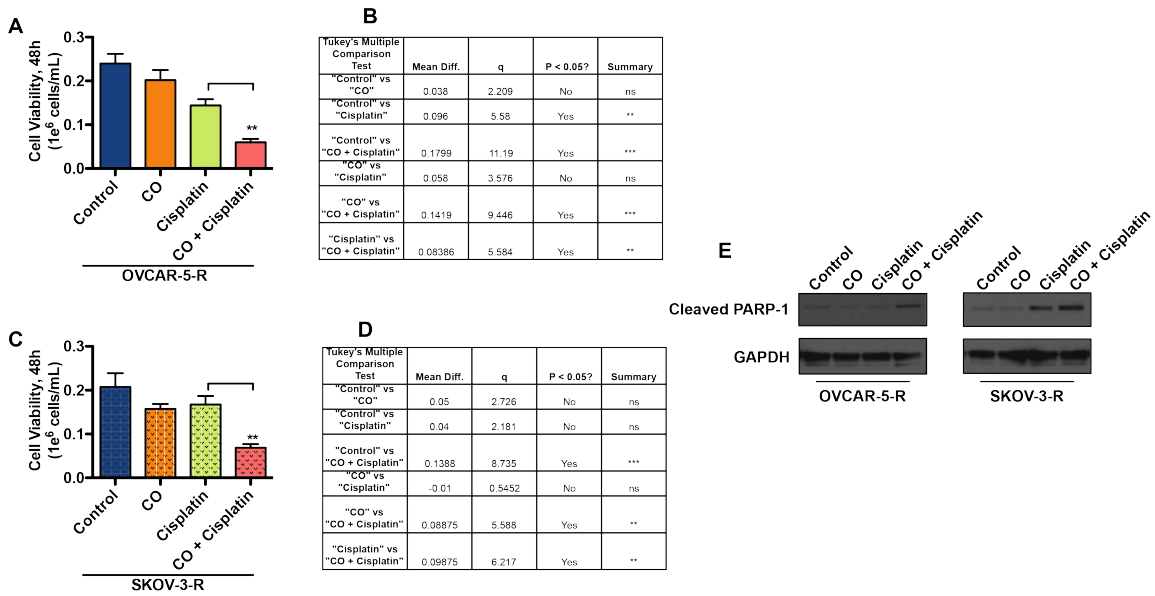


Figure 3.4. Cell viability assays and apoptotic signaling in cisplatin-resistant ovarian cancer cells co-treated with CO and cisplatin. Cisplatin-resistant ovarian cancer cell lines OVCAR-5-R and SKOV-3-R were treated with CO, delivered by 30 μ M photoCORM 1 and/or 20 μ M cisplatin. (A, C) Mean cell viabilities measured by trypan blue exclusion 48 h post-treatment, and (B, D) results from one-way ANOVA/Tukey's test for post-hoc analysis of data. (E) Western analysis of whole cell lysates for PARP-1 and GAPDH as a loading control. Experiments and blots representative of n=3 independent experiments. (* p<0.05, ** p<0.01, ***p,0.001). Abbreviations: carbon monoxide (CO), poly (ADP-ribose) polymerase-1 (PARP-1), glyceraldehyde 3-phosphate dehydrogenase (GAPDH).

The use of photoCORM 1 was a convenient source of CO for study in cell culture conditions, but not without limitations, namely the potential cytotoxicity of the non-CO portion of the molecule. It has been reported that certain CO-releasing molecules (CORMs), specifically the transition metal-containing CORM-2, elicit substantial cell

death independent of CO-release.¹⁴ As photoCORM **1** is a transition metal complex (Figure 3.1), we performed a series of control experiments to assess the ability of the non-CO, molecular scaffold of photoCORM **1** to increase the response of cisplatin-resistant ovarian cancer cells to cisplatin. Light-inactivated photoCORM **1** (iCORM) neither significantly alter cell viability itself nor enhanced the cytotoxicity of cisplatin towards OVCAR-5-R (Figure 3.5), demonstrating the negligible effect of the photoCORM **1**'s molecular scaffolding towards increasing cisplatin sensitivity.

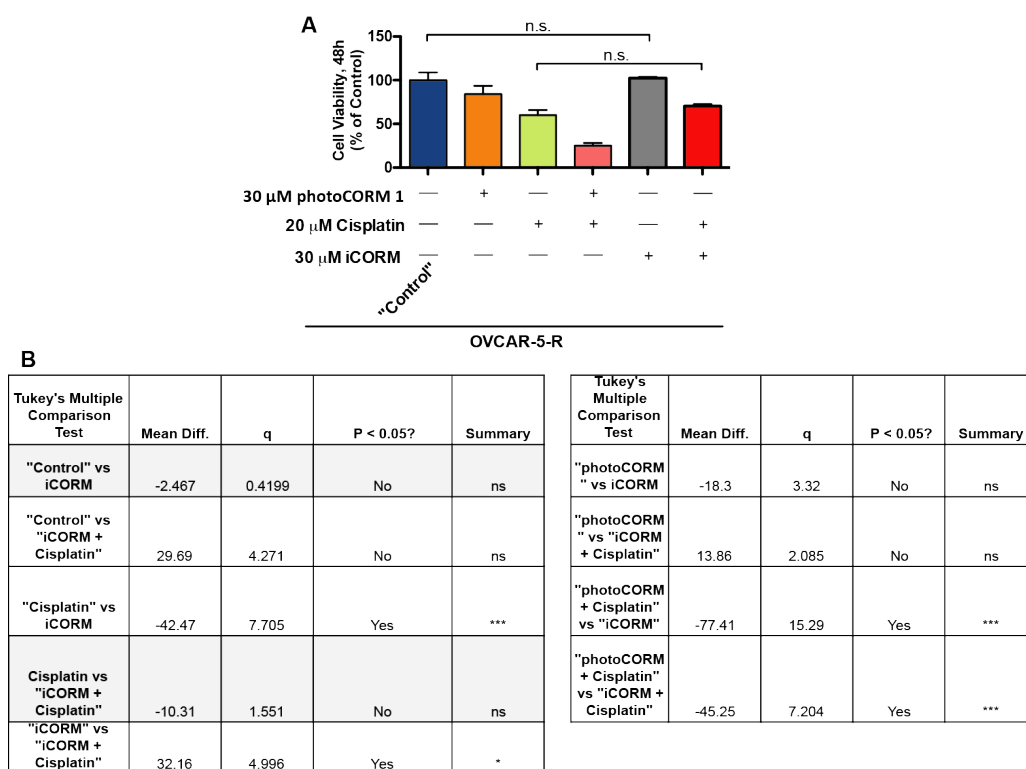


Figure 3.5. Assessment of cytotoxicity and drug sensitizing effects of iCORM on cisplatin-resistant ovarian cancer cells. (Top) Mean +/- SEM cell viabilities of OVCAR-5-R cells treated with 30 μM photoCORM **1**, 30 μM iCORM and/or 20 μM cisplatin assayed 48 h post-treatment by trypan blue exclusion. (Bottom) Results from Tukey's test for post-hoc analysis. Data representative of n=3 experiments. (* p<0.05, ** p<0.01, ***p,0.001). Abbreviations: inactivated, photo-activatable carbon monoxide-releasing molecule (iCORM), photoactivatable, carbon monoxide-releasing molecule (photoCORM).

In a similar manner, iCORM did not significantly alter cell viability of SKOV-3-R cells compared to control treatments and did not increase the sensitivity of those cells to cisplatin (Figure 3.6), further evidence that CO, rather than iCORM, is the cisplatin-sensitizing component of photoCORM 1.

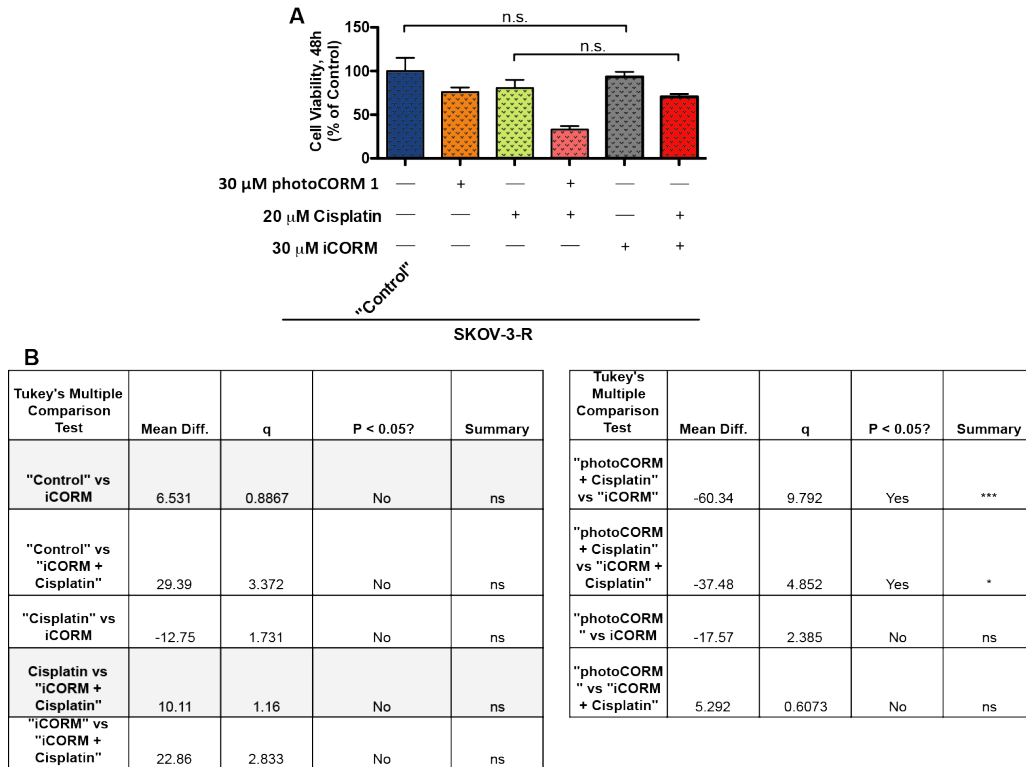


Figure 3.6. Cytotoxicity and drug sensitizing effects of iCORM on cisplatin-resistant ovarian cancer cells. (Top) Mean +/- SEM cell viabilities of SKOV-3-R cells treated with 30 μ M photoCORM, 30 μ M iCORM and/or 20 μ M cisplatin assayed 48 h post-treatment by trypan blue exclusion. (Bottom) Results from Tukey's test for post-hoc analysis. Data representative of n=3 experiments. (* p<0.05, ** p<0.01, ***p,0.001). Abbreviations: inactivated, photo-activatable carbon monoxide-releasing molecule (iCORM). Photoactivatable, carbon monoxide-releasing molecule (photoCORM 1).

Lower doses of CO, delivered by photoCORM 1, also sensitized cisplatin-resistant cells to cisplatin in a concentration-dependent manner (Figure 3.7).

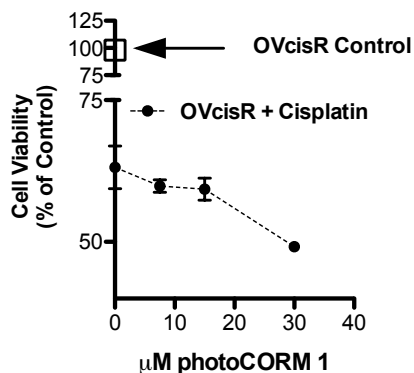


Figure 3.7. Dose-response of cisplatin-resistant ovarian cancer cells to cisplatin in the presence of increasing concentrations of CO. Cell viability, measured by reduction of tetrazolium dye 3-(4,5-dimethylthiazol-2-yl)-2,5-diphenyltetrazolium bromide (MTT). Cisplatin-resistant variant of ovarian cancer cell line OVCAR-5 (OVCAR-5-R) treated with vehicle control, cisplatin and/or photoCORM 1 for 24 h. Data presented as average % of Control +/- SEM of n=3 experiments (*p<0.05).

Interestingly, 24 h treatment with 3 mM *N*-acetylcysteine (NAC), an antioxidant and efficient donor of cysteine, for 24 h was able to largely reverse CO's ability to re-sensitize of OVCAR-5-R and SKOV-3-R to cisplatin (Figure 3.8).

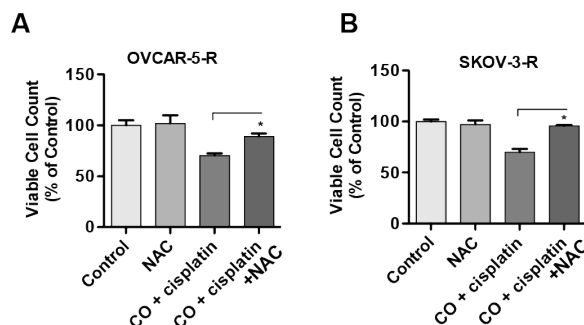


Figure 3.8 NAC reverses the cytotoxic effects of combined CO-cisplatin treatment in cisplatin-resistant ovarian cancer cell lines. (A) OVCAR-5-R and (B) SKOV-3-R. Cells treated with 3mM NAC, 30 μM photoactivatable CO-releasing molecule (photoCORM 1), 20 μM cisplatin or vehicle control(s) as indicated. Cell viability assessed 24 h post-treatment by reduction of tetrazolium dye 3-(4,5-dimethylthiazol-2-yl)-2,5-diphenyltetrazolium bromide (MTT). Data are presented as average % of “Control” +/- SEM of n=3 experiments. (*p<0.05).

Since NAC is an efficient donor of cysteine, we measured steady state levels of intracellular cysteine by HPLC-MS. Indeed, 3 mM NAC treatment for 24 h increased intracellular levels of cysteine in ~4.4-fold in OVCAR-5-R and ~3.8-fold in SKOV-3-R compared with respective vehicle controls (Figure 3.9B). Together, these findings regarding NAC suggested that intracellular levels of cysteine, a sulfur-containing amino acid, might be mechanistically important for the cisplatin-resistance phenotype in OVCAR-5-R and SKOV-3-R.

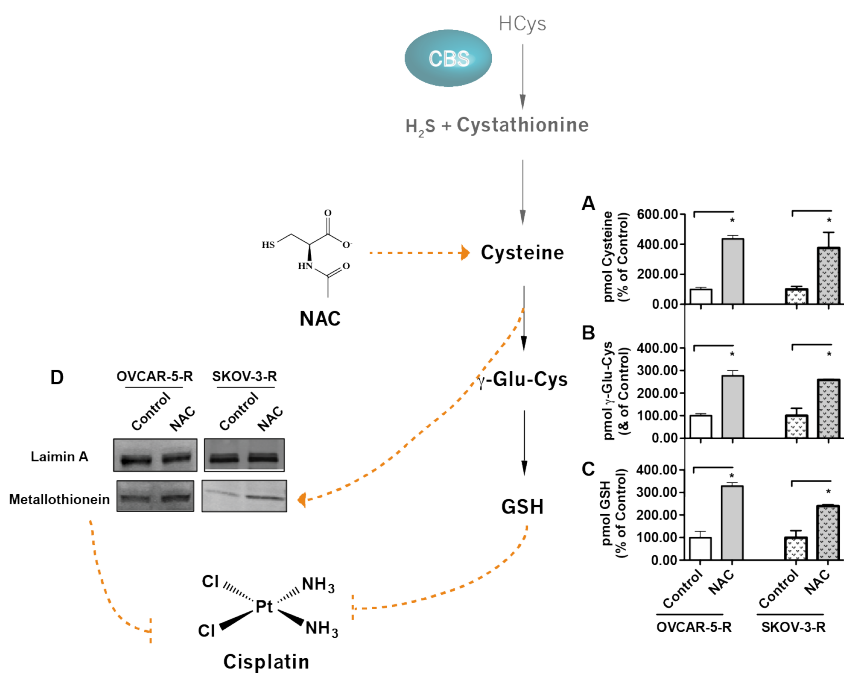


Figure 3.9. Effect of treatment of cisplatin-resistant ovarian cancer cell lines with NAC on markers of cisplatin resistance. Intracellular (B) cysteine levels, (C) γ -Glu-Cys and (D) GSH levels were quantified via high performance liquid chromatography-mass spectrometry (HPLC-MS) in cisplatin-resistant variants of ovarian cancer cell lines OVCAR-5 and SKOV-3 (OVCAR-5-R and SKOV-3-R respectively). (D) Immunoblot of 10 μ g/lane of nuclear fractions of whole cell lysate of cisplatin-resistant ovarian cancer cell lines for metallothionein or Lamin A loading control. Cells treated with 3mM NAC or vehicle control for 24 h. Data presented as average % of “Control” +/- SEM of n=3 independent experiments (*p<0.05).

3.3 CBS is overexpressed in cisplatin-resistant cells

Cisplatin resistance is attributed to increased drug inactivation by sulfur-containing nucleophilic species, GSH and nuclear metallothionein, binding and inactivating the drug.^{15,16} Increased generation of GSH and metallothionein places a significant demand for cysteine, as both GSH and metallothionein require the sulfur-containing amino acid. One of the major sources of cysteine can be from the enzymatic actions of CBS and cystathionine γ -lyase (CGL), transsulfuration pathway enzymes that convert homocysteine to cysteine.¹⁷ We therefore hypothesized that cisplatin-resistant cell lines, OVCAR-5-R and SKOV-3-R, up-regulate transsulfuration pathway enzymes, compared with cisplatin-sensitive cell lines OVCAR-5 and SKOV-3, in order to meet the increased demand for cysteine, GSH and metallothionein. Immunoblot analysis of whole cell lysates revealed dramatically increased expression of both CBS and CGL, transsulfuration pathway enzymes, in cisplatin-resistant versus the corresponding sensitive cells (Figure 3.14).

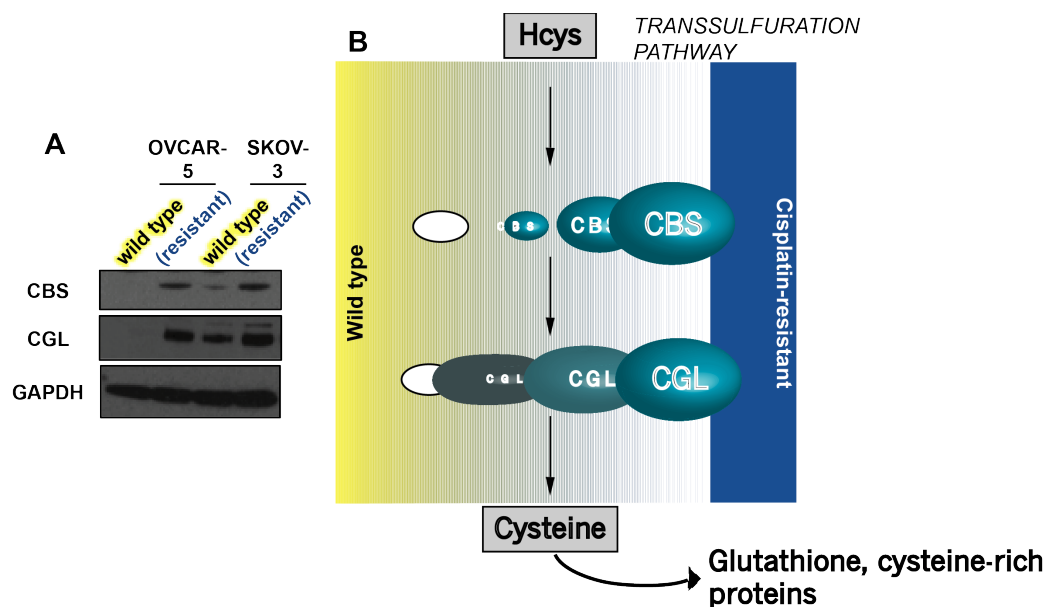


Figure 3.10. Expression of transsulfuration pathway enzymes in wild type ovarian cancer cell lines and their cisplatin-resistant variants. (A) Western analysis for CBS and CGL of whole cell lysates of wild type ovarian cancer cell lines (OVCAR-5, SKOV-3) and cisplatin-resistant variants (OVCAR-5-R, SKOV-3-R). GAPDH probed for as a loading control. (B) Scheme of the expression of transsulfuration pathway enzymes in wild type versus cisplatin-resistant ovarian cancer cell. Blots representative of n=3 independent experiments. Abbreviations: cystathionine β -synthase (CBS), cystathionine γ -lyase (CGL), glyceraldehyde 3-phosphate dehydrogenase (GAPDH).

3.4 CBS is associated with a cisplatin-resistant phenotype

Steady state levels of intracellular CTH, the enzymatic product of CBS, was present ~ 3.1 -fold more in OVCAR-5-R and ~ 7.5 -fold more in SKOV-3-R versus cisplatin-sensitive cell lines OVCAR-5 and SKOV-3 respectively (Figure 3.11A). In addition to overexpressing CBS, cisplatin-resistant ovarian cancer cell lines OVCAR-5-R and SKOV-3-R also exhibited overexpression of CGL (Fig. 3.10), an enzyme downstream of CBS in the transsulfuration pathway. CGL breaks down CTH into the amino acid cysteine, which, like CTH, was found at higher steady state levels in cisplatin-

resistant cell lines, ~2.7-fold more in OVCAR-5-R and ~1.4-fold compared to cisplatin-sensitive cells (Figure 3.11B). CGL, however, is only one of several processes by which cysteine levels are regulated in the cell. In addition to the generation of cysteine through the transsulfuration pathway, uptake of cystine by the glutamate/cystine antiporter (xCT) is known to be an important source of intracellular cysteine for cancer cells, including ovarian cancer.¹⁸ Furthermore, certain cisplatin-resistant ovarian cancer cells are reported to have increased cystine-uptake via xCT.¹⁸ In consideration of this alternate source of cysteine, we compared the intracellular uptake of deuterium-labeled cystine (D4-CC) in cisplatin-resistant ovarian cancer cells with their respective cisplatin-sensitive counterparts.

We observed cisplatin-resistant cells, OVCAR-5-R and SKOV-3-R, contained ~2.1 and ~3.4 times more intracellular D2-cysteine (the reduced form of D4-CC) than OVCAR-5 and SKOV-3, their respective cisplatin-sensitive cells, indicating a greater capacity to uptake cystine (Figure 3.13E). Intracellular D4-CC was not detected at levels above background (data not shown). Despite the increased uptake of cystine in cisplatin-resistant cells, xCT protein expression was not remarkably different between the cisplatin-resistant and cisplatin-sensitive cells (Figure 3.14). This suggested that xCT activity *per se*, and not its expression, was important for the differential uptake of D4-CC.

Next, we wanted to determine whether increased cysteine levels observed in cisplatin-resistant cell lines was correlated with increased biosynthesis of GSH, which

binds and inhibits cisplatin.¹⁵ γ -Glu-Cys, the product of the rate-limiting step in the biosynthesis of GSH, was present at higher steady state levels, ~1.6-fold higher in OVCAR-5-R and ~1.4-fold higher in SKOV-3-R, versus OVCAR-5 and SKOV-3 respectively (Figure 3.11C). Further connecting the dependence of γ -Glu-Cys with intracellular cysteine, treatment of OVCAR-5-R and SKOV-3-R cells with 3 mM NAC significantly increased steady state levels of γ -Glu-Cys: > 2-fold in both cell lines (Figure 3.9B). Such increased levels of γ -Glu-Cys in OVCAR-5-R and SKOV-3-R were supported by concomitant increases in the steady-state levels of GSH. Intracellular levels of GSH were ~2.4-fold higher in OVCAR-5-R and ~1.4-fold higher in SKOV-3-R when compared with OV and SKV, their respective, cisplatin-sensitive, parent cell lines (Figure 3.11D). NAC-treated OVCAR-5-R and SKOV-3-R cells both exhibited ~3.4-fold and ~2.4-fold higher steady state levels of GSH compared with their respective, vehicle treated controls (Figure 3.9C), indicating that the bioavailability of intracellular cysteine levels may be a key regulator of intracellular GSH levels in cisplatin-resistant ovarian cancer cells. In addition to GSH, metallothionein, a cysteine-rich protein, is known to bind and inactivate cisplatin specifically when localized in the nucleus.^{15,16} Qualitative measurement of nuclear metallothionein indicated that OVCAR-5-R and SKOV-3-R cells exhibited considerably increased expression of nuclear metallothionein when compared with OVCAR-5 and SKOV-3 cells (Figure 11F). Addition of 3 mM NAC, a donor of cysteine, also resulted in modest increased nuclear metallothionein expression as determined by Western analysis (Figure 3.9D). Together, these findings demonstrate

the importance of elevated, intracellular cysteine levels toward maintaining higher levels of GSH and nuclear metallothionein, thiols known to bind and in- activate cisplatin.

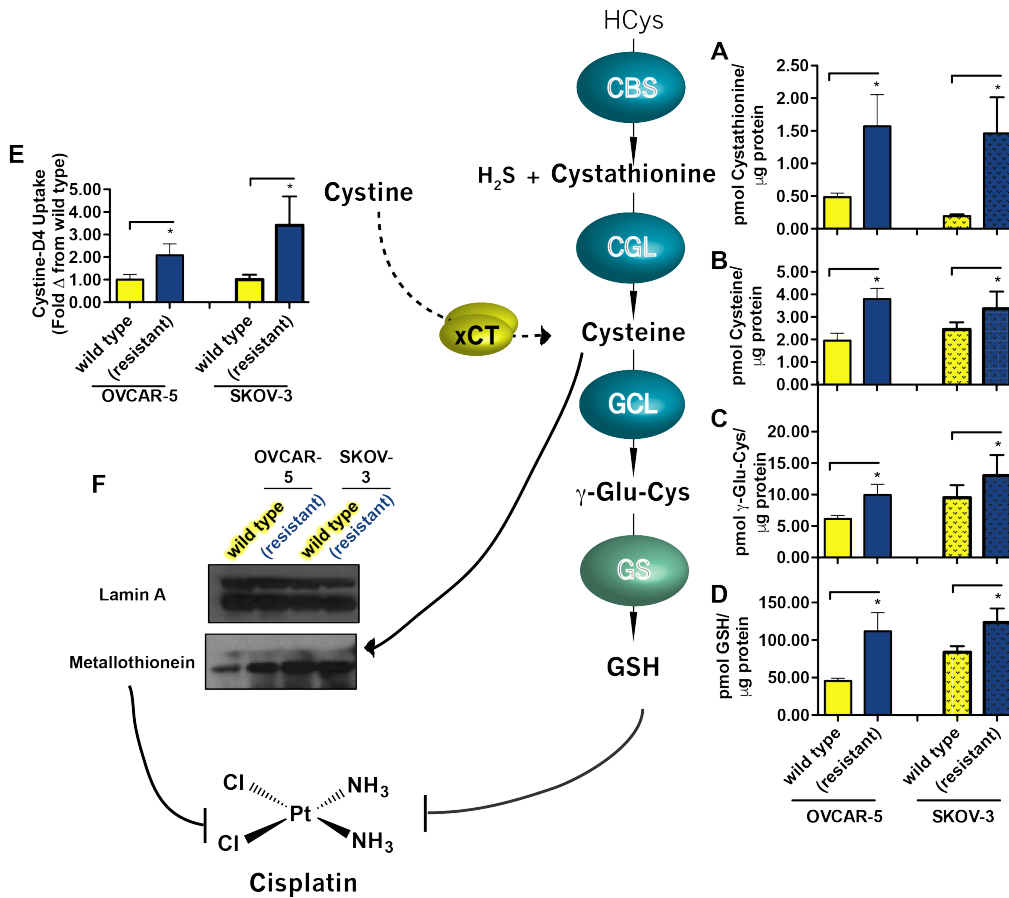


Figure 3.11. Steady state levels of sulfur-containing peptides and proteins in cisplatin-resistant ovarian cancer cells compared to their cisplatin sensitive-derived cell lines. Data and blots representative of n-3 independent experiments. (* $p < 0.05$) Abbreviations: cystathionine β -synthase (CBS), cystathionine γ -lyase (CGL), glutamyl-cysteine ligase (GCL), glutathione synthase (GS), glutathione (GSH), glutamate-cystine antiporter (xCT).

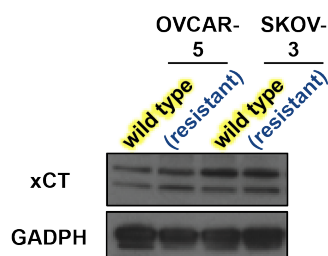


Figure 3.12. Western blot of xCT expression in whole cell lysates of wild type and cisplatin-resistant ovarian cancer cells. Blot representative of n=3 experiments. Abbreviations: glutamate-cystine antiporter (xCT), glyceraldehyde 3-phosphate dehydrogenase (GAPDH).

3.5 Silencing CBS expression sensitizes cisplatin-resistant ovarian cancer cells to cisplatin

In light of the observed correlation between CBS expression and markers for cisplatin resistance, we sought to determine how CBS expression/activity might have been contributing towards cisplatin resistance in OVCAR-5-R and SKOV-3-R. Towards this end, we prepared stable, lentiviral-mediated, CBS-silenced, cisplatin-resistant ovarian cancer cell lines [OVCAR-5-R (shCBS) and SKOV-3-R (shCBS)]. The efficacy of lentiviral-mediated silencing of CBS expression was determined by western analysis on whole cell lysates of OVCAR-5-R (shCBS) and SKOV-3-R (shCBS), observing decreased CBS protein expression in those lysates compared with control, shRNA-transfected cells: OVCAR-5-R (scram) and SKOV-3-R (scram) respectively (Figure 3.14A). Reduced expression of CBS was co-observed with reduced CBS enzymatic activity, as measured by its enzymatic product CTH. Steady state levels of CTH in OVCAR-5-R (shCBS) were ~51% lower compared to

transfection control OVCAR-5-R (scram) (Figure 3.14B). Similarly, SKOV-3-R (shCBS) exhibited ~31% lower levels of intracellular CTH when compared to SKOV-3-R (scram) (Figure 3.14B). To determine whether CBS over-expression in cisplatin-resistant cell lines was at least in part mediating cisplatin resistance, we measured the effects of cisplatin on cell viability in CBS-silenced cells versus scrambled control cells. OVCAR-5-R (shCBS) and SKOV-3-R(shCBS), over a range of concentrations of cisplatin, exhibited significantly reduced cell viability compared to OVCAR-5-R (scram) and SKOV-3-R (shCBS) respectively (Figure 3.13). Calculated ED50 values for cisplatin in OVCAR-5-R (shCBS) and SKOV-3-R (shCBS) were ~2.5 μ M and ~3.6 μ M respectively. These values were lower than the ED50 values for OVCAR-5-R (scram) and SKOV-3-R (scram), ~11 μ M and ~4.4 μ M respectively (Figure 3.13).

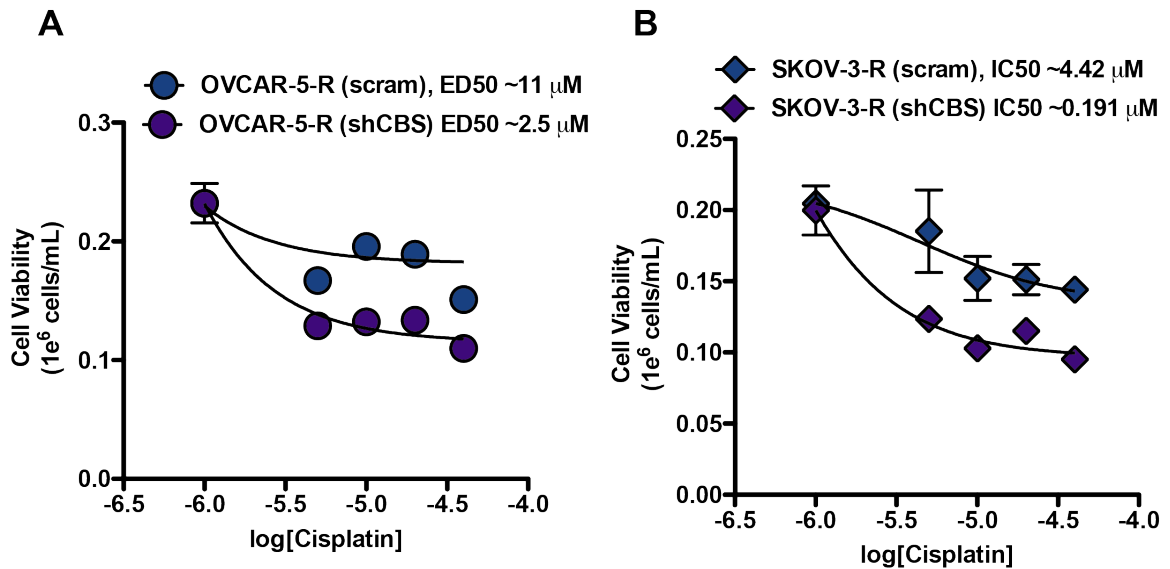


Figure 3.13. Effect of silencing CBS expression on the dose-response relationship between cisplatin and cell viability of cisplatin-resistant ovarian cancer cells. (A) CBS-silenced (shCBS) and control-silenced (scram) OVCAR-5-R and (B) CBS-silenced (shCBS) and control-silenced (scram) SKOV-3-R cells were treated with 0-40 μM cisplatin for 48 h. Cell viability assayed by trypan blue exclusion. Data representative of $n=3$ independent experiments. ED50/IC50 values were calculated from non-linear regression curve fitting of the log(dose)-response curve. Abbreviations: Cystathionine β -synthase (CBS).

3.6 Silencing CBS abates the molecular markers of cisplatin resistance in ovarian cancer cells

Intracellular cysteine levels were ~60% lower in OVCAR-5-R (shCBS) and ~77% in SKOV-3-R (shCBS) compared to their respective scrambled lentiviral controls OVCAR-5-R (scram) and SKOV-3-R (scram) (Figure 3.14C). CBS-silenced cell lines exhibited $\geq 50\%$ reduced D4-CC uptake compared with their respective controls (Figure 3.14F) strongly implicating a role for CBS in regulating cystine uptake. The uptake of cystine may be dependent on the activity and/or expression of xCT. Expression of xCT was however not noticeably different compared with respective

scrambled controls (Figure 3.15C). To partially elucidate the connection between CBS and cystine uptake, we turned our attention to H₂S. H₂S is an enzymatic product of CBS, whereby CBS catalyzes the condensation of homocysteine with cysteine, rather than serine.¹⁷ It has been shown that H₂S allosterically upregulates xCT activity and cystine uptake in neurons,²⁰ though it had not yet been demonstrated in ovarian cancer cells. We therefore wanted to determine if H₂S could at least partially restore the attenuated uptake of D4-CC. CBS-silenced cells treated with 40 μM GYY 4137, a slow releaser of H₂S, exhibited significant yet highly variable increases in D4-CC uptake versus those cells treated with vehicle control: > 600% in OVCAR-5-R (shCBS) and > 33% in SKOV-3-R (shCBS) (Figure 3.15A, B).

Next, we sought to determine whether the observed reduction in steady state levels of cysteine, caused by CBS-silencing (Figure 3.14C), affected the biosynthesis of GSH. Steady state levels of γ-Glu- Cys, the metabolic precursor to GSH, were significantly lower, ~30% less in OVCAR-5-R (shCBS) and ~60% less in SKOV-3-R (shCBS) versus OVCAR-5-R (scram) and SKOV-3-R (scram) respectively (Figure 3.14D). Additionally, we observed steady state levels of GSH in CBS-silenced cell lines, 63 pmol/μg in OVCAR-5-R (shCBS) and 58 pmol/μg SKOV-3-R (shCBS), were > 50% lower than that observed in scrambled controls, 130 pmol/μg in OVCAR-5-R (scram) and 150 pmol/μg in SKOV-3-R (scram) (Figure 3.14 E). CBS-silenced cell lines also expressed relatively less nuclear metallothionein compared with scrambled controls (Figure 3.14G).

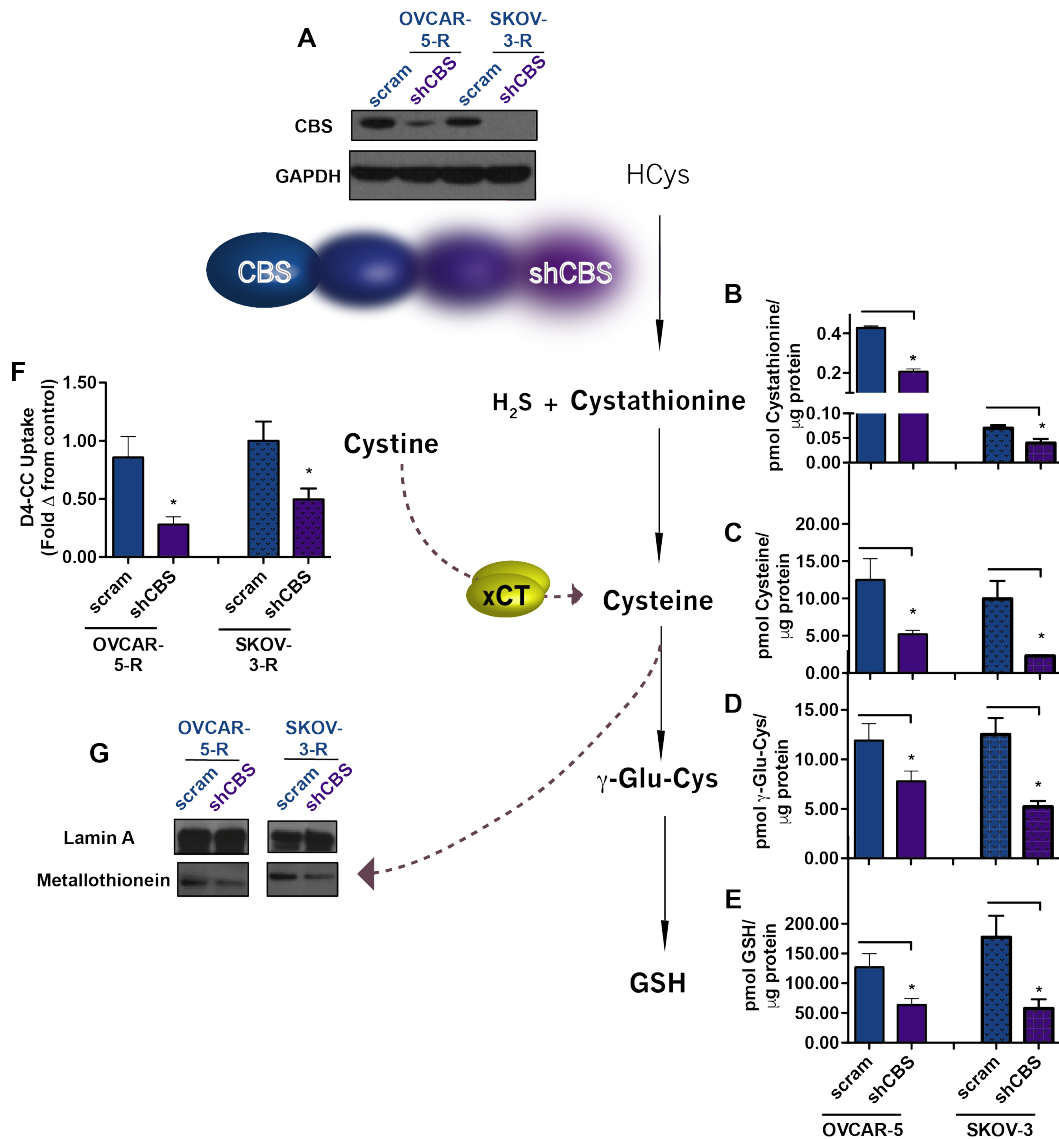


Figure 3.14. Sulfur homeostasis and molecular markers of resistance in cisplatin-resistant ovarian cancer cells exhibiting stable silencing of CBS (shCBS) compared to control transfected cells (scram). Steady state levels of transsulfuration pathway metabolites (A) cystathionine and (B) cysteine, measured by HPLC-MS and normalized to total protein. Steady state levels of GSH synthesis metabolites (D) γ -Glu-Cys and (E) GSH, measured by HPLC-MS and normalized to total protein. (F) xCT activity, as measured by cystine-D4 uptake over 48 h and normalized to total protein. (G) Expression of metallothionein in nuclear extracts, with Lamin A expression to assess equal loading. Data and blots representative of $n=3$ independent experiments. (* $p<0.05$). Abbreviations: cystathionine β -synthase (CBS), high performance liquid chromatography-mass spectrometry (HPLC-MS), glutathione (GSH), glutamate-cystine antiporter (xCT).

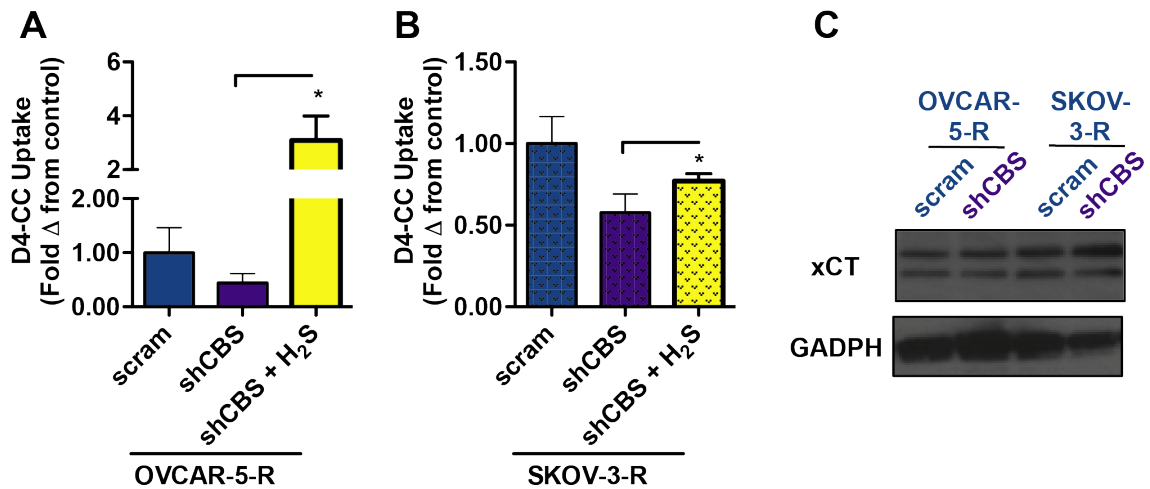


Figure 3.15. Effects of stable silencing of CBS on xCT activities and expressions in cisplatin-resistant ovarian cancer cells. (A) Cystine-D4 uptake, relative to total protein, in OVCAR-5-scram, OVCAR-5-shCBS and OVCARshCBS cells treated with H₂S-donor GYY 4137 for 24 h. (B) Uptake of cystine-D4, normalized to total protein, of SKOV-3-R(scram), SKOV-3-R(shCBS) and SKOV-3-R(shCBS) cells treated with GYY 4137 for 24 h. (C) Immunoblot of xCT expression in whole cell lysates of CBS-silenced and scrambled control cell lines derived from cisplatin-resistant lines OVCAR-5-R and SKOV-3-R. GAPDH expression was measured to determine equal loading. Data and blots representative of n=3 independent experiments. (* p<0.05) Abbreviations: cystathionine β -synthase (CBS), glutamate-cystine antiporter (xCT), glyceraldehyde 3-phosphate dehydrogenase (GAPDH).

3.7 CO sensitizes cisplatin-resistant ovarian cancer cells to cisplatin

Following confirmation of a substantial connection between CBS and cisplatin-resistance in OVCAR-5-R and SKOV-3-R, we investigated whether CO-induced sensitization of cisplatin-resistant cells to cisplatin (Figure 3.4) was in part mediated by inhibition of CBS and the subsequent suppression of nuclear metallothionein and GSH. Treatment of OVCAR-5-R and SKOV-3-R with CO, delivered by 30 μ M photoCORM 1, significantly lowered CBS bioactivity, as measured by decreased steady state levels of intracellular CTH. CTH decreased \sim 2.7- fold in OVCAR-5-R

and ~4.5-fold in SKOV-3-R (Figure 3.16A). In a similar manner to lentiviral-mediated silencing of CBS (Figure 3.14C), CO treatment reduced steady state levels of cysteine > 55% in cisplatin-resistant cell lines OVCAR-5-R and SKOV-3-R (Figure 3.16B). In parallel to the CO-mediated inhibition of CBS and decrease in intracellular cysteine (Figure 3.16A, B), concomitant reduction in the uptake of D4-CC, ~73% in OVCAR-5-R and ~56% in SKOV-3-R, was observed (Figure 3.16E). Steady state levels of γ -Glu-Cys, the product of the rate-limiting step of GSH synthesis, was also significantly lower in cisplatin-resistant cells treated with CO, ~63% lower in OVCAR-5-R and ~66% lower in SKOV-3-R, versus respective controls (Figure 16C). Expression of nuclear metallothionein and steady state levels of GSH were ~40% lower in OVCAR-5-R and ~65% lower in SKOV-3-R upon treatment with CO (Figure 16D, F).

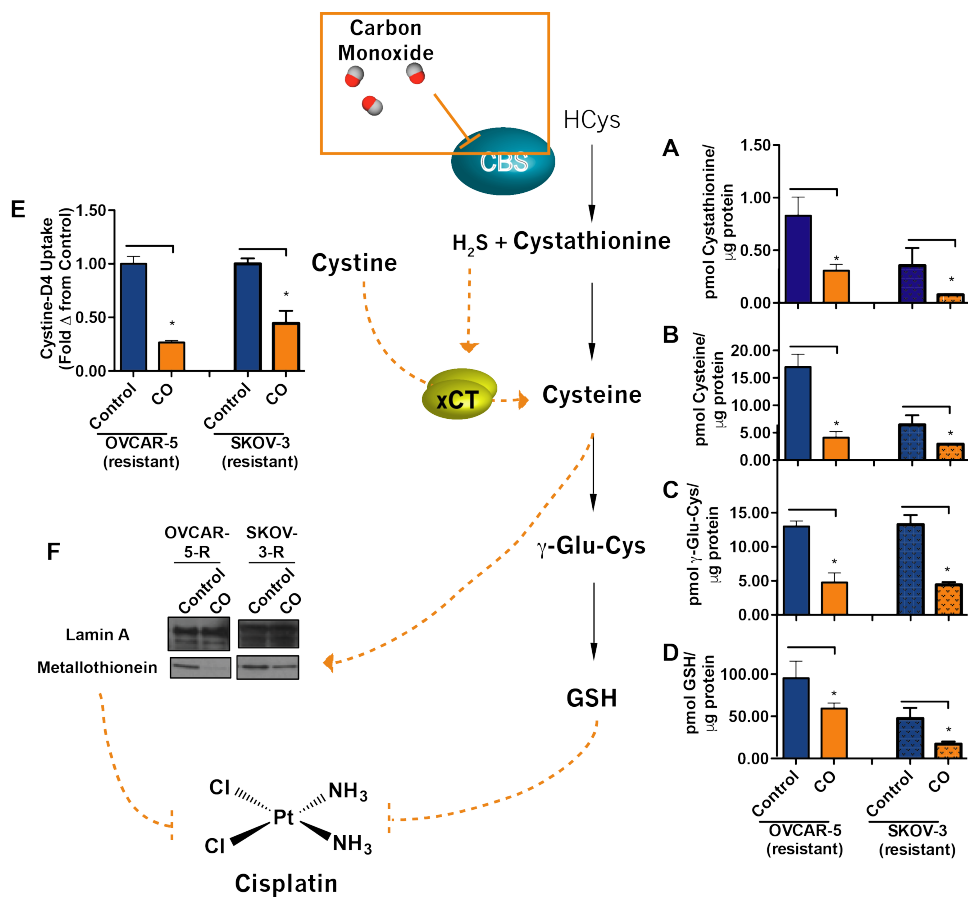


Figure 3.16. Effects of exogenous CO treatment on sulfur homeostasis in cisplatin-resistant ovarian cancer cells. Cisplatin-resistant ovarian cancer cell lines OVCAR-5R and SKOV-3-R were derived from wild type, cisplatin-sensitive cell lines OVCAR-5 and SKOV-3. Average, steady state levels of intracellular metabolites (A) cystathionine, (B) cysteine, (C) γ -Glu-Cys and (D) GSH as measured by HPLC-MS and normalized to total protein. (E) xCT activity quantified by cystine-D4 uptake from extracellular medium over 48h, normalized to total protein. (F) Expression of metallothionein in nuclear extracts. Lamin A was probed for as loading control. Experiments and blots representative of at least n=3 independent experiments. (* p<0.05) Abbreviations: carbon monoxide (CO), glutathione (GSH), high performance liquid chromatography-mass spectrometry (HPLC-MS), glutamate-cysteine antiporter (xCT)

3.8 Discussion

Other investigators have shown that silencing of CBS enhanced drug sensitivity in cisplatin-resistant ovarian cancer cells.¹² CO delivered by tricarbonyldichlororuthenium (II) dimer, has been reported to promote global methylation in U937 human monoblastic leukemia cell, possibly by CO-mediated inhibition of CBS.²¹ These findings, though, may require further validation as the use of tricarbonyldichlororuthenium (II) dimer for studying the effects of CO is controversial; it has significant and potent CO-independent effects on potassium channels in human cells.²² Nevertheless, the direct demonstration of a viable pharmacological inhibition of CBS to alleviate drug resistance in ovarian cancer was lacking.

The present study, for the first time, provides initial evidence that CO, delivered from a photoCORM, inhibits CBS and could be a viable option to circumvent cisplatin resistance in ovarian cancer. Specific small molecule inhibitors of CBS, such as benserazide, have shown promise in eradicating cancer cells.²³ However, if further developed, these could only be used as a systemic therapy that will not spare normal cells. Such systemic therapy will result in serious adverse side effects, as CBS in the liver is the primary source of GSH, the major antioxidant in physiology.²⁴ On the other hand, light-activated CO delivery via appropriate catheters, prototypes for which have already been developed in our laboratory,²⁵ could be used to inhibit CBS locally in accessible cancer tissues. This would bypass systemic delivery and increase the exposure of affected tissues to effective concentrations of

the inhibitor and at the same time minimize adverse side effects. In fact the feasibility of CO-releasing molecules for cancer treatment has recently been reviewed.²⁶

Platinum-containing anti-cancer drugs react readily with the sulfur-containing amino acids in proteins namely methionine and cysteine. Unlike methionine, whose reaction with platinum is readily reversible by replacement with thiols or nucleotide bases, the cysteine-platinum complex is more stable.²⁷ Therefore, cysteine-rich proteins such as GSH and metallothionein, both of which are present at high concentrations in the cancer cell, readily bind and inactivate platinum drugs.^{15,17,27} Indeed, formation of a cisplatin-(GS)₂ complex has been characterized (by NMR spectroscopy and HPLC-atomic absorption spectroscopy) in vitro and in vivo (in murine L1210 cells) in addition to efflux of the complex across the cell membrane.²⁸ Of note, it has been reported that cisplatin adducts, formed by incubation of cisplatin with whole cell lysate from ovarian cancer cell line A2780cisR lysed in distilled water, were comprised of ~20% of cisplatin-(GS)₂ complex, with the other ~80% being cisplatin bound to high molecular weight protein thiols.²⁹ These findings suggest that GSH may be only partially responsible for the binding and inactivation of cisplatin. However, when considering the propensity of extracellular GSH, including that released during preparation of whole cell lysates in a non-reducing environment such as water, to auto-oxidize should be noted. This, under experimental conditions that are far from physiological, the dismissal of GSH towards inactivating cisplatin, as was suggested by Kasherman, et al., perhaps should not be done so readily. Nevertheless, their findings do suggest that higher molecular weight proteins,

such as metallothionein, are very important in the inactivation of cisplatin. Indeed, formation of a ternary complex between metallothionein and Platinum-DNA adduct followed by release of platinum from the DNA (and formation of $[(\text{NH}_3)_2\text{Pt}(\text{S}_2\text{-metallothionein})]$ species) has been suggested to modulate DNA-repair and gene transcription leading to drug resistance.³⁰ Also, immunohistochemical metallothionein expression in various human tumors has been associated either with processes related to carcinogenesis or with resistance against radiation and chemotherapy.³¹ In ovarian tumors an increasing percentage of metallothionein expression has been observed during the progression of malignancy.³²

Results shown in Figure 3.16 now clearly indicate that CO-mediated CBS inhibition leads to the reduction of both GSH and metallothionein (implicated in cisplatin inactivation) in ovarian cancer cells. Our observations are supported by earlier findings that CBS positively regulates GSH levels in breast cancer cells.¹¹ *The fact that exogenous CO could interfere with metallothionein expression as well in refractory ovarian cancer cells, is in itself a novel finding in this study.* The data that CBS silencing could lower levels of nuclear metallothionein underlines the important role of CBS in regulating two major thiol moieties (GSH and metallothionein) implicated in chemotherapeutic drug resistance.³¹⁻³⁴ Nuclear metallothionein expression is induced by cisplatin and seems to protect DNA in cells from toxic effects of the drug. The proportion of the individual contributions of GSH and metallothionein in inactivating cisplatin is however not explored in this work.

Increases in GSH and metallothionein require adequate maintenance of intracellular cysteine levels. The intimate connection between GSH/metallothionein and intracellular cysteine is highlighted by the ability of extracellular treatment of cisplatin-resistant ovarian cancer cells with NAC. Treatment of OVCAR-5-R and SKOV-3-R with 3mM NAC treatments increased both GSH and nuclear metallothionein (Figure 3.9). Data presented here elucidate regulation of sulfur metabolism in cisplatin-resistant ovarian cancer cells by CBS via two processes; flux through the transsulfuration pathway and uptake of extracellular cysteine.

Previous studies have shown that some cancer cell types maintain intracellular cysteine levels by importing cystine via the glutamate/cystine antiporter, xCT.^{35,36} Elevated expression and activity of xCT in response to oxidative stress has been reported in breast cancer cells, alluding to a role for xCT towards protecting cancer cells against oxidative stress induced loss of cell viability (a mechanism often exploited by chemotherapeutic drugs).³⁷ Overexpression of xCT has been shown to increase intracellular GSH and increase resistance to cisplatin.¹⁸ In addition, loss of xCT from cancer cells resulted in suppressed tumor growth of gastric cancer in pre-clinical models.³⁸ In cisplatin-resistant ovarian cancer cells, we observed increased xCT activity, but not increased expression *per se*. We have provided strong evidence for the regulation of xCT activity by CBS via H₂S, as lentiviral-mediated silencing of CBS in OVCAR-5-R (shCBS) and SKOV-3-R (shCBS) reduced the activity of xCT, which was partially reversed by the addition of exogenous H₂S, which is known to allosterically increase xCT activity (Figure 3e-f).²⁰ To the best of our knowledge, this

is the first report that demonstrated that CBS can up-regulate GSH synthesis independent of the transsulfuration pathway in cancer cells by inducing the up regulation of cystine uptake in cancer cells. This study further emphasized that CO mediated inhibition of CBS could exploit this mechanism to compromise the antioxidant potential of cancer cells resulting in their increased sensitivity to cisplatin.

Finally, it is important to note that overexpression of CBS is observed in select malignancies, namely breast and ovarian cancers while the corresponding normal tissues in all such cases exhibit very low levels of expression or none at all.³⁹ For this reason, CBS could be an important target in case of these two types of cancer where modulation of CBS activity by exogenous CO could thwart resistance to conventional chemotherapy. The effect of CO on non-transformed ovarian tissues in the context of resistance to cisplatin is intriguing, as the effect(s) of CO in non-cancerous cells are likely independent of CBS. Elucidation of other binding partners of CO in non-transformed ovarian cell lines could be an interesting follow-up study.

Previous work from this laboratory demonstrated that light-triggered CO delivery by the photoCORM photoCORM can attenuate antioxidant capacity in human breast cancer cells through inhibition of CBS and sensitizes such cells to doxorubicin and paclitaxel.¹⁰ Sensitization of human ovarian cancer cells to cisplatin therapy through administration of CO now demonstrates the general concept of CBS inhibition as a treatment modality to overcome chemoresistance encountered in ovarian cancer therapy.

Strategies that overcome cisplatin resistance may dramatically reduce the mortality of ovarian cancer.⁴ Here we have presented that CO, delivered from a photoCORM, sensitizes established cisplatin-resistant cell lines to cisplatin. Furthermore, we have provided strong evidence that the effects of CO in circumventing chemotherapeutic drug resistance is at least in part mediated by the inactivation of endogenous CBS (as evidenced by the reduction in CTH, the direct metabolic product of CBS).

3.9 Materials and methods

Materials and reagents

[Mn(CO)₃(phen)(PTA)]CF₃SO₃ (photoCORM) was synthesized, analyzed to confirm purity, and applied as previously published.^{10,13} Cisplatin (479306), protease inhibitor cocktail (P8340), puromycin (P8833), N-acetylcysteine (A7250) and other chemicals were products of Sigma Aldrich (St. Louis, MO). GYY 4137 (13345) was purchased from Cayman Chemicals (Ann Arbor, MI). Primary antibodies against CBS (sc-133208), CGL (sc-365382), cleaved PARP-1 (sc-56196), Lamin A (sc-71481), β -tubulin (sc-23949) and GAPDH (sc-47724) were purchased from Santa Cruz Biotechnology (Santa Cruz, CA). Mouse monoclonal antibody against metallothionein (ab12228) and rabbit polyclonal antibody against xCT (ab 37185) were purchased from Abcam (Cambridge, MA).

Cell culture

Ovarian cancer cell lines OVCAR-5 (OV), cisplatin-resistant OVCAR-5 (OVCAR-5-R), SKOV-3 (SKV), and cisplatin-resistant SKOV-3 (SKOV-3-R) were a gift from Dr. Sivakumar Ramadoss and Dr. Gautam Chaudhuri of the David Geffen School of Medicine at University of California at Los Angeles. Cells were grown in 1X RPMI media supplemented with 10% fetal bovine serum, 100 I.U./mL penicillin and 100 µg/mL streptomycin at 37°C + 5% CO₂. Mycoplasma detection was performed regularly to confirm its absence with MycoAlert™ Mycoplasma Detection Kit (LT07-218) from Lonza (Basel, Switzerland). Cells were passaged no more than five times after being received. Unless otherwise indicated, cell cells were allowed to seed overnight prior to treatments, then assayed 24 h post-treatment.

CO and cisplatin treatments of cells

Cells were seeded overnight, 100x10³/well of 6-well tissue culture dishes or 1x10⁶/well of 100 mm tissue culture dishes depending on the experiment being performed, and incubated at 37°C + 5% CO₂ 24 h prior to cell culture treatments. Cells treated with CO were exposed to 30 µM photoCORM in the dark. To control for the effects of the non-CO backbone of the CO-releasing molecule, corresponding control cells were treated with 30 µM light-inactivated photoCORM in the dark. Upon addition of photoCORM or iCORM, cells were exposed to visible light for 30 min at room temperature, then returned back to 37°C + 5% CO₂. In experiments involving cisplatin co-treatment with photoCORM, 20 µM cisplatin or DMSO vehicle control

was administered either by itself or together with 30 μ M photoCORM or iCORM. Subsequent assays were performed 24 h post-treatment.

Cell viability assays

When assessing cell viability via Trypan blue exclusion method, 100×10^3 cells/well of a 6-well tissue culture plate were allowed to seed overnight in a 37°C incubator + 5% CO₂. The next day, cells were treated as indicated and allowed to incubate for 24 h. Following treatment, cells were harvested with 1mL 0.05% Trypsin-EDTA, after which trypsin was neutralized with 1mL cell culture media supplemented with 10% FBS. This cell suspension was then visualized and quantified using a Vi-Cell XR cell viability analyzer from Beckman Coulter (Brea, CA). Cell viability was measured 24 h post-treatment and presented as the mean +/- SEM of three independent experiments.

In cell viability experiments performed using the tetrazolium dye MTT, experiments were performed in 96-well tissue culture plates. Briefly, 4×10^3 cells were allowed to seed overnight in a 37°C incubator + 5% CO₂. The next day, cells were treated as indicated, then assessed for viability 24 h post-treatment. Cell culture media was aspirated from cells, then replaced with 0.5mg/mL 3-(4,5-dimethylthiazol-2-yl)-2,5-diphenyltetrazolium bromide dissolved fresh 1x DMEM and allowed to incubate for 2 h in a 37°C incubator + 5% CO₂. Number of viable cells was assessed by quantifying the amount of 3-(4,5-dimethylthiazol-2-yl)-2,5-diphenyltetrazolium bromide reduced to insoluble formazan. Insoluble formazan was solubilized in 10%

SDS + 0.01 N HCl. The absorbance at 570 nm, with reference wavelength at 690 nm, was measured. Data are presented as average % change +/- SEM from control(s) of n=3 independent experiments.

Western blot analysis

Whole cell lysates from 1×10^6 cells/ 100 mm tissue culture dishes were prepared after treatment in RIPA lysis buffer containing 150 mM NaCl, 5mM EDTA pH 8.0, 50 mM Tris pH 8.0, 1% Triton X-100, 0.5% sodium deoxycholate, 1% SDS and 1X protease inhibitor cocktail. Soluble lysates were quantified using a Pierce™ BCA Protein Assay Kit (23225) from ThermoFisher Scientific (Waltham, MA), 20 µg cell lysates from samples were separated on 4-12% SDS-PAGE gel and transferred to poly(vinylidene difluoride) (PVDF) membrane. Membranes were blocked with 5% nonfat dried milk and incubated for 1 h room temperature or 4°C overnight. Primary (1:1,000 dilution) and horseradish peroxidase (HRP)-conjugated secondary (1:10,000 dilution) antibody incubations were performed at room temperature for 1 h. Immunofluorescent signals were detected with Pierce ECL Plus western blotting substrate (32132) from ThermoFisher Scientific.

High performance liquid chromatography-mass spectrometry

Glutathione (GSH), γ -Glu-Cys, cysteine and cystathionine (CTH) were measured utilizing high pressure, liquid chromatography-mass spectrometry (HPLC-MS) as previously described [10]. $\sim 5 \times 10^6$ cells, harvested via scraping from 100 mm tissue culture dishes, were lysed via three probe sonication in 200 µL of 10 mM N-

ethylmaleimide (NEM) + 10 mM ammonium acetate, pH 7.4. To the lysate, 800 μ L of methanol was added and the samples were vortexed. Samples were then centrifuged at 16,000 \times g for 5 min, then supernatants were collected into microcentrifuge tubes and dried via vacuum centrifugation. Samples were further dried with 100 μ L methanol, then 100 μ L benzene. The carboxy termini of metabolites were esterified with the treatment of 100 μ L of 3N methanolic HCl for 60 min, 60 $^{\circ}$ C. Samples were then dried via vacuum centrifugation, redissolved in 50 μ L of water and transferred to liquid chromatography injector vials. Kinetex XB-C18, 100 \times 2.1 mm, 1.7- μ m particle size, 100 \AA pore diameter, reverse phase column from Phenomenex (Torrance, CA) column was equilibrated with 85% 0.1 mM perfluorooctanoic acid in water (eluant A) and 15% 0.1 mM perfluorooctanoic acid in acetonitrile (eluant B). Samples were injected onto the equilibrated column and eluted at 100 μ L/min with increasing concentration of eluant B (min/% B: 0/15, 5/15, 35/50, 33/ 15, 45/15). The eluants were directed towards an Agilent Jet Stream electrospray ionization (ESI) source connected to a triple quadrupole mass spectrometer (Agilent 6460) operating in positive ion tandem mass spectrometric multiple reaction-monitoring (MRM) mode. The intensities of the CTH parent to fragment transition (461 \rightarrow 318, rt 27.88 min), cysteine-NEM conjugate (261 \rightarrow 244, rt 24.06 min), GSH-NEM conjugate (461 \rightarrow 318, rt 26.06 min) and γ -Glu-Cys-NEM conjugate (404 \rightarrow 244, rt 26.59 min) were recorded using previously-determined settings. Standards were prepared containing known concentrations of CTH (0, 20, 40, 40, 80, 160 pmol), cysteine (0, 80, 160, 320, 640 pmol), GSH (0, 200, 400, 800, 1600

pmol) and γ -Glu-Cys (0, 100, 200, 400, 800 pmol). From these standards, calibration curves were constructed. The amount of the monitored metabolites in biological samples was calculated by interpolation from the curves. Data were normalized to total μg protein and reported in units of pmol metabolite per μg protein or percentage of control/compared group.

D4-cystine uptake assay and H₂S donation

1x DMEM with high glucose but no glutamine, methionine, and cystine (D0422) was procured from Sigma Aldrich. This media was then supplemented with 3.97mM glutamine, 200 μM methionine, 10% FBS and 200 μM D4-CC (DLM-1000-PK), which was purchased from Cambridge Isotope Laboratories (Tewksbury, MA). $\sim 1 \times 10^6$ cells were seeded in 100 mm tissue culture dishes and allowed to grow for 48 h at 37°C + 5% CO₂. In experiments where H₂S-donor GYY 4137 was used, either 40 μM GYY 4137 or DMSO vehicle control was added for 48 h. Cells were harvested and processed in the identical manner described above (Section 2.6). Reported D4-CC uptake was measured by quantifying intracellular D2-cysteine levels. Data was normalized to total μg protein and reported as fold-difference from control/compared group.

Nuclear fraction enrichment

1×10^6 cells were seeded overnight into 100 mm tissue culture dishes, followed by treatments with indicated experimental chemical/agents. By pooling multiple dishes together, $\sim 5 \times 10^6$ cells were scraped from 100 mm tissue culture dishes on ice and

washed with cold, 1X PBS. Cells were suspended in cold lysis buffer containing the following: 10 mM HEPES pH 7.7, 10 mM KCl, 0.1mM EDTA, 1mM DTT, 0.5% NP-40, 0.5mM PMSF and protease inhibitor cocktail. Cells were incubated on ice for 15 min with intermittent mixing, then centrifuged at 12,000 x g at 4°C for 10 min. The supernatant was collected as the cytosolic enriched fraction. The nuclear pellet was washed three times with cold lysis buffer, then resuspended in cold nuclear extraction buffer containing 20 mM HEPES pH 7.5, 400 mM NaCl, 1 mM EDTA, 1 mM DTT, 1 mM PMSF and protease inhibitor cocktail. After incubation on ice for 30 min, the enriched nuclear fraction was collected by centrifugation at 12,000 x g at 4°C for 15 min.

Gene silencing experiments

Stable silencing of CBS expression in OVCAR-5-R and SKOV-3-R was achieved utilizing short hairpin RNA (shRNA) packaged in lentiviral particles purchased from Santa Cruz Biotechnology (Santa Cruz, CA). Cells were transfected with shRNA complimentary to CBS mRNA (sc-60335-V) and selected for in the presence of 1 µg/mL puromycin to generate CBS-silenced cell lines OVCAR-5-R(shCBS) and SKOV-3-R(shCBS). Cells were transfected with scrambled shRNA (sc-108080) and selected for in the presence of 1 µg/mL puromycin to generate transfection control cell lines OVCAR-5-R(scram) and SKOV-3-R(scram).

Statistical analysis

Data are presented as means +/- standard error of n=3 independent experiments. Statistical comparison between two groups was performed using a two-tailed, paired Student's t-test, while comparisons between more than two groups was performed using ANOVA with post-hoc Tukey's test. P values less than 0.05 were considered statistically significant (*p<0.05). Regression analysis and IC50/ED50 estimations were determined using GraphPad Prism purchased from GraphPad Software (La Jolla, CA).

3.10 References

1. Siegel, R. L.; Miller, K. D.; Jemal, A., Cancer statistics, 2017. *Ca-a Cancer Journal for Clinicians* **2017**, *67* (1), 7-30.
2. Seidman, J. D.; Kurman, R. J., Pathology of ovarian carcinoma. *Hematology-Oncology Clinics of North America* **2003**, *17* (4), 909-+.
3. Romero, I.; Bast, R. C., Minireview: Human ovarian cancer: Biology, current management, and paths to personalizing therapy. *Endocrinology* **2012**, *153* (4), 1593-1602.
4. Agarwal, R.; Kaye, S. B., Ovarian cancer: Strategies for overcoming resistance to chemotherapy. *Nature Reviews Cancer* **2003**, *3* (7), 502-516.
5. Koberle, B.; Tomicic, M. T.; Usanova, S.; Kaina, B., Cisplatin resistance: Preclinical findings and clinical implications. *Biochimica Et Biophysica Acta-Reviews on Cancer* **2010**, *1806* (2), 172-182.
6. Galluzzi, L.; Senovilla, L.; Vitale, I.; Michels, J.; Martins, I.; Kepp, O.; Castedo, M.; Kroemer, G., Molecular mechanisms of cisplatin resistance. *Oncogene* **2012**, *31* (15), 1869-1883.

7. Wegiel, B.; Gallo, D.; Csizmadia, E.; Harris, C.; Belcher, J.; Vercellotti, G. M.; Penacho, N.; Seth, P.; Sukhatme, V.; Ahmed, A.; Pandolfi, P. P.; Helczynski, L.; Bjartell, A.; Persson, J. L.; Otterbein, L. E., Carbon monoxide expedites metabolic exhaustion to inhibit tumor growth. *Cancer Research* **2013**, *73* (23), 7009-7021.
8. Vitek, L.; Gbelcova, H.; Muchova, L.; Vanova, K.; Zelenka, J.; Konickova, R.; Suk, J.; Zadinova, M.; Knejzlik, Z.; Ahmad, S.; Fujisawa, T.; Ahmed, A.; Ruml, T., Antiproliferative effects of carbon monoxide on pancreatic cancer. *Digestive and Liver Disease* **2014**, *46* (4), 369-375.
9. Yamamoto, T.; Takano, N.; Ishiwata, K.; Ohmura, M.; Nagahata, Y.; Matsuura, T.; Kamata, A.; Sakamoto, K.; Nakanishi, T.; Kubo, A.; Hishiki, T.; Suematsu, M., Reduced methylation of PFKFB3 in cancer cells shunts glucose towards the pentose phosphate pathway. *Nature Communications* **2014**, *5*.
10. Kawahara, B.; Moller, T.; Hu-Moore, K.; Carrington, S.; Faull, K. F.; Sen, S.; Mascharak, P. K., Attenuation of antioxidant capacity in human breast cancer cells by carbon monoxide through inhibition of cystathionine β -synthase activity: implications in chemotherapeutic drug sensitivity. *Journal of Medicinal Chemistry* **2017**, *60* (19), 8000-8010.
11. Sen, S.; Kawahara, B.; Gupta, D.; Tsai, R.; Khachatryan, M.; Roy-Chowdhuri, S.; Bose, S.; Yoon, A.; Faull, K.; Farias-Eisner, R.; Chaudhuri, G., Role of cystathionine beta-synthase in human breast cancer. *Free Radical Biology and Medicine* **2015**, *86*, 228-238.
12. Bhattacharyya, S.; Saha, S.; Giri, K.; Lanza, I. R.; Nair, K. S.; Jennings, N. B.; Rodriguez-Aguayo, C.; Lopez-Berestein, G.; Basal, E.; Weaver, A. L.; Visscher, D. W.; Cliby, W.; Sood, A. K.; Bhattacharya, R.; Mukherjee, P., Cystathionine beta-synthase (CBS) contributes to advanced ovarian cancer progression and drug resistance. *Plos One* **2013**, *8* (11).
13. Chakraborty, I.; Carrington, S. J.; Roseman, G.; Mascharak, P. K., Synthesis, structures, and CO release capacity of a family of water-soluble photoCORMs:

- assessment of the biocompatibility and their phototoxicity toward human breast cancer cells. *Inorganic Chemistry* **2017**, *56* (3), 1534-1545.
14. Winburn, I. C.; Gunatunga, K.; McKernan, R. D.; Walker, R. J.; Sammut, I. A.; Harrison, J. C., Cell Damage following carbon monoxide releasing molecule exposure: implications for therapeutic applications. *Basic & Clinical Pharmacology & Toxicology* **2012**, *111* (1), 31-41.
 15. Jansen, B. A. J.; Brouwer, J.; Reedijk, J., Glutathione induces cellular resistance against cationic dinuclear platinum anticancer drugs. *Journal of Inorganic Biochemistry* **2002**, *89* (3-4), 197-202.
 16. Surowiak, P.; Materna, V.; Maciejczyk, A.; Pudelko, M.; Markwitz, E.; Spaczynski, M.; Dietel, M.; Zabel, M.; Lage, H., Nuclear metallothionein expression correlates with cisplatin resistance of ovarian cancer cells and poor clinical outcome. *Virchows Archiv* **2007**, *450* (3), 279-285.
 17. Kabil, O.; Banerjee, R., Enzymology of H₂S biogenesis, decay and signaling. *Antioxidants & Redox Signaling* **2014**, *20* (5), 770-782.
 18. Savaskan, N. E.; Eyupoglu, I. Y., xCT modulation in gliomas: Relevance to energy metabolism and tumor microenvironment normalization. *Annals of Anatomy-Anatomischer Anzeiger* **2010**, *192* (5), 309-313.
 19. Okuno, S.; Sato, H.; Kuriyama-Matsumura, K.; Tamba, M.; Wang, H.; Sohda, S.; Hamada, H.; Yoshikawa, H.; Kondo, T.; Bannai, S., Role of cystine transport in intracellular glutathione level and cisplatin resistance in human ovarian cancer cell lines. *British Journal of Cancer* **2003**, *88* (6), 951-956.
 20. Kimura, Y.; Kimura, H., Hydrogen sulfide protects neurons from oxidative stress. *Faseb Journal* **2004**, *18* (7), 1165-+.
 21. Yamamoto, T.; Takano, N.; Ishiwata, K.; Suematsu, M., Carbon monoxide stimulates global protein methylation via its inhibitory action on cystathionine beta-synthase. *Journal of Clinical Biochemistry and Nutrition* **2011**, *48* (1), 96-100.

22. Gessner, G.; Sahoo, N.; Swain, S. M.; Hirth, G.; Schonherr, R.; Mede, R.; Westerhausen, M.; Brewitz, H. H.; Heimer, P.; Imhof, D.; Hoshi, T.; Heinemann, S. H., CO-independent modification of K⁺ channels by tricarbonyldichlororuthenium(II) dimer (CORM-2). *European Journal of Pharmacology* **2017**, *815*, 33-41.
23. Druzhyna, N.; Szczesny, B.; Olah, G.; Modis, K.; Asimakopoulou, A.; Pavlidou, A.; Szoleczky, P.; Gero, D.; Yanagi, K.; Toro, G.; Lopez-Garcia, I.; Myriantopoulos, V.; Mikros, E.; Zatarain, J. R.; Chao, C.; Papapetropoulos, A.; Hellmich, M. R.; Szabo, C., Screening of a composite library of clinically used drugs and well-characterized pharmacological compounds for cystathionine beta-synthase inhibition identifies benserazide as a drug potentially suitable for repurposing for the experimental therapy of colon cancer. *Pharmacological Research* **2016**, *113*, 18-37
24. Kaplowitz, N., The importance and regulation of hepatic glutathione. *Yale Journal of Biology and Medicine* **1981**, *54* (6), 497-502.
25. Pinto, M. N.; Chakraborty, I.; Sandoval, C.; Mascharak, P. K., Eradication of HT-29 colorectal adenocarcinoma cells by controlled photorelease of CO from a CO-releasing polymer (photoCORP-1) triggered by visible light through an optical fiber-based device. *Journal of Controlled Release* **2017**, *264*, 192-202.
26. Kourti, M.; Jiang, W. G.; Cai, J., Aspects of carbon monoxide in form of CO-releasing molecules used in cancer treatment: More light on the way. *Oxidative Medicine and Cellular Longevity* **2017**.
27. Reedijk, J., Why does cisplatin reach guanine-N7 with competing S-donor ligands available in the cell? *Chemical Reviews* **1999**, *99* (9), 2499-2510.
28. Ishikawa, T.; Aliosman, F., Glutathione-associated cis-diamminedichloroplatinum(II) metabolism and ATP-dependent efflux from leukemia-cells – molecular characterization of platinum complex and its biological significance. *Journal of Biological Chemistry* **1993**, *268* (27), 20116-20125.

29. Kasherman, Y.; Sturup, S.; Gibson, D., Is glutathione the major cellular target of cisplatin? A study of the interactions of cisplatin with cancer cell extracts. *Journal of Medicinal Chemistry* **2009**, *52* (14), 4319-4328.
30. Karotki, A. V.; Vasak, M., Interaction of metallothionein-2 with platinum-modified 5'-guanosine monophosphate and DNA. *Biochemistry* **2008**, *47* (41), 10961-10969.
31. Theocharis, S. E.; Margeli, A. P.; Klijanienko, J. T.; Kouraklis, G. P., Metallothionein expression in human neoplasia. *Histopathology* **2004**, *45* (2), 103-118.
32. Tan, Y.; Sinniah, R.; Bay, B. H.; Singh, G., Expression of metallothionein and nuclear size in discrimination of malignancy in mucinous ovarian tumors. *International Journal of Gynecological Pathology* **1999**, *18* (4), 344-350.
33. Lewis, A. D.; Hayes, J. D.; Wolf, C. R., Glutathione and glutathione-dependent enzymes in ovarian adenocarcinoma cell-lines derived from a patient before and after the onset of drug-resistance – intrinsic differences and cell-cycle effects. *Carcinogenesis* **1988**, *9* (7), 1283-1287.
34. Chen, H. H. W.; Kuo, M. T., Role of glutathione in the regulation of cisplatin resistance in cancer chemotherapy. *Metal-Based Drugs* **2010**, 430939-Article No.: 430939.
35. Ungard, R. G.; Seidlitz, E. P.; Singh, G., Inhibition of breast cancer-cell glutamate release with sulfasalazine limits cancer-induced bone pain. *Pain* **2014**, *155* (1), 28-36.
36. Sharma, M. K.; Seidlitz, E. P.; Singh, G., Cancer cells release glutamate via the cystine/glutamate antiporter. *Biochemical and Biophysical Research Communications* **2010**, *391* (1), 91-95.
37. Habib, E.; Linher-Melville, K.; Lin, H. X.; Singh, G., Expression of xCT and activity of system X-c(-) are regulated by NRF2 in human breast cancer cells in response to oxidative stress. *Redox Biology* **2015**, *5*, 33-42.

38. Ishimoto, T.; Nagano, O.; Yae, T.; Tamada, M.; Motohara, T.; Oshima, H.; Oshima, M.; Ikeda, T.; Asaba, R.; Yagi, H.; Masuko, T.; Shimizu, T.; Ishikawa, T.; Kai, K.; Takahashi, E.; Imamura, Y.; Baba, Y.; Ohmura, M.; Suematsu, M.; Baba, H.; Saya, H., CD44 Variant Regulates Redox Status in Cancer Cells by Stabilizing the xCT Subunit of System xc(-) and Thereby Promotes Tumor Growth. *Cancer Cell* **2011**, *19* (3), 387-400.
39. Uhlen, M.; Fagerberg, L.; Hallstrom, B. M.; Lindskog, C.; Oksvold, P.; Mardinoglu, A.; Sivertsson, A.; Kampf, C.; Sjostedt, E.; Asplund, A.; Olsson, I.; Edlund, K.; Lundberg, E.; Navani, S.; Szigartyo, C. A.; Odeberg, J.; Djureinovic, D.; Takanen, J. O.; Hober, S.; Alm, T.; Edqvist, P. H.; Berling, H.; Tegel, H.; Mulder, J.; Rockberg, J.; Nilsson, P.; Schwenk, J. M.; Hamsten, M.; von Feilitzen, K.; Forsberg, M.; Persson, L.; Johansson, F.; Zwahlen, M.; von Heijne, G.; Nielsen, J.; Ponten, F., Tissue-based map of the human proteome. *Science* **2015**, *347* (6220).

3.11 Reprint of publication

Rightslink® by Copyright Clearance Center



RightsLink®



Home



Help



Email Support



Brian Kawahara ▾



Carbon monoxide sensitizes cisplatin-resistant ovarian cancer cell lines toward cisplatin via attenuation of levels of glutathione and nuclear metallothionein

Author:

Brian Kawahara, Sivakumar Ramadoss, Gautam Chaudhuri, Carla Janzen, Suvajit Sen, Pradip K. Mascharak

Publication: Journal of Inorganic Biochemistry

Publisher: Elsevier

Date: February 2019

© 2018 Published by Elsevier Inc.

Please note that, as the author of this Elsevier article, you retain the right to include it in a thesis or dissertation, provided it is not published commercially. Permission is not required, but please ensure that you reference the journal as the original source. For more information on this and on your other retained rights, please visit: <https://www.elsevier.com/about/our-business/policies/copyright#Author-rights>

BACK

CLOSE WINDOW

© 2020 Copyright - All Rights Reserved | [Copyright Clearance Center, Inc.](#) | [Privacy statement](#) | [Terms and Conditions](#)
Comments? We would like to hear from you. E-mail us at customer-care@copyright.com



Contents lists available at ScienceDirect

Journal of Inorganic Biochemistry

journal homepage: www.elsevier.com/locate/jinorgbio

Carbon monoxide sensitizes cisplatin-resistant ovarian cancer cell lines toward cisplatin via attenuation of levels of glutathione and nuclear metallothionein



Brian Kawahara^a, Sivakumar Ramadoss^b, Gautam Chaudhuri^b, Carla Janzen^b, Suvajit Sen^{b,*}, Pradip K. Mascharak^{b,*}

^a Contribution from Department of Chemistry and Biochemistry, University of California, Santa Cruz, CA 95064, United States of America

^b Department of Obstetrics and Gynecology, David Geffen School of Medicine at University of California at Los Angeles, Los Angeles, CA 90095, United States of America

ARTICLE INFO

Keywords:

Carbon monoxide
Ovarian cancer
Cisplatin-resistance
Cystathionine β-synthase
Glutathione
Metallothionein

ABSTRACT

Cisplatin resistance remains a major impediment to effective treatment of ovarian cancer. Despite initial platinum responsiveness, thiol-containing peptides and proteins, glutathione (GSH) and metallothionein (MT), bind and inactivate cisplatin in cancer cells. Indeed, high levels of GSH and MT in ovarian cancers impart cisplatin resistance and are predictive of poor prognosis. Cystathionine β-synthase (CBS), an enzyme involved in sulfur metabolism, is overexpressed in ovarian cancer tissues and is itself associated with cisplatin resistance. Treatment with exogenous carbon monoxide (CO), a known inhibitor of CBS, may mitigate cisplatin resistance in ovarian cancer cells by attenuation of GSH and MT levels. Using a photo-activated CO-releasing molecule (photoCORM), [Mn(CO)₃(phen)(PTA)]CF₃SO₃ (phen = 1,10-phenanthroline, PTA = 1,3,5-triaza-7-phosphaadamantane) we assessed the ability of CO to sensitize established cisplatin-resistant ovarian cancer cell lines to cisplatin. Cisplatin-resistant cells, treated with both cisplatin and CO, exhibited significantly lower cell viability and increased poly (ADP-ribose) polymerase (PARP) cleavage versus those treated with cisplatin alone. These cisplatin-resistant cell lines overexpressed CBS and had increased steady state levels of GSH and expression of nuclear MT. Both CO treatment and lentiviral-mediated silencing of CBS attenuated GSH and nuclear MT expression in cisplatin resistant cells. We have demonstrated that CO, delivered from a photoCORM, sensitizes established cisplatin-resistant cell lines to cisplatin. Furthermore, we have presented strong evidence that the effects of CO in circumventing chemotherapeutic drug resistance is at least in part mediated by the inactivation of endogenous CBS.

1. Introduction

Ovarian cancer is the fifth most prevalent and the most lethal gynecological cancer in the United States [1]. The overall 5-year survival rate for advanced ovarian cancer patients is only ~40% and has remained largely static over the past 20 years [2]. The current standard of care includes cytoreductive surgery and combination platinum/taxane chemotherapy [3]. However, ~90% of ovarian cancer deaths are caused by chemotherapeutic resistance and metastasis [4]. Clearly there is an unmet need for treatment modalities to mitigate chemotherapeutic resistance.

Cisplatin is one of the most widely used and effective anti-cancer drugs. In addition to ovarian cancer, it is the standard of care for other solid cancers of the head and neck, bowel and colon, cervix and lung.

By localizing to the nucleus and binding to DNA, cisplatin gives rise to intrastrand DNA adducts and triggers G2 cell cycle arrest and subsequent apoptosis. The effectiveness of cisplatin, however, is limited by the high incidences of drug resistance [5,6]. In the cases of colorectal, lung and prostate cancers, intrinsic resistance is common [5]. In ovarian cancer, however, resistance is mainly acquired after initial treatment and response to cisplatin therapy [5]. Understanding the cellular changes that occur in the development of cisplatin resistance will help in developing more effective means of circumventing cisplatin resistance in ovarian cancer.

Exogenous carbon monoxide (CO) has recently been shown to decrease chemotherapeutic resistance and proliferation in various cancer cell types [7–9]. Our group has recently reported that CO increased the sensitivity of human breast cancer cells to doxorubicin mediated cell

* Corresponding authors.

E-mail addresses: ssen@mednet.ucla.edu (S. Sen), pradip@uclsc.edu (P.K. Mascharak).

<https://doi.org/10.1016/j.jinorgbio.2018.11.003>

Received 8 June 2018; Received in revised form 31 October 2018; Accepted 4 November 2018

Available online 10 November 2018

0162-0134/ © 2018 Published by Elsevier Inc.

Abbreviations

CBS	cystathionine β -synthase
CGL	cystathionine γ -lyase
CO	carbon monoxide
CTH	cystathionine
FBS	fetal bovine serum
GSH	glutathione

MT	metallothionein
NEM	N-ethylmaleimide
OV	OVCAR-5
OVcisR	cisplatin-resistant OVCAR-5
PARP	poly (ADP-ribose) polymerase
PMSF	phenylmethane sulfonyl fluoride
SKV	SKOV-3
SKVcisR	cisplatin-resistant SKOV-3

death by > 40% via the inhibition of endogenous cystathionine β -synthase (CBS) enzymatic activity [10]. CBS is overexpressed selectively in human breast cancer tissues and not in normal human breast tissues making it a potential therapeutic target [11]. Interestingly, CBS is overexpressed in only a few other neoplasms, one of which is ovarian cancer, where CBS has been implicated in resistance to cisplatin [12]. However, the mitigation of chemotherapeutic drug resistance, using a pharmacological inhibitor of CBS has not yet been demonstrated in ovarian cancer cells. This study for the first time assessed the pharmacological inhibition of CBS by a light-induced CO delivery modality to counter chemotherapeutic drug resistance in human ovarian cancer cells. The results underscore the important role of the transsulfuration pathway in the development of chemotherapeutic drug resistance in ovarian cancer.

The noxious nature of gaseous CO often poses challenging delivery issues in hospital settings. To avoid this problem, a designed metal carbonyl complex namely $[\text{Mn}(\text{CO})_3(\text{phen})(\text{PTA})]\text{CF}_3\text{SO}_3$ (phen = 1,10-phenanthroline; PTA = 1,3,5-triaza-7-phosphaadamantane; abbreviated “photoCORM” hereafter) has been employed as the exogenous CO source in this study (Scheme 1). This designed manganese carbonyl complex is water-soluble and rapidly releases CO only when exposed to low-power (10 mW/cm^2) broadband visible light. This photoactive CO-releasing molecule (photoCORM) has been a convenient source of CO in delivery under controlled conditions [10,13].

2. Materials and methods**2.1. Materials and reagents**

$[\text{Mn}(\text{CO})_3(\text{phen})(\text{PTA})]\text{CF}_3\text{SO}_3$ (photoCORM) was synthesized, analyzed to confirm purity, and applied as previously published [10,13]. Cisplatin (479306), protease inhibitor cocktail (P8340), puromycin (P8833), N-acetylcysteine (A7250), 3-(4,5-Dimethylthiazol-2-yl)-2,5-Diphenyltetrazolium Bromide (MTT) and other chemicals were products of Sigma Aldrich (St. Louis, MO). GYY 4137 (13345) was purchased from Cayman Chemicals (Ann Arbor, MI). Primary antibodies against CBS (sc-133208), cystathionine γ -lyase (CGL, sc-365382), poly (ADP-ribose) polymerase (PARP-1, sc-56196), Lamin A (sc-71481), β -tubulin (sc-23949) and Glyceraldehyde 3-phosphate dehydrogenase (GAPDH, sc-47724) were purchased from Santa Cruz Biotechnology (Santa Cruz, CA). Mouse monoclonal antibody against metallothionein (ab12228) and rabbit polyclonal antibody against xCT (ab 37185) were purchased from Abcam (Cambridge, MA).

2.2. Cell culture

Ovarian cancer cell lines OVCAR-5 (OV), cisplatin-resistant OVCAR-5 (OVcisR), SKOV-3 (SKV), and cisplatin-resistant SKOV-3 (SKVcisR) were a gift from Dr. Sivakumar Ramadoss and Dr. Gautam Chaudhuri of the David Geffen School of Medicine at University of California at Los Angeles. Cells were grown in $1 \times$ RPMI media supplemented with 10% fetal bovine serum, 100 I.U./mL penicillin and 100 $\mu\text{g}/\text{mL}$ streptomycin at $37^\circ\text{C} + 5\% \text{ CO}_2$. Mycoplasma detection was performed regularly to confirm its absence with MycoAlert™ Mycoplasma Detection Kit (LT07-218) from Lonza (Basel, Switzerland). Cells were passaged no more

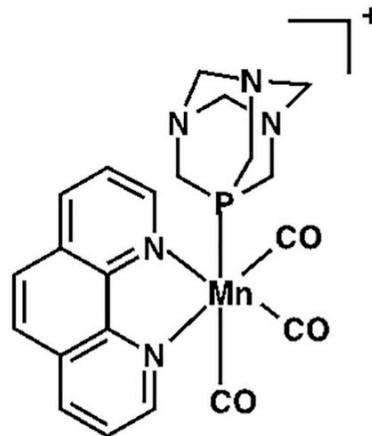
than five times after being received. Unless otherwise indicated, cells were allowed to seed overnight prior to treatments, then assayed 24 h post-treatment.

2.3. CO and cisplatin treatments of cells

Cells were seeded overnight, $100 \times 10^3/\text{well}$ of 6-well tissue culture dishes or $1 \times 10^6/\text{well}$ of 100 mm tissue culture dishes depending on the experiment being performed, and incubated at $37^\circ\text{C} + 5\% \text{ CO}_2$ 24 h prior to cell culture treatments. Cells treated with CO were exposed to $30 \mu\text{M}$ photoCORM in the dark. To control for the effects of the non-CO backbone of the CO-releasing molecule, corresponding control cells were treated with $30 \mu\text{M}$ light-inactivated photoCORM (iCORM) in the dark. Upon addition of photoCORM or iCORM, cells were exposed to visible light for 30 min at room temperature, then returned back to $37^\circ\text{C} + 5\% \text{ CO}_2$. In experiments involving cisplatin, $20 \mu\text{M}$ cisplatin or DMSO vehicle control was administered either by itself or together with $30 \mu\text{M}$ photoCORM or iCORM. In experiments utilizing NAC, 3 mM NAC or vehicle control were added to cells along with photoCORM and cisplatin. Subsequent assays were performed 24 h post-treatment.

2.4. Cell viability (Trypan blue exclusion and MTT) assay

When assessing cell viability via Trypan blue exclusion method, 100×10^3 cells/well of a 6-well tissue culture plate were allowed to seed overnight in a 37°C incubator + $5\% \text{ CO}_2$. The next day, cells were treated as indicated and allowed to incubate for 24 h. Following treatment, cells were harvested with 1 mL 0.05% Trypsin-EDTA, after which trypsin was neutralized with 1 mL cell culture media



Scheme 1. Structure of $[\text{Mn}(\text{CO})_3(\text{phen})(\text{PTA})]\text{CF}_3\text{SO}_3$, the photoCORM used in this study.

supplemented with 10% FBS. This cell suspension was then visualized and quantified using a Vi-Cell XR cell viability analyzer from Beckman Coulter (Brea, CA). Cell viability was measured 24 h post-treatment and presented as the mean % of control or comparison group \pm SEM of three independent experiments.

In cell viability experiments performed using the tetrazolium dye MTT, experiments were performed in 96-well tissue culture plates. Briefly, 4×10^3 cells were allowed to seed overnight in a 37 °C incubator + 5% CO₂. The next day, cells were treated as indicated, then assessed for viability 24 h post-treatment. Cell culture media was aspirated from cells, then replaced with 0.5 mg/mL MTT dissolved in fresh 1 \times DMEM and allowed to incubate for 2 h in a 37 °C incubator + 5% CO₂. Number of viable cells was assessed by quantifying the amount of MTT reduced to insoluble formazan. Insoluble formazan was solubilized in 10% SDS + 0.01 N HCl. The absorbance at 570 nm, with reference wavelength at 690 nm, was measured. Data are presented as average % change \pm SEM from control(s) of $n = 3$ independent experiments.

2.5. Western blot analysis

Whole cell lysates were prepared after treatment in RIPA lysis buffer containing 150 mM NaCl, 5 mM EDTA pH 8.0, 50 mM Tris pH 8.0, 1% Triton X-100, 0.5% sodium deoxycholate, 1% SDS and 1 \times protease inhibitor cocktail. Soluble lysates were quantified using a Pierce™ BCA Protein Assay Kit (23225) from ThermoFisher Scientific (Waltham, MA), 20 μ g cell lysates from samples were separated on 4–12% SDS-PAGE gel and transferred to poly(vinylidene difluoride) (PVDF) membrane. Membranes were blocked with 5% nonfat dried milk and incubated for 1 h room temperature or 4 °C overnight. Primary (1:1000 dilution) and horseradish peroxidase (HRP)-conjugated secondary (1:10,000 dilution) antibody incubations were performed at room temperature for 1 h. Immunofluorescent signals were detected with Pierce ECL Plus Western blotting substrate (32132) from ThermoFisher Scientific.

2.6. High performance liquid chromatography-mass spectrometry

Glutathione (GSH), γ -Glu-Cys, cysteine and cystathionine (CTH) were measured utilizing high pressure, liquid chromatography-mass spectrometry (HPLC-MS) as previously described [10]. $\sim 5 \times 10^6$ cells were lysed via three probe sonication in 200 μ L of 10 mM *N*-ethylmaleimide (NEM) + 10 mM ammonium acetate, pH 7.4. To the lysate, 800 μ L of methanol was added and the samples were vortexed. Samples were then centrifuged at 16,000 \times g for 5 min, then supernatants were collected into microcentrifuge tubes and dried via vacuum centrifugation. Samples were further dried with 100 μ L methanol, then 100 μ L benzene. The carboxy termini of metabolites were esterified with the treatment of 100 μ L of 3 N methanolic HCl for 60 min, 60 °C. Samples were then dried via vacuum centrifugation, redissolved in 50 μ L of water and transferred to liquid chromatography injector vials. Kinetex XB-C18, 100 \times 2.1 mm, 1.7- μ m particle size, 100 Å pore diameter, reverse phase column from Phenomenex (Torrance, CA) column was equilibrated with 85% 0.1 mM perfluorooctanoic acid in water (eluant A) and 15% 0.1 mM perfluorooctanoic acid in acetonitrile (eluant B). Samples were injected onto the equilibrated column and eluted at 100 μ L/min with increasing concentration of eluant B (min/% B: 0/15, 5/15, 35/50, 33/ 15, 45/15). The eluants were directed toward an Agilent Jet Stream electrospray ionization (ESI) source connected to a triple quadrupole mass spectrometer (Agilent 6460) operating in positive ion tandem mass spectrometric multiple reaction-monitoring (MRM) mode. The intensities of the CTH parent to fragment transition (461 \rightarrow 318, rt 27.88 min), cysteine-NEM conjugate (261 \rightarrow 244, rt 24.06 min), GSH-NEM conjugate (461 \rightarrow 318, rt 26.06 min) and γ -Glu-Cys-NEM conjugate (404 \rightarrow 244, rt 26.59 min) were recorded using previously-determined settings. Standards were prepared containing

known concentrations of CTH (0, 20, 40, 80, 160 pmol), cysteine (0, 80, 160, 320, 640 pmol), GSH (0, 200, 400, 800, 1600 pmol) and γ -Glu-Cys (0, 100, 200, 400, 800 pmol). From these standards, calibration curves were constructed. The amount of the monitored metabolites in biological samples was calculated by interpolation from the curves. Signals for monitored metabolites were normalized to total μ g protein and expressed as either average pmol/ μ g protein OR average percentage/fold-difference from control or comparison group \pm SEM of $n = 3$ independent experiments.

2.7. D4-cystine uptake assay and H₂S donation

1 \times DMEM with high glucose but no glutamine, methionine, and cystine (D0422) was procured from Sigma Aldrich. This media was then supplemented with 3.97 mM glutamine, 200 μ M methionine, 10% FBS and 200 μ M D4-CC (DLM-1000-PK), which was purchased from Cambridge Isotope Laboratories (Tewksbury, MA). $\sim 1 \times 10^6$ cells were seeded in 100 mm tissue culture dishes and allowed to grow for 48 h at 37 °C + 5% CO₂. In experiments where H₂S-donor GYY 4137 was used, either 40 μ M GYY 4137 or DMSO vehicle control was added for 48 h. Cells were harvested and processed in the identical manner described above (Section 2.6). Reported D4-CC uptake was measured by quantifying intracellular D2-cysteine levels normalized to total μ g protein. Data are presented as average fold-difference from control or comparison group \pm SEM of $n = 3$ independent experiments.

2.8. Nuclear fraction enrichment

5×10^6 cells were scraped from 100 mm tissue culture dishes on ice and washed with cold, 1 \times PBS (phosphate buffer saline). Cells were suspended in cold lysis buffer containing the following: 10 mM HEPES pH 7.7, 10 mM KCl, 0.1 mM EDTA, 1 mM dithiothreitol (DTT), 0.5% NP-40, 0.5 mM PMSF and protease inhibitor cocktail. Cells were incubated on ice for 15 min with intermittent mixing, then centrifuged at 12,000 \times g at 4 °C for 10 min. The supernatant was collected as the cytosolic enriched fraction. The nuclear pellet was washed three times with cold lysis buffer, then resuspended in cold nuclear extraction buffer containing 20 mM HEPES pH 7.5, 400 mM NaCl, 1 mM EDTA, 1 mM DTT, 1 mM PMSF and protease inhibitor cocktail. After incubation on ice for 30 min, the enriched nuclear fraction was collected by centrifugation at 12,000 \times g at 4 °C for 15 min.

2.9. Gene silencing experiments

Stable silencing of CBS expression in OVcisR and SKVcisR was achieved utilizing short hairpin RNA (shRNA) packaged in lentiviral particles purchased from Santa Cruz Biotechnology (Santa Cruz, CA). Cells were transfected with shRNA complimentary to CBS mRNA (sc-60335-V) and selected for in the presence of 1 μ g/mL puromycin to generate CBS-silenced cell lines OVcisR(shCBS) and SKVcisR(shCBS). Cells were transfected with scrambled shRNA (sc-108080) and selected for in the presence of 1 μ g/mL puromycin to generate transfection control cell lines OVcisR(scram) and SKVcisR(scram).

2.10. Statistical analysis

Data are presented as means \pm SEM of $n = 3$ independent experiments. Statistical comparison between two groups was performed using a two-tailed, paired Student's *t*-test, while comparisons between more than two groups was performed using ANOVA with post hoc Tukey's test. *p* values < 0.05 were considered statistically significant (**p* < 0.05). Regression analysis and IC₅₀/ED₅₀ estimations were determined using GraphPad Prism purchased from GraphPad Software (La Jolla, CA).

3. Results

3.1. Cisplatin-resistant ovarian cancer cell lines were re-sensitized to cisplatin upon co-treatment with CO

Previous studies have demonstrated the ability of CO to sensitize

cancer cells to chemotherapeutics [7,9,10], though cisplatin resistance and ovarian cancer had yet to be addressed. In this study, we wanted to assess the ability of CO, delivered by 30 μM photoCORM, to sensitize established cisplatin-resistant ovarian cancer cells. 30 μM of photoCORM was used in this study because CO concentrations higher than that delivered from > 30 μM photoCORM, were cytotoxic to the cells

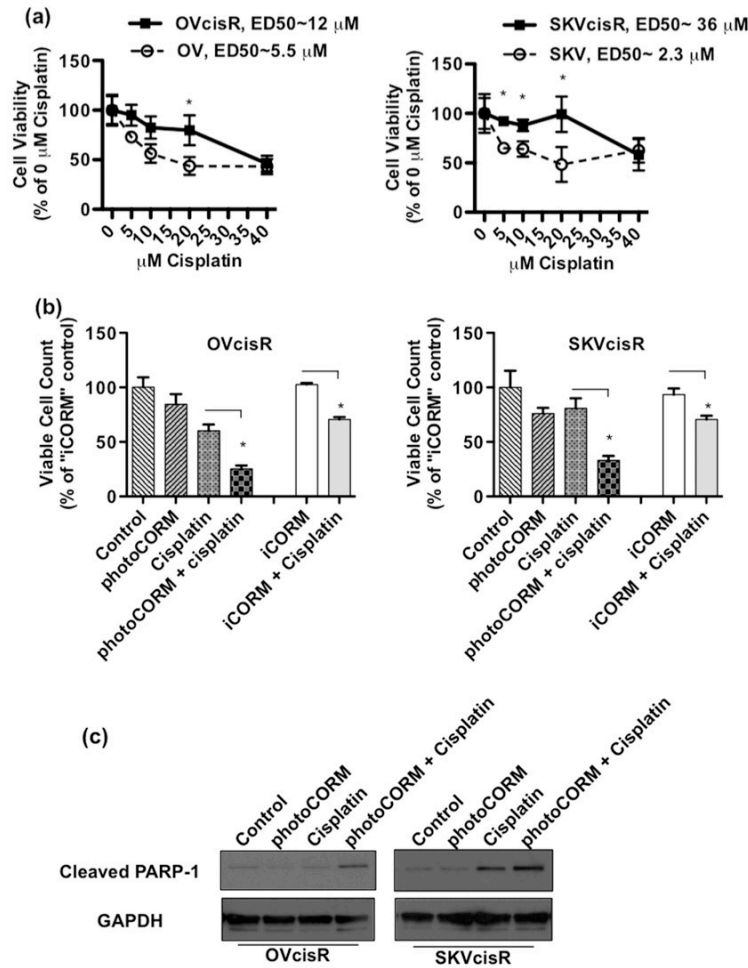


Fig. 1. Cisplatin-resistant ovarian cancer cell lines are sensitized to cisplatin upon co-treatment with carbon monoxide (CO), delivered from a photo-activated CO-releasing molecule (photoCORM). (a) Dose-dependency of cisplatin on cell viability in cisplatin-sensitive and resistant cell lines. Cells were treated with 0–40 μM cisplatin and/or DMSO vehicle control. Cell viability was then measured 24 h post-treatment via Trypan blue exclusion. Data are presented as average % of 0 μM cisplatin \pm SEM of $n = 3$ independent experiments. (* $p < 0.05$). (b) Cell viability 24 h post-treatment, as measured by trypan blue exclusion, of cisplatin-resistant ovarian cancer cell lines, assessing the ability of CO to sensitize cisplatin-resistant ovarian cancer cell lines cells to cisplatin. iCORM, photo-inactivated photoCORM, was used as control for the non-CO scaffolding of the photoCORM. In lieu of cisplatin treatment, cells were treated with DMSO as vehicle control. Data are presented as average percentages of “Control” \pm SEM of $n = 3$ independent experiments. (* $p < 0.05$). (c) Immunoblot of 20 μg whole cell lysate for cleaved PARP-1 in cisplatin-resistant ovarian cancer cell lines treated with CO and/or cisplatin. GAPDH was probed to assess equal protein loading. Blots presented are representative blots of $n = 3$ independent experiments.

used in this study (Supporting information, Fig. S1). Cisplatin-resistant versions of ovarian cancer cell lines OVCA-5 and SKOV-3 (abbreviated OVcisR and SKVcisR respectively) were assessed for their resistance to therapeutically relevant concentrations of cisplatin compared to their respective parent cancer cell lines, OVCA-5 and SKOV-3 (abbreviated OV and SKV respectively). Dose-response experiments revealed that OVcisR, and SKVcisR exhibited significant cisplatin resistance, with > 2-fold increased ED50 values for cisplatin compared with OV and SKV respectively (Fig. 1a). Because CO has been shown to sensitize certain cancer cells to chemotherapeutics, we wanted to assess whether CO, delivered from a photoCORM, could work similarly in an ovarian cancer model, attenuating drug resistance for platinum-based chemotherapies in ovarian cancer cell lines. To determine this, we treated cisplatin-resistant cell lines, OVcisR and SKVcisR, with 30 μ M photoCORM and 20 μ M cisplatin and compared these cell viability to cells treated with cisplatin alone. We observed that CO significantly enhanced the ability of cisplatin to reduce cell viability of cisplatin-resistant cell lines compared with cisplatin treatment alone (Fig. 1b). OVcisR and SKVcisR cells treated with cisplatin alone exhibited ~40% and ~29% decreases in cell viability, which was enhanced > 2-fold in both cell lines by CO, delivered from 30 μ M photoCORM (Fig. 1b). Light-inactivated photoCORM (iCORM) neither significantly alter cell viability itself nor enhanced the cytotoxicity of cisplatin toward OVcisR and SKVcisR (Fig. 1b), demonstrating the negligible effect of the molecular scaffolding of the photoCORM toward increasing cisplatin sensitivity in OVcisR and SKVcisR. Lower doses of photoCORM also sensitized cisplatin-resistant cells to cisplatin in a concentration-dependent manner (Supporting information, Fig. S2). To determine whether the actions of CO and cisplatin together were apoptotic in nature, we assessed PARP-1 cleavage. Indeed, the sensitization of OVcisR and SKVcisR to cisplatin by co-treatment with 30 μ M CO corresponded to increased PARP-1 cleavage in whole cell lysates, indicating an apoptotic process (Fig. 1c). Interestingly, we found 24 h treatment with that co-addition of 3 mM N-acetylcysteine (NAC), an antioxidant and efficient donor of cysteine, for 24 h was able to largely reverse CO's ability to re-sensitize of OVcisR and SKVcisR to cisplatin (Supporting information, Fig. S3). This finding indicated that NAC, and its effect on OVcisR and SKVcisR, disrupted the cellular processes by which CO sensitizes these cells to cisplatin. Since NAC is an efficient donor of cysteine, we measured steady state levels of intracellular cysteine by HPLC-MS. Indeed, 3 mM NAC treatment for 24 h increased intracellular levels of cysteine in ~4.4-fold in OVcisR and ~3.8-fold in SKVcisR compared with respective vehicle controls (Supporting information, Fig. S4). Together, these findings regarding NAC suggested that intracellular levels of cysteine, a sulfur-containing amino acid, might be mechanistically important for the cisplatin-resistance phenotype in OVcisR and SKVcisR.

3.2. Cisplatin resistance in ovarian cancer cells was associated with increased expression and activity of CBS

Cisplatin resistance is attributed to increased drug inactivation by sulfur-containing nucleophilic species GSH and nuclear metallothionein (MT) binding and inactivating the drug [14,15]. Increased generation of GSH and MT places a significant demand for cysteine, as both GSH and MT require the same sulfur-containing amino acid. One of the major sources of cysteine can be from the enzymatic actions of CBS and cystathionine γ -lyase (CGL), transsulfuration pathway enzymes that convert homocysteine to cysteine [16]. Immunoblot analysis of 20 μ g whole cell lysates revealed dramatically increased expression of both CBS and CGL, transsulfuration pathway enzymes, in cisplatin-resistant versus the corresponding sensitive cells (Fig. 2a). Additionally, steady state levels of intracellular CTH, the enzymatic product of CBS, was present ~3.1-fold more in OVcisR and ~7.5-fold more in SKVcisR versus cisplatin-sensitive cell lines OV and SKV respectively (Fig. 2b).

3.3. Cisplatin-resistant ovarian cancer cell lines exhibited increased uptake of cystine and steady state levels of cysteine versus corresponding cisplatin-sensitive cell lines

In addition to overexpressing CBS, cisplatin-resistant ovarian cancer cell lines OVcisR and SKVcisR also exhibited overexpression of CGL (Fig. 2a), an enzyme downstream of CBS in the transsulfuration pathway. CGL breaks down CTH into the amino acid cysteine, which, like CTH, was found at higher steady state levels in cisplatin-resistant cell lines, ~2.7-fold more in OVcisR and ~1.4-fold compared to cisplatin-sensitive cells (Fig. 3a). CGL, however, is only one of several processes by which cysteine levels are regulated in the cell. In addition to the generation of cysteine through the transsulfuration pathway, uptake of cystine, an oxidized disulfide of two cysteine molecules, by the glutamate/cystine antiporter (xCT) is known to be an important source of intracellular cysteine for cancer cells, including ovarian cancer [18]. Furthermore, certain cisplatin-resistant ovarian cancer cells are reported to have increased cysteine-uptake via xCT [18]. In consideration of this alternate source of cysteine, we measured relative uptake of extracellular deuterium-labeled cystine (D4-CC) by cisplatin-resistant ovarian cancer cells compared to their respective cisplatin-sensitive counterparts. The relative uptake of D4-CC was quantified by measuring intracellular levels of heavy labeled cystine and cysteine

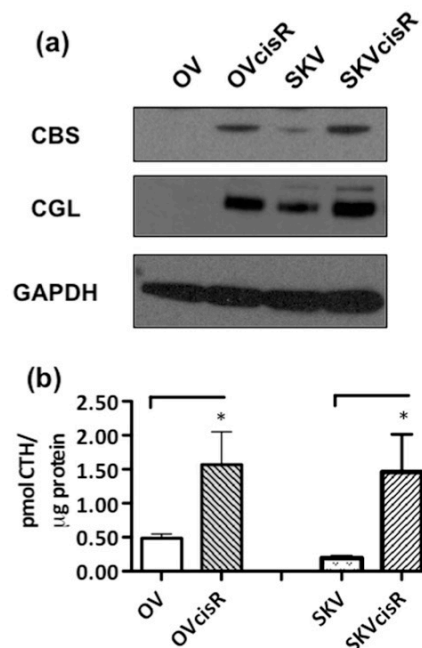


Fig. 2. Cystathionine β -synthase (CBS) expression and activity correlates with cisplatin-resistance in ovarian cancer cells. (a) Immunoblot for CBS and cystathionine γ -lyase (CGL) of 20 μ g whole cell lysate of ovarian cancer cells, both cisplatin-sensitive and cisplatin-resistant cells. GAPDH expression was used as a loading control. Blots are representative of $n = 3$ independent experiments. (b) Steady state levels of cystathionine (CTH) in ovarian cancer cell lines, as determined by HPLC-MS. Data presented as average pmol CTH per μ g protein \pm SEM of $n = 3$ independent experiments. (* $p < 0.05$).

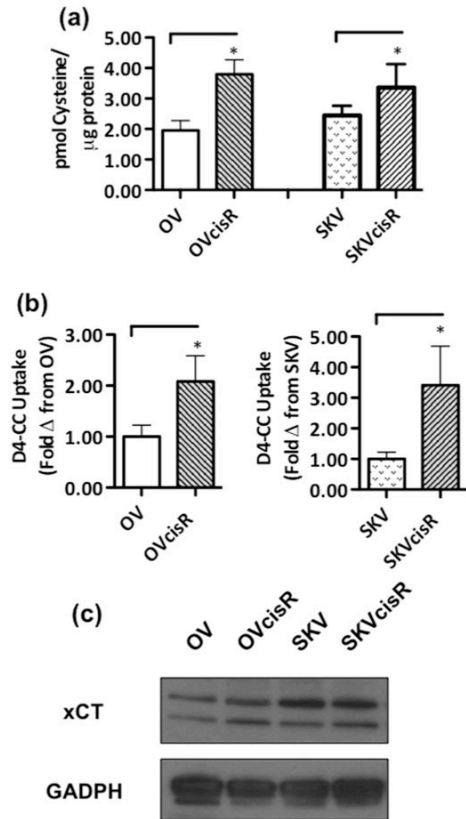


Fig. 3. Cisplatin-resistant ovarian cancer cell lines, OVcisR and SKVcisR, maintain higher levels of intracellular cysteine compared with cisplatin-sensitive cell lines. (a) Steady state levels of cysteine in OVcisR and SKVcisR, cisplatin-resistant ovarian cancer cell lines, compared with OV and SKV, cisplatin-sensitive ovarian cancer cell lines. Data are presented as average pmol cysteine/ μg protein \pm SEM of $n = 3$ independent experiments. ($*p < 0.05$) (b) Relative uptake of D4-cysteine (D4-CC) by OVcisR and SKVcisR compared to OV and SKV respectively. Data expressed as average fold difference from OV and SKV \pm SEM of $n = 3$ independent experiments. ($*p < 0.05$). (c) Representative immunoblot of three independent experiments, showing the relative expression of xCT in 20 μg whole cell lysate of cisplatin-sensitive and cisplatin-resistant cell lines. GAPDH was used as a loading control.

(D4-CC and D2-cysteine respectively). We observed cisplatin-resistant cells, OVcisR and SKVcisR, contained ~ 2.1 and ~ 3.4 times more intracellular D2-cysteine (the reduced form of D4-CC) than OV and SKV, their respective cisplatin-sensitive cells, indicating a greater capacity to uptake cysteine (Fig. 3b). Intracellular D4-CC was not detected at levels above background (data not shown). This is in accordance with previous observations because intracellular cysteine is quickly reduced to two cysteine residues, due to the reducing environment of the cytosol [18]. Despite the increased uptake of cysteine in cisplatin-resistant cells, xCT protein expression was not remarkably different between the

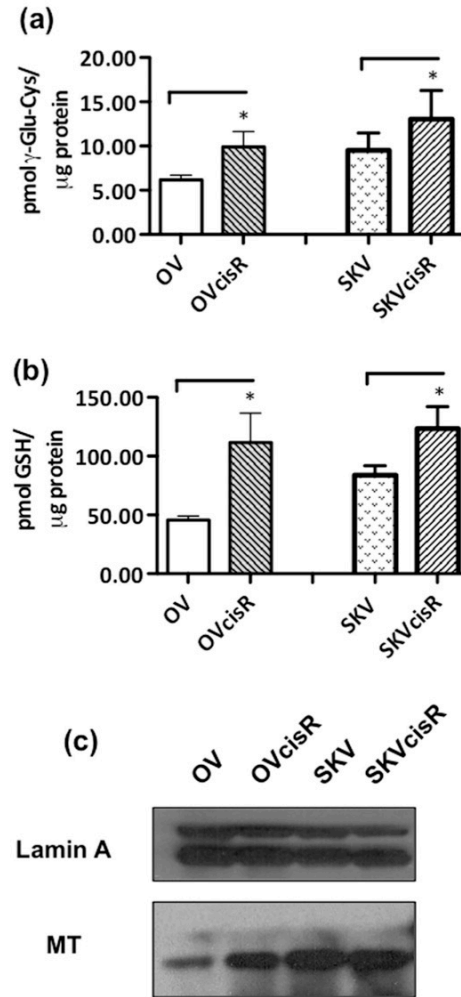


Fig. 4. Glutathione (GSH) and metallothionein (MT) are up regulated in cisplatin-resistant ovarian cancer cell lines. (a–b) Steady state levels of γ -Glu-Cys and GSH as measured by HPLC-MS in cisplatin-resistant cell lines, OVcisR and SKVcisR, and cisplatin-sensitive cell lines, OV and SKV. Data are presented as average pmol metabolite per total μg protein \pm SEM of $n = 3$ independent experiments. ($*p < 0.05$). (c) Immunoblot of MT in 15 μg nuclear-enriched fractions of ovarian cancer cells. Lamin A was probed for determining equal loading of nuclear fractions. Blot is representative of $n = 3$ independent experiments.

cisplatin-resistant and cisplatin-sensitive cells (Fig. 3c). This suggested that xCT activity per se, and not its expression, was important for the differential uptake of D4-CC.

3.4. GSH and MT were found at increased levels in cisplatin-resistant ovarian cancer cell lines compared with cisplatin-sensitive ovarian cancer cell lines

Next, we wanted to determine whether increased cysteine levels observed in cisplatin-resistant cell lines was correlated with increased biosynthesis of GSH and MT, cysteine-containing species that bind and inactivate cisplatin [14]. γ -Glu-Cys, the product of the rate-limiting step in the biosynthesis of GSH, was present at higher steady state levels, \sim 1.6-fold higher in OVCisR and \sim 1.4-fold higher in SKVcisR, versus OV and SKV respectively (Fig. 4a). Further connecting the dependence of γ -Glu-Cys with intracellular cysteine, 3 mM NAC significantly increased steady state levels of γ -Glu-Cys: $>$ 2-fold in both OVCisR and SKVcisR (Supporting information, Fig. S5). Such increased levels of γ -Glu-Cys in OVCisR and SKVcisR were supported by concomitant increases in the steady-state levels of GSH. Intracellular levels of GSH were \sim 2.4-fold higher in OVCisR and \sim 1.4-fold higher in SKVcisR when compared with OV and SKV, their respective, cisplatin-sensitive, parent cell lines (Fig. 4b). NAC-treated OVCisR and SKVcisR cells both exhibited \sim 3.4-fold and \sim 2.4-fold higher steady state levels of GSH compared with their respective, vehicle treated controls (Supporting information, Fig. S6), demonstrating intracellular cysteine levels can influence GSH levels in cisplatin-resistant ovarian cancer cells.

In addition to GSH, MT, a cysteine-rich protein, is known to bind and inactivate cisplatin specifically when localized in the nucleus [14,15]. Qualitative measurement of nuclear MT indicated that OVCisR and SKVcisR cells exhibited considerably increased expression of nuclear MT when compared with OV and SKV cells (Fig. 4c). Addition of 3 mM NAC, a donor of cysteine, also resulted in modest increased nuclear MT expression as determined by Western analysis (Supporting information, Fig. S7). Together, these findings demonstrate the importance of elevated, intracellular cysteine levels toward maintaining

higher levels of GSH and nuclear MT, thiols known to bind and inactivate cisplatin.

3.5. Stable silencing of CBS expression in cisplatin-resistant ovarian cancer cell lines sensitized those cells to cisplatin

We next wanted to assess if and, if so, how CBS expression/activity was imparting cisplatin resistance. Toward this end, we prepared stable, lentiviral-mediated CBS-silenced cisplatin-resistant ovarian cancer cell lines [OVCisR(shCBS) and SKVcisR(shCBS)]. Western analysis on whole cell lysates of OVCisR(shCBS) and SKVcisR(shCBS) revealed decreased CBS protein expression in those lysates compared to control shRNA-transfected cells OVCisR(scram) and SKVcisR(scram) respectively (Fig. 5a). Reduced expression of CBS also resulted in reduced bioactivity, as measured by its enzymatic product CTH. Steady state levels of CTH in OVCisR(shCBS) were \sim 51% lower compared to transfection control OVCisR(scram) (Fig. 5b, left). Similarly, SKVcisR(shCBS) exhibited \sim 31% lower levels of intracellular CTH when compared to SKVcisR(scram) (Fig. 5b, right). To determine whether CBS over-expression in cisplatin-resistant cell lines was at least in part mediating cisplatin resistance, we measured the effects of cisplatin on cell viability in CBS-silenced cells versus scrambled controls. OVCisR(shCBS) and SKVcisR(shCBS), over a range of concentrations of cisplatin, exhibited significantly reduced cell viability compared to OVCisR(scram) and SKVcisR(scram) respectively (Fig. 5c). Calculated ED50 values for cisplatin in OVCisR(shCBS) and SKVcisR(shCBS) were \sim 2.5 μ M and \sim 3.6 μ M respectively. These values were lower than the ED50 values for OVCisR(scram) and SKVcisR(scram), \sim 11 μ M and \sim 30 μ M respectively, reflecting increased sensitivity to cisplatin due to silencing CBS (Fig. 5c).

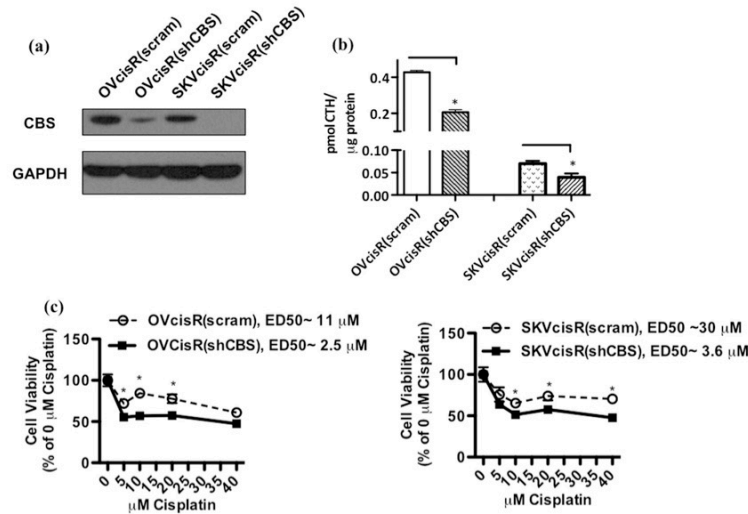


Fig. 5. Silencing cystathionine β -synthase (CBS) protein expression attenuates cisplatin resistance in cisplatin-resistant ovarian cancer cell lines OVCisR and SKVcisR. (a) Immunoblot for CBS of 20 μ g whole cell lysate to measure efficacy of lentiviral-mediated gene silencing of CBS. Blots are representative of $n = 3$ independent experiments. (b) Intracellular cystathionine (CTH), as measured by HPLC-MS, to determine relative CBS enzymatic activity in CBS-silenced cell lines versus scrambled controls. Data presented as average pmol CTH per total μ g protein \pm SEM of $n = 3$ independent experiments. (c) Graph depicting the dose-dependency of cisplatin on cell viability 24 h post-treatment in cisplatin-resistant cell lines silenced for CBS (shCBS) versus those treated with scrambled controls (scram). ED50 values calculated from modeling of data shown. Data presented as average percentage of 0 μ M cisplatin treatment \pm SEM of $n = 3$ independent experiments. (* $p < 0.05$).

3.6. CBS-silencing in cisplatin-resistant ovarian cancer cell lines decreased steady state levels of intracellular cysteine

Intracellular cysteine levels were ~60% lower in OVcisR(shCBS) and ~77% in SKVcisR(shCBS) compared to their respective scrambled lentiviral controls OVcisR(scram) and SKVcisR(scram) (Fig. 6a). CBS-silenced cell lines exhibited $\geq 50\%$ reduced D4-CC uptake compared with their respective controls (Fig. 6b) strongly implicating a role for CBS in regulating cystine uptake. The uptake of cystine, as addressed in Results Section 3.3, may be dependent on the activity and/or expression of xCT. Expression of xCT was however not noticeably different compared with respective scrambled controls (Fig. 6c). To partially elucidate the connection between CBS and cystine uptake, we turned our attention to H₂S. H₂S is a possible enzymatic product of CBS, whereby CBS catalyzes the condensation of homocysteine with cysteine, rather than serine [18]. It has been shown that H₂S can allosterically upregulate xCT activity and cystine uptake in neurons [19], though it had not yet been demonstrated in ovarian cancer cells. We therefore wanted to determine if H₂S could at least partially restore the attenuated uptake of D4-CC. CBS-silenced cells treated with 40 μ M GYY 4137, a slow releaser of H₂S, exhibited significant yet highly variable increases in D4-CC uptake versus those cells treated with vehicle control: > 600% in OVcisR(shCBS) and > 33% in SKVcisR(shCBS) (Fig. 6b).

3.7. Cystathionine β -synthase (CBS) in cisplatin-resistant ovarian cancer cell lines regulated GSH biosynthesis and expression of nuclear MT

In our next step we sought to determine whether the observed reduction in steady state levels of cysteine, caused by CBS-silencing (Fig. 6a), affected the biosynthesis of GSH. Steady state levels of γ -Glu-Cys, the metabolic precursor to GSH, were significantly lower, ~30% less in OVcisR(shCBS) and ~60% less in SKVcisR(shCBS) versus OVcisR(scram) and SKVcisR(scram) respectively (Fig. 7a). Additionally, we observed steady state levels of GSH in CBS-silenced cell lines, 63 pmol/ μ g in OVcisR(shCBS) and 58 pmol/ μ g SKVcisR(shCBS), were > 50% lower than that observed in scrambled controls, 130 pmol/ μ g in OVcisR(scram) and 150 pmol/ μ g in SKVcisR(scram) (Fig. 7b). CBS-silenced cell lines also expressed relatively less nuclear MT compared with scrambled controls (Fig. 7c).

3.8. CO inhibited CBS, thereby decreasing nuclear metallothionein and GSH

Following confirmation of a substantial connection between CBS and cisplatin-resistance in OVcisR and SKVcisR, we investigated whether CO-induced sensitization of cisplatin-resistant cells to cisplatin (Fig. 1b–c) was in part mediated by inhibition of CBS and the subsequent suppression of nuclear MT and GSH. CO, delivered by 30 μ M photoCORM, significantly lowered CBS bioactivity, as measured by decreased steady state levels of intracellular CTH. CTH decreased ~2.7-fold in OVcisR and ~4.5-fold in SKVcisR (Fig. 8a). In a similar manner to lentiviral-mediated silencing of CBS (Fig. 6a), CO treatment reduced steady state levels of cysteine > 55% in the both cisplatin-resistant cell lines, OVcisR and SKVcisR (Fig. 8b). Concomitantly, CO reduced D4-CC uptake, ~73% in OVcisR and ~56% in SKVcisR (Fig. 8c). Steady state levels of γ -Glu-Cys, the product of the rate-limiting step of GSH synthesis, was also significantly lower in cisplatin-resistant cells treated with CO, ~63% lower in OVcisR and ~66% lower in SKVcisR, versus respective controls (Fig. 8d). Expression of nuclear MT, the thiol-containing peptide that is known to bind and inactivate cisplatin, was also lower in OVcisR and SKVcisR cells following treatment with CO (Fig. 8e). Treatment of cells with CO significantly lowered steady state levels of GSH in cisplatin-resistant cells, by ~40% in OVcisR and 65% SKVcisR (Fig. 8f).

4. Discussion

The results reported above require critical evaluation. In previous studies, investigators have shown that silencing of CBS (by lentiviral transduction) enhances drug sensitivity in cisplatin-resistant ovarian cancer cells [12]. Also, CO delivered by tricarbonyldichlororuthenium (II) dimer, has been shown to promote global methylation in U937

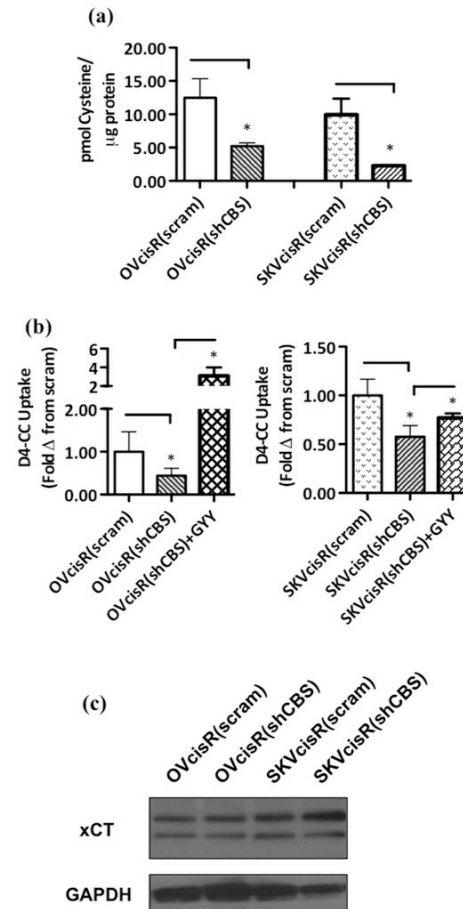


Fig. 6. Cystathionine β -synthase (CBS) expression in cisplatin-resistant ovarian cancer cells correlates to the bioavailability of cysteine. (a) Steady state levels of intracellular cysteine, as measured by HPLC-MS, normalized to μ g protein. Data presented as averages \pm SEM of $n = 3$ independent experiments. (b) Relative D4-cystine (D4-CC) uptake from extracellular media in CBS-silenced cells. Cells treated with either 40 μ M GYY or DMSO vehicle control, then incubated for 48 h. Data are presented as average fold difference from scrambled controls \pm SEM of $n = 3$ independent experiments. (* $p < 0.05$). (c) Expression of xCT in 20 μ g whole cell lysates of CBS-silenced ovarian cancer cells versus respective scrambled controls. GAPDH was used as a loading control. Blot representative of $n = 3$ independent experiments.

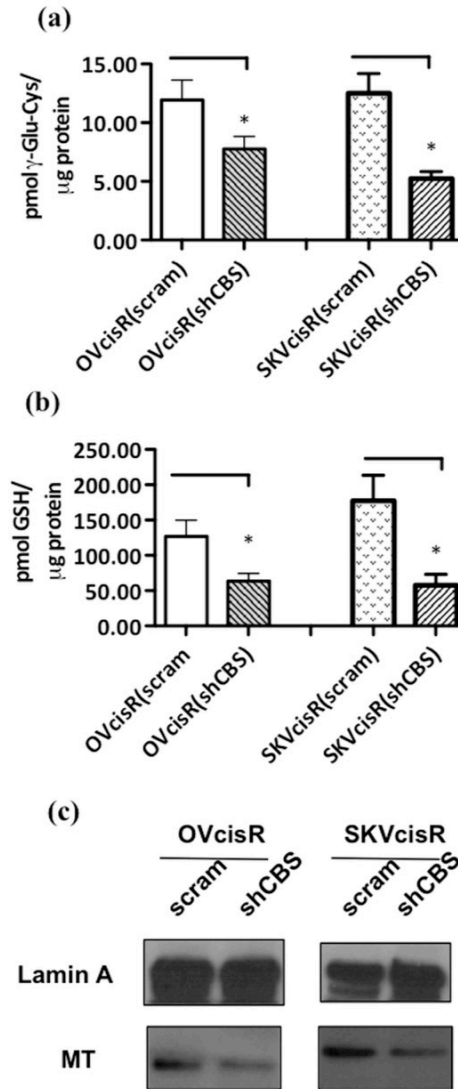


Fig. 7. Cisplatin resistance and cystathionine β -synthase (CBS) expression correlate to glutathione (GSH) biosynthesis and expression of nuclear metallothionein (MT) in cisplatin-resistant ovarian cancer cells. (a–b) Steady state levels of γ -Glu-Cys and GSH, normalized to total μ g protein, in CBS-silenced cell lines (shCBS) compared with respective scrambled controls (scram), measured by HPLC-MS. Data presented as average pmol of metabolite per total μ g protein \pm SEM of $n = 3$ independent experiments. (c) Immunoblot of MT in 15 μ g nuclear extracts of CBS-silenced cells (shCBS) versus transduction controls (scram). Lamin A is used as a nuclear fraction loading control. Blots representative of $n = 3$ independent experiments.

human monoblastic leukemia cell, presumably by CO-mediated inhibition of CBS [20]. However, direct demonstration of a viable pharmacological inhibition of CBS to alleviate drug resistance in ovarian cancer has not been achieved. The present study for the first time provides evidence that CO, delivered from a photoCORM, inhibits CBS and such delivery could be a viable option to circumvent chemo-resistance in ovarian cancer. Specific small molecule inhibitors of CBS, such as benserazide, have shown promise in eradicating cancer cells [21]. However, if further developed, these could only be used as a systemic therapy that will not spare normal cells. Such systemic therapy will result in serious adverse side effects, as CBS in the liver is the primary source of GSH, the major antioxidant in physiology [22]. On the other hand, light-activated CO delivery via appropriate catheters, prototypes for which have already been developed in our laboratory [23], could be used to inhibit CBS locally in accessible cancer tissues. This would bypass systemic delivery and increase the exposure of affected tissues to effective concentrations of the inhibitor and at the same time minimize adverse side effects. In fact the feasibility of CO-releasing molecules for cancer treatment has recently been reviewed [24].

Platinum-containing anti-cancer drugs react readily with the sulfur-containing amino acids in proteins namely methionine and cysteine. Unlike methionine, whose reaction with platinum is readily reversible by replacement with thiols or nucleotide bases, the cysteine-platinum complex is more stable [25]. Therefore, cysteine-rich proteins such as GSH and MT, both of which are present at high concentrations in the cancer cell, readily bind and inactivate platinum drugs. Indeed, formation of a cisplatin-(GS)₂ complex has been characterized (by NMR spectroscopy and HPLC-atomic absorption spectroscopy) *in vitro* and *in vivo* (in murine L1210 cells) in addition to efflux of the complex across the cell membrane [26]. Along the same line, formation of a ternary complex between MT and Platinum-DNA adduct followed by release of platinum from the DNA (and formation of [(NH₃)₂Pt(S₂-MT)] species) has been suggested to modulate DNA-repair and gene transcription leading to drug resistance [27]. Immunohistochemical MT expression in various human tumours has been associated either with processes related to carcinogenesis or with resistance against radiation and chemotherapy [28]. In ovarian tumours an increasing percentage of MT expression has been observed during the progression of malignancy [29]. Results shown in Fig. 8 now clearly indicate that CO-mediated CBS inhibition leads to the reduction of both GSH and MT (implicated in cisplatin inactivation) in ovarian cancer cells. Our observations are supported by earlier findings that CBS positively regulates GSH levels in breast cancer cells [11]. *The fact that exogenous CO could interfere with MT expression as well in refractory ovarian cancer cells, is in itself a novel finding in this study.* The data that CBS silencing could lower levels of nuclear MT underlines the important role of CBS in regulating two major thiol moieties (GSH and MT) implicated in chemotherapeutic drug resistance [28–31]. Nuclear MT expression is induced by cisplatin and seems to protect DNA in cells from toxic effects of the drug. The proportion of the individual contributions of GSH and MT in inactivating cisplatin is however not explored in this work.

Increases in GSH and MT require adequate maintenance of intracellular cysteine levels. The intimate connection between GSH/MT and intracellular cysteine is highlighted by the ability of extracellular treatment of cisplatin-resistant ovarian cancer cells with NAC. Treatment of OVCisR and SKVcisR with 3 mM NAC treatments increased both GSH and nuclear MT (Fig. S6 and S7, Supporting information). These results strongly suggest that regulation of sulfur metabolism in cisplatin-resistant ovarian cancer cells by CBS consists of two processes: flux through the transsulfuration pathway and uptake of extracellular cysteine. Previous studies have shown that some cancer cell types maintain intracellular cysteine levels by importing cystine via the glutamate/cystine antiporter, xCT [32,33]. Elevated expression and activity of xCT in response to oxidative stress has been reported in breast cancer cells, alluding to a role for xCT toward protecting cancer cells

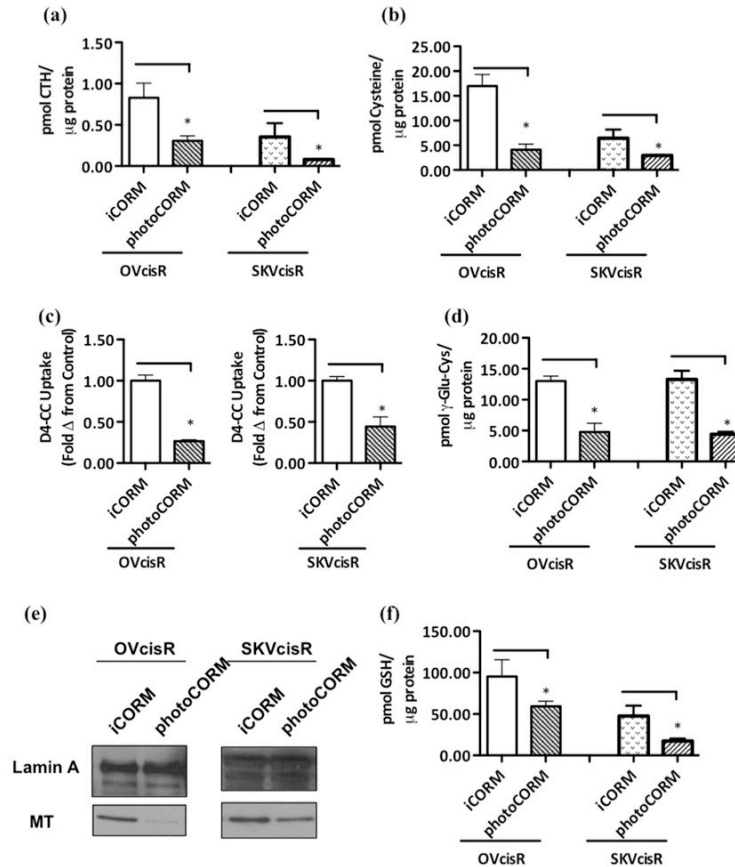


Fig. 8. Carbon monoxide (CO) inhibits CBS activity in cisplatin-resistant ovarian cancer cell lines OVcisR and SKVcisR. (a) CBS activity as measured by intracellular cystathionine (CTH). Levels of (b) cysteine, (d) γ -Glu-Cys and (f) GSH as measured by HPLC-MS in cisplatin-resistant ovarian cancer cell lines (normalized to total μ g protein). Cells treated with either 30 μ M photoCORM or 30 μ M of inactivated photoCORM (iCORM) for 24 h. Data presented as averages \pm SEM of $n = 3$ independent experiments. For GSH, data presented as average pmol GSH/ μ g protein \pm SEM of $n = 3$ independent experiments (* $p < 0.05$). (c) Effect of 30 μ M photoCORM treatment on D4-cystine (D4-CC) uptake in OVcisR and SKVcisR. Cells grown for 48 h in media supplemented with D4-CC. Data presented as average fold difference from "iCORM" control \pm SEM of $n = 3$ independent experiments. (e) Immunoblot of MT expression in 15 μ g nuclear enriched fractions of cisplatin-resistant cell lines. Cell treated with 30 μ M photoCORM or respective iCORM controls for 24 h prior to nuclear fraction isolation.

against oxidative stress induced loss of cell viability (a mechanism often exploited by chemotherapeutic drugs) [34]. Overexpression of xCT has been shown to increase intracellular GSH and increase resistance to cisplatin [17]. In addition, loss of xCT from cancer cells resulted in suppressed tumor growth of gastric cancer in pre-clinical models [35]. In cisplatin-resistant ovarian cancer cells, we observed increased xCT activity, but not increased expression per se. We have provided strong evidence for the regulation of xCT activity by CBS via H_2S , as lentiviral-mediated silencing of CBS in OVcisR(shCBS) and SKVcisR(shCBS) reduced the activity of xCT, which was partially reversed by the addition of exogenous H_2S , known to allosterically increase xCT activity [Fig. 6b] [19]. To the best of our knowledge, this is the first report that demonstrated that CBS can upregulate GSH synthesis independent of

the transsulfuration pathway in cancer cells by inducing the upregulation of cystine uptake in cancer cells. This study further emphasized that CO mediated inhibition of CBS could exploit this mechanism to compromise the anti-oxidant potential of cancer cells resulting in their increased sensitivity to cisplatin.

The importance of overexpression of CBS in imparting cisplatin resistance was observed in SKV cells, which despite being sensitive to cisplatin, express detectable levels of CBS and CGL. This is in contrast to OV cells, where the expression of CBS and CGL is nearly undetectable. Interestingly, regression analysis of the effects of cisplatin on ovarian cancer cell lines in this study revealed that the ED50 of cisplatin for SKV cells is higher than that of OV cells (5.5 μ M versus 2.3 μ M, respectively, data not shown). The lower sensitivity of SKV cells to cisplatin versus

OV (Fig. 1a) could possibly be attributed to the higher protein expression of CBS and CGL in the former (Fig. 2a).

Finally, it is important to note that overexpression of CBS is observed in select malignancies, namely breast and ovarian cancers while the corresponding normal tissues in all such cases exhibit very low levels of expression or none at all [36]. For this reason, CBS could be an important target in case of these two types of cancer where modulation of CBS activity by exogenous CO could thwart resistance to conventional chemotherapy. The effect of CO on non-transformed ovarian tissues in the context of resistance to cisplatin is intriguing, as the effect (s) of CO in non-cancerous cells are likely independent of CBS. Elucidation of other binding partners of CO in non-transformed ovarian cell lines could be an interesting follow-up study.

5. Conclusions

Previous work from this laboratory demonstrated that light-triggered CO delivery by the photoCORM can attenuate antioxidant capacity in human breast cancer cells through inhibition of CBS and sensitizes such cells to doxorubicin and paclitaxel [10]. Sensitization of human ovarian cancer cells to cisplatin therapy through administration of CO now demonstrates the general concept of CBS inhibition as a treatment modality to overcome chemoresistance encountered in ovarian cancer therapy. Strategies that overcome cisplatin resistance may dramatically reduce the mortality of ovarian cancer [4]. Here we have presented that CO, delivered from a photoCORM, sensitizes established cisplatin-resistant cell lines to cisplatin. Furthermore, we have provided strong evidence that the effects of CO in circumventing chemotherapeutic drug resistance is at least in part mediated by the inactivation of endogenous CBS (as evidenced by the reduction in CTH, the direct metabolic product of CBS).

Notes

The authors declare no competing financial interests.

Acknowledgments

Financial support from the NSF grant DMR-1409335 (to PM) and Departmental funding from the Department of Department of Obstetrics and Gynecology, David Geffen School of Medicine at UCLA is gratefully acknowledged. CJ acknowledges support from the NIH U01 grant HD087221. Statistical analysis by Ariel Wen, M.B.A. of the UCLA Anderson School of Management is gratefully acknowledged.

Appendix A. Supplementary data

Supplementary data to this article can be found online at <https://doi.org/10.1016/j.jinorgbio.2018.11.003>.

References

- [1] R.L. Siegel, K.D. Miller, A. Jemal, *CA Cancer J. Clin.* 67 (2017) 7–30.

- [2] J.D. Seidman, R.J. Kurman, *Hematol. Oncol. Clin. North Am.* 17 (2003) 909–925.
- [3] I. Romero, R.C. Bast, *Endocrinology* 153 (2012) 1593–1602.
- [4] R. Agarwal, S.B. Kaye, *Nat. Rev. Cancer* 3 (2003) 502–516.
- [5] B. Koberle, M.T. Tomcic, S. Usanova, B. Kaina, *Biochim. Biophys. Acta* 1806 (2010) 172–182.
- [6] L. Galluzzi, L. Senovilla, I. Vitale, J. Michels, I. Martins, O. Kepp, M. Castedo, G. Kroemer, *Oncogene* 31 (2012) 1869–1883.
- [7] B. Węgiel, D. Gallo, E. Cizmáda, C. Harris, J. Belcher, G.M. Vercellotti, N. Penacho, P. Seth, V. Sukhame, A. Ahmed, P.P. Pandolfi, L. Helczynski, A. Bjartell, J.L. Persson, L.E. Otterbein, *Cancer Res.* 73 (2013) 7009–7021.
- [8] L. Vitek, H. Gbelcova, L. Muchova, K. Vanova, J. Zelenka, R. Konickova, J. Suk, M. Zadinova, Z. Knezlik, S. Ahmad, T. Fujisawa, A. Ahmed, T. Ruml, *Dig. Liver Dis.* 46 (2014) 369–375.
- [9] T. Yamamoto, N. Takano, K. Ishiwata, M. Ohmura, Y. Nagahata, T. Matsuura, A. Kamata, K. Sakamoto, T. Nakanishi, A. Kubo, T. Hishiki, M. Suematsu, *Nat. Commun.* 5 (2014) 3480.
- [10] B. Kawahara, T. Moller, K. Hu-Moore, S. Carrington, K.F. Faull, S. Sen, P.K. Mascharak, *J. Med. Chem.* 60 (2017) 8000–8010.
- [11] S. Sen, B. Kawahara, D. Gupta, R. Tsai, M. Khachatryan, S. Roy-Chowdhuri, S. Bose, A. Yoon, K. Faull, R. Farias-Elsner, G. Chaudhuri, *Free Radic. Biol. Med.* 86 (2015) 228–238.
- [12] S. Bhattacharyya, S. Saha, K. Giri, I.R. Lanza, K.S. Nair, N.B. Jennings, C. Rodriguez-Aguayo, G. Lopez-Berestein, E. Basal, A.L. Weaver, D.W. Visscher, W. Cliby, A.K. Sood, R. Bhattacharya, P. Mukherjee, *PLoS One* 8 (2013) e79167.
- [13] I. Chakraborty, S.J. Carrington, G. Roseman, P.K. Mascharak, *Inorg. Chem.* 56 (2017) 1534–1545.
- [14] B.A.J. Jansen, J. Brouwer, J. Reedijk, *J. Inorg. Biochem.* 89 (2002) 197–202.
- [15] P. Surowiak, V. Materna, A. Maciejczyk, M. Pudelko, E. Markwitz, M. Spaczynski, M. Dietel, M. Zabel, H. Lage, *Virchows Arch.* 450 (2007) 279–285.
- [16] O. Kabil, R. Banerjee, *Antioxid. Redox Signal.* 20 (2014) 770–782.
- [17] N.E. Savaskan, I.Y. Eypoglu, *Ann. Anat.* 192 (2010) 309–313.
- [18] S. Okuno, H. Sato, K. Kuriyama-Matsumura, M. Tamba, H. Wang, S. Sohma, H. Himada, H. Yoshikawa, T. Kondo, S. Bannai, *Br. J. Cancer* 88 (2003) 951–956.
- [19] Y. Kimura, H. Kimura, *FASEB J.* 18 (2004) 1165–1167.
- [20] T. Yamamoto, N. Takano, K. Ishiwata, M. Suematsu, *J. Clin. Biochem. Nutr.* 48 (2011) 96–100.
- [21] N. Druzhyina, B. Szczesny, G. Olah, K. Modis, A. Asimakopoulou, A. Pavlidou, P. Szoleczky, D. Gero, K. Yanagi, G. Toro, I. Lopez-Garcia, V. Myrianthopoulos, E. Mikros, J.R. Zatarain, C. Chao, A. Papapetropoulos, M.R. Hellmich, C. Szabo, *Pharmacol. Res.* 113 (2016) 18–37.
- [22] N. Kaplowitz, *Yale J. Biol. Med.* 54 (1981) 497–502.
- [23] M.N. Pinto, I. Chakraborty, C. Sandoval, P.K. Mascharak, *J. Control. Release* 264 (2017) 192–202.
- [24] M. Kourti, W.G. Jiang, J. Cai, *Oxidative Med. Cell. Longev.* 2017 (2017) 9326454.
- [25] J. Reedijk, *Chem. Rev.* 99 (1999) 2499–2510.
- [26] T. Ishikawa, F. Aliosman, *J. Biol. Chem.* 268 (1993) 20116–20125.
- [27] A.V. Karotki, M. Vasak, *Biochemistry* 47 (2008) 10961–10969.
- [28] S.E. Theoharidis, A.P. Margeli, J.T. Klijanienko, G.P. Kouraklis, *Histopathology* 45 (2004) 103–118.
- [29] Y. Tan, R. Sinniah, B.H. Bay, G. Singh, *J. Pathol.* 18 (1999) 344–350.
- [30] A.D. Lewis, J.D. Hayes, C.R. Wolf, *Carcinogenesis* 9 (1988) 1283–1287.
- [31] H.H.W. Chen, M.T. Kuo, *Metal-Based Drugs* 2010 (2010) 430939.
- [32] R.G. Ungard, E.P. Seidltz, G. Singh, *Pain* 155 (2014) 28–36.
- [33] M.K. Sharma, E.P. Seidltz, G. Singh, *Biochem. Biophys. Res. Commun.* 391 (2010) 91–95.
- [34] E. Habib, K. Linher-Melville, H.X. Lin, G. Singh, *Redox Biol.* 5 (2015) 33–42.
- [35] T. Ishimoto, O. Nagano, T. Yae, M. Tamada, T. Motohara, H. Oshima, M. Oshima, T. Ikeda, R. Asaba, H. Yagi, T. Masuko, T. Shimizu, T. Ishikawa, K. Kai, E. Takahashi, Y. Imamura, Y. Baba, M. Ohmura, M. Suematsu, H. Baba, H. Saya, *Cancer Cell* 19 (2011) 387–400.
- [36] M. Uhlen, C. Zhang, S. Lee, E. Sjostedt, L. Fagerberg, G. Bidkhori, R. Benfais, M. Arif, Z.T. Liu, F. Edfors, K. Sanli, K. von Feilitzen, P. Oksvold, E. Lundberg, S. Hober, P. Nilsson, J. Mattsson, J.M. Schwenk, H. Brunstrom, B. Glimelius, T. Sjblom, P.H. Edqvist, D. Djureinovic, P. Mücke, C. Lindskog, A. Mardinglu, F. Ponten, *Science* 357 (2017), <https://doi.org/10.1126/science.aan2507>.

Supporting Information
For
Carbon Monoxide Sensitizes Cisplatin-resistant Ovarian Cancer Cell
Lines toward Cisplatin via Attenuation of Levels of Glutathione and
Nuclear Metallothionein

Brian Kawahara^a, Sivakumar Ramadoss^b, Gautam Chaudhuri^b, Carla Janzen^b, Suvajit Sen^{b*} and Pradip K. Mascharak^{a*}

^a *Contribution from Department of Chemistry and Biochemistry, University of California, Santa Cruz, CA 95064 and*

^b *Department of Obstetrics and Gynecology, David Geffen School of Medicine at University of California at Los Angeles, Los Angeles, CA 90095*

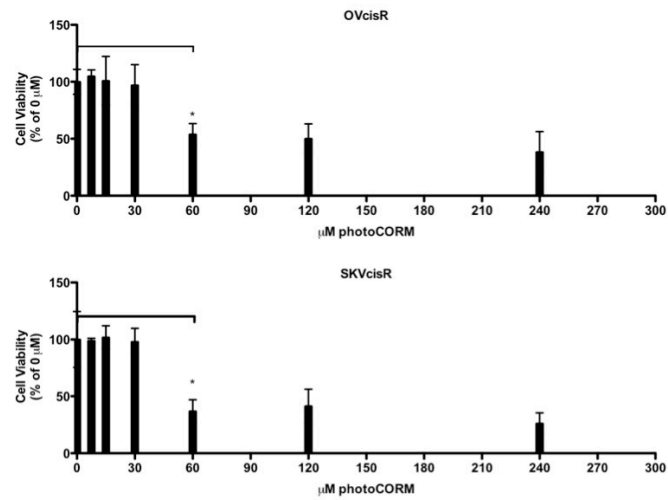


Figure S1. Carbon monoxide (CO), delivered from > 30 μM photoCORM, is lethal to cisplatin resistant ovarian cancer cell lines. Cell viability of cisplatin-resistant cells OVcisR (top) and SKVcisR (bottom), determined by trypan blue exclusion, 24 h post-treatment with varying doses of CO, delivered from the indicated concentration of photoCORM. Data presented as average % change from 0 μM photoCORM treatment +/- SEM of n=3 independent experiments. (*p<0.05)

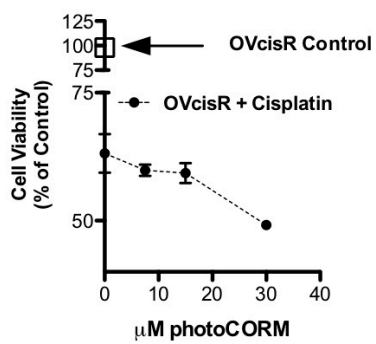


Figure S2. Carbon monoxide (CO), delivered from photoCORM, sensitizes cisplatin-resistant cells to cisplatin in dose-dependent manner. Cell viability, measured by reduction of tetrazolium dye 3-(4,5-dimethylthiazol-2-yl)-2,5-diphenyltetrazolium bromide (MTT). Cisplatin-resistant cells (OVcisR) treated with vehicle control, cisplatin and/or photoCORM for 24 h. Data presented as average % of Control +/- SEM of n=3 experiments (*p<0.05).

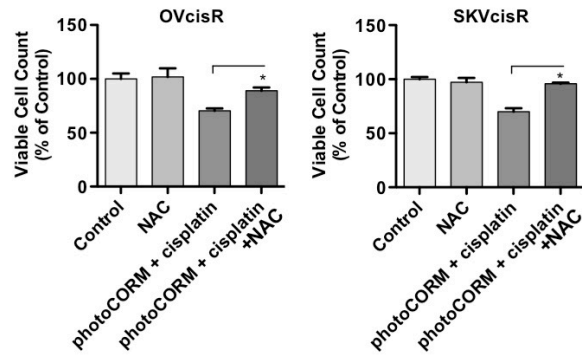


Figure S3. N-acetyl-cysteine (NAC) reverses the cytotoxic effects of combined carbon monoxide (CO)-cisplatin treatment in cisplatin-resistant ovarian cancer cell lines OVcisR (left) and SKVcisR (right). Cells treated with 3mM NAC, 30 μ M photoCORM, 20 μ M cisplatin or vehicle control(s) as indicated. Cell viability assessed 24 h post-treatment by reduction of tetrazolium dye 3-(4,5-dimethylthiazol-2-yl)-2,5-diphenyltetrazolium bromide (MTT). Data are presented as average % of "Control" \pm SEM of n=3 experiments. (*p<0.05).

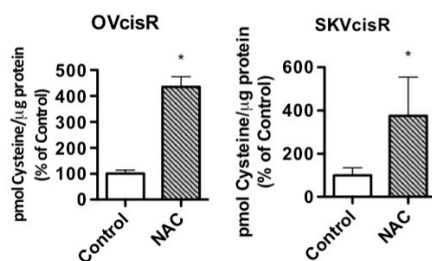


Figure S4. Extracellular treatment of cisplatin-resistant ovarian cancer cell lines with N-acetylcysteine (NAC) significantly increases steady state levels of intracellular cysteine. Intracellular cysteine levels quantified via high pressure, liquid chromatography-mass spectrometry (HPLC-MS) in cisplatin-resistant cell lines OVcisR and SKVcisR. Cells treated with 3mM NAC or vehicle control for 24 h. Data presented as average % of “Control” \pm SEM of n=3 independent experiments (*p<0.05).

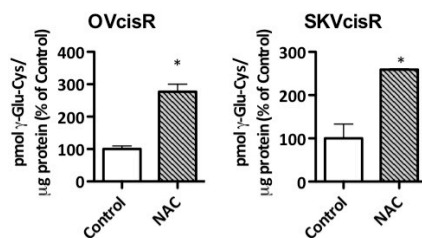


Figure S5. Upon treatment with N-acetylcysteine (NAC), steady state levels of γ -Glu-Cys increase significantly in cisplatin-resistant cell lines. Measurement of intracellular γ -Glu-Cys by high pressure, liquid chromatography-mass spectrometry (HPLC-MS). Cells treated with vehicle control or 3mM NAC for 24 h. Data are presented as average % of Control +/- SEM of n=3 independent experiments, (*p>0.05).

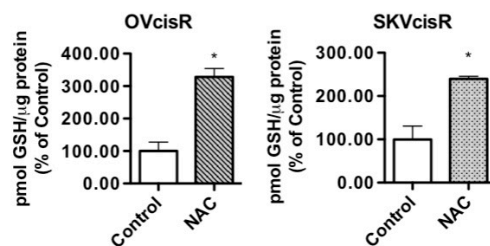


Figure S6. Steady state levels of intracellular glutathione (GSH) increase in cisplatin-resistant ovarian cancer cell lines upon treatment with N-acetylcysteine (NAC). GSH levels, as measured by high pressure, liquid chromatography-mass spectrometry (HPLC-MS) after treatment with vehicle control or 3 mM NAC for 24 h. Data presented as average % of Control +/- SEM of n=3 independent experiments, (*p<0.05).

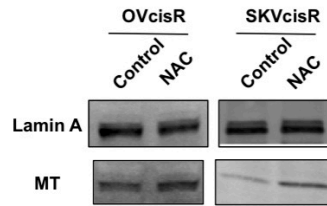


Figure S7. Expression of nuclear metallothionein (MT) increases in cisplatin-resistant ovarian cancer cells upon treatment with N-acetylcysteine (NAC). Immunoblot of 10 $\mu\text{g}/\text{lane}$ of nuclear fractions of whole cell lysate of cisplatin-resistant ovarian cancer cell lines OVcisR (left) and SKVcisR (right) for metallothionein (MT) or Lamin A loading control. Cells treated with vehicle control or 3mM NAC for 24h. Blots are representative of n=3 experiments.

Chapter 4

Antigen-specific delivery of carbon monoxide through a new class of antibody- drug conjugate

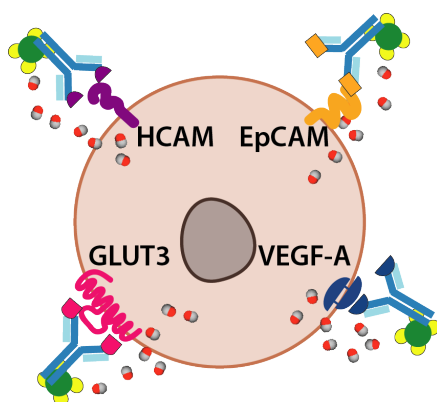


Table 4.1 Table of Content

4.1 Background

The challenge of delivering efficacious concentrations of CO to a target tissue has been approached by our group and others by synthesizing CO-releasing molecules (CORMs) with properties necessary for a potential therapeutic, including water solubility,¹ incorporation within biocompatible materials^{2,3} and controllable release of CO.⁴⁻⁷ Very recently, with the use of photoactivatable CORMs (photoCORMs) our group has elucidated mechanism(s) by which CO exerts deleterious effects against human breast and ovarian cancer cell models.^{8,9} In such studies we have observed sensitization of ovarian cancer cells to drugs like cisplatin and paclitaxel through co-

administration of CO.⁹ Because sensitization to conventional chemotherapeutics could mitigate the poor outcome of ovarian cancer treatment, precise target-specific delivery of CO to the malignant tissue appears to be a very desirable goal.

Although a number of CORMs and photoCORMs has been developed in recent years,⁴⁻⁷ most have notably lacked the ability to highly discriminate between targeted versus non-targeted tissues. With this in mind, we sought to conjugate a photoCORM to a monoclonal antibody with the goal of improving target specificity of CO-release. Antibody-drug conjugates (ADCs) are fast emerging as an effective strategy for anticancer therapies. In most cases small molecule drugs are combined with monoclonal antibodies to achieve high selectivity.¹⁰ Conjugation of photoCORMs (i.e. the warhead) to monoclonal antibodies using a biotin-streptavidin linker is a novel, currently unexplored and potentially effective strategy that could be employed for the controlled delivery of CO to specific tissues.

Herein we report the successful conjugation of a biotinylated-photoCORM to streptavidin-conjugated mouse monoclonal immunoglobulin G (IgG) antibodies to isolate Ab-photoCORMs for the controlled delivery of CO to ovarian cancer cell cultures with high specificity. Utilizing different monoclonal antibodies, a family of Ab-photoCORMs was synthesized with the goal of localizing and delivering cytotoxic levels of CO to ovarian cancer cells expressing different tumor-specific surface antigens. To the best of our knowledge, this communication is the first report of an antibody-drug conjugate in which the drug is a gaseous molecule, namely CO.

4.2 Synthesis of biotinylated, photo-activatable carbon monoxide-releasing molecule

The present work utilized a designed photoCORM $[\text{Mn}(\text{CO})_3(\text{phen})(4\text{-pyAl})](\text{CF}_3\text{SO}_3)$ (where phen = 1,10-phenanthroline, 4-pyAl = pyridine-4-carboxaldehyde) as the photoactivatable CO donor.

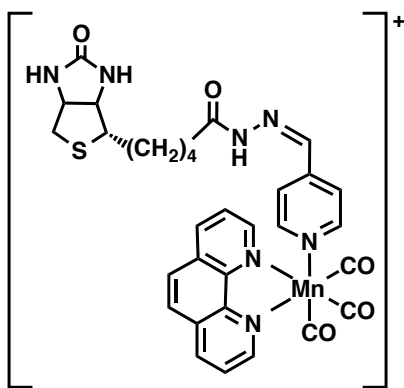


Figure 4.1. Structure of biotinylated photoCORM (Complex 1). Abbreviations: photoactivatable carbon monoxide-releasing molecule, photoCORM.

Biotinylation of this photoCORM (Figure 4.1, Complex 1) was achieved through reaction with biotin-hydrazide in trifluoroethanol at room temperature (Figure 4.2).

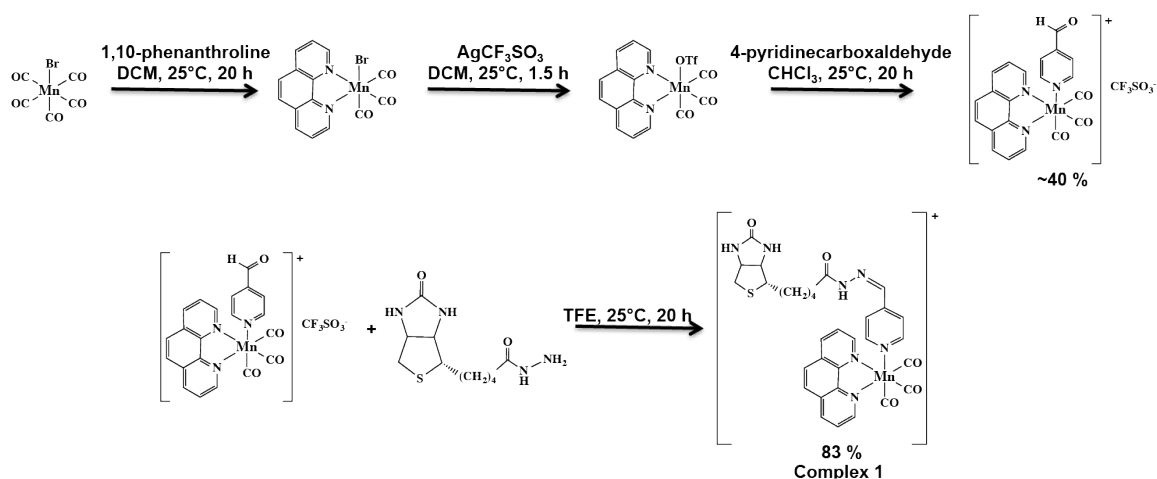


Figure 4.2. Synthetic scheme for Complex 1: a biotinylated, photoactivatable CO-releasing molecule (photoCORM).

The composition of Complex 1 was confirmed by electrospray ionization Fourier Transform mass spectrometry (ESI FTMS); (M^+) $m/z = 666.13539$ (calculated for $C_{31}H_{29}N_7O_5SMn$: 666.13313, Δ ppm = 3.4 ppm, Δ mDa = 2.2 (Figure 4.3), and 1H NMR (Figure 4.4).

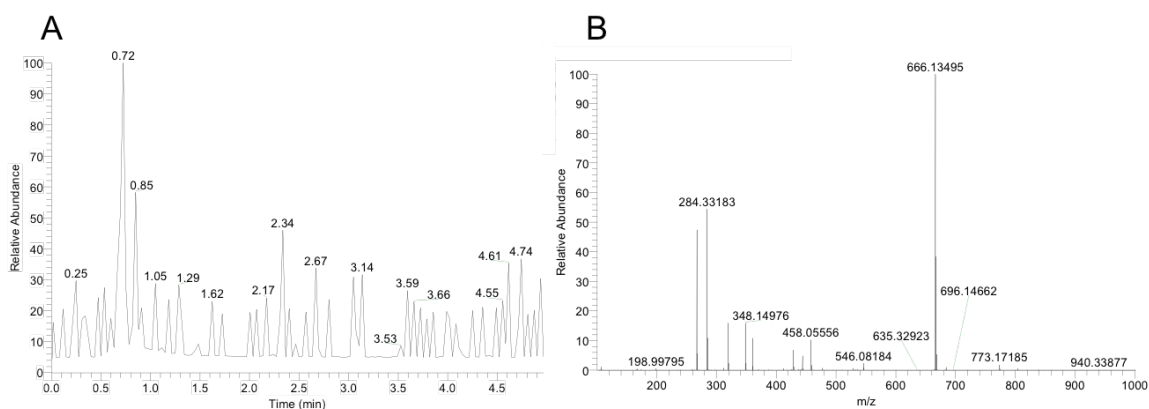


Figure 4.3. Electrospray ionization mass spectrometry (ESI-MS) of Complex 1. (A) Total ion count (TIC) chromatogram of 0-5 min for a 5 min run of Complex 1 via flow injection analysis and (B) full mass spectrum (100-1000 m/z) for retention time=0.70-0.72. Found: 666.13495, calculated for $C_{31}H_{29}N_7O_5SMn$ 666.13314, Δ ppm = 3.4 ppm, Δ mDa = 2.2.

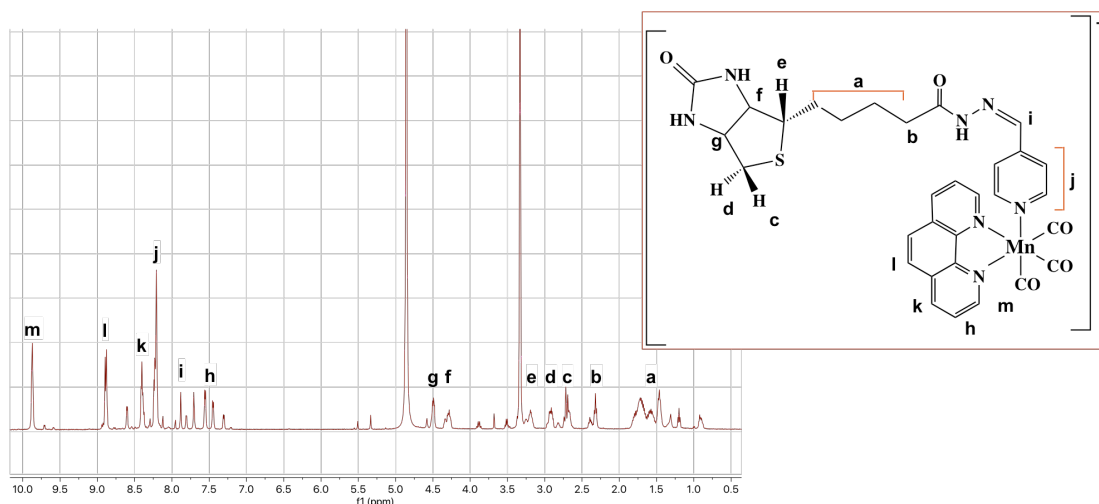


Figure 4.4. ^1H NMR for Complex 1. For Complex 1, ^1H NMR (400 MHz, $[\text{D}_4]$ -methanol): $\delta=1.37$ - 1.84 (m, 6H), 2.30 (t, 2H, 7.4 Hz), 2.68 (m, 1H), 2.89 (m, 1H), 3.18 (m, 1H), 4.24 (m, 1H), 4.47 (m, 1H), 7.53 (m, 2H), 7.86 (s, 1H), 8.20 (m, 4H), 8.38 (m, 2H), 8.87 (m, 2H), 9.88 (m, 2H).

The Infrared spectrum of Complex 1 showed the presence of two $\nu_{\text{C}=\text{O}}$ bands at 2039 and 1939 cm^{-1} , characteristic of the manganese tricarbonyl moiety, and one $\nu_{\text{C}=\text{O}}$ band at 1685 cm^{-1} derived from the biotin unit (Figure 4.4).

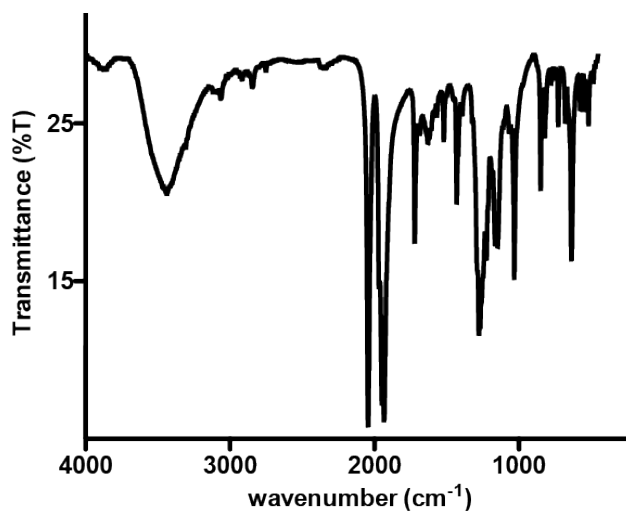


Figure 4.4. Infrared (IR) spectrum of Complex 1. IR spectrum of solid Complex 1 was recorded in KBr matrix. $\nu_{\text{C}=\text{O}}$: (cm^{-1}): 2030, 1941, 1687.

Electronic absorption spectra of solutions of Complex **1** in 1x phosphate-buffered saline (PBS) exhibited a broad absorbance band in the visible region between 320 and 450 nm (Figure 4.5).

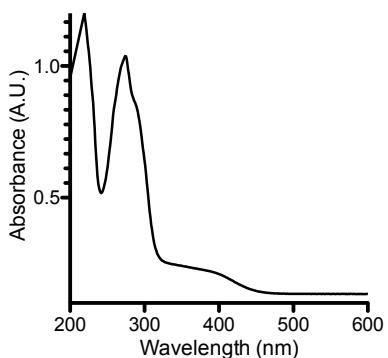


Figure 4.5. Electronic absorption spectrum of Complex **1** in 1X PBS, 298 K (25°C).

Exposure of Complex **1** to visible light resulted in systematic changes in the absorption spectra (Figure 4.6) arising from the loss of CO.³ Integration of the rate law for the photodegradation of Complex **1** was performed to determine pseudo-first order kinetics for CO release, with apparent visible light activated CO release rate $k_{app} = 0.0030 \pm 0.010 \text{ s}^{-1}$ determined in 1x PBS (Figure 4.6).

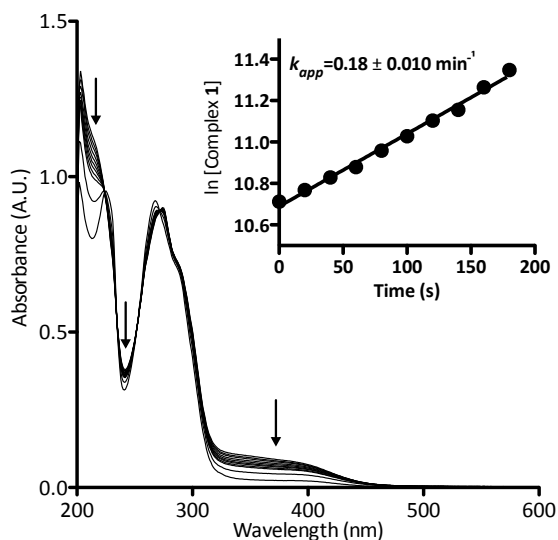


Figure 4.6. Electronic absorption spectrum of Complex **1** upon illumination with low power (10 mW/cm^2), broadband visible light in 20-second intervals at 25°C . Inset: Integration of the release rate for the photodegradation of Complex **1**, calculated at 390 nm , with low power (10 mW/cm^2), broadband visible light for indicated time.

Complex **1** was stable in $1\times$ PBS in the dark for $\sim 48 \text{ h}$, releasing CO only upon illumination with low power (10 mW/cm^2), broadband, visible light (Figure 4.7A). Furthermore, Complex **1** exhibited stability in human serum for 24 h at 37°C , retaining the property of photorelease of CO, as confirmed by myoglobin assay (Figure 4.7B).

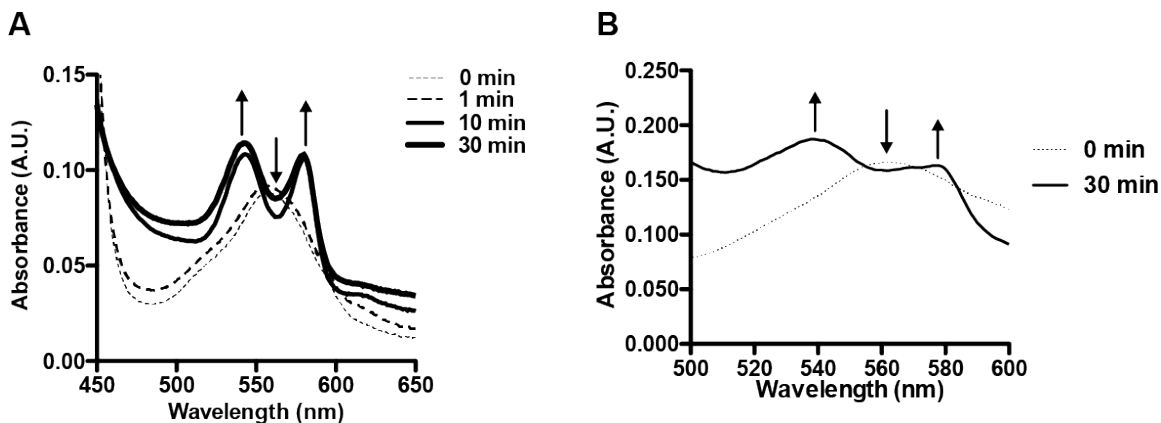


Figure 4.7. Myoglobin assay for CO release of Complex 1. (A) Myoglobin assay for CO release of Complex 1 dissolved and performed in 1X phosphate buffered saline (PBS), triggered by low power ($10\text{mW}/\text{cm}^2$), visible light for indicated time. (B) Myoglobin assay for CO release of Complex 1 dissolved in human serum and incubated for ≥ 1 h at 37°C , followed by exposure to low power, broadband visible light for 30 min.

Previous studies from this laboratory have demonstrated that sufficient levels of CO, delivered from photoCORMs, can induce apoptotic cell death in a wide variety of cancer cells.^{2,3,11-13} Likewise, Complex 1 upon illumination with visible light, significantly reduced cell viability in two ovarian cancer cell lines OVCAR-5 and SKOV-3 ($\text{ED}_{50} = 48$ and $25 \mu\text{M}$ respectively) assayed 24 h post-treatment (Figure 4.8).

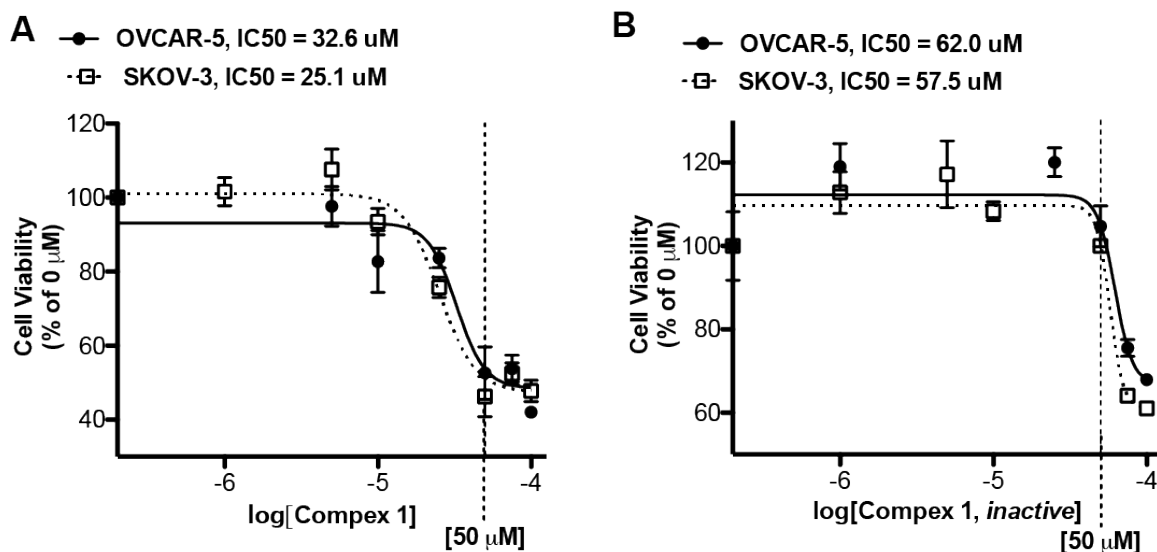


Figure 4.8. Effect of treatment of ovarian cancer cell lines with indicated concentrations of Complex 1 upon illumination with visible light on cell viability, measured 24 h post-treatment in ovarian cancer cell lines. (A) Log[dose]-response curves of ovarian cancer cell lines OVCAR-5 and SKOV-3 to Complex 1. (B) Log[dose]-response curves of OVCAR-5 and SKOV-3 to photo-inactivated Complex 1. Data representative of n=3 independent experiments.

4.3 Synthesis of streptavidin-conjugated antibody

A streptavidin-biotin strategy was used to link Complex 1 to IgG, exploiting the strong affinity ($K_d = 10^{-14}$ M) and stability of the streptavidin-biotin interaction.¹⁶ The streptavidin-IgG conjugate was synthesized using a commercially available kit (Supporting Information). Native gel electrophoresis (Figure 4.9A) and size exclusion chromatography (Figure 4.9B) revealed conjugation of a variable number of streptavidin molecules to IgG which was expected as per manufacturer's notes. Fractionation of crude streptavidin-IgG conjugates following size exclusion chromatography was performed to resolve and isolate antibodies conjugated with 1-4

streptavidin molecules (Figure 4.9C). These fractions were then pooled together (abbreviated hereafter as Complex 2) for cellular studies.

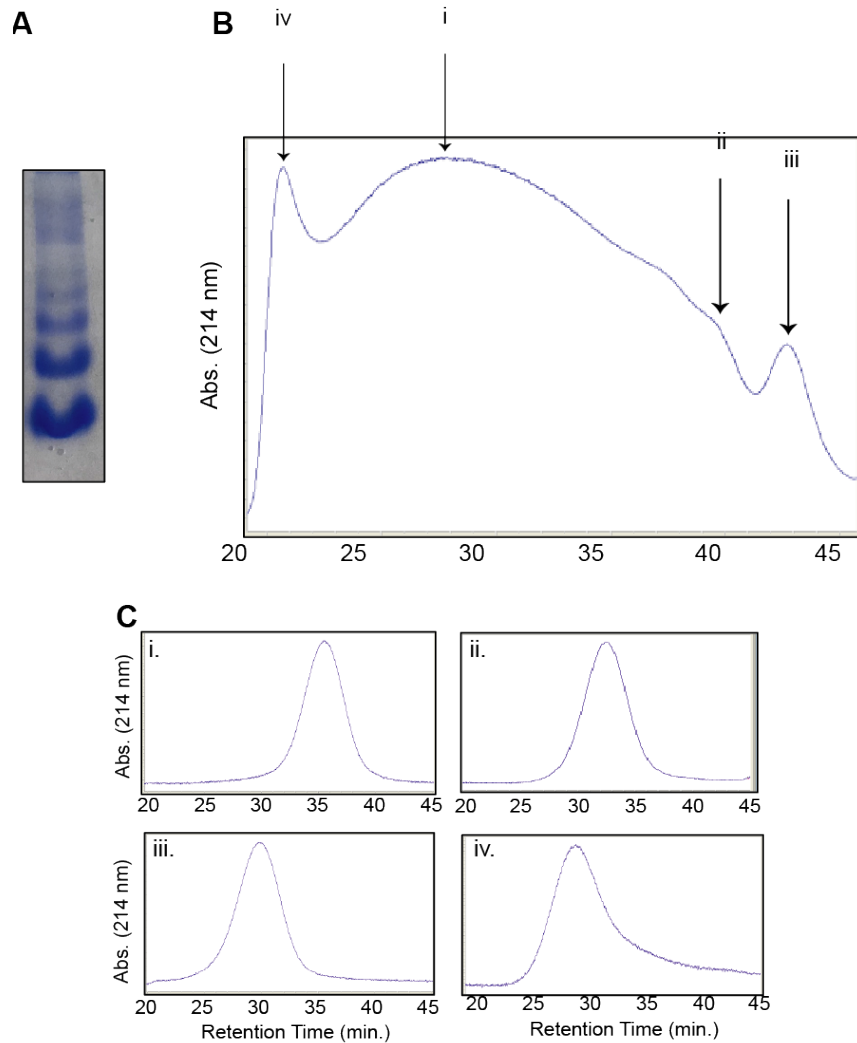


Figure 4.9. Complex 2: streptavidin-conjugated IgG. (A) Native protein gel electrophoresis of crude Complex 2. (B) Chromatogram of Complex 2 following size exclusion chromatography. [Retention time, ~molecular weight, identity] (i) [28.4 min, 366 kDa, IgG + 4 streptavidin]. (ii) [39.6 min, ~155 kDa, IgG + 0 streptavidin]. (iii) [42.7 min, ~121 kDa, IgG Fragments]. (iv) [20.6 min, ~659 kDa, void volume]. (C) Size-exclusion chromatograms of fractions of Complex 2. [Retention time, ~molecular weight, identity] (i) [35.4 min, ~210 kDa, IgG + 1 streptavidin]. (ii) [32.2 min, ~260 kDa, IgG + 2 streptavidin]. (iii) [29.9 min, ~313 kDa, IgG + 3 streptavidin]. (iv) [28.6 min, ~366 kDa, IgG + 4 streptavidin].

4.4 Synthesis of antibody-photoCORM conjugate

Reaction of Complex 2 with excess Complex 1 afforded the antibody-photoCORM conjugate (Ab-photoCORM) through a streptavidin-biotin interaction, then purified to remove any trace of unbound streptavidin, unconjugated IgG and unincorporated Complex 1 by size-exclusion chromatography (Figure 4.10).

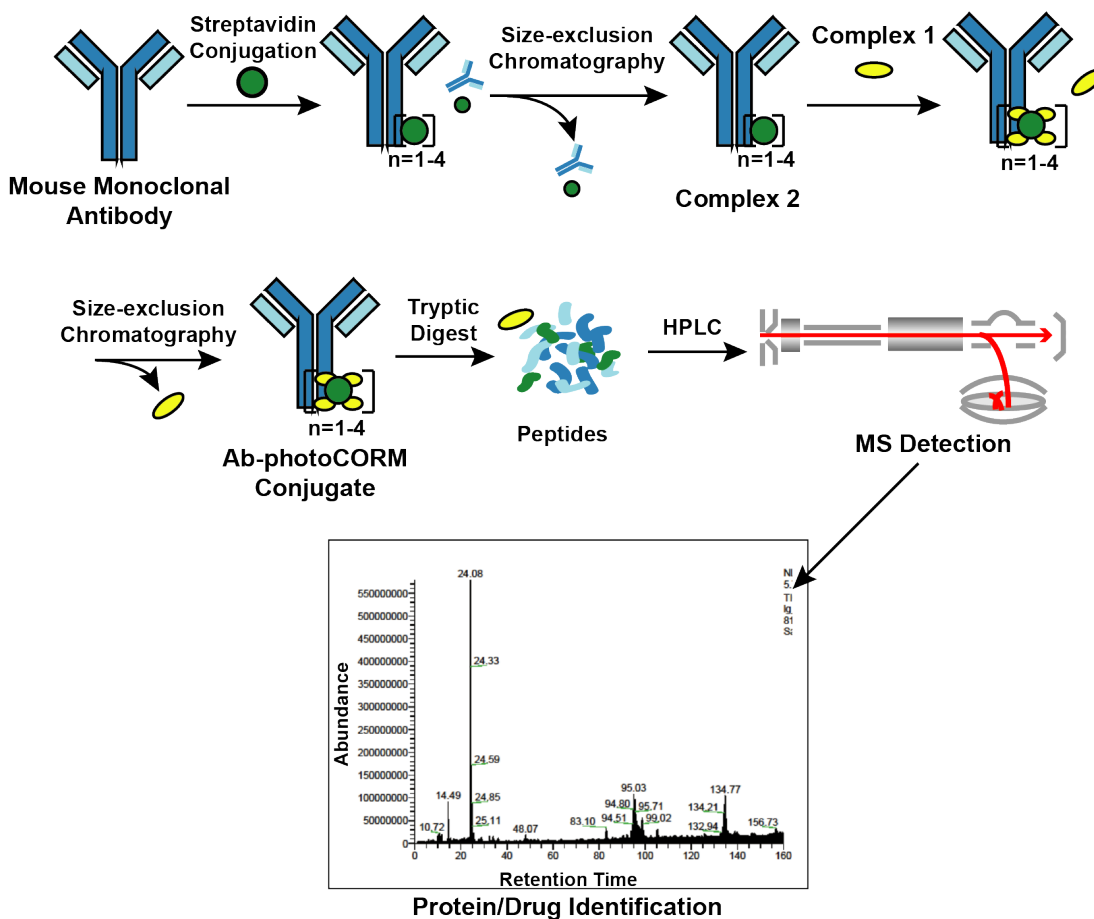


Figure 4.10. Synthesis and characterization of the antibody-photoCORM conjugate (Ab-photoCORM) and proteomic analysis of Ab-photoCORM. The scheme of bottom-up proteomics of the Ab-photoCORM is also shown.

Bottom-up proteomic analysis of the Ab-photoCORM confirmed the presence of streptavidin in the Ab-photoCORM (Figure 4.11).

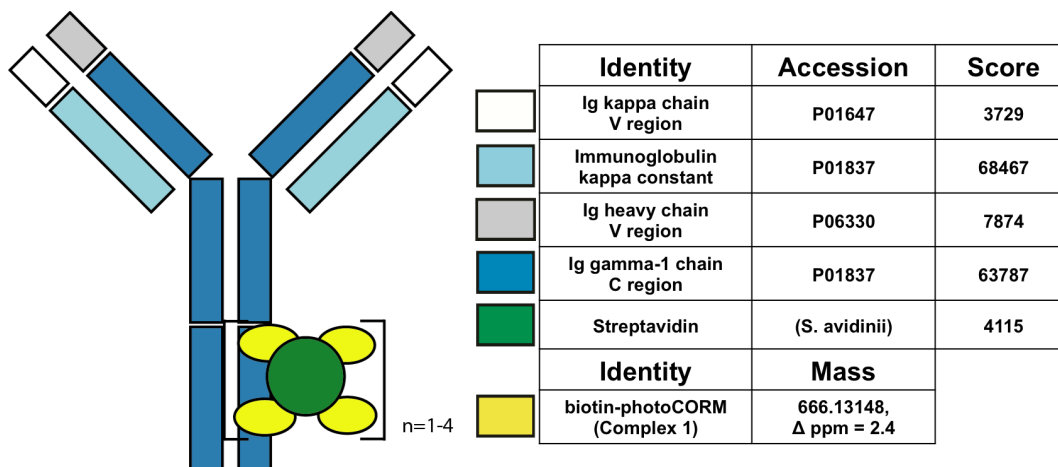


Figure 4.11. Proteomic scores of the Ab-photoCORMs synthesized in this study. Biotin-photoCORM (Complex 1) was observed in the full MS scan of the tryptic digest of Ab-photoCORM. Protein scores greater than 67 are significant (i.e. $p < 0.05$).

Additionally, Complex 1 (M^+) incorporated into the Ab-photoCORM was observed in the full MS scan of the tryptic digest (Figure 4.12).

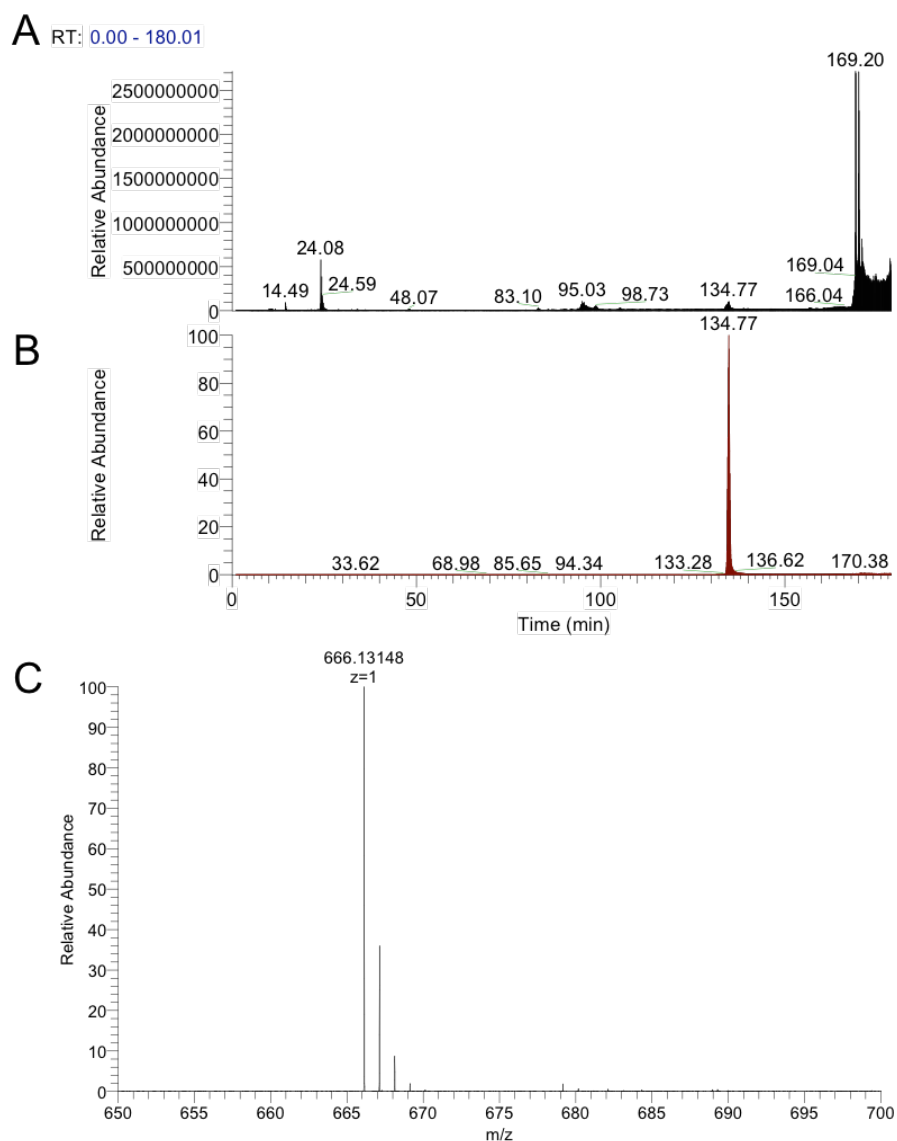


Figure 4.12. Detection of Complex 1 in tryptic digest of antibody-photoCORM conjugate (Ab-photoCORM). (A) Total ion count (TIC) of Ab-photoCORM sample. (B) Chromatogram of Ab-photoCORM, mass filter range $m/z = 666.12593-666.13925$. (C) Full mass spectrum at retention time 134.16-135.34 min.

The Ab-photoCORM, by merit of Complex 1 incorporation, exhibited photo-activated release of CO, as determined by myoglobin assay performed in 1x PBS (Figure 4.13A). Furthermore, the Ab-photoCORM exhibited stability in a biological

fluid, as evidenced by its retained photo-activatable release of CO following incubation in human for 1 h at 37°C (Figure 4.13B).

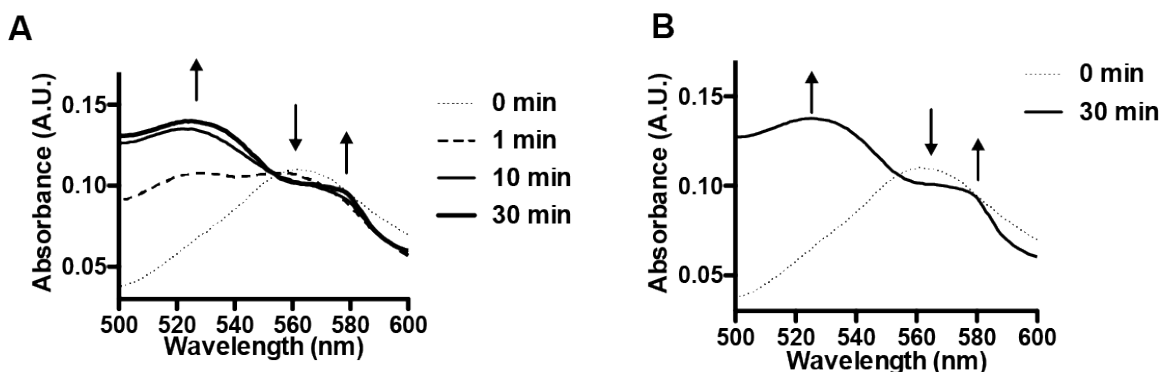


Figure 4.13. Myoglobin assay for light-triggered CO release from antibody-photoCORM conjugate (Ab-photoCORM). (A) Absorbance spectrum of myoglobin for determination of CO release from Ab-photoCORM dissolved in 1X phosphate buffered saline (PBS), triggered by low power (10mW/cm²), broadband visible light for indicated times. (B) Absorbance spectrum of myoglobin for determination of CO release from Ab-photoCORM dissolved and incubated in human serum for >1 h at 37°C by low power, broadband visible light for indicated times.

A family of Ab-photoCORM conjugates was synthesized (Table 4.2) using this synthetic strategy with commercially available mouse monoclonal IgG raised against four surface-expressed antigens implicated in ovarian cancer, namely homing cell adhesion molecule (HCAM),¹⁵ epithelial cell adhesion molecule (EpCAM),¹⁶ glucose transporter 3 (GLUT3),¹⁷ and vascular endothelial growth factor A (VEGF).¹⁸ Immunoblot analysis of whole cell lysates of cell line models utilized, OVCAR-5 and SKOV-3, confirmed the presence of the antigens recognized by the family of Ab-photoCORMs (Figure 4.15A). An Ab-photoCORM utilizing IgG *not raised against any specific antigen* (α -Control-photoCORM) was also synthesized for application in

cell viability experiments in order to account for any non-CO-mediated effects of the antigen-specific Ab-photoCORMs.

Original Mouse IgG	Epitope Recognized	Streptavidin-IgG (Complex 2)	Antibody-photoCORM conjugate (Ab-photoCORM)
HCAM (sc-7297)	Homing cell adhesion molecule (human)	Complex 2- (α -HCAM)	α -HCAM-photoCORM
EpCAM (sc-53277)	Epithelial cell adhesion molecule (human)	Complex 2- (α -EpCAM)	α -HCAM-photoCORM
GLUT3 (sc-74399)	Glucose transporter 3 (human)	Complex 2- (α -GLUT3)	α -GLUT3-photoCORM
VEGF-A (365578)	Vascular endothelial growth factor A (human)	Complex 2- (α -VEGF)	α -VEGF-photoCORM
Normal mouse IgG (sc-2025)	None	Complex 2- (α -Control)	α -Control-photoCORM

Table 4.2. Family of antibody-photoCORM conjugates (Ab-photoCORMs) synthesized from commercial antibodies, recognizing indicated human cell surface antigens implicated in ovarian cancer.

4.5 Antigen-mediated delivery of carbon monoxide to ovarian cancer cells

The antigen-recognizing family of Ab-photoCORMs was finally assessed for their ability to localize and deliver cytotoxic levels of CO to OVCAR-5 and SKOV-3 cell cultures using a live-cell, immunosorbent assay (Figure 4.14.). Adherent cells were first treated with 2 μ g/mL of Ab-photoCORMs for 60 min in the dark and then washed 3 times with 1X PBS to remove any non-specific association. Next fresh media was added to the cells and they were exposed to low-power visible light for 30

min for CO photorelease. After an incubation period of 24 h, cell viability was assessed by cellular reduction of MTT.

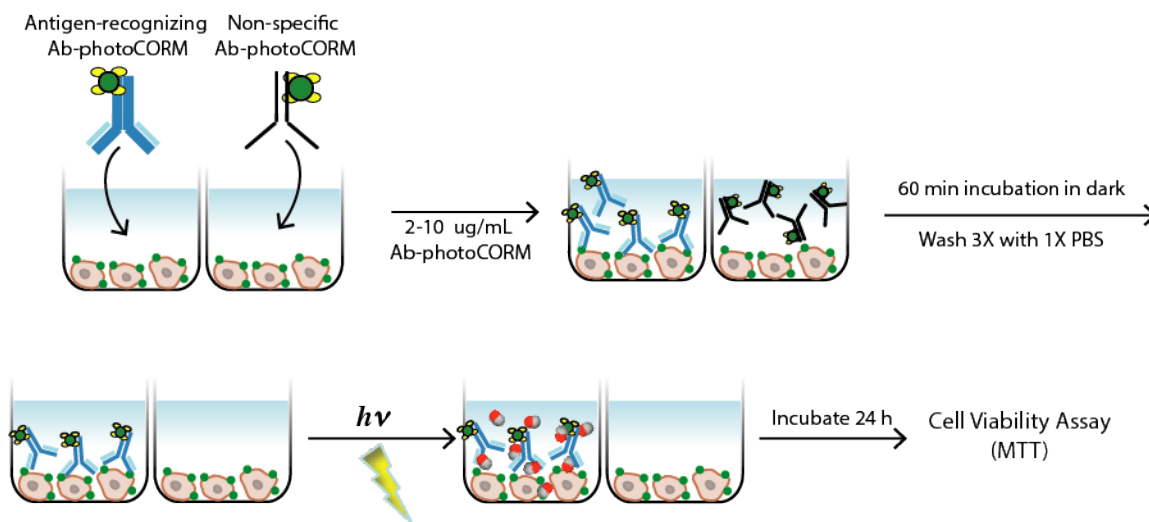


Figure 4.14. Live-cell, immunosorbent assay scheme utilized for assessment of the efficacy of antigen-recognition of an antibody-(photo-activated carbon monoxide-releasing molecule) conjugate (Ab-photoCORM) to deliver cytotoxic levels of carbon monoxide to ovarian cancer cells compared to a non-specific Ab-photoCORM conjugate.

The viability study clearly demonstrated that treatment of OVCAR-5 and SKOV-3 cells with Ab-photoCORM conjugates recognizing epitopes expressed in those ovarian cancer cell lines delivered cytotoxic levels of CO and dramatically decreased cell viability (Figure 4.15B). α -Control-photoCORM did not significantly reduce cell viability (Figure 4.15B), demonstrating that (a) CO alone was responsible for the cytotoxicity of the Ab-photoCORM complexes against the cancer cells, and (b) the presence of the antigen specific to the Ab-photoCORM on cancer cell surface was required for the targeted delivery of CO.

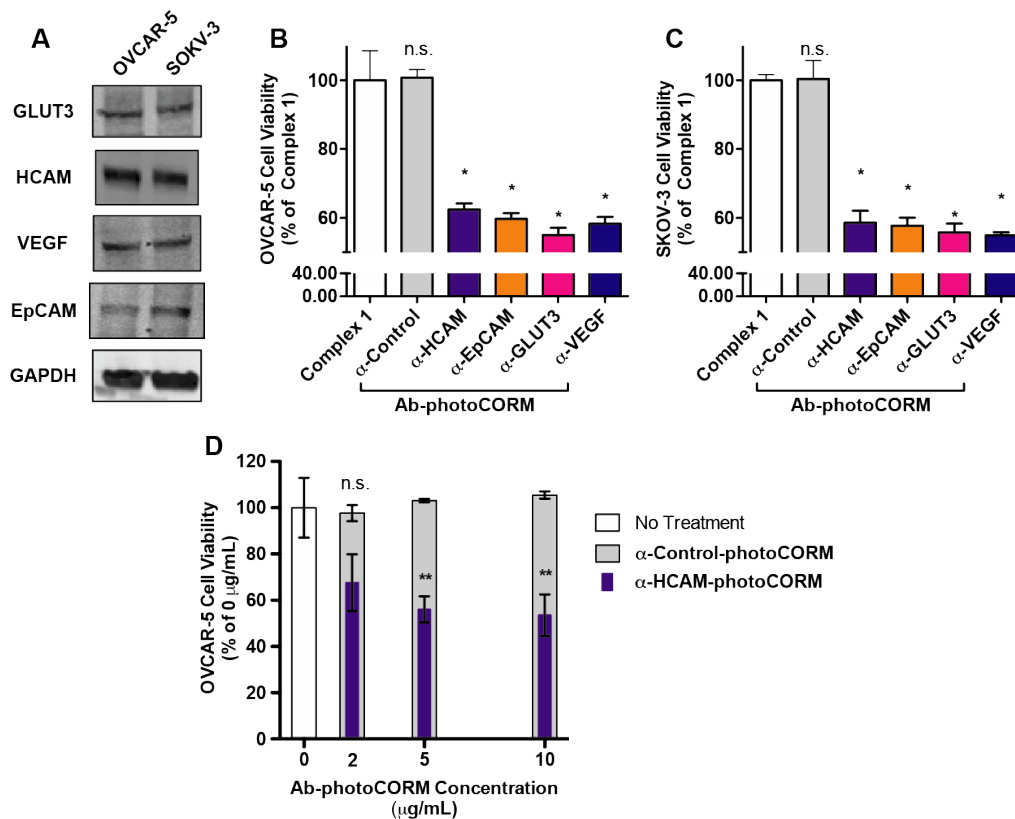


Figure 4.15. Antibody-photoCORM conjugates (Ab-photoCORMs) deliver cytotoxic levels to ovarian cancer cell lines via immunosorbent assay. (A) Western analysis of whole cell lysates of cell lines OVCAR-5 and SKOV-3, probing for antigens recognized by a family of Ab-photoCORMs. (B) Cell viability, as measured by cellular reduction of MTT, of OVCAR-5 and SKOV-3 24 h post-immunosorbent assay utilizing 2 µg/mL Ab-photoCORM conjugates. (C) Dose-dependency of α-HCAM-photoCORM, compared to α-Control-photoCORM, on cell viability. Data representative of n=3 independent experiments. (* p<0.05)

Additionally, no significant cell death was observed either with light-inactivated Complex 1 or Complex 1 in the dark. No statistically significant differences were observed between treatments for OVCAR-5 as determined by one-way ANOVA ($F(2,13) = 2.046$, $p = 0.167$) (Figure 4.16A). Similarly, no statistically

significant differences were observed between treatments for SKOV-3 as determined by one-way ANOVA ($F(2,11) = 0.219$, $p = 0.807$) (Figure 4.16B).

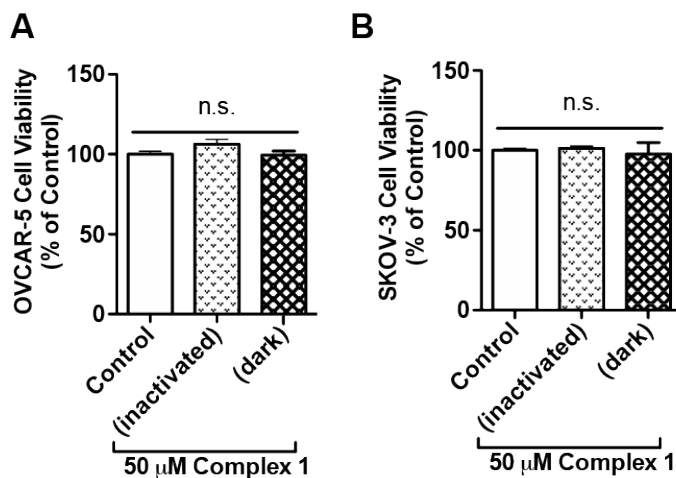


Figure 4.16. Cell viability of ovarian cancer cell lines OVCAR-5 and SKOV-3 treated with light-inactivated Complex 1 and Complex 1 in the dark to assess the cytotoxicity of the non-CO components of Complex 1. Data representative of $n=3$ independent experiments. (* $p<0.05$)

Complex 2 by itself also did not exhibit significant toxicity to both ovarian cancer cells, with no statistically significant differences observed between groups. Between treatments of OVCAR-5 with Complex 2 of varying antigen recognitions, no statistically significant differences between treatments were observed as determined by one-way ANOVA $F(6,30) = 2.632$, $p = 0.0548$). Conversely, statistically significant differences between Complex 2 treatments of SKOV-3 cells were observed as determined by one-way ANOVA $F(6,30) = 3.474$, $p = 0.0104$), though post-hoc analysis revealed no significant differences between any pairs, likely due to the relatively small sample sizes ($n=6$ for each group) or the high number of factor levels (Figure 4.17B).

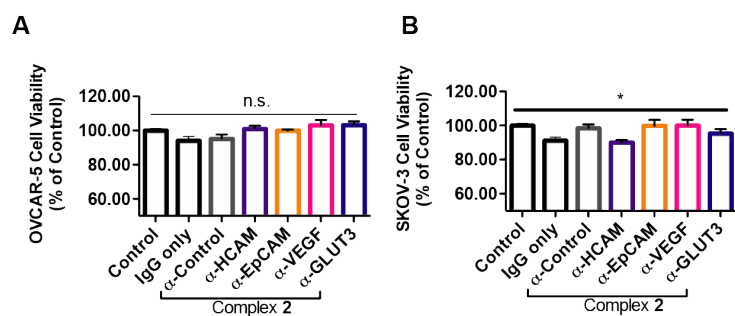


Figure 4.17. Cell viability, as measured by reduction of MTT 24 h post-treatment, of (A) OVCAR-5 and (B) SKOV-3 treated with 2 $\mu\text{g}/\text{mL}$ Complex 2 and control antibodies. Family of Complex 2 constructed from mouse monoclonal antibodies raised against human HCAM ($\alpha\text{-HCAM}$), EpCAM ($\alpha\text{-EpCAM}$), GLUT3 ($\alpha\text{-GLUT3}$) and VEGF-1 ($\alpha\text{-VEGF}$). Control treatments with vehicle control (Control), IgG without streptavidin (IgG) and Complex 2 synthesized from control mouse IgG ($\alpha\text{-Control}$) included. Data representative of $n=3$ independent experiments. (* $p<0.05$)

In order to establish a dose-dependence of Ab-photoCORM in CO-induced cell death, the $\alpha\text{-HCAM}$ -photoCORM was utilized. $\alpha\text{-HCAM}$ -photoCORM elicited dose-dependent decreases in cell viability of the OVCAR-5 and SKOV-3 compared to $\alpha\text{-Control}$ -photoCORM (Figure 4.15D). It is important to note that in previous experiments, similar photoCORMs with no conjugation with antibodies exhibited CO-induced cell death at much higher concentrations (10-50 μM range) compared to the present study where cell death is evident in presence of hundreds of picomoles of CO (Figure 4.18).

$$\left(\frac{2-10 \mu\text{g}}{\text{mL}} \right) \left(\frac{0.2 \text{ mL cell}}{\text{culture media}} \right) \left(\frac{1-4 \text{ mol streptavidin}}{1 \text{ mol Ab-photoCORM}} \right) \left(\frac{4 \text{ mol Complex 1}}{1 \text{ streptavidin}} \right) \left(\frac{3 \text{ mol CO}}{1 \text{ mol Complex 1}} \right) = \sim 23-262 \text{ pmol CO}$$

Figure 4.18. Calculations for estimation of molar release of CO from antibody-photoCORM conjugates.

While the greater potency of CO can be attributed to the improved localization of the Ab-photoCORM imparted by antigen recognition, much of this improved potency could likely be due to other mechanisms of action attributed ADCs generally, including antibody-mediated receptor signaling blockades and inflammatory responses due to the Fc component of the antibody.¹⁹ The relative contributions and synergism of these processes are poorly understood,¹⁹ but are nevertheless potent actions that can be attributed to the Ab-photoCORMs synthesized in this study. Taken together, these findings demonstrate the superior ability of the antigen-specific Ab-photoCORMs to accumulate onto ovarian cancer cells via recognition of surface proteins and deliver cytotoxic levels of CO in a much more efficient manner.

4.6 Discussion

The application of CO-releasing drugs face the challenge of strict site-specificity to avoid off-target effects of CO in normal cells. In the present work we have described an open strategy for site-specific and controlled delivery of CO to a desired biological target. Light-triggered release of a therapeutic molecule had, until this study, remained an unexplored approach for ADCs. This approach may be an effective strategy for reducing premature/off-target drug release by illumination of light directly to the tumor site. Furthermore, the frequency and length of illumination could be modulated to precisely control the kinetics of CO release from Ab-photoCORMs.

In support of this strategy, a recent study has demonstrated the feasibility of light-triggered release of a CO-releasing material in an *in vivo* mouse models.²⁰

The use of light for the remote control over the activity of pharmaceuticals, a concept known as photopharmacology, has a nearly 100 year old history in medicine and oncology.²¹ The successful clinical use of visible light to control drug activity in time and space to regulate biological processes is well documented.²²⁻²⁴ While photopharmacological treatment is naturally suitable for localized and exposed targets, optic fibers inserted through small and minimally invasive incisions allow for illumination of most body organs to be illuminated with intense, visible, broad spectrum light from non-laser sources.²⁵

Photopharmacological approaches have even been successfully applied for metastatic ovarian cancer, where intraoperative and laparoscopic light sources were successfully used in photodynamic therapy, resulting in substantial benefits for patients in clinical trials.²⁶ Visible light offers unparalleled therapeutic benefits as an external control element for pharmacological activity, which allows for the delivery and activity of photo-activatable pharmaceuticals with very high spatiotemporal precision. Furthermore, unlike chemicals, light exhibits high orthogonality towards biological systems with minimal contamination of the study subject and low to negligible toxicity.²¹ Visible light activation of photoCORMs and Ab-photoCORM conjugates for the therapeutic delivery of CO may soon mature beyond an academic

strategy at this point in time considering the well-documented success of the clinical use of visible light in photopharmacology and photodynamic therapy.^{21, 22}

The high selectivity and diversity of monoclonal antibodies towards surface expressing antigens suggest that Ab-photoCORM conjugates could be designed to deliver CO to a wide range of cell/tissues with high specificity. Antibodies inherently exhibit a wide range of binding specificities due to amino acid residues contained within six short lengths, three each in the heavy and light chains of the antibody.²⁷ As antibodies have the potential to recognize $>10^{12}$ unique antigens,²⁸ this can be exploited to improve the specificity of delivery of therapeutic molecules. The Ab-photoCORMs synthesized in this study have successfully exploited the antigen-recognition of antibodies to improve specificity of delivery of CO, a therapeutic, gaseous molecule. The Ab-photoCORMs reported here thus represent a novel class of ADCs that could be described as “immunoCORMs”.

The biotin-streptavidin linker utilized in these studies allow for the facile conjugation of the photoCORMs to any monoclonal antibody. Furthermore, the biotinylation of the photoCORM in this study was synthetically straightforward and performed under mild conditions. Biotinylation of not only other designed CORMs, but also hydrogen sulfide/nitric oxide donating molecules and nanoparticles is feasible. By this approach, the biotin-streptavidin linkage to monoclonal antibodies could be a new direction in the field of gasotransmitters, namely, the delivery of gaseous molecules driven by antibody-conjugation and antigen recognition.

Conventional ADCs require a number of specific properties in order to exhibit sufficient potency and stability. As one of the main mechanisms of drug resistance is ADC efflux,²⁹ lack of susceptibility to multidrug resistant protein 1 (MDR1) is essential. CO, as a drug delivered by an ADC, could be intriguing in that it would be unaffected by efflux mechanisms of drug resistance like MDR1. Furthermore, traditional ADCs are limited by the frequency of internalization and trafficking through the endosomal-lysosomal pathway, a relatively infrequent event.¹⁹ The ability of CO to readily diffuse across cellular membranes could circumvent the need for antibody internalization per se. A photoCORM (a prodrug) conjugated to an antibody also requires that drug release is not dependent on linker cleavage or through complete degradation of the antibody within the tumor cell. The cleavable linkers impart small molecule drug ADCs with poor pharmacokinetics and circulation instability.¹⁹ The biotin-streptavidin linker used in this design is expected to maximize stability and mitigate the problems related to esterases and proteases within cellular milieu. The antibody-photoCORM conjugates (Ab-photoCORM) could be an intriguing tool for addressing some of the fundamental limitations of ADCs.

4.7 Materials and methods

Materials and reagents

Biotin-hydrazide (A8007-100mg) was procured from Apex Biotech, Ltd. (Xuzhuang, Shaanxi, PRC). Mouse monoclonal antibodies raised against HCAM (sc-7297),

EpCAM (sc-53277), GLUT3 (sc-74399), VEGF-1 (365578) and normal mouse IgG (sc-2025) were obtained from Santa Cruz Biotechnology (Santa Cruz, CA, USA). All other chemicals were purchased from Sigma-Aldrich (St. Louis, MO, USA) unless otherwise stated.

Synthesis of biotin-photoCORM (Complex I)

[Mn(CO)₅(Br)] (100 mg, 0.36 mmol) and 1,10-phenanthroline (phen) (66 mg, 0.36 mmol) was dissolved in 25 mL dichloromethane (DCM) and allowed to stir in the dark for 20 h at 25°C. The solution, initially dark yellow, was dried down under vacuum to a yellow powder. Next, 1.5-fold excess AgCF₃SO₃ (140 mg, 0.54 mmol) was dissolved in 20 mL DCM and added to the yellow product, and allowed to stir for 1.5 h at 25°C in the dark. The cloudy green solution was subsequently filtered through a wet Celite pad, and the filtrate was evaporated to dryness. The resulting yellow powder was dissolved in 50 mL chloroform. To that stirring solution, 4-pyridinecarboxaldehyde (pyAl) (385 mg, 3.6 mmol) was added drop wise and allowed to stir for 20 h at 25°C in the dark. The next day, the solution was dried down under vacuum, revealing orange/yellow microcrystals of [Mn(CO)₃(phen)(PyrAl)CF₃SO₃] (155 mg, 0.27 mmol, 75%). To 223 mg (0.39 mmol) of [Mn(CO)₃(phen)(PyrAl)CF₃SO₃], biotin-hydrazide (100 mg, 0.39 mmol) dissolved in 20 mL of freshly distilled 2,2,2-trifluoroethanol was added, in a similar manner to a previous study.²⁹ The dark yellow solution was allowed to stir for 20 h at 25°C in the dark. The yellow brown solution was concentrated under vacuum to ~2 mL, then

chromatographed on a basic alumina column (50-200 μm particle diameter). The column was then washed with DCM (to remove unreacted $[\text{Mn}(\text{CO})_3(\text{phen})(\text{PyrAl})\text{CF}_3\text{SO}_3$ and biotin-hydrazide and finally Complex **1** was eluted with DCM/methanol (3/2 v/v).

^1H NMR (400 MHz, $[\text{D}_4]$ -methanol): δ =1.37-1.84 (m, 6H), 2.30 (t, 2H, 7.4 Hz), 2.68 (m, 1H), 2.89 (m, 1H), 3.18 (m, 1H), 4.24 (m, 1H), 4.47 (m, 1H), 7.53 (m, 2H), 7.86 (s, 1H), 8.20 (m, 4H), 8.38 (m, 2H), 8.87 (m, 2H), 9.88 (m, 2H); IR (KBr): ν = 2039, 1939, 1685 cm^{-1} (C=O); HRMS (ESI): m/z calcd for $\text{C}_{31}\text{H}_{29}\text{N}_7\text{O}_5\text{SMn}$: 666.13315 $[M^+]$; found: 666.13539, Δ ppm = 3.4 ppm, Δ mDa = 2.2; elemental analysis calculated (%) for $\text{C}_{31}\text{H}_{29}\text{N}_7\text{O}_5\text{SMn}$: C 55.86, H 4.35, N 14.71, O 12.01, S 4.80, Mn 8.26; found: C 55.84, H 4.39, N 14.71, O 12.01, S 4.80, Mn 8.25.

Physical measurements

^1H NMR spectra of Complex **1** were collected at 298 K on a Varian Unity Inova 500 MHz instrument. FT-IR of Complex **1** was collected on a PerkinElmer Spectrum-One FT-IR. UV-vis data of Complex **1** were recorded on a Varian Cary 50 UV-vis spectrophotometer.

Myoglobin assay

Horse heart myoglobin was dissolved in 1X PBS, pH = 7.4 to a final concentration of 50 μM and reduced with 0.1 % sodium dithionite in quartz cuvette under aerobic conditions. In a second cuvette, Complex **1** was dissolved in 1X PBS to a final

concentration of 50 μM . Antibody-photoCORM conjugates (Ab-photoCORM) were dissolved in 1X PBS to a final concentration of 10 $\mu\text{g/mL}$. For myoglobin assays performed in human serum, either Complex **1** or Ab-photoCORMs was dissolved to final concentrations of 50 μM or 10 $\mu\text{g/mL}$ respectively in human serum, followed by $\geq 1\text{h}$ incubation at 37°C. Photogenerated CO, triggered by low power, broadband visible light (10mW/cm²) from Complex **1** or Ab-photoCORM was released into the headspace and transferred to the reduced Mb solution via a cannula and positive pressure with N₂(g). The extent of the conversion of Mb to carboxymyoglobin (MbCO) was monitored by the change in absorbance at 540 nm. The source of low power, broadband visible light was an IL 410 Illumination System purchased from Electro Optical Components, Inc. (Santa Rosa, CA, USA). Visible light power was measured with a Field MaxII-TO laser power meter purchased from Coherent (Palo Alto, CA, USA).

Photolysis experiments

The rate of CO release (k_{CO}) for Complex **1** at 25°C in 1x PBS was assessed with in 1 cm x 1 cm quartz cuvettes. The k_{CO} of Complex **1** (concentration = 3.0×10^{-5} M, 390 nm, 25°C) was determined by recording the electronic absorption spectra, monitoring changes in the spectra following exposure to light at regular intervals. k_{CO} was then calculated from the $\ln[\text{Complex } \mathbf{1}]$ versus time (t) plot.

*Synthetic strategy of streptavidin-conjugated mouse IgG (Complex **2**)*

Conjugation of 1 mg mouse IgG, either control or antigen-specific IgG, with streptavidin was performed utilizing the Streptavidin Conjugation Kit (ab102921, Cambridge, MA, USA). Native gel electrophoresis and size exclusion chromatography were used to analyze and characterize streptavidin-conjugated antibodies. Complex **2** was quantified for use in subsequent cellular studies by measuring total protein using a Pierce™ BCA Protein Assay Kit (23225, ThermoFisher Scientific, Waltham, MA).

Native gel electrophoresis

2 µg of streptavidin-IgG conjugate was combined with native loading dye (62.5 mM Tris-HCl, pH=7.4, 40% glycerol and 0.01% bromophenol blue) and loaded onto a 4-12% Mini-PROTEAN TGX Precast Protein Gels (#4561095, Bio-Rad, Hercules, CA, USA) and separated under non-reducing, native conditions. Protein bands were visualized using Coomassie Brilliant Blue R-250 (#161-0436).

Size exclusion chromatography

Separation and simultaneous UV absorbance detection at 214 nm of streptavidin-conjugated antibodies and antibody-photoCORM conjugates was performed using a 7.5 D x 60 cm, 3 µm Tosoh TSK G4000SW (stainless steel) column. The column was preconditioned with molecular weight standards. The mobile phase was prepared with 137 mM NaCl, 2.7 mM KCl, 4.3 mM Na₂HPO₄, 1.47 mM KH₂PO₄, pH = 6.8 and sterile filtered and degassed prior to use. Separation species based on size was performed at a flow rate of 0.5 mL/min, 25 °C. Fractions of streptavidin-conjugated

antibodies and antibody-photoCORM conjugates were further characterized by bottom up proteomics.

Synthesis of antibody-photoCORM conjugates (Ab-photoCORM)

Complex **2** (100 µg, ~273 pmol) pre-dissolved in 500 µL 1X PBS was reacted with excess Complex **1** (40.0 ng, 60 nmol) pre-dissolved in 500 µL 1X PBS for 1h at 25°C in the dark. The antibody-photoCORM conjugates (Ab-photoCORMs) were purified using size exclusion chromatography. Bottom up proteomics and HPLC-MS/MS analysis was utilized to characterize the composition of Ab- photoCORMs. Detection of Complex **1** in Ab-photoCORMs was observed in full MS scans in the bottom up proteomic assays.

Bottom-up proteomics analysis

10 µg of each antibody-photoCORM conjugate, as determined by BCA Protein Assay, were solubilized in 200 µL lysis buffer (12 mM sodium lauroyl sarcosine, 0.5% sodium deoxycholate, 50 mM triethylammonium bicarbonate (TEAB)) followed by 10 min bath sonication and heating at 95°C for 5 min. The samples were then diluted to 0.5 mg total protein/mL with lysis buffer, then a 100 µL aliquot was treated with 5 mM tris(2-carboxyethyl) phosphine (TCEP) prepared in 50 mM aqueous TEAB at 60°C for 30 min. Next, the samples were treated with 10mM chloroacetamide, prepared in 50 mM TEAB, for 30 min at 25°C in the dark. Samples were diluted 5-fold in 50 mM TEAB, then incubated overnight with Sequencing Grade Modified Trypsin (1:100, mg trypsin: mg total protein). The next day, an equal volume of ethyl

acetate/trifluoroacetic acid (TFA, 100/1, v/v) was added to samples, followed by 5 min vigorous vortexing and centrifugation (13,000 x g, 5 min). Desalting of samples was performed similar to that previously described.[3] Dried samples were reconstituted in acetonitrile/water/TFA (2/98/0.1, v/v/v), loaded onto a C18-silica disk (3M, Maplewood, MN, USA) placed inside a 200 μ L pipet tip. Prior to sample loading onto the disk, it was equilibrated with methanol (20 μ L), acetonitrile/water/TFA (20 μ L, 80/20/0.1, v/v/v), then finally acetonitrile/water/TFA (2/98/0.1, v/v/v). The samples were loaded onto the disks were washed with acetonitrile/water/TFA (20 μ L, 2/98/0.1, v/v/v) and eluted with acetonitrile/water/TFA (40 μ L, 80/20/0.1, v/v/v). Eluents were concentrated under vacuum centrifugation and reconstituted in 10 μ L water/acetonitrile/formic acid, 98/2/0.1, v/v/v). 5 μ L aliquots were injected onto a reverse phase nanobore HPLC column (AcuTech Scientific, C18, 1.8 μ m particle size, 360 μ m x 20 cm, 150 μ m ID), equilibrated in water/acetonitrile/formic acid (98/2/0.1, v/v/v: min/%; 0/0, 5/3, 18/7, 74/12, 144/24, 153/27, 162/40, 164/80, 174/80, 176/0, 180/0) using an Eksigent NanoLC-2D system (Sciex, Framingham, MA, USA). The flow from the column was directed towards nanospray ionization source connected to a Q ExactiveTM Hybrid Quadrupole-OrbitrapTM Mass Spectrometer (Thermo Fisher Scientific). Data-dependent mass spectra were acquired alternating between full scan (m/z 350-2000, automated gain control target 3×10^3 , 50 ms maximum injection time, FWHM resolution 70,000 at m/z 200) and up to 10 MS/MS scans (quadrupole isolation of charge states ≥ 1 , isolation width 1.2 Th) with optimized fragmentation conditions

(normalized collision energy of 32, dynamic exclusion of 30 s, AGC target 1×10^6 , 100 ms maximum injection time, FWHM resolution 35,000 at m/z 200). Analysis of raw data and peptide/protein identification of the antibody- photoCORM conjugates was performed using Mascot to search the UniProt- Mouse database. Common Contaminants database was also searched to identify streptavidin. Probability based scoring was used to determine significance of data, where reported scores = $-10 \times \text{Log}_{10}(P)$, where P is the absolute probability that the observed match between the experimental data and the database sequence is a random event.[4,5] Scores >67 are considered significant ($p < 0.05$).[4,5] Complex 1 associated with Ab-photoCORM was observed in the full MS scan data (Figure 4.12).

Cell culture

Ovarian cancer cell lines OVCAR-5 and SKOV-3 were obtained from American Type Culture Collection (Manassas, VA, USA). OVCAR-5 and SKOV-3 were grown in RPMI 1640 Medium (11875119, ThermoFisher Scientific) supplemented with 10% fetal bovine serum (FBS, 16000) and 100 U/mL penicillin-streptomycin (15070063) were all purchased from ThermoFisher Scientific. Cells were passaged ≤ 10 times after acquisition from the manufacturer.

Cell viability assay

Cell viability was assessed by the cellular reduction of tetrazolium dye MTT performed in 96-well tissue culture plates. 2×10^3 cells/well were allowed to seed overnight in a 37 °C incubator + 5% CO₂. The following day, cells were treated as

indicated with Complex 1 or Complex 2, then assessed for viability 24 h post-treatment. Following removal of cell culture media, 0.5 mg/mL MTT dissolved in fresh 1× DMEM was added and allowed to incubate for 2 h in a 37°C incubator + 5% CO₂. Cell viability was quantified by measuring the relative amount of MTT reduced to insoluble formazan. Following solubilization of formazan in 10% SDS + 0.01 N HCl, formazan was measured by taking the absorbance at 570 nm, reference wavelength taken at 690 nm.

Western analysis

Whole cell lysates were extracted using RIPA lysis buffer (150 mM NaCl, 5 mM EDTA pH 8.0, 50 mM Tris pH 8.0, 1% Triton X-100, 0.5% sodium deoxycholate, 1% SDS and 1× protease inhibitor cocktail. BCA Protein Assay assayed soluble fractions for total protein content. 20 µg of soluble cell lysates from samples were resolved on 10% SDS-PAGE gel and transferred to poly(vinylidene difluoride) (PVDF) membrane. All following blocking and antibody solutions were prepared in 1x PBS + 0.1% Tween 20. Membranes, following blocking in 5% nonfat dried milk for 18 h at 4°C, were probed with primary (1:1000 dilution) antibody overnight at 4°C and then horseradish peroxidase (HRP)-conjugated secondary (1:10,000 dilution) antibody for 1 h at 25°C. Immunofluorescent signals were amplified with Pierce ECL Plus Western blotting substrate (32132, ThermoFisher Scientific).

Live-cell immunosorbent assay

2 x 10³ cells/well of 96-well tissue culture plates were allowed to seed overnight at 37°C + 5% CO₂. The next day, cells were treated as indicated with 0-10 µg/mL antibody-photoCORM conjugates (Ab-photoCORM), as measured by BCA Protein Assay. Immunosorbence of Ab-photoCORMs to the adherent live cells was allowed to occur for 60 min in the dark at 37°C + 5% CO₂. α -Control Ab- photoCORM, utilizing control mouse IgG (sc-2025, Santa Cruz Biotechnology), was utilized as control to assess the specificity of the other antibody-photoCORM conjugates. Following incubation, the media was gently aspirated, followed by three 250 µL washes with 1X PBS in the dark to remove any non-specific binding. 100 µL fresh cell culture media was added, followed by illumination with low power, visible light for 30 min to trigger release of CO from any Ab-photoCORM present after immunosorbence and washing. Cell viability, as measured by the reduction of MTT, was assayed 24 h post-illumination of light.

Statistical analysis

Data are expressed as the mean \pm standard error mean (range) or as percentage of control value where indicated. Comparisons between two groups were made using the Student's t-test. Comparisons between more than two groups were made using the One-way ANOVA/ Tukey's post hoc test. p-values < 0.05 were considered statistically significant. All calculations were performed using GraphPad Prism software package (GraphPad Software Inc., San Diego, USA).

4.9 References

1. Chakraborty, I.; Carrington, S. J.; Roseman, G.; Mascharak, P. K., Synthesis, structures, and CO release capacity of a family of water-soluble photoCORMs: assessment of the biocompatibility and their phototoxicity toward human breast cancer cells. *Inorganic Chemistry* **2017**, *56* (3), 1534-1545.
2. Chakraborty, I.; Carrington, S. J.; Hauser, J.; Oliver, S. R. J.; Mascharak, P. K., Rapid eradication of human breast cancer cells through trackable light-triggered co delivery by mesoporous silica nanoparticles packed with a designed photoCORM. *Chemistry of Materials* **2015**, *27* (24), 8387-8397.
3. Chakraborty, I.; Jimenez, J.; Mascharak, P. K., CO-Induced apoptotic death of colorectal cancer cells by a luminescent photoCORM grafted on biocompatible carboxymethyl chitosan. *Chemical Communications* **2017**, *53* (40), 5519-5522.
4. Schatzschneider, U., Novel lead structures and activation mechanisms for CO-releasing molecules (CORMs). *British Journal of Pharmacology* **2015**, *172* (6), 1638-1650.
5. Garcia-Gallego, S.; Bernardes, G. J. L., Carbon-monoxide-releasing molecules for the delivery of therapeutic CO in vivo. *Angewandte Chemie-International Edition* **2014**, *53* (37), 9712-9721.
6. Heinemann, S. H.; Hoshi, T.; Westerhausen, M.; Schiller, A., Carbon monoxide - physiology, detection and controlled release. *Chemical Communications* **2014**, *50* (28), 3644-3660.
7. Rimmer, R. D.; Pierri, A. E.; Ford, P. C., Photochemically activated carbon monoxide release for biological targets. Toward developing air-stable photoCORMs labilized by visible light. *Coordination Chemistry Reviews* **2012**, *256* (15-16), 1509-1519.
8. Kawahara, B.; Moller, T.; Hu-Moore, K.; Carrington, S.; Faull, K. F.; Sen, S.; Mascharak, P. K., attenuation of antioxidant capacity in human breast cancer cells by carbon monoxide through inhibition of cystathionine β -synthase activity:

- implications in chemotherapeutic drug sensitivity. *Journal of Medicinal Chemistry* **2017**, *60* (19), 8000-8010.
9. Kawahara, B.; Ramadoss, S.; Chaudhuri, G.; Janzen, C.; Sen, S.; Mascharak, P. K., Carbon monoxide sensitizes cisplatin-resistant ovarian cancer cell lines toward cisplatin via attenuation of levels of glutathione and nuclear metallothionein. *Journal of Inorganic Biochemistry* **2019**, *191*, 29-39.
 10. Beck, A.; Goetsch, L.; Dumontet, C.; Corvaia, N., Strategies and challenges for the next generation of antibody drug conjugates. *Nature Reviews Drug Discovery* **2017**, *16* (5), 315-337.
 11. Pinto, M. N.; Chakraborty, I.; Sandoval, C.; Mascharak, P. K., Eradication of HT-29 colorectal adenocarcinoma cells by controlled photorelease of CO from a CO-releasing polymer (photoCORP-1) triggered by visible light through an optical fiber-based device. *Journal of Controlled Release* **2017**, *264*, 192-202.
 12. Carrington, S. J.; Chakraborty, I.; Bernard, J. M. L.; Mascharak, P. K., A theranostic two-tone luminescent photoCORM derived from Re(i) and (2-pyridyl)-benzothiazole: trackable co delivery to malignant cells. *Inorganic Chemistry* **2016**, *55* (16), 7852-7858.
 13. Carrington, S. J.; Chakraborty, I.; Mascharak, P. K., Rapid CO release from a Mn(I) carbonyl complex derived from azopyridine upon exposure to visible light and its phototoxicity toward malignant cells. *Chemical Communication* **2013**, *49* (96), 11254-11256.
 14. Hermanson, G. T., (Strept)avidin-Biotin Systems. *Bioconjugate Techniques*, *3rd Edition* **2013**, 465-505.
 15. Sacks, J. D.; Barbolina, M. V., Expression and function of CD44 in epithelial ovarian carcinoma. *Biomolecules* **2015**, *5* (4), 3051-3066.
 16. Akhter, M. Z.; Sharawat, S. K.; Kumar, V.; Kochat, V.; Eqbal, Z.; Ramakrishnan, M.; Kumar, U.; Mathur, S.; Kumar, L.; Mukhopadhyay, A., Aggressive serous epithelial ovarian cancer is potentially propagated by EpCAM(+)CD45(+) phenotype. *Oncogene* **2018**, *37* (16), 2089-2103.

17. Tsukioka, M.; Matsumoto, Y.; Noriyuki, M.; Yoshida, C.; Nobeyama, H.; Yoshida, H.; Yasui, T.; Sumi, T.; Honda, K. I.; Ishiko, O., Expression of glucose transporters in epithelial ovarian carcinoma: Correlation with clinical characteristics and tumor angiogenesis. *Oncology Reports* **2007**, *18* (2), 361-367.
18. Mukherjee, S.; Pal, M.; Mukhopadhyay, S.; Das, I.; Hazra, R.; Ghosh, S.; Mondal, R. K.; Bal, R., VEGF expression to support targeted therapy in ovarian surface epithelial neoplasms. *Journal of Clinical Diagnostic Research* **2017**, *11* (4), EC43-EC46
19. Khera, E.; Thurber, G. M., pharmacokinetic and immunological considerations for expanding the therapeutic window of next-generation antibody-drug conjugates. *Biodrugs* **2018**, *32* (5), 465-480.
20. Wang, C. C.; Li, Y. Q.; Shi, X. Q.; Zhou, J. H.; Zhou, L.; Wei, S. H., Use of an NIR-light-responsive CO nanodonor to improve the EPR effect in photothermal cancer treatment. *Chemical Communications* **2018**, *54* (95), 13403-13406.
21. Velema, W. A.; Szymanski, W.; Feringa, B. L., Photopharmacology: Beyond proof of principle. *Journal of the American Chemical Society* **2014**, *136* (6), 2178-2191.
22. Hull, K.; Morstein, J.; Trauner, D., In vivo photopharmacology. *Chemical Reviews* **2018**, *118* (21), 10710-10747.
23. Mehta, Z. B.; Johnston, N. R.; Nguyen-Tu, M. S.; Broichhagen, J.; Schultz, P.; Larner, D. P.; Leclerc, I.; Trauner, D.; Rutter, G. A.; Hodson, D. J., Remote control of glucose homeostasis in vivo using photopharmacology. *Scientific Reports* **2017**, *7*.
24. Broichhagen, J.; Schonberger, M.; Cork, S. C.; Frank, J. A.; Marchetti, P.; Bugliani, M.; Shapiro, A. M. J.; Trapp, S.; Rutter, G. A.; Hodson, D. J.; Trauner, D., Optical control of insulin release using a photoswitchable sulfonyleurea. *Nature Communications* **2014**, *5*.

25. Allison, R. R.; Cuenca, R.; Downie, G. H.; Randall, M. E.; Bagnato, V. S.; Sibata, C. H., PD/PDT for gynecological disease: A clinical review. *Photodiagnosis and Photodynamic Therapy* **2005**, *2* (1), 51-63.
26. Wierrani, F.; Fiedler, D.; Grin, W.; Henry, M.; Dienes, E.; Gharehbaghi, K.; Krammer, B.; Grunberger, W., Clinical effect of meso-tetrahydroxyphenylchlorine based photodynamic therapy in recurrent carcinoma of the ovary: Preliminary results. *British Journal of Obstetrics and Gynaecology* **1997**, *104* (3), 376-378.
27. Rose, D. R., The generation of antibody diversity. *American Journal of Hematology* **1982**, *13* (1), 91-99.
28. Salomon, P. L.; Singh, R., Sensitive ELISA method for the measurement of catabolites of antibody-drug conjugates (ADCs) in Target Cancer Cells. *Molecular Pharmaceutics* **2015**, *12* (6), 1752-1761.
29. Salmain, M.; Fischer-Durand, N.; Cavalier, L.; Rudolf, B.; Zakrzewski, J.; Jaouen, G., Transition metal-carbonyl labeling of biotin and avidin for use in solid-phase carbonyl metallo immunoassay (CMIA). *Bioconjugate Chemistry* **2002**, *13* (3), 693-8.

4.9 Reprint of Publication

1/18/2020

Diminished viability of human ovarian cancer cells by antigen-specific delivery of carbon monoxide with a family of photoactivatable antibody-photo...



Diminished viability of human ovarian cancer cells by antigen-specific delivery of carbon monoxide with a family of photoactivatable antibody-photoCORM conjugates

B. Kawahara, L. Gao, W. Cohn, J. P. Whitelegge, S. Sen, C. Janzen and P. K. Mascharak, *Chem. Sci.*, 2020, **11**, 467

DOI: 10.1039/C9SC03166A

This article is licensed under a [Creative Commons Attribution 3.0 Unported Licence](#). Material from this article can be used in other publications provided that the correct acknowledgement is given with the reproduced material.


Reproduced material should be attributed as follows:

- For reproduction of material from NJC:
[Original citation] - Published by The Royal Society of Chemistry (RSC) on behalf of the Centre National de la Recherche Scientifique (CNRS) and the RSC.
- For reproduction of material from PCCP:
[Original citation] - Published by the PCCP Owner Societies.
- For reproduction of material from PPS:
[Original citation] - Published by The Royal Society of Chemistry (RSC) on behalf of the European Society for Photobiology, the European Photochemistry Association, and RSC.
- For reproduction of material from all other RSC journals:
[Original citation] - Published by The Royal Society of Chemistry.

Information about reproducing material from RSC articles with different licences is available on our [Permission Requests page](#).



Cite this: DOI: 10.1039/c9sc03166a

 All publication charges for this article have been paid for by the Royal Society of ChemistryReceived 27th June 2019
Accepted 18th November 2019DOI: 10.1039/c9sc03166a
rsc.li/chemical-science

Diminished viability of human ovarian cancer cells by antigen-specific delivery of carbon monoxide with a family of photoactivatable antibody-photoCORM conjugates†

Brian Kawahara,^a Lucy Gao,^b Whitaker Cohn,^b Julian P. Whitelegge,^b Suvajit Sen,^c Carla Janzen^c and Pradip K. Mascharak^{*,a}

Carbon monoxide (CO)-releasing antibody conjugates were synthesized utilizing a photoactivatable CO-releasing molecule (photoCORM) and mouse monoclonal antibodies linked by a biotin-streptavidin system. Different monoclonal antibodies raised against different surface-expressed antigens that are implicated in ovarian cancer afforded a family of antibody-photoCORM conjugates (Ab-photoCORMs). In an immunosorbent/cell viability assay, Ab-photoCORMs accumulated onto ovarian cancer cells expressing the target antigens, delivering cytotoxic doses of CO *in vitro*. The results described here provide the first example of an “immunoCORM”, a proof-of-the-concept antibody-drug conjugate that delivers a gaseous molecule as a warhead to ovarian cancer.

Introduction

Carbon monoxide (CO), while long recognized as a toxic gas, is an endogenously produced gasotransmitter that regulates immune/inflammatory processes and vascular tone through reactions with heme-containing proteins.¹ In recent years, exogenous delivery of CO has shown promise as a novel therapeutic in a variety of disease and injury models, including cancer.²

The challenge of delivering efficacious concentrations of CO to a target tissue has been approached by our group and others by synthesizing CO-releasing molecules (CORMs) with properties necessary for a potential therapeutic, including water solubility,³ incorporation within biocompatible materials^{4,5} and controllable release of CO.^{6–9} Very recently, with the use of photoactivatable CORMs (photoCORMs) our group has elucidated mechanism(s) by which CO exerts deleterious effects against human breast and ovarian cancer cell models.^{10,11} In such studies we have observed sensitization of ovarian cancer

cells to drugs like cisplatin and paclitaxel through co-administration of CO.¹¹ Because sensitization to conventional chemotherapeutics could mitigate the poor outcome of ovarian cancer treatment, precise target-specific delivery of CO to the malignant tissue appears to be a very desirable goal.

Although a number of CORMs and photoCORMs has been developed in recent years,^{1,2,6–9} most have notably lacked the ability to highly discriminate between targeted *versus* non-targeted tissues. With this in mind, we sought to conjugate a photoCORM to a monoclonal antibody with the goal of improving target specificity of CO-release. Antibody-drug conjugates (ADCs) are fast emerging as an effective strategy for anticancer therapies. In most cases small molecule drugs are combined with monoclonal antibodies to achieve high selectivity.¹² Conjugation of photoCORMs (*i.e.* the warhead) to monoclonal antibodies using a biotin-streptavidin linker is a novel, currently unexplored and potentially effective strategy that could be employed for the controlled delivery of CO to specific tissues.

Herein we report the successful conjugation of a biotinylated-photoCORM to streptavidin-conjugated mouse monoclonal immunoglobulin G (IgG) antibodies to isolate Ab-photoCORMs for the controlled delivery of CO to ovarian cancer cell cultures with high specificity. Utilizing different monoclonal antibodies, a family of Ab-photoCORMs was synthesized with the goal of localizing and delivering cytotoxic levels of CO to ovarian cancer cells expressing different tumor-specific surface antigens. To the best of our knowledge, this communication is the first report of an antibody-drug conjugate in which the drug is a gaseous molecule, namely CO.

^aDepartment of Chemistry and Biochemistry, University of California, Santa Cruz, CA 95064, USA. E-mail: pradip@ucsc.edu

^bPasarrow Mass Spectrometry Laboratory, Jane and Terry Semel Institute for Neuroscience and Human Behavior, University of California at Los Angeles, Los Angeles, CA 90095, USA

^cDepartment of Obstetrics and Gynecology, David Geffen School of Medicine, University of California at Los Angeles, Los Angeles, CA 90095, USA

† Electronic supplementary information (ESI) available: Synthetic scheme and calculations for CO release (Schemes S1 and S2). Spectroscopic, chromatography and mass spectrometry data (Fig. S1–S4, S8 and S9). Myoglobin assays and cell toxicity/viability data (Fig. S5–S7 and S10–S13). Description of the experimental procedures. See DOI: 10.1039/c9sc03166a



Results and discussion

Synthesis of biotinylated photoCORM (Complex 1)

The present work utilized a designed photoCORM [Mn(CO)₃(phen)(4-pyAl)](CF₃SO₃) (where phen = 1,10-phenanthroline, 4-pyAl = pyridine-4-carboxaldehyde) as the photoactivatable CO donor. Biotinylation of this photoCORM (Fig. 1, Complex 1) was achieved through reaction with biotin-hydrazide in trifluoroethanol at room temperature (Scheme S1†). The composition of Complex 1 was confirmed by electrospray ionization Fourier Transform mass spectrometry (ESI FTMS); (*M*⁺) *m/z* = 666.13539 (calculated for C₃₁H₂₉N₇O₅SMn: 666.13313, Δ ppm = 3.4 ppm, Δ mDa = 2.2) (Fig. S1†), and ¹H NMR spectrum (ESI†). The infrared spectrum of Complex 1 showed the presence of two $\nu_{C=O}$ bands at 2039 and 1939 cm⁻¹, characteristic of the manganese tricarbonyl moiety, and one $\nu_{C=O}$ band at 1685 cm⁻¹ derived from the biotin unit (Fig. S2†). Electronic absorption spectra of solutions of Complex 1 in 1x phosphate-buffered saline (PBS) exhibited a broad absorbance band in the visible region between 320 and 450 nm (Fig. S3†). Exposure of Complex 1 to visible light resulted in systematic changes in the absorption

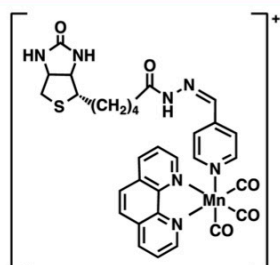


Fig. 1 Structure of biotinylated photoCORM (Complex 1).

spectra (Fig. S4†) arising from the loss of CO.³ Integration of the rate law for the photodegradation of Complex 1 was performed to determine pseudo-first order kinetics for CO release, with apparent visible light activated CO release rate $k_{app} = 0.0030 \pm 0.010$ s⁻¹ determined in 1x PBS (Fig. S4†). Complex 1 was stable in 1x PBS in the dark for ~48 h, releasing CO only upon illumination with low power (10 mW cm⁻²), broadband, visible light (Fig. S5†). Furthermore, Complex 1 exhibited stability in human serum for 24 h at 37 °C, retaining the property of photorelease of CO, as confirmed by myoglobin assay (Fig. S6†).

Previous studies from this laboratory have demonstrated that sufficient levels of CO, delivered from photoCORMs, can induce apoptotic cell death in a wide variety of cancer cells.^{4,5,13-15} Likewise, Complex 1 upon illumination with visible light, significantly reduced cell viability in two ovarian cancer cell lines OVCAR-5 and SKOV-3 (ED₅₀ = 48 and 25 μ M respectively) assayed 24 h post-treatment (Fig. S7†).

Synthesis of streptavidin-conjugated IgG (Complex 2)

A streptavidin-biotin strategy was used to link Complex 1 to IgG, exploiting the strong affinity ($K_d = 10^{-14}$ M) and stability of the streptavidin-biotin interaction.¹⁶ The streptavidin-IgG conjugate was synthesized using a commercially available kit (ESI†). Native gel electrophoresis (Fig. 2A) and size exclusion chromatography (Fig. S8†) revealed conjugation of a variable number of streptavidin molecules to IgG which was expected as per manufacturer's notes. Fractionation of crude streptavidin-IgG conjugates following size exclusion chromatography was performed to resolve and isolate antibodies conjugated with 1–4 streptavidin molecules (Fig. 2B). These fractions were then pooled together (abbreviated hereafter as Complex 2) for cellular studies.

Construction of Ab-photoCORM conjugate

Reaction of Complex 2 with excess Complex 1 afforded the antibody-photoCORM conjugate (Ab-photoCORM) through

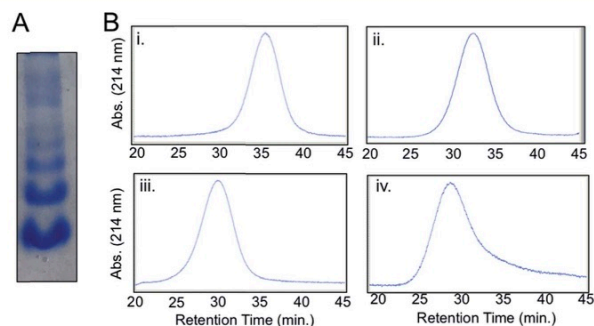


Fig. 2 Complex 2: streptavidin-conjugated IgG. (A) Native protein gel electrophoresis of crude Complex 2. (B) Size-exclusion chromatograms of fractions of Complex 2. [Retention time, ~molecular weight, identity] (i) [35.4 min, ~210 kDa, IgG + 1 streptavidin]. (ii) [32.2 min, ~260 kDa, IgG + 2 streptavidin]. (iii) [29.9 min, ~313 kDa, IgG + 3 streptavidin]. (iv) [28.6 min, ~366 kDa, IgG + 4 streptavidin].



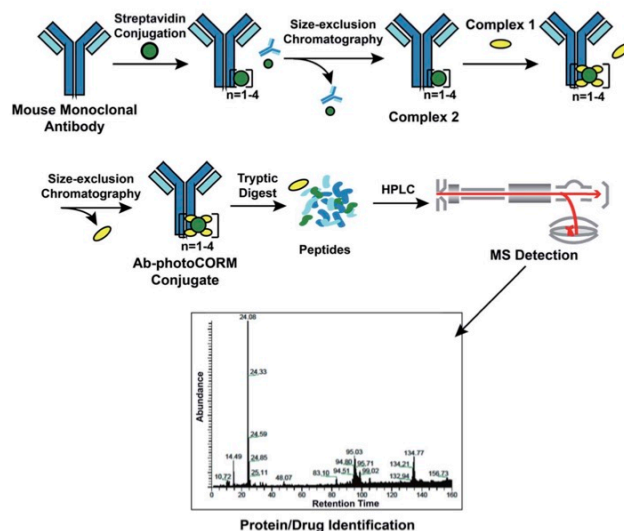


Fig. 3 Synthesis and characterization of the antibody-photoCORM conjugate (Ab-photoCORM) and proteomic analysis of Ab-photoCORM. The scheme of bottom-up proteomics of the Ab-photoCORM is also shown.

a streptavidin-biotin interaction (Fig. 3) (ESI[†]). The Ab-photoCORM was then purified to remove any trace of unbound streptavidin, unconjugated IgG and unincorporated Complex 1 by size-exclusion chromatography (Fig. 3).

Bottom-up proteomic analysis of the Ab-photoCORM confirmed the presence of streptavidin in the Ab-photoCORM (Fig. 4). Additionally, Complex 1 (M[†]) incorporated into the Ab-photoCORM was observed in the full MS scan (Fig. 4 and S9[†]). The Ab-photoCORM, by merit of Complex 1 incorporation,

exhibited photo-activated release of CO, as determined by myoglobin assay performed in 1x PBS (Fig. S10[†]). Furthermore, the Ab-photoCORM exhibited stability in a biological fluid, as evidenced by its retained photo-activatable release of CO following incubation in human blood serum for 1 h at 37 °C (Fig. S11[†]).

A family of Ab-photoCORM conjugates was synthesized (Table 1) using this synthetic strategy with commercially available mouse monoclonal IgG raised against four surface-expressed antigens implicated in ovarian cancer, namely

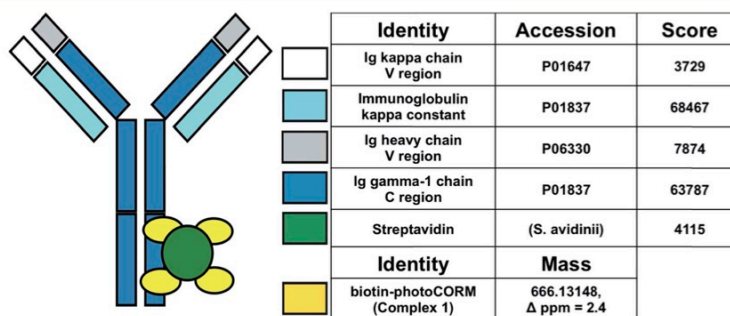


Fig. 4 Proteomic scores of the Ab-photoCORMs synthesized in this study. Biotin-photoCORM (Complex 1) was observed in the full MS scan of the tryptic digest of Ab-photoCORM. Protein scores greater than 67 are significant (*i.e.* $p < 0.05$).



Table 1 Family of antibody-photoCORM conjugates (Ab-photoCORMs) synthesized from commercial antibodies, recognizing indicated human cell surface antigens implicated in ovarian cancer

Original mouse IgG	Epitope recognized	Streptavidin-IgG (Complex 2)	Antibody-photoCORM conjugate (Ab-photoCORM)
HCAM (sc-7297)	Homing cell adhesion molecule (human)	Complex 2-(α -HCAM)	α -HCAM-photoCORM
EpCAM (sc-53277)	Epithelial cell adhesion molecule (human)	Complex 2-(α -EpCAM)	α -EpCAM-photoCORM
GLUT3 (sc-74399)	Glucose transporter 3 (human)	Complex 2-(α -GLUT3)	α -GLUT3-photoCORM
VEGF-A (365578)	Vascular endothelial growth factor A (human)	Complex 2-(α -VEGF)	α -VEGF-photoCORM
Normal mouse IgG (sc-2025)	None	Complex 2-(α -control)	α -Control-photoCORM

homing cell adhesion molecule (HCAM),¹⁷ epithelial cell adhesion molecule (EpCAM),¹⁸ glucose transporter 3 (GLUT3),¹⁹ and vascular endothelial growth factor A (VEGF).²⁰ Immunoblot analysis of whole cell lysates of cell line models utilized, OVCAR-5 and SKOV-3, confirmed the presence of the antigens recognized by the family of Ab-photoCORMs (Fig. 5A). An Ab-photoCORM utilizing IgG *not raised against any specific antigen* (α -Control-photoCORM) was also synthesized for application in

cell viability experiments in order to account for any non-CO-mediated effects of the antigen-specific Ab-photoCORMs.

Cell viability assays of Ab-photoCORMs in ovarian cancer cell model

The antigen-recognizing family of Ab-photoCORMs was finally assessed for their ability to localize and deliver cytotoxic levels

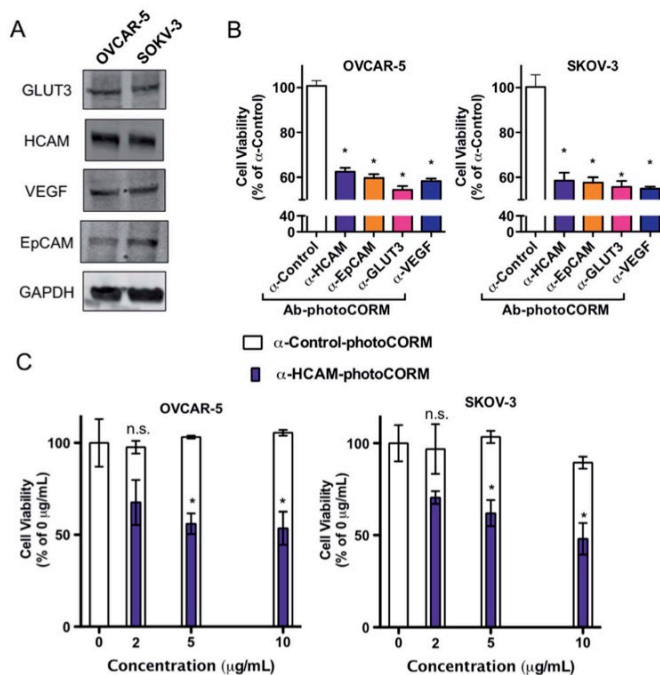
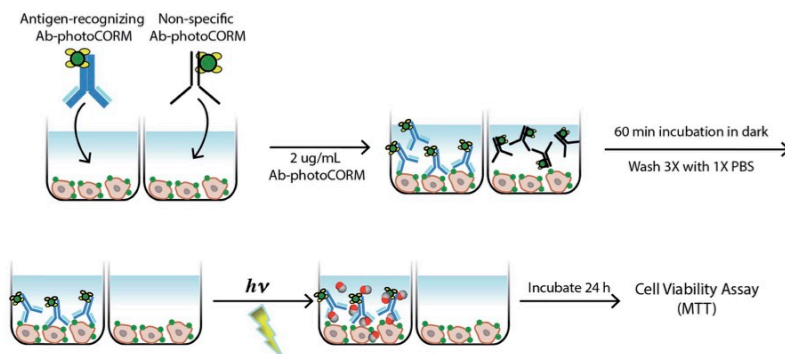


Fig. 5 Antibody-photoCORM conjugates (Ab-photoCORMs) deliver cytotoxic levels to ovarian cancer cell lines *via* immunosorbent assay. (A) Western analysis of whole cell lysates of cell lines OVCAR-5 and SKOV-3, probing for antigens recognized by a family of Ab-photoCORMs. (B) Cell viability, as measured by cellular reduction of MTT, of OVCAR-5 and SKOV-3 24 h post-immunosorbent assay utilizing 2 μ g mL⁻¹ Ab-photoCORM conjugates. (C) Dose-dependency of α -HCAM-photoCORM, compared to α -Control-photoCORM, on cell viability. Data representative of $n = 3$ independent experiments. (* $p < 0.05$).





Scheme 1 Live-cell, immunosorbent assay scheme utilized for assessment of the efficacy of antigen-recognition of an antibody-(photo-activated carbon monoxide-releasing molecule) conjugate (Ab-photoCORM) to deliver cytotoxic levels of carbon monoxide to ovarian cancer cells compared to a non-specific Ab-photoCORM conjugate.

of CO to OVCAR-5 and SKOV-3 cell cultures using a live-cell, immunosorbent assay (Scheme 1). Adherent cells were first treated with $2 \mu\text{g mL}^{-1}$ of Ab-photoCORMs for 60 min in the dark and then washed 3 times with 1x PBS to remove any non-specific association. Next fresh media was added to the cells and they were exposed to low-power visible light for 30 min for CO photorelease. After an incubation period of 24 h, cell viability was assessed by cellular reduction of MTT. The viability study clearly demonstrated that treatment of OVCAR-5 and SKOV-3 cells with Ab-photoCORM conjugates recognizing epitopes expressed in those ovarian cancer cell lines delivered cytotoxic levels of CO and dramatically decreased cell viability (Fig. 5B). α -Control-photoCORM did not significantly reduce cell viability (Fig. 5B), demonstrating that (a) CO alone was responsible for the cytotoxicity of the Ab-photoCORM complexes against the cancer cells, and (b) the presence of the right antigen on cancer cell surface was required for the targeted delivery of CO. Additionally, no significant cell death was observed either with light-inactivated Complex 1 or Complex 1 in the dark (Fig. S12[†]). Complex 2 by itself also did not exhibit significant toxicity to both ovarian cancer cells (Fig. S13[†]).

In order to establish a dose-dependence of Ab-photoCORM in CO-induced cell death, the α -HCAM-photoCORM was utilized in similar assay. As shown in Fig. 5C, α -HCAM-photoCORM elicited dose-dependent decreases in cell viability of the OVCAR-5 and SKOV-3 compared to α -Control-photoCORM. It is important to note that in previous experiments, similar photoCORMs with no conjugation with antibodies exhibited CO-induced cell death at much higher concentrations (10–50 μM range) compared to the present study where cell death is evident in presence of hundreds of picomoles of CO (Scheme S2[†]). While the greater potency of CO can be attributed to the improved localization of the Ab-photoCORM imparted by antigen recognition, much of this

improved potency could likely be due to other mechanisms of action attributed ADCs generally, including antibody-mediated receptor signaling blockades and inflammatory responses due to the Fc component of the antibody.²¹ The relative contributions and synergism of these processes are poorly understood,²¹ but are nevertheless potent actions that can be attributed to the Ab-photoCORMs synthesized in this study. Taken together, these findings demonstrate the superior ability of the antigen-specific Ab-photoCORMs to accumulate onto ovarian cancer cells *via* recognition of surface proteins and deliver cytotoxic levels of CO in a much more efficient manner.

Conclusions

The application of CO-releasing drugs face the challenge of strict site-specificity to avoid off-target effects of CO in normal cells. In the present work we have described an open strategy for site-specific and controlled delivery of CO to a desired biological target. Light-triggered release of a therapeutic molecule had, until this study, remained an unexplored approach for ADCs. This approach may be an effective strategy for reducing premature/off-target drug release by illumination of light directly to the tumor site. Furthermore, the frequency and length of illumination could be modulated to precisely control the kinetics of CO release from Ab-photoCORMs. In support of this strategy, a recent study has demonstrated the feasibility of light-triggered release of a CO-releasing material in an *in vivo* mouse models.²²

The use of light for the remote control over the activity of pharmaceuticals, a concept known as photopharmacology, has a nearly 100 year old history in medicine and oncology.²³ The successful clinical use of visible light to control drug activity in time and space to regulate biological processes is well documented.^{24–26} While photopharmacological treatment is naturally suitable for localized and exposed targets, optic fibers inserted



through small and minimally invasive incisions allow for illumination of most body organs to be illuminated with intense, visible, broad spectrum light from non-laser sources.²⁷

Photopharmacological approaches have even been successfully applied for metastatic ovarian cancer, where intraoperative and laparoscopic light sources were successfully used in photodynamic therapy, resulting in substantial benefits for patients in clinical trials.²⁸ Visible light offers unparalleled therapeutic benefits as an external control element for pharmacological activity, which allows for the delivery and activity of photo-activatable pharmaceuticals with very high spatiotemporal precision. Furthermore, unlike chemicals, light exhibits high orthogonality towards biological systems with minimal contamination of the study subject and low to negligible toxicity.²³ Visible light activation of photoCORMs and Ab-photoCORM conjugates for the therapeutic delivery of CO may soon mature beyond an academic strategy at this point in time considering the well-documented success of the clinical use of visible light in photopharmacology and photodynamic therapy.^{23,24}

The high selectivity and diversity of monoclonal antibodies towards surface expressing antigens suggest that Ab-photoCORM conjugates could be designed to deliver CO to a wide range of cell/tissues with high specificity. Antibodies inherently exhibit a wide range of binding specificities due to amino acid residues contained within six short lengths, three each in the heavy and light chains of the antibody.²⁹ As antibodies have the potential to recognize $>10^{12}$ unique antigens,³⁰ this can be exploited to improve the specificity of delivery of therapeutic molecules. The Ab-photoCORMs synthesized in this study have successfully exploited the antigen-recognition of antibodies to improve specificity of delivery of CO, a therapeutic, gaseous molecule. The Ab-photoCORMs reported here thus represent a novel class of ADCs that could be described as "immunoCORMs".

The biotin-streptavidin linker utilized in these studies allow for the facile conjugation of the photoCORMs to any monoclonal antibody. Furthermore, the biotinylation of the photoCORM in this study was synthetically straightforward and performed under mild conditions. Biotinylation of not only other designed CORMs, but also hydrogen sulfide/nitric oxide donating molecules and nanoparticles is feasible. By this approach, the biotin-streptavidin linkage to monoclonal antibodies could be a new direction in the field of gasotransmitters, namely, the delivery of gaseous molecules driven by antibody-conjugation and antigen recognition.

Conventional ADCs require a number of specific properties in order to exhibit sufficient potency and stability. As one of the main mechanisms of drug resistance is ADC efflux,³¹ lack of susceptibility to multidrug resistant protein 1 (MDR1) is essential. CO, as a drug delivered by an ADC, could be intriguing in that it would be unaffected by efflux mechanisms of drug resistance like MDR1. Furthermore, traditional ADCs are limited by the frequency of internalization and trafficking through the endosomal-lysosomal pathway, a relatively infrequent event.³¹ The ability of CO to readily diffuse across cellular membranes could circumvent the need for antibody

internalization *per se*. A photoCORM (a prodrug) conjugated to an antibody also requires that drug release is not dependent on linker cleavage or through complete degradation of the antibody within the tumor cell. The cleavable linkers impart small molecule drug ADCs with poor pharmacokinetics and circulation instability.²¹ The biotin-streptavidin linker used in this design is expected to maximize stability and mitigate the problems related to esterases and proteases within cellular milieu. The antibody-photoCORM conjugates (Ab-photoCORM) could be an intriguing tool for addressing some of the fundamental limitations of ADCs.

Conflicts of interest

The authors declare no conflict of interest.

Acknowledgements

Financial support from the NSF grant DMR-1409335 and the Cancer Research Coordinating Committee (UC) grant CTR-19-580346 is gratefully acknowledged. Research in UCLA was supported by the NIH U01 grant HD087221.

Notes and references

- 1 R. Motterlini and R. Foresti, Biological signaling by carbon monoxide and carbon monoxide-releasing molecules, *Am. J. Physiol.*, 2017, **312**(3), C302–C313.
- 2 R. Motterlini and L. E. Otterbein, The therapeutic potential of carbon monoxide, *Nat. Rev. Drug Discovery*, 2010, **9**(9), 728–743.
- 3 I. Chakraborty, S. J. Carrington, G. Roseman and P. K. Mascharak, Synthesis, Structures, and CO Release Capacity of a Family of Water-Soluble PhotoCORMs: Assessment of the Biocompatibility and Their Phototoxicity toward Human Breast Cancer Cells, *Inorg. Chem.*, 2017, **56**(3), 1534–1545.
- 4 I. Chakraborty, S. J. Carrington, J. Hauser, S. R. J. Oliver and P. K. Mascharak, Rapid Eradication of Human Breast Cancer Cells through Trackable Light-Triggered CO Delivery by Mesoporous Silica Nanoparticles Packed with a Designed photoCORM, *Chem. Mater.*, 2015, **27**(24), 8387–8397.
- 5 I. Chakraborty, J. Jimenez and P. K. Mascharak, CO-Induced apoptotic death of colorectal cancer cells by a luminescent photoCORM grafted on biocompatible carboxymethyl chitosan, *Chem. Commun.*, 2017, **53**(40), 5519–5522.
- 6 U. Schatzschneider, Novel lead structures and activation mechanisms for CO-releasing molecules (CORMs), *Br. J. Pharmacol.*, 2015, **172**(6), 1638–1650.
- 7 S. Garcia-Gallego and G. J. L. Bernardes, Carbon-Monoxide-Releasing Molecules for the Delivery of Therapeutic CO In Vivo, *Angew. Chem.*, 2014, **53**(37), 9712–9721.
- 8 S. H. Heinemann, T. Hoshi, M. Westerhausen and A. Schiller, Carbon monoxide – physiology, detection and controlled release, *Chem. Commun.*, 2014, **50**(28), 3644–3660.
- 9 R. D. Rimmer, A. E. Pierri and P. C. Ford, Photochemically activated carbon monoxide release for biological targets.



- Toward developing air-stable photoCORMs labilized by visible light, *Coord. Chem. Rev.*, 2012, **256**(15–16), 1509–1519.
- 10 B. Kawahara, T. Moller, K. Hu-Moore, S. Carrington, K. F. Faulk, S. Sen and P. K. Mascharak, Attenuation of Antioxidant Capacity in Human Breast Cancer Cells by Carbon Monoxide through Inhibition of Cystathionine β -Synthase Activity: Implications in Chemotherapeutic Drug Sensitivity, *J. Med. Chem.*, 2017, **60**(19), 8000–8010.
- 11 B. Kawahara, S. Ramadoss, G. Chaudhuri, C. Janzen, S. Sen and P. K. Mascharak, Carbon monoxide sensitizes cisplatin-resistant ovarian cancer cell lines toward cisplatin via attenuation of levels of glutathione and nuclear metallothionein, *J. Inorg. Biochem.*, 2019, **191**, 29–39.
- 12 A. Beck, L. Goetsch, C. Dumontet and N. Corvaia, Strategies and challenges for the next generation of antibody drug conjugates, *Nat. Rev. Drug Discovery*, 2017, **16**(5), 315–337.
- 13 M. N. Pinto, I. Chakraborty, C. Sandoval and P. K. Mascharak, Eradication of HT-29 colorectal adenocarcinoma cells by controlled photorelease of CO from a CO-releasing polymer (photoCORP-1) triggered by visible light through an optical fiber-based device, *J. Controlled Release*, 2017, **264**, 192–202.
- 14 S. J. Carrington, I. Chakraborty, J. M. L. Bernard and P. K. Mascharak, A Theranostic Two-Tone Luminescent PhotoCORM Derived from Re(I) and (2-Pyridyl)-benzothiazole: Trackable CO Delivery to Malignant Cells, *Inorg. Chem.*, 2016, **55**(16), 7852–7858.
- 15 S. J. Carrington, I. Chakraborty and P. K. Mascharak, Rapid CO release from a Mn(I) carbonyl complex derived from azopyridine upon exposure to visible light and its phototoxicity toward malignant cells, *Chem. Commun.*, 2013, **49**(96), 11254–11256.
- 16 G. T. Hermanson, (Strept)avidin-Biotin Systems, *Bioconjug. Techniques*, 3rd edn, 2013, pp. 465–505.
- 17 J. D. Sacks and M. V. Barbolina, Expression and Function of CD44 in Epithelial Ovarian Carcinoma, *Biomolecules*, 2015, **5**(4), 3051–3066.
- 18 M. Z. Akhter, S. K. Sharawat, V. Kumar, V. Kochat, Z. Equbal, M. Ramakrishnan, U. Kumar, S. Mathur, L. Kumar and A. Mukhopadhyay, Aggressive serous epithelial ovarian cancer is potentially propagated by EpCAM(+)/CD45(+) phenotype, *Oncogene*, 2018, **37**(16), 2089–2103.
- 19 M. Tsukioka, Y. Matsumoto, M. Noriyuki, C. Yoshida, H. Nobeyama, H. Yoshida, T. Yasui, T. Sumi, K. I. Honda and O. Ishiko, Expression of glucose transporters in epithelial ovarian carcinoma: correlation with clinical characteristics and tumor angiogenesis, *Oncol. Rep.*, 2007, **18**(2), 361–367.
- 20 S. Mukherjee, M. Pal, S. Mukhopadhyay, I. Das, R. Hazra, S. Ghosh, R. K. Mondal and R. Bal, VEGF Expression to Support Targeted Therapy in Ovarian Surface Epithelial Neoplasms, *J. Clin. Diagn. Res.*, 2017, **11**(4), EC43–EC46.
- 21 E. Khera and G. M. Thurber, Pharmacokinetic and Immunological Considerations for Expanding the Therapeutic Window of Next-Generation Antibody-Drug Conjugates, *BioDrugs*, 2018, **32**(5), 465–480.
- 22 C. C. Wang, Y. Q. Li, X. Q. Shi, J. H. Zhou, L. Zhou and S. H. Wei, Use of an NIR-light-responsive CO nanodonor to improve the EPR effect in photothermal cancer treatment, *Chem. Commun.*, 2018, **54**(95), 13403–13406.
- 23 W. A. Velema, W. Szymanski and B. L. Feringa, *J. Am. Chem. Soc.*, 2014, **136**, 2178–2191.
- 24 K. Hull, J. Morstein and D. Trauner, *Chem. Rev.*, 2018, **118**, 10710–10747.
- 25 Z. B. Mehta, N. R. Johnston, M. S. Nguyen-Tu, J. Broichhagen, P. Schultz, D. P. Lerner, I. Leclerc, D. Trauner, G. A. Rutter and D. J. Hodson, *Sci. Rep.*, 2017, **7**, 291.
- 26 J. Broichhagen, M. Schonberger, S. C. Cork, J. A. Frank, P. Marchetti, M. Bugliani, A. M. J. Shapiro, S. Trapp, G. A. Rutter, D. J. Hodson and D. Trauner, *Nat. Commun.*, 2014, **5**, 5116.
- 27 R. R. Allison, R. Cuenca, G. H. Downie, M. E. Randall, V. S. Bagnato and C. H. Sibata, *Photodiagn. Photodyn. Ther.*, 2005, **2**, 51–63.
- 28 F. Wierrani, D. Fiedler, W. Grin, M. Henry, E. Dienes, K. Gharehbaghi, B. Krammer and W. Grunberger, *BJOG*, 1997, **104**, 376–378.
- 29 D. R. Rose, The generation of antibody diversity, *Am. J. Hematol.*, 1982, **13**(1), 91–99.
- 30 B. Alberts; A. Johnson; J. Lewis, R. Martin; K. Roberts; and P. Walte, The Generation of Antibody Diversity, *Molecular Biology of the Cell*, 4th edn, New York, Garland Science, 2002.
- 31 P. L. Salomon and R. Singh, Sensitive ELISA Method for the Measurement of Catabolites of Antibody-Drug Conjugates (ADCs) in Target Cancer Cells, *Mol. Pharm.*, 2015, **12**(6), 1752–1761.

Supporting Information

For

Diminished Viability of Human Ovarian Cancer Cells by Antigen-specific Delivery of Carbon Monoxide with a Family of Photoactivatable Antibody-photoCORM Conjugates

Brian Kawahara,[†] Lucy Gao,[§] Whitaker Cohn,[§] Julian P. Whitelegge,[§] Suvajit Sen,[‡] Carla Janzen,[‡] Pradip K. Mascharak^{†*}

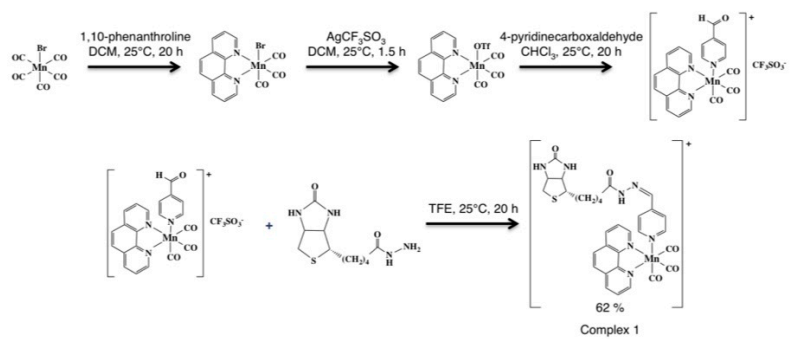
Contribution from

[†]Department of Chemistry and Biochemistry, University of California, Santa Cruz, CA 95064, USA

[§]Pasarow Mass Spectrometry Laboratory, Jane and Terry Semel Institute for Neuroscience and Human Behavior, University of California at Los Angeles, Los Angeles, CA 90095, USA

and

[‡]Department of Obstetrics and Gynecology, David Geffen School of Medicine, University of California at Los Angeles, Los Angeles, CA 90095, USA



Scheme S1. Synthetic scheme for Complex 1: biotinylated, photoactivatable CO-releasing molecule (photoCORM).

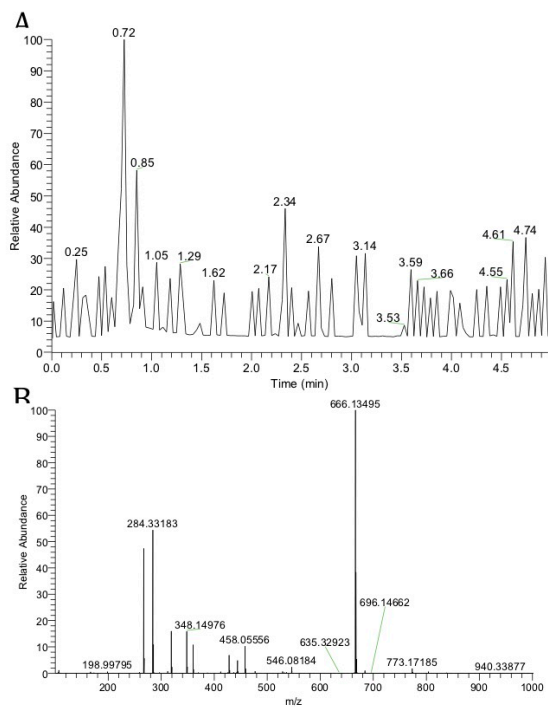


Figure S1. By electrospray ionization mass spectrometry (ESI-MS), (A) Total ion count (TIC) chromatogram of 0-5 min for a 5 min run of Complex **1** via flow injection analysis and (B) full mass spectrum (100-1000 m/z) for retention time=0.70-0.72. Found: 666.13495, calculated for $C_{31}H_{29}N_7O_5Smn$ 666.13314, Δ ppm = 3.4 ppm, Δ mDa = 2.2.

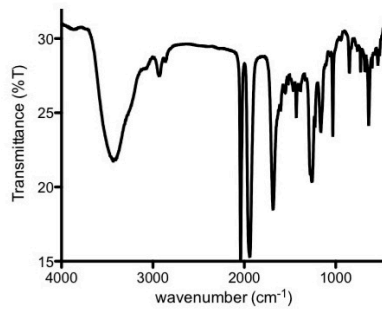


Figure S2. Infrared (IR) spectrum of Complex 1. IR spectrum of solid Complex 1 was recorded in KBr matrix. $\nu_{\text{C=O}}$: (cm⁻¹): 2030, 1941, 1687.

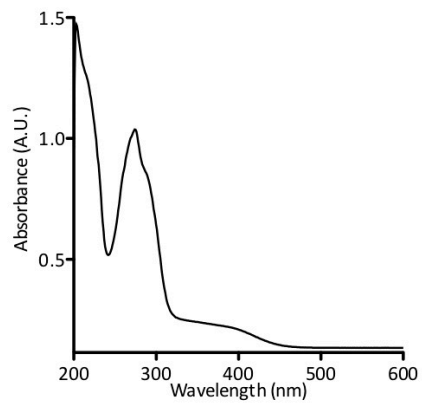


Figure S3. Electronic absorption spectrum of Complex 1 in 1x PBS, 25°C.

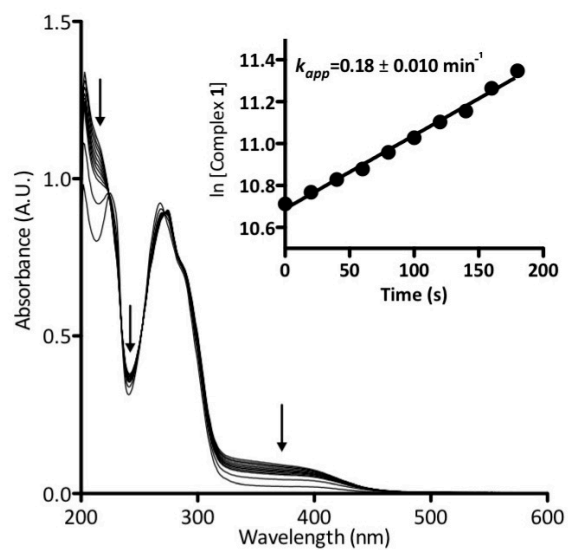


Figure S4. Electronic spectrum of Complex 1 upon illumination with low power (10 mW/cm^2), broadband visible light in 20-second intervals. Inset: Integration of the release rate for the photodegradation of Complex 1, calculated at 390 nm, with low power (10 mW/cm^2), broadband visible light for indicated time.

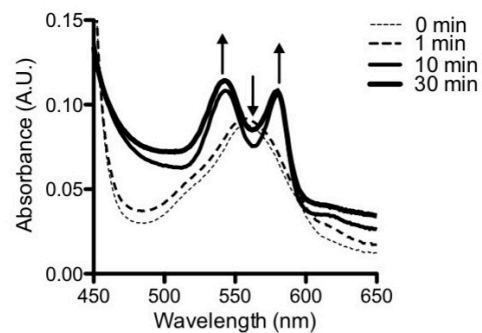


Figure S5. Myoglobin assay for CO release from Complex 1 dissolved and performed in 1X phosphate buffered saline (PBS), triggered by low power (10 mW/cm²), visible light for indicated time.

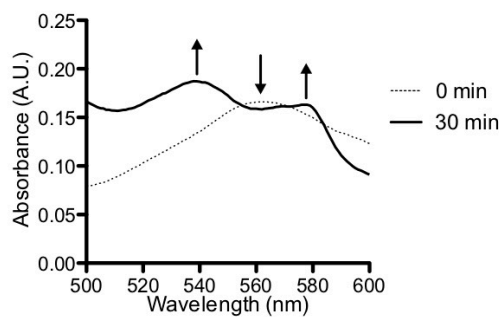


Figure S6. Myoglobin assay for CO release from Complex 1 dissolved in human serum and incubated for ≥ 1 h at 37°C, followed by exposure to low power (10 mW/cm²), broadband visible light for 30 min.

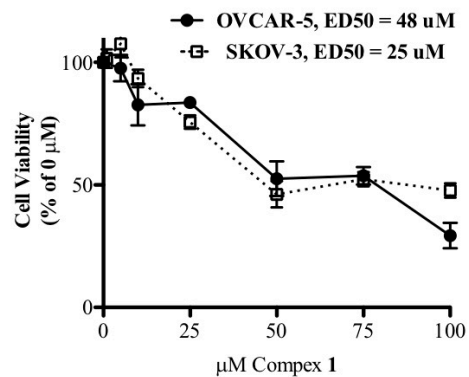


Figure S7. Effect of treatment of ovarian cancer cell lines with indicated concentrations of Complex 1 upon illumination with visible light on cell viability, measured 24 h post-treatment in ovarian cancer cell lines OVCAR-5 and SKOV-3. Data representative of n=3 independent experiments.

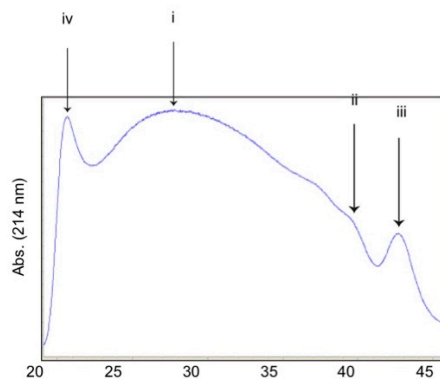


Figure S8. Chromatogram of Complex 2 following size exclusion chromatography. [retention time, ~molecular weight, identity] (i) [28.4 min, 366 kDa, IgG + 4 streptavidin]. (ii) [39.6 min, ~155 kDa, IgG + 0 streptavidin]. (iii) [42.7 min, ~121 kDa, IgG Fragments]. (iv) [20.6 min, ~659 kDa, void volume].

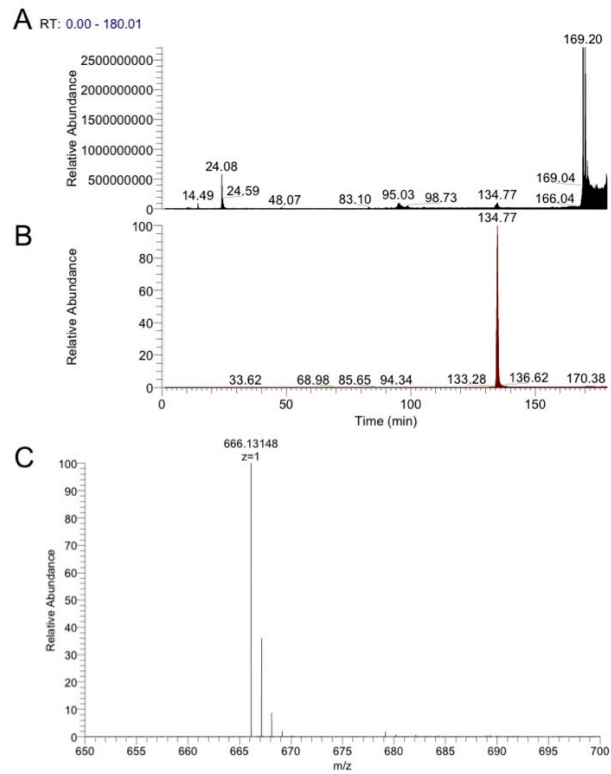


Figure S9. Detection of Complex 1 in tryptic digest of antibody-photoCORM conjugate (Ab-photoCORM). (A) Total ion count (TIC) of Ab-photoCORM sample. (B) Chromatogram of Ab-photoCORM, mass filter range $m/z = 666.12593-666.13925$. (C) Full mass spectrum at retention time 134.16-135.34 min.

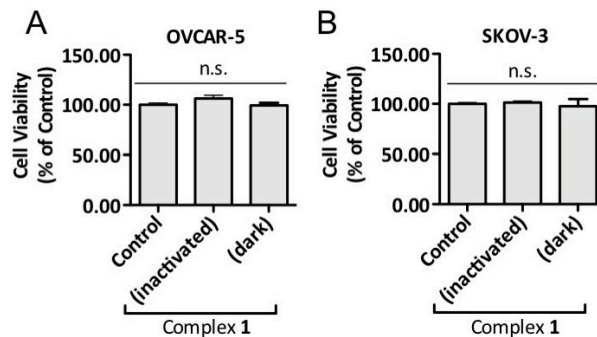


Figure S12. Cell viability of ovarian cancer cell lines OVCAR-5 and SKOV-3 treated with light-inactivated Complex 1 and Complex 1 in the dark to assess the cytotoxicity of non-CO components of Complex 1. Data representative of n=3 independent experiments. (* p<0.05)

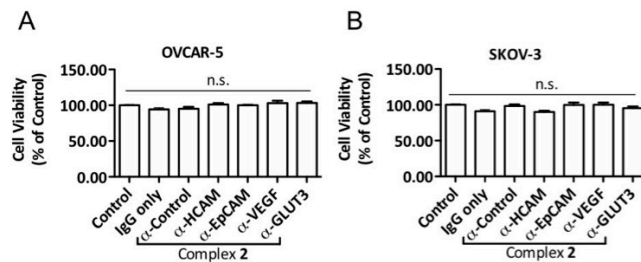


Figure S13. Cell viability, as measured by reduction of MTT 24 h post-treatment, of (A) OVCAR-5 and (B) SKOV-3 treated with 2 µg/mL Complex 2 and control antibodies. Family of Complex 2 constructed from mouse monoclonal antibodies raised against human HCAM (α-HCAM), EpCAM (α-EpCAM), GLUT3 (α-GLUT3) and VEGF-1 (α-VEGF). Control treatments with vehicle control (Control), IgG without streptavidin (IgG) and Complex 2 synthesized from control mouse IgG (α-Control) included. Data representative of n=3 independent experiments. (*p<0.05)

$$\left(\frac{2-10 \mu\text{g}}{\text{Ab-photoCORM}}\right) \left(\frac{0.2 \text{ mL cell}}{\text{culture media}}\right) \left(\frac{1-4 \text{ mol streptavidin}}{1 \text{ mol Ab-photoCORM}}\right) \left(\frac{4 \text{ mol Complex 1}}{1 \text{ streptavidin}}\right) \left(\frac{3 \text{ mol CO}}{1 \text{ mol Complex 1}}\right) = \frac{\sim 23-262 \text{ pmol}}{\text{CO}}$$

Scheme S2. Calculations for estimation of molar release of CO from antibody-photoCORM conjugates.

Experimental Section

Materials

Biotin-hydrazide (A8007-100mg) was procured from Apex Biotech, Ltd. (Xuzhuang, Shaanxi, PRC). Mouse monoclonal antibodies raised against HCAM (sc-7297), EpCAM (sc-53277), GLUT3 (sc-74399), VEGF-1 (365578) and normal mouse IgG (sc-2025) were obtained from Santa Cruz Biotechnology (Santa Cruz, CA, USA). All other chemicals were purchased from Sigma-Aldrich (St. Louis, MO, USA) unless otherwise stated.

Synthesis of biotin-photoCORM (Complex 1)

[Mn(CO)₅(Br)] (100 mg, 0.36 mmol) and 1,10-phenanthroline (phen) (66 mg, 0.36 mmol) was dissolved in 25 mL dichloromethane (DCM) and allowed to stir in the dark for 20 h at 25°C. The solution, initially dark yellow, was dried down under vacuum to a yellow powder. Next, 1.5-fold excess AgCF₃SO₃ (140 mg, 0.54 mmol) was dissolved in 20 mL DCM and added to the yellow product, and allowed to stir for 1.5 h at 25°C in the dark. The cloudy green solution was subsequently filtered through a wet Celite pad, and the filtrate was evaporated to dryness. The resulting yellow powder was dissolved in 50 mL chloroform. To that stirring solution, 4-pyridinecarboxaldehyde (pyAl) (385 mg, 3.6 mmol) was added drop wise and allowed to stir for 20 h at 25°C in the dark. The next day, the solution was dried down under vacuum, revealing orange/yellow microcrystals of [Mn(CO)₃(phen)(PyrAl)]CF₃SO₃ (155 mg, 0.27 mmol, 75%). To 223 mg (0.39 mmol) of [Mn(CO)₃(phen)(PyrAl)]CF₃SO₃, biotin-hydrazide (100 mg, 0.39 mmol) dissolved in 20 mL of freshly distilled 2,2,2-trifluoroethanol was added, in a similar manner to a previous study.^[1] The dark yellow solution was allowed to stir for 20h at 25°C in the dark. The yellow brown solution was concentrated under vacuum to ~2 mL, then chromatographed on a basic alumina column (50-200 μm particle diameter). The column was then washed with DCM (to remove unreacted [Mn(CO)₃(phen)(PyrAl)]CF₃SO₃ and biotin-hydrazide and finally Complex 1 was eluted with DCM/methanol (3/2 v/v).

¹H NMR (400 MHz, [D₄]-methanol): δ=1.37-1.84 (m, 6H), 2.30 (t, 2H, 7.4 Hz), 2.68 (m, 1H), 2.89 (m, 1H), 3.18 (m, 1H), 4.24 (m, 1H), 4.47 (m, 1H), 7.53 (m, 2H), 7.86 (s, 1H), 8.20 (m, 4H), 8.38 (m, 2H), 8.87 (m, 2H), 9.88 (m, 2H); IR (KBr): ν = 2039, 1939, 1685 cm⁻¹(C=O); HRMS (ESI): *m/z* calcd for C₃₁H₂₉N₇O₅SMn: 666.13315 [*M*+]; found: 666.13539, Δ ppm = 3.4 ppm, Δ mDa = 2.2; elemental analysis calcd (%) for C₃₁H₂₉N₇O₅SMn: C 55.86, H 4.35, N 14.71,

O 12.01, S 4.80, Mn 8.26; found: C 55.84, H 4.39, N 14.71, O 12.01, S 4.80, Mn 8.25.

Physical Measurements

¹H NMR spectra of Complex **1** were collected at 298 K on a Varian Unity Inova 500 MHz instrument. FT-IR of Complex **1** was collected on a PerkinElmer Spectrum-One FT-IR. UV-vis data of Complex **1** were recorded on a Varian Cary 50 UV-vis spectrophotometer.

Myoglobin Assay

Horse heart myoglobin was dissolved in 1X PBS, pH=7.4 to a final concentration of 50 μM and reduced with 0.1 % sodium dithionite in quartz cuvette under aerobic conditions. In a second cuvette, Complex **1** was dissolved in 1X PBS to a final concentration of 50 μM. Antibody-photoCORM conjugates (Ab-photoCORM) were dissolved in 1X PBS to a final concentration of 10 μg/mL. For myoglobin assays performed in human serum, either Complex **1** or Ab-photoCORMs was dissolved to final concentrations of 50 μM or 10 μg/mL respectively in human serum, followed by ≥1h incubation at 37°C. Photogenerated CO, triggered by low power, broadband visible light (10mW/cm²) from Complex **1** or Ab-photoCORM was released into the headspace and transferred to the reduced Mb solution via a cannula and positive pressure with N₂(g). The extent of the conversion of Mb to carboxymyoglobin (MbCO) was monitored by the change in absorbance at 540 nm, a reliable determination of CO-release from organometallic carbonyl complexes.^[2] The source of low power, broadband visible light was an IL 410 Illumination System purchased from Electro Optical Components, Inc. (Santa Rosa, CA, USA). Visible light power was measured with a Field MaxII-TO laser power meter purchased from Coherent (Palo Alto, CA, USA).

Photolysis Experiments

The rate of CO release (k_{CO}) for Complex **1** at 25 °C in 1x PBS was assessed with in 1 cm x 1 cm quartz cuvettes. The k_{CO} of Complex **1** (concentration = 3.0×10^{-5} M, 390 nm, 25°C) was determined by recording the electronic absorption spectra, monitoring changes in the spectra following exposure to light at regular intervals. k_{CO} was then calculated from the ln[Complex **1**] versus time (t) plot.

Synthetic strategy of streptavidin-conjugated mouse IgG (Complex 2)

Conjugation of 1 mg mouse IgG, either control or antigen-specific IgG, with streptavidin was performed utilizing the Streptavidin Conjugation Kit (ab102921, Cambridge, MA, USA). Native gel electrophoresis and size exclusion chromatography were used to analyze and characterize streptavidin-conjugated antibodies. Complex **2** was quantified for use in subsequent cellular studies by measuring total protein using a Pierce™ BCA Protein Assay Kit (23225, ThermoFisher Scientific, Waltham, MA).

Native Gel Electrophoresis

2 µg of streptavidin-IgG conjugate was combined with native loading dye (62.5 mM Tris-HCl, pH=7.4, 40% glycerol and 0.01% bromophenol blue) and loaded onto a 4-12% Mini-PROTEAN TGX Precast Protein Gels (#4561095, Bio-Rad, Hercules, CA, USA) and separated under non-reducing, native conditions. Protein bands were visualized using Coomassie Brilliant Blue R-250 (#161-0436).

Size Exclusion Chromatography

Separation and simultaneous UV absorbance detection at 214 nm of streptavidin-conjugated antibodies and antibody-photoCORM conjugates was performed using a 7.5 D x 60 cm, 3 µm Tosoh TSK G4000SW (stainless steel) column. The column was preconditioned with molecular weight standards. The mobile phase was prepared with 137 mM NaCl, 2.7 mM KCl, 4.3 mM Na₂HPO₄, 1.47 mM KH₂PO₄, pH = 6.8 and sterile filtered and degassed prior to use. Separation species based on size was performed at a flow rate of 0.5 mL/min, 25 °C. Fractions of streptavidin-conjugated antibodies and antibody-photoCORM conjugates were further characterized by bottom up proteomics.

Synthesis of antibody-photoCORM Conjugates (Ab-photoCORM)

Complex 2 (100 µg, ~273 pmol) pre-dissolved in 500 µL 1X PBS was reacted with excess Complex 1 (40.0 ng, 60 nmol) pre-dissolved in 500 µL 1X PBS for 1h at 25°C in the dark. The antibody-photoCORM conjugates (Ab-photoCORMs) were purified using size exclusion chromatography. Bottom up proteomics and HPLC-MS/MS analysis was utilized to characterize the composition of Ab-photoCORMs. Detection of Complex 1 in Ab-photoCORMs was observed in full MS scans in the bottom up proteomic assays.

Bottom Up Proteomics Analysis

10 µg of each antibody-photoCORM conjugate, as determined by BCA Protein Assay, were solubilized in 200 µL lysis buffer (12 mM sodium lauroyl sarcosine, 0.5% sodium deoxycholate, 50 mM triethylammonium bicarbonate (TEAB)) followed by 10 min bath sonication and heating at 95°C for 5 min. The samples were then diluted to 0.5 mg total protein/mL with lysis buffer, then a 100 µL aliquot was treated with 5 mM tris(2-carboxyethyl) phosphine (TCEP) prepared in 50 mM aqueous TEAB at 60°C for 30 min. Next, the samples were treated with 10mM chloroacetamide, prepared in 50 mM TEAB, for 30 min at 25°C in the dark. Samples were diluted 5-fold in 50 mM TEAB, then incubated overnight with Sequencing Grade Modified Trypsin (1:100, □g trypsin: □g total protein). The next day, an equal volume of ethyl acetate/trifluoroacetic acid (TFA, 100/1, v/v) was added to samples, followed by 5 min vigorous vortexing and centrifugation (13,000 x g, 5 min). Desalting of samples was performed similar to that previously described.^[3] Dried samples were reconstituted in acetonitrile/water/TFA (2/98/0.1, v/v/v), loaded onto a C18-silica disk (3M, Maplewood, MN, USA) placed inside a 200 µL pipet tip. Prior to sample loading onto the disk, it was equilibrated with methanol (20 µL), acetonitrile/water/TFA (20 µL, 80/20/0.1, v/v/v), then finally acetonitrile/water/TFA (2/98/0.1, v/v/v). The

samples loaded onto the disks were washed with acetonitrile/water/TFA (20 μ L, 2/98/0.1, v/v/v) and eluted with acetonitrile/water/TFA (40 μ L, 80/20/0.1, v/v/v). Eluents were concentrated under vacuum centrifugation and reconstituted in 10 μ L water/acetonitrile/formic acid, 98/2/0.1, v/v/v). 5 μ L aliquots were injected onto a reverse phase nanobore HPLC column (AcuTech Scientific, C18, 1.8 μ m particle size, 360 μ m x 20 cm, 150 μ m ID), equilibrated in water/acetonitrile/formic acid (98/2/0.1, v/v/v: min/%; 0/0, 5/3, 18/7, 74/12, 144/24, 153/27, 162/40, 164/80, 174/80, 176/0, 180/0) using an Eksigent NanoLC-2D system (Sciex, Framingham, MA, USA). The flow from the column was directed towards nanospray ionization source connected to a Q Exactive™ Hybrid Quadrupole-Orbitrap™ Mass Spectrometer (Thermo Fisher Scientific). Data-dependent mass spectra were acquired alternating between full scan (m/z 350-2000, automated gain control target 3×10^3 , 50 ms maximum injection time, FWHM resolution 70,000 at m/z 200) and up to 10 MS/MS scans (quadrupole isolation of charge states ≥ 1 , isolation width 1.2 Th) with optimized fragmentation conditions (normalized collision energy of 32, dynamic exclusion of 30 s, AGC target 1×10^6 , 100 ms maximum injection time, FWHM resolution 35,000 at m/z 200). Analysis of raw data and peptide/protein identification of the antibody-photoCORM conjugates was performed using Mascot to search the UniProt-Mouse database. Common Contaminants database was also searched to identify streptavidin. Probability based scoring was used to determine significance of data, where reported scores = $-10 \times \log_{10}(P)$, where P is the absolute probability that the observed match between the experimental data and the database sequence is a random event.^[4,5] Scores >67 are considered significant ($p < 0.05$).^[4,5] Complex 1 associated with Ab-photoCORM was observed in the full MS scan data (Figure S6).

Cell culture

Ovarian cancer cell lines OVCAR-5 and SKOV-3 were obtained from American Type Culture Collection (Manassas, VA, USA). OVCAR-5 and SKOV-3 were grown in RPMI 1640 Medium (11875119, ThermoFisher Scientific) supplemented with 10% fetal bovine serum (FBS, 16000) and 100 U/mL penicillin-streptomycin (15070063) were all purchased from ThermoFisher Scientific. Cells were passaged ≤ 10 times after acquisition from the manufacturer.

Cell Viability (MTT) Assay

Cell viability was assessed by the cellular reduction of tetrazolium dye MTT performed in 96-well tissue culture plates. 2×10^3 cells/well were allowed to seed overnight in a 37 °C incubator + 5% CO₂. The following day, cells were treated as indicated with Complex 1 or Complex 2, then assessed for viability 24 h post-treatment. Following removal of cell culture media, 0.5 mg/mL MTT dissolved in fresh 1x DMEM was added and allowed to incubate for 2 h in a 37 °C incubator + 5% CO₂. Cell viability was quantified by measuring the relative amount of MTT reduced to insoluble formazan. Following solubilization of formazan in 10% SDS

+ 0.01 N HCl, formazan was measured by taking the absorbance at 570 nm, reference wavelength taken at 690 nm.

Western Analysis

Whole cell lysates were extracted using RIPA lysis buffer (150 mM NaCl, 5 mM EDTA pH 8.0, 50 mM Tris pH 8.0, 1% Triton X-100, 0.5% sodium deoxycholate, 1% SDS and 1× protease inhibitor cocktail. BCA Protein Assay assayed soluble fractions for total protein content. 20 µg of soluble cell lysates from samples were resolved on 10% SDS-PAGE gel and transferred to poly(vinylidene difluoride) (PVDF) membrane. All following blocking and antibody solutions were prepared in 1× PBS + 0.1% Tween 20. Membranes, following blocking in 5% nonfat dried milk for 18 h at 4°C, were probed with primary (1:1000 dilution) antibody overnight at 4°C and then horseradish peroxidase (HRP)-conjugated secondary (1:10,000 dilution) antibody for 1 h at 25°C. Immunofluorescent signals were amplified with Pierce ECL Plus Western blotting substrate (32132, ThermoFisher Scientific).

Live-cell Immunosorbent Assay

2×10^3 cells/well of 96-well tissue culture plates were allowed to seed overnight at 37°C + 5% CO₂. The next day, cells were treated as indicated with 0-10 µg/mL antibody-photoCORM conjugates (Ab-photoCORM), as measured by BCA Protein Assay. Immunosorbence of Ab-photoCORMs to the adherent live cells was allowed to occur for 60 min in the dark at 37°C + 5% CO₂. α-Control Ab-photoCORM, utilizing control mouse IgG (sc-2025, Santa Cruz Biotechnology), was utilized as control to assess the specificity of the other antibody-photoCORM conjugates. Following incubation, the media was gently aspirated, followed by three 250 µL washes with 1X PBS in the dark to remove any non-specific binding. 100 µL fresh cell culture media was added, followed by illumination with low power, visible light for 30 min to trigger release of CO from any Ab-photoCORM present after immunosorbence and washing. Cell viability, as measured by the reduction of MTT, was assayed 24 h post-illumination of light.

Statistical Analysis

Data are expressed as the mean ± standard error mean (range) or as percentage of control value where indicated. Comparisons between two groups were made using the Student's t-test. Comparisons between more than two groups were made using the One-way ANOVA/ Tukey's post hoc test. p-values < 0.05 were considered statistically significant. All calculations were performed using GraphPad Prism software package (GraphPad Software Inc., San Diego, USA).

Supporting References

[1] M. Salmain, N. Fischer-Durand, L. Cavalier, B. Rudolf, J. Zakrzewski, G. Jaouen, *Bioconjug. Chem.* **2002**, *13*, 693-698.

- [2] A. J. Atkin, J. M. Lynam, B. E. Moulton, P. Sawle, R. Motterlini, N. M. Boyle, M. T. Pryce, I. J. S. Fairlamb, *Dalton Trans.* **2011**, 40, 5755-5761.
- [3] J. Rappsilber, M. Mann, Y. Ishihama, *Nat. Protoc.* **2007**, 2, 1896-1906.
- [4] T. Koenig, B. H. Menze, M. Kirchner, F. Monigatti, K. C. Parker, T. Patterson, J. J. Steen, F. A. Hamprecht, H. Steen, *J. Proteome Res.* **2008**, 7, 3708-3717.
- [5] D. J. C. Pappin, P. Hojrup, A. J. Bleasby, *Curr. Biol.* **1993**, 3, 327-332.

Chapter 5

Carbon monoxide inhibits cytochrome P450 enzymes CYP3A4/2C8 in human breast cancer cells, increasing sensitivity to paclitaxel

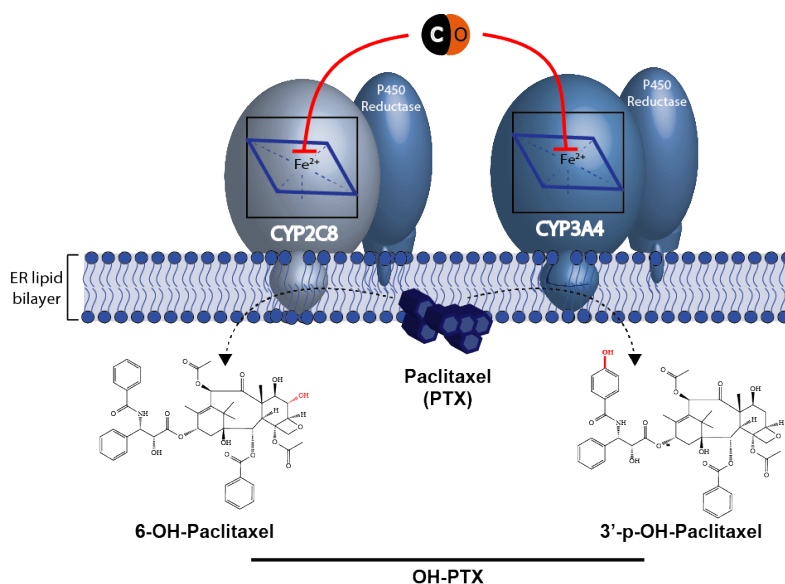


Table 5.1. Table of Content

5.1 Background

Cytochrome P450 enzymes (CYPs) are a large class of heme-containing monooxygenases that catalyze NADPH-dependent substrate oxidation via the homolytic cleavage of molecular oxygen. Functionally, CYPs are classified into two groups: those that catalyze endogenous substrate oxidation, such as hormones, and those that catalyze exogenous substrate oxidation such as drugs and other xenobiotics. Drug-metabolizing CYP expression is largely localized in the liver and gastrointestinal tract, though aberrant expression of specific isoforms of CYP have been identified in many solid tumors, including breast tissue.¹ Multiple studies have

reported the overexpression of drug-metabolizing CYPs in breast cancer, where they are believed to play roles in imparting drug resistance.^{2,3} Of these CYPs, CYP3A4 is one of the more promising therapeutic targets. CYP3A4 has broad substrate recognition, metabolizing 60% of the drugs currently on the market and a number of anti-cancer drugs utilized in the treatment of breast cancer, including paclitaxel (PTX).^{4,5}

PTX is a taxane-based therapy and one of the most important anti-cancer drugs available today. It is the most widely used anti-cancer drug and frequently used as the first-line treatment of breast cancer. However, like other anti-cancer drugs, PTX resistance arises often and quickly in human breast cancer cells.⁶ There is substantial evidence that CYP isoforms 3A4 and 2C8 (CYP3A4 and CYP2C8) are overexpressed in malignant breast tissue and that their activity may limit the intracellular concentrations of taxanes, like PTX, and impart drug resistance.^{7,8} Furthermore, CYP3A4 expression in malignant breast tissue is predictive of resistance to taxane therapy.⁹ CYP3A4 and CYP2C8 metabolize paclitaxel (PTX) into inactive metabolites 3'-para-hydroxy-paclitaxel (3'-p-OH-PTX) and 6 α -hydroxy-paclitaxel (6-OH-PTX) respectively.¹⁰ CYP3A4/2C8 metabolism of PTX is likely one mechanism of drug resistance in the breast cancer cells as the PTX metabolites are an order of magnitude less active.¹¹ Inhibition of CYP-mediated PTX inactivation in breast cancer cells in situ could improve the efficacy of PTX and decrease the incidence of PTX resistance, revitalizing its use in the clinical setting.

Inhibition of CYPs is well characterized and understood as it is the basis of drug-drug interactions in pharmacology. Perhaps the simplest inhibitor of CYP activity is carbon monoxide (CO). CO binds the ferrous state of the heme center in CYP, preventing the binding of molecular oxygen (O₂), which upon spectroscopic analysis, affords an absorption maxima at ~450 nm, thus its name.¹² The inhibition of metabolic processes by CO is indicative of CYP involvement.^{13,14} Until recently, however, the use of CO, a diffusible gas, as a therapeutic agent to inhibit CYP activity in a target tissue was not feasible. The development of CO-releasing molecules (CORMs) and specifically photoactivatable CO-releasing molecules (photoCORMs), small molecules capable of introducing CO to a biological target with temporal and dose control, has improved the prospect for therapeutic CO.¹⁵ Additionally, CO has demonstrated anti-cancer effects, reported to circumvent drug resistance in both cellular and animal models of cancer.¹⁶⁻¹⁸ CO is a promiscuous inhibitor of ferrous heme enzymes and exerts anti-cancer and drug sensitizing effects through multiple targets concertedly, though likely to different extents. CYP appears a likely therapeutic target of CO in cancer models where CYP expression is substantial, though no such study has been performed to this date.

CYP isoforms CYP3A4 and CYP2C8 metabolically inactivate PTX, are overexpressed in malignant breast tissues and are correlated with poorer patient prognosis. CYP3A4 expression in malignant breast tissues is also predictive of resistance to taxane therapy. Additionally, a known inhibitor of CYP activity, CO, is a demonstrated anti-cancer drug-sensitizing agent in human breast cancer cells. We

therefore initiated the present study to determine whether CO could sensitize human breast cancer cells to PTX and whether it was due to CYP inhibition.

5.2. Expression and activity of CYP3A4 in breast cancer cells and tissues

Three human breast cancer cell lines were selected for this study, along with a human hepatocellular carcinoma cell line, a model that is known to express numerous CYP isoforms and other enzymes associated with multidrug resistance.¹⁹ The greatest relative expression of CYP3A4 was detected in MCF-7 compared to MDA-MB-231, MDA-MB-468 and HepG2 (Figure 5.1A). CYP2C8 protein expression was also detected in whole cell lysates of the human breast cancer cells, though at lower levels relative to HepG2 (Figure 5.1A). Similar to relative expression levels, CYP3A4 activity was greatest, >3-fold, in MCF-7 compared to MDA-MB-231 and MDA-MB-468 (Figure 5.1B). Additionally, CYP3A4 expression was generally higher in human breast cancer tissues compared to normal human breast tissues (Figure 5.1C), providing further evidence for a meaningful role for CYP3A4 in human breast cancer biology.

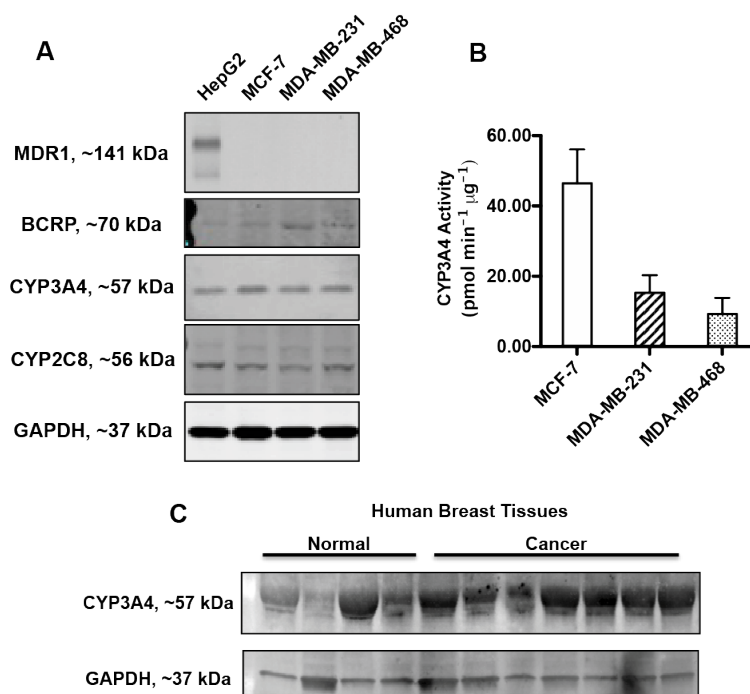


Figure 5.1. Expression and activity of CYP3A4 in human breast cancer cells and tissues. (A) Western blots detecting expressions of cytochrome P450 3A4/2C8 (CYP3A4/2C8) and ATP-binding cassette transporters multi-drug resistance protein 1 (MDR1) and breast cancer resistance protein (BCRP) in 20 μg whole cell lysate of human breast cancer cell lines (MCF-7, MDA-MB-231 and MDA-MB-468) and human hepatocellular carcinoma cell line HepG2. GAPDH expression was used as a loading control. (B) CYP3A4 activity assay in human breast cancer cell lines. (C) Western blots of CYP3A4 expression in 20 μg extracts of normal and cancerous human breast tissues. GAPDH was again used as a loading control. Blots representative of at least n=3 independent experiments. Data representative of n=3 independent experiments.

5.3. CYP3A4 activity in human breast cancer cells in the presence of CO, delivered by photoCORM

The role of CYP3A4 in human breast cancer and drug resistance to PTX was explored by inhibiting its enzymatic activity using CO. Controlled delivery CO to cells in culture conditions was achieved with a designed photoCORM (Figure 5.2).

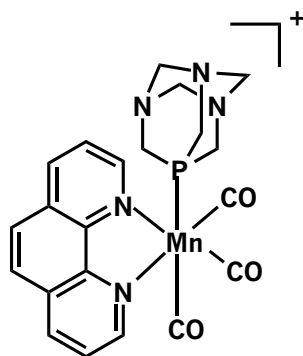


Figure 5.2 $[\text{Mn}(\text{CO})_3(\text{phen})(\text{PTA})]\text{CF}_3\text{SO}_3$ (photoCORM) where phen is 1,10-phenanthroline, PTA is 1,3,5-Triaza-7-phosphaadamantane and CF_3SO_3 is trifluoromethylsulfonate. Protons and CF_3SO_3 counterion have been omitted for clarity.

CO, delivered by 50 and 100 μM photoCORM, inhibited recombinant CYP3A4 activity ~ 2.3 and ~ 3.4 -fold, respectively, compared to control, though only 100 μM photoCORM treatment resulted in a statistically significant difference from control (Figure 5.3A). In cell culture models, CO from 100 μM photoCORM inhibited CYP3A4 activity to an even greater degree, ~ 3.7 -fold in MCF-7 and ~ 3.1 -fold in MDA-MB-231 cell cultures (Figure 5.3B). While CYP3A4 activity appears to be inhibited by CO in MDA-MB-468, which exhibited the lowest basal CYP3A4 activity among the breast cancer cell lines, the difference was not statistically significant (Figure 5.3B).

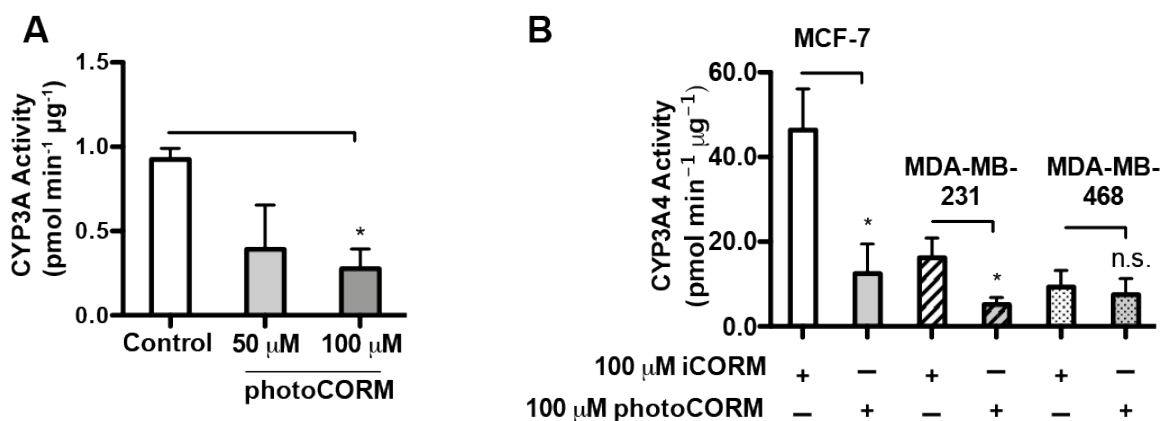


Figure 5.3. CYP3A4 activity in the presence of carbon monoxide (CO), delivered by photoactivatable CO-releasing molecule (photoCORM). (A) Recombinant CYP3A4 enzyme activity in the presence of CO delivered from 0-100 μM photoCORM. Enzyme activity was assayed 20 min after light-triggered release of CO from photoCORM. (B) CYP3A4 activity in human breast cancer cell lines MCF-7, MDA-MB-231 and MDA-MB-468 in the presence and absence of CO, delivered by 100 μM photoCORM. Photo-inactivated photoCORM (iCORM) was used as the control treatment to account for any effects of the non-CO, molecular scaffold of the photoCORM on CYP3A4 activity in cells. Enzyme activity was assayed 24 h post-treatment with CO. Data representative of n=5 independent experiments (* p<0.05).

5.4. Pharmacokinetics and pharmacodynamics of PTX in immortalized, human breast cancer cell cultures

The metabolism of PTX in the four cell lines was monitored by LC-MS/MS-MRM, by adapting a previously published method.²⁰ Protonated PTX and the collisionally induced dissociation (CID) fragment ions were used to establish and optimize an MRM for quantitating PTX in cell culture extracts (Figure 5.4). However, 6-OH-PTX and 3'-p-OH-PTX, structural isomers with identical reversed phase retention times and parent m/z values, only formed sodiated adducted during LC-MS, and these were refractory to CID dissociation, as is frequently the case for alkali-metal adducts. In

this case we monitored the parent-to-parent $(M+Na)^+$ signal intensity of the two metabolites, affording one signal, OH-PTX, for the sum of both (Figure 5.4).

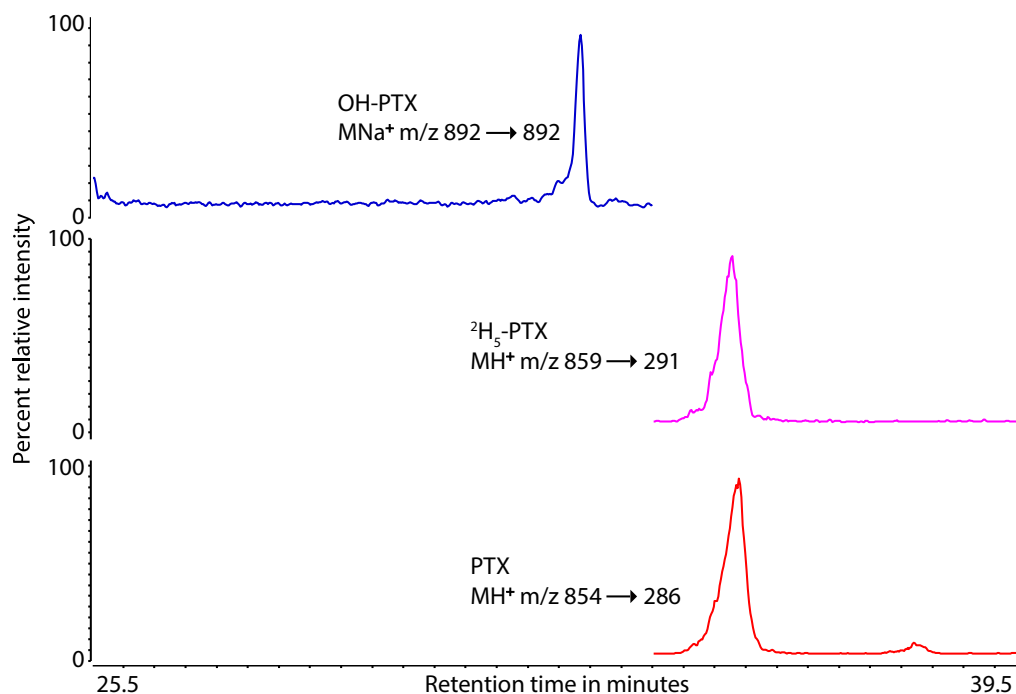


Figure 5.4. Representative chromatograms of the measurement, by high performance liquid chromatography-mass spectrometry (HPLC-MS), of intracellular paclitaxel (PTX) ($[M+H]^+$ m/z: 854 \rightarrow 286, rt \sim 35.4 min) and hydroxy-paclitaxel (OH-PTX) ($[M+Na]^+$ m/z: 892 \rightarrow 892, rt \sim 32.8 min) in PTX-treated human breast cancer cells. Deuterated PTX (2H_5 -PTX) ($[M+H]^+$ m/z: 859 \rightarrow 509, rt \sim 52.3) was used as an internal standard.

LC-MS/MS-MRM measurements of standard solutions of 6-OH-PTX and 3'-p-OH-PTX, prepared in MCF-7 lysate, afforded standard curves which, when combined together, had acceptable goodness-of-fit (Figure 5.5).

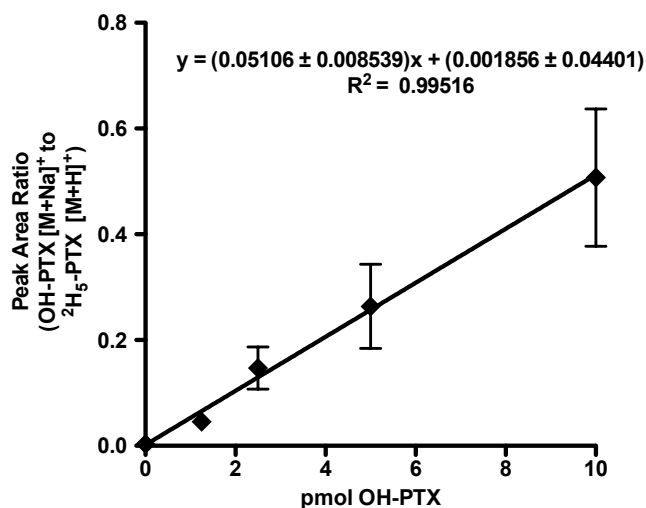


Figure 5.5. Standard curve of hydroxyl-paclitaxel (OH-PTX) prepared in cell lysate. Standard solutions of 0-10 pmol OH-PTX prepared in human breast cancer cell line lysate MCF-7. OH-PTX ($[M+Na]^+$ m/z: 892 \rightarrow 892, rt \sim 32.8 min). Internal Deuterated PTX (2H_5 -PTX) ($[M+H]^+$ m/z: 859 \rightarrow 509, rt \sim 52.3) was used. Data representative of n=5 independent experiments.

In PTX-treated cells, intracellular OH-PTX was detected only in MCF-7 cells, \sim 1-7 fmol μg^{-1} (Figure 5.6A). Intracellular concentrations of the parent substrate, PTX, in the cell lines were highest in MCF-7, \sim 2-fold lower in MDA-MB-231, 2.4-fold lower in MDA-MB-468 and \sim 2000-fold less in HepG2 (Figure 5.6B). As ABCs are believed to influence intracellular accumulation of many anti-cancer drugs and are implicated in multidrug resistance, the relative expression levels of multidrug resistance protein 1 (MDR1 or ABCB1/P-glycoprotein) and breast cancer resistance protein (BCRP or ABCG2), two transporters shown to play mediating roles in multidrug resistance, were determined.²¹⁻²³ MDR1 expression was only detected in HepG2 (Figure 5.1A), while BCRP expression was low in all cell lines, though

immunoblot bands for BCRP in MDA-MB-231 and MDA-MB-468 were slightly more intense (Figure 5.1A).

PTX-induced expression of CYPs and ABCs was also considered, as CYPs and ABCs are capable of co-induction and have overlapping substrate specificity, as is the case with CYP3A4/2C8, MDR1 and BCRP.²⁴ Furthermore, induction of CYPs and ABCs in cancer cells in the presence of a xenobiotic drug is well documented and implicated as the mechanism of acquired drug resistance in cancer.²⁵ In the timescales of our experiments, 24 h treatments of MCF-7 cells with 0.5 and 1 μ M PTX, only CYP3A4 exhibited minor induction compared to control, while CYP2C8, MDR1 and BCRP expression did not exhibit visible expression changes with increasing concentrations of PTX (Figure 5.6C). Levels of intracellular OH-PTX and PTX, however, increased in MCF-7 with increasing doses of PTX (Figure 5.6D-E).

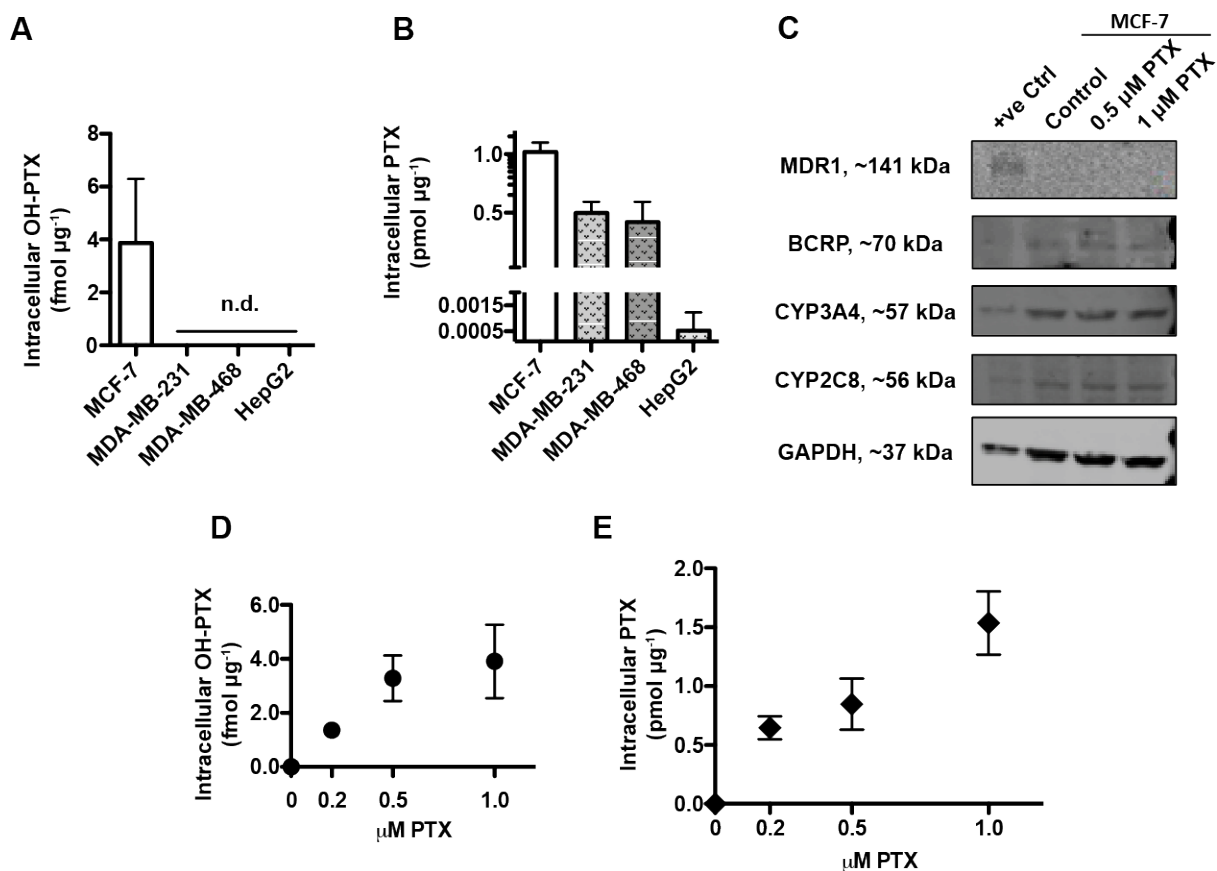


Figure 5.6. Pharmacokinetics and pharmacodynamics of paclitaxel (PTX) in immortalized, human breast cancer cell cultures. (A) Intracellular hydroxy-PTX (OH-PTX) concentrations in cell cultures treated with PTX (1 μM) for 24 h measured by LC-MS/MS-MRM. Data were normalized to total protein. (B) Intracellular PTX concentrations in cell cultures treated with 1 μM PTX for 24 h also as measured by LC-MS/MS-MRM. Data were normalized to total protein. (C) Representative western blots of 20 μg per lane whole cell lysates of MCF-7 cells treated with 0-1 μM PTX for 24 h. Positive control (+ve Ctrl) of 10 μg HepG2 whole cell lysate was used. GAPDH expression was used as a loading control. Measurement, by HPLC-MS/MS-MRM, of (D) intracellular OH-PTX and (E) intracellular PTX in MCF-7 cells treated with 0-1 μM PTX for 24 h. Data were normalized to total protein. Data representative of $n=5$ independent experiments. Blots representative of $n=3$ independent experiments.

5.5. Effect of CO on the pharmacokinetics of PTX and the effects in human breast cancer cells

Having found that CYP activity was inhibited by CO (Figure 5.3B) and that CYP-mediated metabolism of PTX occurred in human breast cancer cells (Figure 5.6A, D), we sought to determine if CO could alter the pharmacokinetics of PTX in human breast cancer cells. Intracellular levels of OH-PTX in MCF-7 treated with PTX declined in a dose-dependent manner with CO co-treatment (Figure 5.7A). Treatment of MCF-7 with increasing concentrations of CO did not result in any statistically significant changes in intracellular PTX, though linear regression analysis of the data revealed a possible correlation between CO and increasing intracellular levels of PTX (Figure 5.7B). The response of human breast cancer cells to PTX, as measured by decreased cell viability, was enhanced in the presence of CO. Delivered from 50 μ M and 100 μ M photoCORM, CO led to diminution of the IC₅₀ of PTX for cells ~140-fold and ~210-fold compared to control-treated cells (Figure 5.7C).

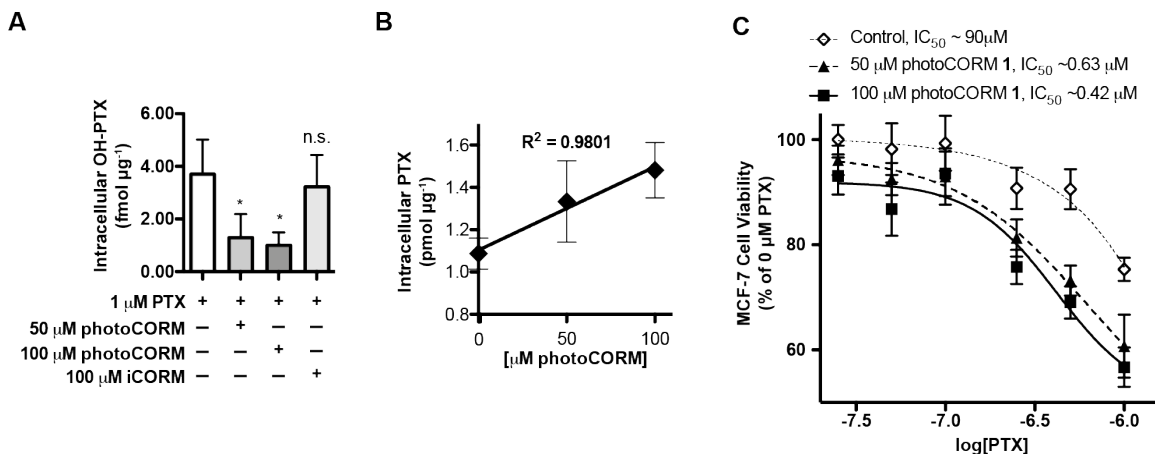


Figure 5.7. Effects of carbon monoxide (CO) on the pharmacokinetics of paclitaxel (PTX) and the effects in human breast cancer cells. (A) Intracellular hydroxy-paclitaxel (OH-PTX), as measured 24 h post-treatment by LC-MS/MS-MRM in 1 μ M PTX-treated MCF-7 cells with co-treatment of CO delivered by 50/100 μ M photoactivatable CO-releasing molecule (photoCORM). 100 μ M light-inactivated photoCORM (iCORM) was used as a treatment to control for effects of the molecular scaffold on intracellular OH-PTX levels. (B) Intracellular PTX levels in MCF-7 cells treated with 1 μ M PTX in the presence of increasing concentrations of CO, delivered by 50 and 100 μ M photoCORM. Measurements were performed by LC-MS/MS-MRM 24 h post-treatment. Linear regression of the data was performed to predict the effect of CO on intracellular PTX levels. (C) Dose-response curves of PTX treatment on cell viability of MCF-7 cells in the presence of CO, delivered by 50 and 100 μ M photoCORM 24 h post-treatment. Data representative of n=5 independent experiments (* p<0.05).

The photoCORM-normalized dose-response curves of MCF-7 to PTX also revealed increased cell death response to PTX in the presence of CO compared to controls (Figure 5.8).

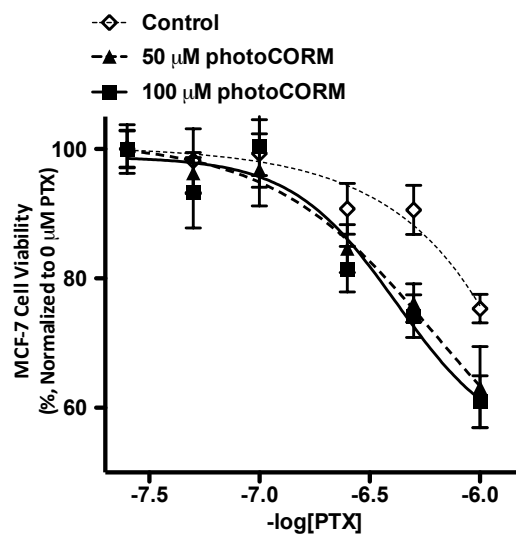


Figure 5.8. Normalization to 0 μM PTX ($\log[0 \mu\text{M PTX}] \sim -7.8$) of cell viability curves of human breast cancer cell line MCF-7, presenting the dose-response of paclitaxel (PTX) on cell viability in the absence (Control) and presence of carbon monoxide (CO), delivered by 50/100 μM photoactivatable CO-releasing molecule (photoCORM)). Cell viability was measured 24 h post-treatment by the cellular reduction of tetrazolium salt (3-(4,5-dimethylthiazol-2-yl)-2,5-diphenyltetrazolium bromide or MTT). Data representative of $n=5$ independent experiments.

In contrast, in MDA-MB-231 cells where intracellular OH-PTX formation was not detected (Figure 5.6A) and intracellular levels of PTX were ~ 2 -fold lower than in MCF-7 (Figure 5.6B), the increase in sensitivity of MDA-MB-231 cells to PTX in the presence of CO was orders of magnitude less than in MCF-7 cells, ~ 1.6 -fold and ~ 2.4 -fold respectively in the presence of CO (Figure 5.9).

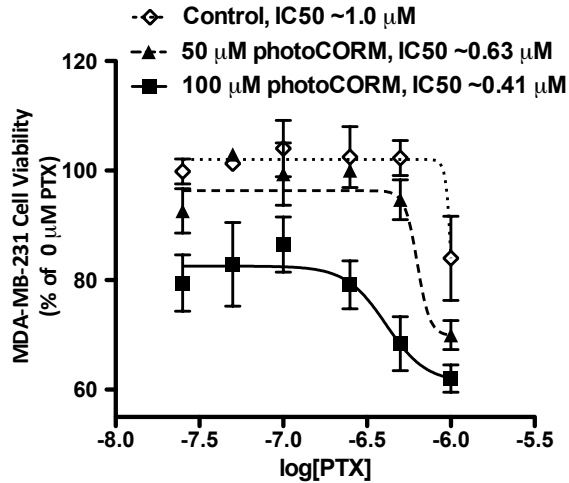


Figure 5.9. Effect of carbon monoxide (CO) co-treatment on the dose-response of paclitaxel (PTX) on the cell viability of human breast cancer cell line MDA-MB-231. Cells were treated in the absence (Control) and presence of CO, delivered by 50/100 μM photoactivatable CO-releasing molecule (photoCORM). Cell viability was measured 24 h post-treatment by the cellular reduction of tetrazolium salt (3-(4,5-dimethylthiazol-2-yl)-2,5-diphenyltetrazolium bromide or MTT). Data representative of $n=3$ independent experiments.

Of note, CO alone elicited significantly greater cell death in MDA-MB-231 compared to MCF-7 cells (Figure 5.10).

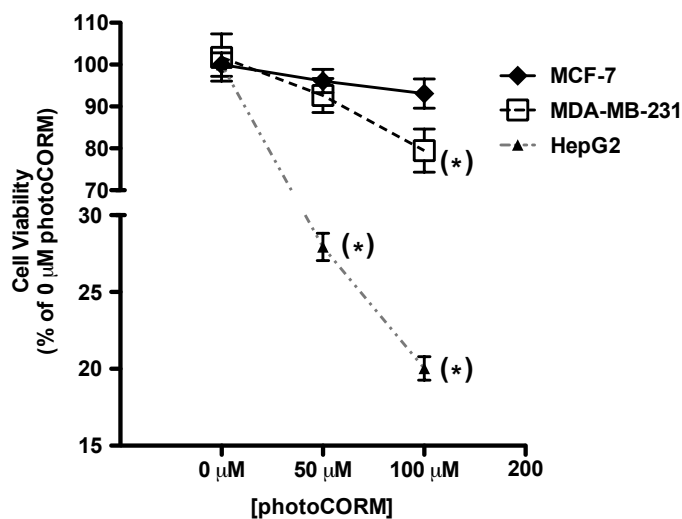


Figure 5.10. Cell viability of human breast cancer and human hepatocellular carcinoma cell lines in the presence of carbon monoxide (CO). MCF-7, MDA-MB-231 and HepG2 cells were treated with CO, delivered by indicated concentrations of photoactivatable CO-releasing molecule (photoCORM) for 24 h, then assayed for cell viability by the cellular reduction of tetrazolium salt (3-(4,5-dimethylthiazol-2-yl)-2,5-diphenyltetrazolium bromide or MTT). Data representative of n=3 independent experiments.

Additionally, the photoCORM-normalized response of MDA-MB-231 cell viability to PTX was not markedly different in the presence and absence of CO (Figure 5.11).

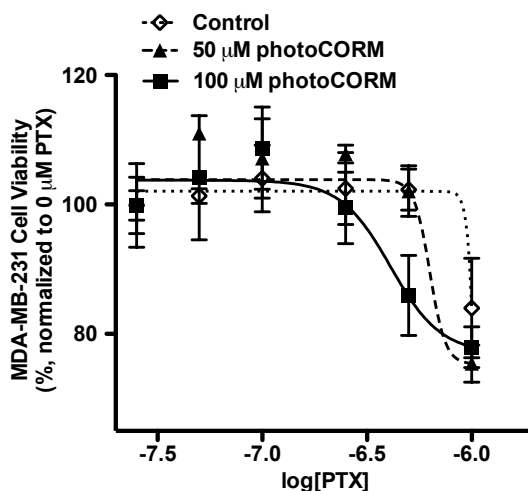


Figure 5.11. Initial value-normalized dose-response curves to paclitaxel (PTX) on cell viability of human breast cancer cell line MDA-MB-231 in the absence (Control) and presence of carbon monoxide (CO), delivered by 50/100 μM photoactivatable CO-releasing molecule (photoCORM). Cell viability was measured 24 h post-treatment by the cellular reduction of tetrazolium salt (3-(4,5-dimethylthiazol-2-yl)-2,5-diphenyltetrazolium bromide or MTT). Data representative of $n=3$ independent experiments.

5.6. Effects of chloramphenicol on CYP3A4/2C8-mediated metabolism of PTX in human breast cancer cells

Because it was not possible to distinguish between 3'-p-OH-PTX and 6-OH-PTX by LC-MS/MS-MRM (Figure 5.4), chloramphenicol (CAM), a potent inhibitor of CYP3A4, $K_i = 10.6 \mu\text{M}$, but not CYP2C8,²⁶ was used. The sensitivity of MCF-7 cells to PTX was assessed in the presence of CAM, where it was found that both 10 and 20 μM inhibitor increased the sensitivity of MCF-7 to PTX ~ 120 -fold compared to control treatments (Figure 5.12A).

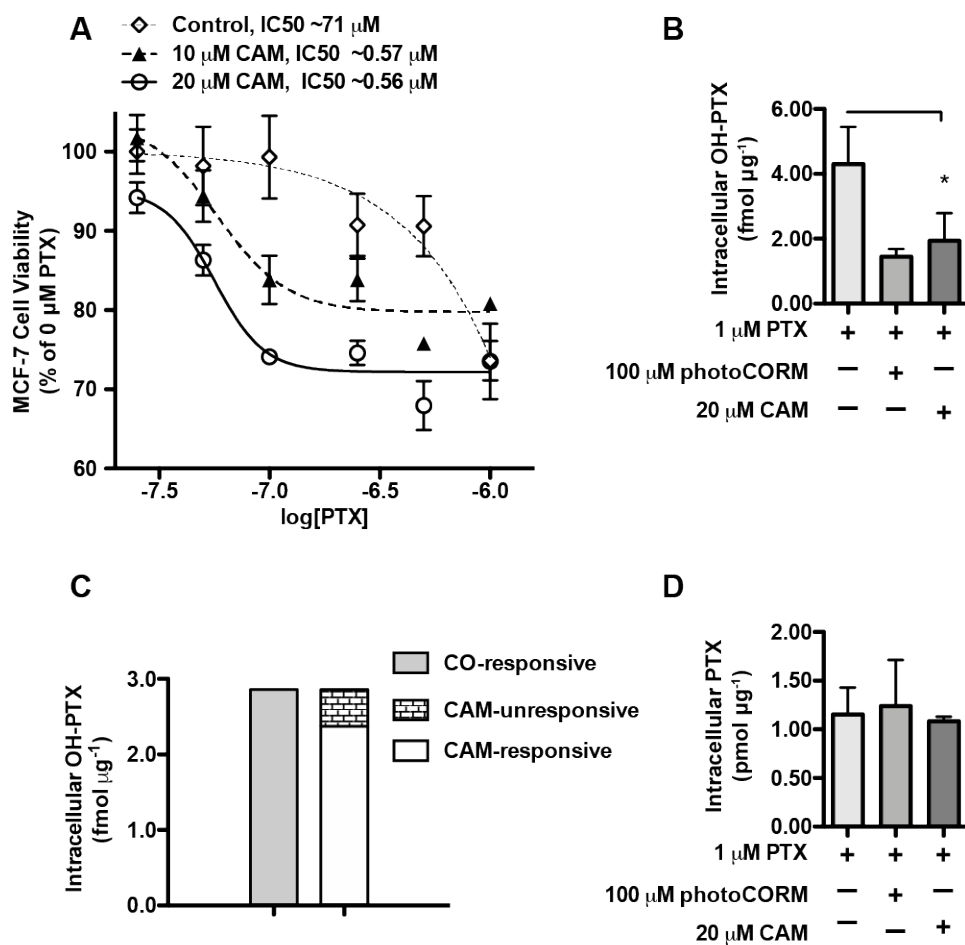


Figure 5.12. Effects of small molecule, pharmacological inhibition of CYP3A4-mediated metabolism of PTX in human breast cancer cells. (A) Representative cell viability curves, showing the effect of CAM co-treatment on the dose-response of PTX on the cell viability of human breast cancer cell line MCF-7. Cells were treated in the absence (Control) and presence of 10 and 20 μ M CAM. Cell viability was measured 24 h post-treatment by the cellular reduction of tetrazolium salt (3-(4,5-dimethylthiazol-2-yl)-2,5-diphenyltetrazolium bromide or MTT). (B) LC-MS/MS-MRM measurements of intracellular OH-PTX levels in MCF-7 cells 24 h post-treatment with 1 μ M PTX and either CO, delivered by 100 μ M photoCORM, or 20 μ M CAM. (C) Graphical summary of magnitude of perturbations in intracellular OH-PTX in PTX-treated MCF-7 cells in response to CO and CAM treatments. (D) Intracellular PTX levels, measured by LC-MS/MS-MRM, in MCF-7 cells 24 h post-treatment with 1 μ M PTX and either CO, delivered by 100 μ M photoCORM, or 20 μ M CAM. Data representative of n=5 independent experiments. (* p<0.05)

Initial condition-normalized response curves of MCF-7 cell viability to PTX afforded dose-response curves showing increased response to lower concentrations of PTX in the presence of CAM (Figure 5.13).

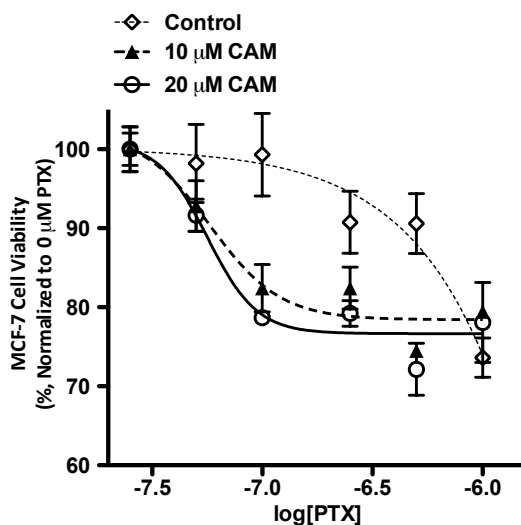


Figure 5.13. Initial value-normalized cell viability curves of the dose-response of paclitaxel (PTX) on cell viability of human breast cancer cell line MCF-7 in the absence (Control) and presence of 10/20 μM chloramphenicol (CAM). Cell viability was measured 24 h post-treatment by the cellular reduction of tetrazolium salt (3-(4,5-dimethylthiazol-2-yl)-2,5-diphenyltetrazolium bromide or MTT). Data representative of $n=5$ independent experiments.

The 20 μM CAM dose decreased the levels of intracellular OH-PTX $\sim 55\%$ in MCF-7, while CO decreased OH-PTX levels to a greater magnitude, $\sim 67\%$ (Figure 5.12B). Further analysis of intracellular measurements of these data (Figure 5.12B) afforded insight and an estimation of the enzymatic sources of OH-PTX. Of the $\sim 2.86 \text{ fmol } \mu\text{g}^{-1}$ OH-PTX measured in MCF-7 that was CO-responsive, $\sim 83\%$ of that was CAM-responsive, leaving $\sim 17\%$ that was sensitive to CO-mediated, but not CAM-mediated inhibition (Figure 5.12C). Additionally, intracellular PTX levels in PTX-treated

MCF-7 did not change significantly in the presence of either CO or CAM (Figure 5.12D). In case of MDA-MB-231, cell viability was decreased to a greater extent in the presence of CAM and PTX compared to PTX alone (Figure 5.14).

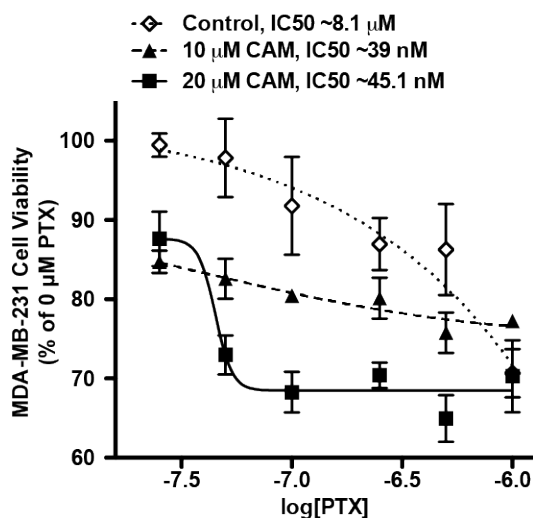


Figure 5.14. Effect of chloramphenicol (CAM) co-treatment on the dose-response of paclitaxel (PTX) on the cell viability of human breast cancer cell line MDA-MB-231. Cells were treated in the absence (Control) and presence of 10 and 20 μM chloramphenicol (CAM). Cell viability was measured 24 h post-treatment by the cellular reduction of tetrazolium salt (3-(4,5-dimethylthiazol-2-yl)-2,5-diphenyltetrazolium bromide or MTT). Data representative of $n=3$ independent experiments.

Normalization of the data to initial conditions revealed increased sensitivity of MDA-MB-231 cells to PTX in the presence of 20 μM CAM only, though this effect was limited to PTX concentrations $<0.5 \mu\text{M}$ PTX (Figure 5.15).

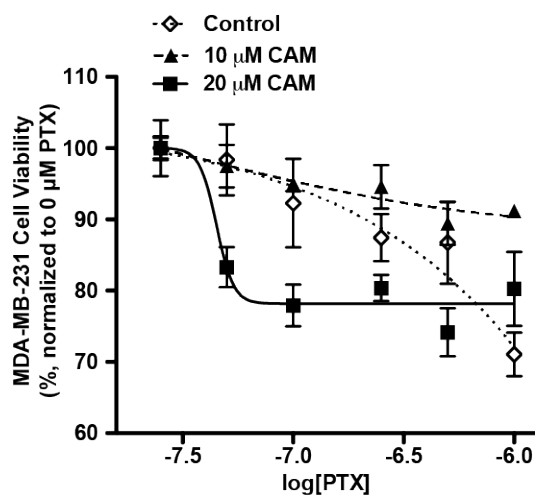


Figure 5.15. Initial value-normalized cell viability curves of human breast cancer cell line MDA-MB-231 of the dose-response of paclitaxel (PTX) on cell viability in the absence (Control) and presence of 10/20 μM chloramphenicol (CAM). Cell viability was measured 24 h post-treatment by the cellular reduction of tetrazolium salt (3-(4,5-dimethylthiazol-2-yl)-2,5-diphenyltetrazolium bromide or MTT). Data representative of $n=3$ independent experiments.

5.7. CO and the pharmacokinetics of PTX in HepG2 cells

HepG2, a cell line model of a disease characterized by multidrug resistance,²⁷ was highly sensitive to CO-mediated growth restriction and/or cell death, $\text{IC}_{50} \sim 1.19 \mu\text{M}$ (Figure 5.16A). This was in contrast to human breast cancer cells, which were significantly more tolerant of CO alone compared with HepG2 (Figure 5.10). Therefore, to assess the ability of CO to sensitize HepG2 cells to PTX, rather than assess the cytotoxic effects of CO itself, lower doses of CO, delivered by photoCORM, were used in PTX-cell viability dose-response experiments. In these experiments, HepG2 was observed to have a >200-fold response in cell death in the

presence of CO, delivered by 1 and 10 μM photoCORM, compared to its absence (Control) (Figure 5.16B).

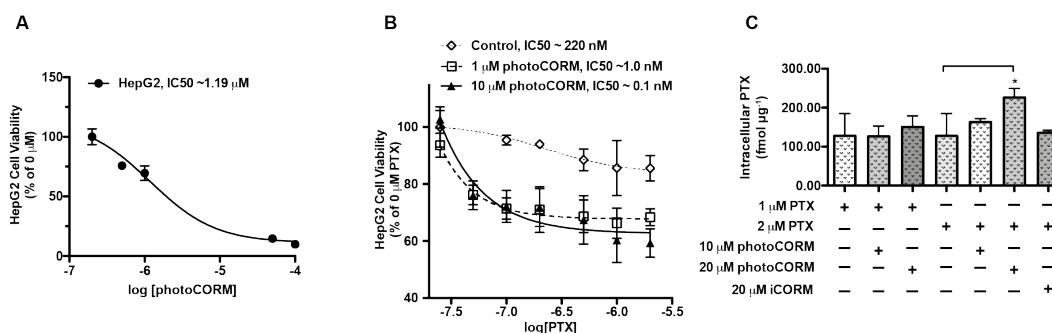


Figure 5.16. Effects of carbon monoxide (CO) on the pharmacokinetics of paclitaxel (PTX) in human hepatocellular carcinoma cells. (A) Cell viability curve of the response of HepG2 cells to CO, delivered by photoCORM. Cell viability was measured 24 h post-treatment by the cellular reduction of tetrazolium salt (3-(4,5-dimethylthiazol-2-yl)-2,5-diphenyltetrazolium bromide or MTT). (B) Dose-response of HepG2 cell viability to PTX in the presence of CO, delivered by 1 and 10 μM photoactivatable CO-releasing molecule (photoCORM), and absence of CO (Control). Cell viability was measured 24 h post-treatment by MTT assay. (C) Intracellular PTX levels in HepG2 24 h post-treatment with PTX and or CO, delivered by photoCORM, assayed by LC-MS/MS-MRM. Light-inactivated photoCORM (iCORM) treatments were performed as a control for the non-CO molecular scaffold of photoCORM. Viability curves representative of n=3 independent experiments. LC-MS/MS-MRM data are representative of n=5 independent experiments. (* p<0.05)

Normalization of these dose-response curves to initial conditions also revealed increased cell death response to PTX in the presence of CO compared to controls (Figure 5.17).

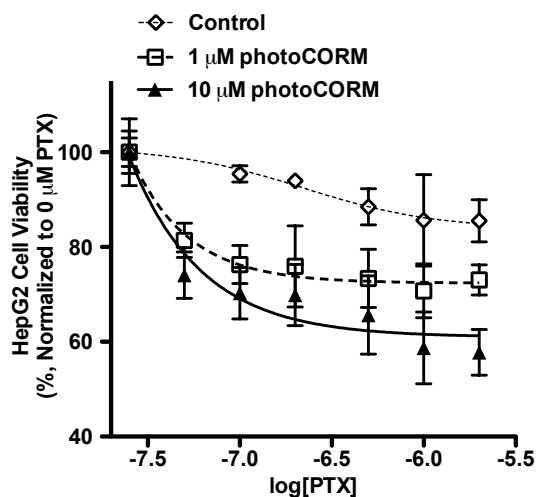


Figure 5.17. Initial condition-normalized cell viability curves of the response of human hepatocellular carcinoma cells to paclitaxel (PTX) in the absence (Control) and presence of carbon monoxide (CO) delivered by 1 and 10 μM photoactivatable CO-releasing molecule (photoCORM). Cell viability of HepG2 cells was measured 24 h post-treatment by the cellular reduction of tetrazolium salt (3-(4,5-dimethylthiazol-2-yl)-2,5-diphenyltetrazolium bromide or MTT). Data representative of $n=3$ independent experiments.

A significant effect on intracellular PTX levels of HepG2 was observed between treatments of varying concentrations of PTX and/or CO, as determined by one-way ANOVA ($F(6,25) = 3.343$, $p = 0.0148$), though the only statistically significant difference observed, that was relevant to the pharmacokinetics of PTX, was between 2 μM PTX-treated and 2 μM PTX + 20 μM photoCORM-treated cells (Figure 5.16C).

5.8 Discussion

The importance of CYP3A4 in drug resistance in breast cancer is highlighted by the observation that its expression positively correlates with poor prognosis and

therapeutic failure of taxanes.^{9,28} Until the findings presented here, however, no study had directly demonstrated that CYP3A4 expression and activity influences the sensitivity of human breast cancer cells to PTX.

While CYP3A4/2C8 was expressed in human breast cancer cells and HepG2 (Figure 5.1A), our results indicated that the formation of detectable levels of OH-PTX (Figure 5.6A) in PTX-treated cell cultures was contingent on both high CYP3A4 activity/expression (Figure 5.1A, B) and sufficient intracellular accumulation of PTX (Figure 5.6B) in the cell line; thus OH-PTX was only detected in MCF-7 (Figure 5.6A). In addition, although the expression of MDR1 and BCRP appeared to influence intracellular PTX levels in the cell cultures, it should be noted that broadly speaking, the contribution of ABCs to drug resistance is controversial. They have been the most popular therapeutic target for circumventing drug resistance, and yet clinical studies targeting ABCs have generally afforded poor results, with the majority failing due to lack of efficacy or toxicity.²⁹ There is no strong evidence that MDR1 expression contributes directly to drug resistance.³⁰ While their expression patterns explain some of the observed differences in the pharmacokinetics of PTX (Figure 5.1A, 5.6A, 5.6B), CYP3A4/2C8-mediated inactivation of PTX in certain human breast cancer models, i.e. MCF-7, appeared to be a key mode of drug resistance in cancer; CO *sensitized* MCF-7 to PTX (Figure 5.7C, 5.8) and CYP3A4 inhibitor CAM elicited similar sensitization (Figure 5.12A, 5.13). The use of CAM also afforded an estimate of the relative activities of CYP3A4 and CYP2C8, with

CYP3A4 identified as the major enzyme, and CYP2C8 the minor enzyme, in the metabolic inactivation of PTX in human breast cancer (Figure 5.12C).

Additionally, our findings indicated that the expression of CYP3A4/2C8 alone was not necessarily indicative of appreciable CYP-mediated inactivation of PTX as explained by our studies with MDA-MB-231. The ability of CO to increase the cell death response of MDA-MB-231 to PTX (Figure 5.9, 5.11) was qualitatively different compared to MCF-7. Unlike in MCF-7, in MDA-MB-231 CO and PTX co-treatment appeared to elicit a more simple, cumulative cytotoxic effect on MDA-MB-231 cell viability (Figure 5.9) that was revealed upon normalization of the curves to initial conditions (Figure 5.11). Interestingly, CAM co-treatment elicited greater response of MDA-MB-231 to PTX (Figure 5.14, 5.15) despite the lack of detectable intracellular OH-PTX (Figure 5.6A). In addition to its specific inhibition of CYP3A4, CAM has been reported to induce mitochondrial stress and deplete intracellular ATP levels in cancer cells.³¹ Interestingly, a similar depletion in intracellular ATP levels has been reported to be a mechanism of CO-induced uncoupled mitochondrial respiration and drug sensitization in cancer cells.^{32,33} Depletion of cellular ATP levels, a shared mechanism of action between CAM and CO, could have been the reason for their cumulative, cytotoxic effects against MDA-MB-231.

CYP3A4 is also a marker for poor prognosis in human hepatocellular carcinoma and HepG2 cells possess a strong, multidrug resistant phenotype.³⁴ We initially had hoped to demonstrate inhibition of CYP3A4-mediated inactivation of PTX by CO in HepG2

cells in addition to human breast cancer cells, but high MDR1 expression compared to human breast cancer cells (Figure 5.1A) resulted in low intracellular accumulation of PTX (Figure 5.6B). These observations indicated that MDR1, and not CYP3A4/2C8, was the main effector of PTX pharmacokinetics. While this would seemingly contradict the importance of CYP3A4 as a biomarker for poor prognosis in hepatocellular carcinoma, it should be noted that HepG2, despite possessing many markers for multidrug resistance, possesses surprisingly low levels of CYP expression, especially compared to primary hepatocytes,¹⁹ a possible consequence of selection pressures during immortalization of the cell line. This was evidenced here, as HepG2 possessed some of the lowest CYP3A4 expression compared to the breast cancer cell lines (Figure 5.1A). While the use of cell culture models was key to demonstrate direct involvement of CYP activity in resistance to PTX in this study, clear understanding of the differences between hepatocellular carcinoma immortalized cell lines and clinical samples/data is necessary as well.

While our studies with HepG2 did not offer greater insight into CYP-mediated metabolism of PTX, its extreme sensitivity to CO-induced cell death (Figure 5.16A) was notable. Increased responses of HepG2 to PTX in the presence of 1 and 10 μ M CO (Figure 5.16B) were similar in magnitude to the increased responses of MCF-7 (Figure 5.7C) and MDA-MB-231 (Figure 5.9) to PTX in the presence of 10 and 100-fold greater amounts of CO. As CO is a promiscuous inhibitor of not only CYPs, but all ferrous heme-containing enzymes, albeit to varying degrees,³⁵ the great sensitivity of HepG2 to CO suggests a particular importance of heme-containing enzyme activity

in HepG2 cell viability. Only at high doses of CO, delivered by 20 μ M photoCORM, the pharmacokinetics of PTX were significantly changed in PTX-treated HepG2 cells (Figure 5.16C), though the cytotoxicity of CO alone to HepG2 (Figure 5.16A) may be responsible for the observed difference.

CO-sensitive, heme-containing enzymes like CYP3A4 also appears to be particularly important to the breast cancer cell and drug resistance. Heme biosynthesis is up-regulated 20-fold in malignant breast tissue compared to adjacent normal tissue.³⁶ Furthermore, increased heme uptake and biosynthesis in cancer tissues and the synthesis of heme-containing enzymes are believed to be key in driving cellular processes favorable to uncontrolled growth and drug resistance.³⁷ Previous studies have identified other heme-containing enzymes, including cystathionine β -synthase (CBS), as direct effectors of drug resistance in malignant breast, ovarian and hepatic tissues.^{17,38,39} In this present study, the direct demonstration of the role CYP3A4 had in imparting resistance to PTX in human breast cancer further highlights the importance of heme-containing enzymes to drug resistance in cancer. Furthermore, CO appears to be an ideal candidate to concomitantly inhibit heme-containing therapeutic targets in human breast cancer.

Inhibition of specific CYP isoforms in human cancers to mitigate drug resistance has shown some promise,⁴⁰ though genetic/structural variances and heterogeneous expression of certain CYP isoforms in patient populations has made some question how effective CYP-specific, small molecule inhibitors will be in a clinical setting.⁴¹

Findings in this study corroborate the trepidation in viewing CYPs, including CYP3A4, as an *independent* marker and effector of PTX resistance. Drug resistance in cancer is well understood and known to be multifactorial. Targeting single markers of resistance is unlikely to be any more successful than the unimaginative and expensive endeavor in targeting of individual growth signaling pathways.⁴² Even for the newest, most promising, targeted inhibitors of cancer growth signaling proteins like B-raf and Bcr-Abl, resistance quickly develops.^{43,44} A fresh approach to cancer therapy is needed.

CO, unlike most pharmacological CYP inhibitors, is a polypharmacological drug, a small molecule that can interact with multiple targets to elicit a more dynamic, salutary effect.⁴⁵ Ferrous heme-containing enzymes and other low-valent metal center containing enzymes are all susceptible to CO inhibition.⁴⁶ Tumor heterogeneity and rapid growth rate impart the cancer cell the ability to quickly adapt and evolve drug resistance.⁴⁷ CO, through simultaneous blockade of multiple, heme-containing targets and pathways offers the opportunity overcome adaptive drug resistance. In the present study, we have demonstrated the utility of CO as a polypharmacology drug, in inhibiting both CYP3A4 and CYP2C8 simultaneously to sensitize human breast cancer cells to PTX. This is in addition to the other known mechanisms of action of CO in human cancer.⁴⁸

PTX is one the most important anti-cancer drugs available today.⁴⁹ It is the most widely used anti-cancer drug and frequently used as the first-line treatment of breast

cancer.⁵⁰ Now available in generic form, PTX is relatively affordable to most populations and represents the promise of equal access healthcare, in stark contrast to the newer, expensive drugs that possess arguably trivial advantages over PTX.^{51,52} An intriguing strategy, which could invigorate the field of cancer therapy, and not only for the upper socioeconomic classes of society, is the direct targeting of the molecular machinery in cancer cells that promote drug resistance to PTX. In combination with PTX therapy, such a strategy could prevent and/or circumvent PTX resistance by blocking the cancer cell's evolutionary escape routes. We have provided direct evidences for the role of CYP3A4 in resistance to PTX in human breast cancer cells by using CO. In combination with PTX therapy, the use of therapeutic CO is a promising strategy to mitigate or even prevent PTX resistance in human breast cancer.

5.9 Materials and methods

Chemicals and reagents

[Mn(CO)₃(phen)(PTA)]CF₃SO₃ (photoCORM) was synthesized and characterized as previously reported (Chakraborty et al. 2017). Paclitaxel (479306), protease inhibitor cocktail (P8340), chloramphenicol (C0378-5G) and other chemicals were products of Sigma Aldrich (St. Louis, MO). Paclitaxel-d₅ (22092) and 6 α -hydroxy paclitaxel (10009027) were purchased from Cayman Chemical Company (Ann Arbor, MI). 3'-Para-hydroxy paclitaxel and frozen, human breast tissue samples were supplied by the Pasarow Mass Spectrometry Laboratory (PMSL), Department of Psychiatry &

Biobehavioral Sciences at the UCLA David Geffen School of Medicine. Primary antibodies against CYP2C8 (BML-CR3280-0025) was purchased from Enzo Life Sciences, Inc. (Farmingdale, NY), Multidrug Resistance Protein 1/P-glycoprotein (ab170904) was from AbCam (Cambridge, MA), while antibodies against CYP3A4 (sc-53850) and GAPDH (sc-47724) were purchased from Santa Cruz Biotechnology (Santa Cruz, CA). Anti-mouse (926-32210) and anti-rabbit (926-68071) secondary antibodies were purchased from LI-COR (Lincoln, NB).

Cell culture and treatments

Human breast cancer cell lines MCF-7, MDA-MB-231, MDA-MB-468 and human hepatocellular carcinoma cell line HepG2 were obtained from American Type Culture Collection (Manassas, VA). MDA-MB-231, MDA-MB-468 and HepG2 were grown in 1× DMEM supplemented with 10 mM HEPES buffer, 1× antibiotic–antimycotic, and 10% fetal bovine serum (FBS). MCF-7 cells were also grown in 1× DMEM supplemented with 1 µg/mL insulin, 1 mM sodium pyruvate, 1× antibiotic–antimycotic, and 10% FBS. The absence of mycoplasma was determined periodically using a MycoAlert mycoplasma detection kit (LT07-318, Lonza, Basel, Switzerland). Cells were seeded overnight prior to treatments and were observed through light microscopy to be <70% confluent prior to treatments with paclitaxel and chloramphenicol.

Treatment of cell cultures with CO, delivered by photoCORM

Cells were treated with CO, delivered by 0-100 µM photoCORM in respective cell

culture media. Cells were seeded, $2-4 \times 10^3$ cells per well of a 96-well plate, or $1-2 \times 10^6$ cells into 100 mm tissue culture dishes, and allowed to incubate overnight at $37^\circ\text{C} + 5\% \text{CO}_2$. The next day, in the dark, the media was removed and replaced with photoCORM dissolved in cell culture media supplemented with 10% FBS to final concentrations of 0-100 μM photoCORM. Cells were then exposed to low power (10 mW/cm^2) visible light to trigger the release of CO. To control for the effects of the non-CO molecular scaffold of the photoCORM, photoCORM was dissolved in cell culture media then exposed to low power (10 mW/cm^2) for 60 min to prematurely release the CO, then added to the cells. Cells were incubated at $37^\circ\text{C} + 5\% \text{CO}_2$ for 24 h prior to analysis by the indicated methods.

Western analysis

Cells were harvested by scraping, pelleted via centrifugation and extracted using RIPA lysis buffer (150 mM NaCl, 5 mM EDTA pH 8.0, 50 mM Tris pH 8.0, 1% Triton X-100, 0.5% sodium deoxycholate, 1% SDS and $1\times$ protease inhibitor cocktail). Frozen human tissue samples (~ 10 mg) were bead sonicated in RIPA lysis buffer. BCA Protein Assay was performed on all samples to measure total protein content of soluble fractions. Samples assayed for membrane bound proteins were not boiled while all other samples were boiled. 20 μg cell lysate were separated on 4-20% SDS-PAGE gel and transferred to poly(vinylidene difluoride) (PVDF) membranes. Blocking and antibody solutions were prepared in $1\times$ PBS + 0.1% Tween 20. Membranes, following blocking in 5% non-fat dried milk for 18 h at 4°C , were

incubated with primary (1:1000 dilution) antibody overnight at 4°C and then an infra-red (IR) dye conjugated secondary (1:10,000 dilution) antibody for 1 h at 25°C in the dark. Immunofluorescent signals were detected using a Li-cor Odyssey 9120 Imaging System.

CYP3A4 activity assay

A commercially available CYP3A4 Activity Assay Kit (ab211076, Abcam) was used as per manufacturer's instructions. After treatments, cell cultures ($\sim 5 \times 10^6$ cells) were harvested by scraping, counted and collected by centrifugation ($250 \times g$, 10 min) in a conical tube. The supernatant was removed and discarded while the pellets were washed with cold 1X PBS, then homogenized in ice-cold assay buffer (500 μ L). The lysate was incubated on ice for 5 min and centrifuged ($10,000 \times g$, 15 min, 4°C). After performing a BCA protein assay, enzymatic activity was determined in a 96-well flat-bottomed, clear bottom, black side microplate with lysate (100 μ g protein/well), the fluorogenic substrate, and an NADPH-generating system, with fluorescent signal monitored over time, as per manufacturer's instructions. Recombinant CYP3A4 (200 μ g/well) was used to determine the effect of CO on acellular enzyme activity. In the dark, photoCORM was solubilized in assay buffer and added to each well such that the final concentration of was 0-100 μ M. The microplate was then exposed to visible light for 20 min to trigger release of CO. As per manufacturer's instructions, the fluorogenic substrate and NADPH-generating-system were added, and the subsequent

fluorescent signal monitored over time. Data for CYP3A4 activity are reported as pmol of substrate metabolized per minute per μg protein.

Treatment and measurement of paclitaxel (PTX) and its metabolites by high performance liquid chromatography-tandem mass spectrometry (LC-MS/MS)

All stock and working solutions of paclitaxel (PTX), 6 α -hydroxy-paclitaxel (6-OH-PTX), 3'-para-hydroxy-paclitaxel (3'-p-OH-PTX) and penta-deuterated paclitaxel ($^2\text{H}_5$ -PTX) were prepared in methanol and stored at -20°C . Cells to be assayed were treated with indicated concentrations of paclitaxel (PTX) in the presence and absence of CO, delivered by photoCORM, and chloramphenicol, then incubated overnight for 24 h at $37^\circ\text{C} + 5\% \text{CO}_2$. The next day, approximately 5×10^6 cells were harvested from the 100 mm tissue culture dishes by scraping, and washed 3 times with cold, 1X phosphate buffered saline (PBS). $^2\text{H}_5$ -PTX (1 nmol in 10 μL) was added to each sample and the cells were lysed via sonication in 200 μL methanol and incubated at room temperature for 30 min, followed by centrifugation (16000 x g, 5 min). Supernatants were transferred to microcentrifuge tubes and dried by vacuum centrifugation. Samples were redissolved in 25 μL methanol, centrifuged at 16000 x g for 5 min. The supernatants were transferred to LC injector vials from which 20 μL was injected onto a reversed phase column (Kinetex XB-C18, 100×2.1 mm, 1.7 μm particle size, 100 \AA pore diameter, Phenomenex, Torrance, CA) equilibrated with 95% eluant A (water + 0.1% formic acid) and 5% eluant B (acetonitrile + 0.1% formic acid) and eluted ($200 \mu\text{L min}^{-1}$) with increasing concentration of eluant B

(min %B⁻¹: 0 5%⁻¹, 5 5%⁻¹, 60 100%⁻¹, 62 5%⁻¹, 80 5%⁻¹). The eluant was passed through an electrospray ionization (ESI) source connected to a triple quadrupole mass spectrometer (Agilent 6460). Analytes were detected via multiple reaction-monitoring (MRM) in positive ion mode: PTX ([M+H]⁺ m/z: 854 → 286, rt = 35.4 min) parent to fragment and OH-PTX ([M+Na]⁺ m/z: 892 → 892, rt = 32.8 min) parent to parent transitions were recorded using optimized settings. In each independent experiment, standards, spiked with 1 nmol ²H₅-PTX, were prepared with known concentrations of paclitaxel (0, 125, 250, 500, 1000 pmol) and 6-OH-PTX (0, 1.25, 2.5, 5, 10 pmol). Amounts of PTX and OH-PTX in each sample were calculated by interpolation from constructed standard curves.

Cell viability assay

The cellular reduction of tetrazolium dye MTT was performed in 96-well tissue culture plates to assay cell viability. Batches of $2-4 \times 10^3$ cells in each well were allowed to seed overnight in a 37 °C incubator + 5% CO₂. The following day, cells were treated with PTX, CAM or photoCORM as indicated, incubated for 24 h, then assessed for viability. Following removal of cell culture media, 0.5 mg/mL MTT dissolved in 1× DMEM was added and allowed to incubate for 2 h in a 37 °C incubator + 5% CO₂. Cell viability was quantified by measuring the relative amount of MTT reduced to insoluble formazan. Following solubilization of formazan in 10% SDS + 0.01 N HCl, the concentration of formazan was measured by taking the absorbance at 570 nm, reference wavelength taken at 690 nm.

Statistical analysis

Data are expressed as the mean +/- standard error of the mean (range) or as a percentage of control value. For results of n=5 or greater, comparisons between two groups were made using the Student's t-test. For results of n=5 or greater, where comparison between more than two groups was analyzed, the One-way ANOVA and Tukey's *post hoc* test were performed. Non-linear regression analyses of dose-response curves were fitted to three parameters by least squares. To make cell viability curves easily comparable to negative controls (i.e. Controls), dose-response curves were also normalized to the initial values and conditions of the system. Goodness-of-fit of linear regression analyses were reported with coefficients of determination.

5.10. References

1. McFadyen, M. C. E.; Melvin, W. T.; Murray, G. I., Cytochrome P450 enzymes: Novel options for cancer therapeutics. *Molecular Cancer Therapeutics* **2004**, *3* (3), 363-371.
2. Murray, G. I.; Patimalla, S.; Stewart, K. N.; Miller, I. D.; Heys, S. D., Profiling the expression of cytochrome P450 in breast cancer. *Histopathology* **2010**, *57* (2), 202-211.
3. van Eijk, M.; Boosman, R. J.; Schinkel, A. H.; Huitema, A. D. R.; Beijnen, J. H., Cytochrome P450 3A4, 3A5, and 2C8 expression in breast, prostate, lung, endometrial, and ovarian tumors: relevance for resistance to taxanes. *Cancer Chemotherapy and Pharmacology* **2019**, *84* (3), 487-499.

4. Zhou, S.; Chan, E.; Li, X.; Huang, M., Clinical outcomes and management of mechanism-based inhibition of cytochrome P450 3A4. *Ther Clin Risk Manag* **2005**, *1* (1), 3-13.
5. Rodriguez-Antona, C.; Ingelman-Sundberg, M., Cytochrome P450 pharmacogenetics and cancer. *Oncogene* **2006**, *25* (11), 1679-1691.
6. Moreno-Aspitia, A.; Perez, E. A., Treatment Options for Breast Cancer Resistant to Anthracycline and Taxane. *Mayo Clinic Proceedings* **2009**, *84* (6), 533-545.
7. Kapucuoglu, N.; Coban, T.; Raunio, H.; Pelkonen, O.; Edwards, R. J.; Boobis, A. R.; Iscan, M., Expression of CYP3A4 in human breast tumour and non-tumour tissues. *Cancer Letters* **2003**, *202* (1), 17-23.
8. Oyama, T.; Kagawa, N.; Kunugita, N.; Kitagawa, K.; Ogawa, M.; Yamaguchi, T.; Suzuki, R.; Kinaga, T.; Yashima, Y.; Ozaki, S.; Isse, T.; Kim, Y. D.; Kim, H.; Kawamoto, T., Expression of cytochrome P450 in tumor tissues and its association with cancer development. *Frontiers in Bioscience-Landmark* **2004**, *9*, 1967-1976.
9. Miyoshi, Y.; Ando, A.; Takamura, Y.; Taguchi, T.; Tamaki, T.; Noguchi, S., Prediction of response to docetaxel by CYP3A4 mRNA expression in breast cancer tissues. *International Journal of Cancer* **2002**, *97* (1), 129-132.
10. Walle, T., Assays of CYP2C8- and CYP3A4-mediated metabolism of taxol in vivo and in vitro. *Cytochrome P450, Pt B* **1996**, *272*, 145-151.
11. Monsarrat, B.; Mariel, E.; Cros, S.; Gares, M.; Guenard, D.; Guerittevoegelein, F.; Wright, M., Taxol metabolism – isolation and identification of 3 major metabolites of taxol in rat bile. *Drug Metabolism and Disposition* **1990**, *18* (6), 895-901.
12. Leemann, T.; Bonnabry, P.; Dayer, P., Selective-inhibition of major-drug metabolizing cytochrome-P450 isozymes in human liver-microsomes by carbon-monoxide. *Life Sciences* **1994**, *54* (14), 951-956.
13. Cooper, D. Y.; Schleyer, H.; Levin, S. S.; Eisenhardt, R. H.; Novack, B. G.; Rosenthal, O., A re-evaluation of the role of cytochrome-P-450 as the terminal

- oxidase in hepatic-microsomal mixed-function oxidase catalyzed-reactions. *Drug Metabolism Reviews* **1979**, *10* (2), 153-185.
14. Dasilva, D. F.; Schroder, U.; Diehl, H., Metabolism of tetraorganolead compounds by rat-liver microsomal mono-oxygenase .2. enzymic dealkylation of tetraethyl lead. *Xenobiotica* **1983**, *13*(10), 583-590.
 15. Chakraborty, I.; Carrington, S. J.; Roseman, G.; Mascharak, P. K., Synthesis, structures, and co release capacity of a family of water-soluble photocorms: assessment of the biocompatibility and their phototoxicity toward human breast cancer cells. *Inorganic Chemistry* **2017**, *56* (3), 1534-1545.
 16. Wegiel, B.; Gallo, D.; Csizmadia, E.; Harris, C.; Belcher, J.; Vercellotti, G. M.; Penacho, N.; Seth, P.; Sukhatme, V.; Ahmed, A.; Pandolfi, P. P.; Helczynski, L.; Bjartell, A.; Persson, J. L.; Otterbein, L. E., Carbon monoxide expedites metabolic exhaustion to inhibit tumor growth. *Cancer Research* **2013**, *73* (23), 7009-7021.
 17. Kawahara, B.; Moller, T.; Hu-Moore, K.; Carrington, S.; Faull, K. F.; Sen, S.; Mascharak, P. K., Attenuation of antioxidant capacity in human breast cancer cells by carbon monoxide through inhibition of cystathionine β -synthase activity: implications in chemotherapeutic drug sensitivity. *Journal of Medicinal Chemistry* **2017**, *60* (19), 8000-8010.
 18. Li, Y. J.; Dang, J. J.; Liang, Q. J.; Yin, L. C., Thermal-responsive carbon monoxide (co) delivery expedites metabolic exhaustion of cancer cells toward reversal of chemotherapy resistance. *Acs Central Science* **2019**, *5* (6), 1044-1058
 19. Westerink, W. M. A.; Schoonen, W., Cytochrome P450 enzyme levels in HepG2 cells and cryopreserved primary human hepatocytes and their induction in HepG2 cells. *Toxicology in Vitro* **2007**, *21* (8), 1581-1591.
 20. Fernandez-Peralbo, M. A.; Priego-Capote, F.; de Castro, M. D. L.; Casado-Adam, A.; Arjona-Sanchez, A.; Munoz-Casares, F. C., LC-MS/MS quantitative analysis of paclitaxel and its major metabolites in serum, plasma and tissue from women

- with ovarian: cancer after intraperitoneal chemotherapy. *Journal of Pharmaceutical and Biomedical Analysis* **2014**, *91*, 131-137.
21. Doyle, L. A.; Ross, D. D., Multidrug resistance mediated by the breast cancer resistance protein BCRP (ABCG2). *Oncogene* **2003**, *22* (47), 7340-7358.
 22. Pires, M. M.; Emmert, D.; Hrycyna, C. A.; Chmielewski, J., Inhibition of P-glycoprotein-mediated paclitaxel resistance by reversibly linked quinine homodimers. *Molecular Pharmacology* **2009**, *75* (1), 92-100.
 23. Louisa, M.; Soediro, T. M.; Suyatna, F. D., in vitro modulation of P-glycoprotein, MRP-1 and BCRP expression by mangiferin in doxorubicin-treated MCF-7 cells. *Asian Pacific Journal of Cancer Prevention* **2014**, *15* (4), 1639-1642.
 24. Rochat, B., importance of influx and efflux systems and xenobiotic metabolizing enzymes in intratumoral disposition of anticancer agents. *Current Cancer Drug Targets* **2009**, *9* (5), 652-674.
 25. AbuHammad, S.; Zihlif, M., Gene expression alterations in doxorubicin resistant MCF7 breast cancer cell line. *Genomics* **2013**, *101* (4), 213-220.
 26. Park, J. Y.; Kim, K. A.; Kim, S. L., Chloramphenicol is a potent inhibitor of cytochrome P450 isoforms CYP2C19 and CYP3A4 in human liver microsomes. *Antimicrobial Agents and Chemotherapy* **2003**, *47* (11), 3464-3469.
 27. Duan, B.; Huang, C.; Bai, J.; Zhang, Y. L.; Wang, X.; Yang, J.; Li, J., *Multidrug Resistance in Hepatocellular Carcinoma*. Codon Publications: Brisbane (AU), 2019; Vol. Chapter 8.
 28. Floriano-Sanchez, E.; Rodriguez, N. C.; Bandala, C.; Coballase-Urrutia, E.; Lopez-Cruz, J., CYP3A4 expression in breast cancer and its association with risk factors in Mexican women. *Asian Pacific Journal of Cancer Prevention* **2014**, *15* (8), 3805-3809.
 29. Kartal-Yandim, M.; Adan-Gokbulut, A.; Baran, Y., Molecular mechanisms of drug resistance and its reversal in cancer. *Critical Reviews in Biotechnology* **2016**, *36* (4), 716-+.

30. Jungsuwadee, P.; Vore, M. E., *Comprehensive Toxicology, Second Edition*. Elsevier Ltd.: 2010; Vol. 4.
31. Li, C. H.; Tzeng, S. L.; Cheng, Y. W.; Kang, J. J., Chloramphenicol-induced mitochondrial stress increases p21 expression and prevents cell apoptosis through a p21-dependent pathway. *Journal of Biological Chemistry* **2005**, *280* (28), 26193-26199.
32. Queiroga, C. S. F.; Almeida, A. S.; Vieira, H. L. A., Carbon monoxide targeting mitochondria. *Biochemistry Research International* **2012**.
33. Li, Y. J.; Dang, J. J.; Liang, Q. J.; Yin, L. C., Thermal-Responsive Carbon Monoxide (CO) Delivery Expedites Metabolic Exhaustion of Cancer Cells toward Reversal of Chemotherapy Resistance. *Acs Central Science* **2019**, *5* (6), 1044-1058.
34. Ashida, R.; Okamura, Y.; Ohshima, K.; Kakuda, Y.; Uesaka, K.; Sugiura, T.; Ito, T.; Yamamoto, Y.; Sugino, T.; Urakami, K.; Kusuhara, M.; Yamaguchi, K., CYP3A4 gene is a novel biomarker for predicting a poor prognosis in hepatocellular carcinoma. *Cancer Genomics & Proteomics* **2017**, *14* (6), 445-453
35. Motterlini, R.; Foresti, R., Biological signaling by carbon monoxide and carbon monoxide-releasing molecules. *American Journal of Physiology-Cell Physiology* **2017**, *312* (3), C302-C313.
36. Navone, N. M.; Polo, C. F.; Frisardi, A. L.; Andrade, N. E.; Batlle, A. M. D., Heme-biosynthesis in human breast-cancer mimetic invitro studies and some heme enzymatic-activity levels. *International Journal of Biochemistry* **1990**, *22* (12), 1407-1411.
37. Fiorito, V.; Chiabrando, D.; Petrillo, S.; Bertino, F.; Tolosano, E., The multifaceted role of heme in cancer. *Frontiers in Oncology* **2020**, *9*.
38. Wang, L. P.; Han, H. X.; Liu, Y.; Zhang, X. L.; Shi, X. Y.; Wang, T. X., Cystathionine beta-synthase induces multidrug resistance a metastasis in hepatocellular carcinoma. *Current Molecular Medicine* **2018**, *18* (7), 496-506.

39. Kawahara, B.; Ramadoss, S.; Chaudhuri, G.; Janzen, C.; Sen, S.; Mascharak, P. K., Carbon monoxide sensitizes cisplatin-resistant ovarian cancer cell lines toward cisplatin via attenuation of levels of glutathione and nuclear metallothionein. *Journal of Inorganic Biochemistry* **2019**, *191*, 29-39.
40. Noll, E. M.; Eisen, C.; Stenzinger, A.; Espinet, E.; Muckenhuber, A.; Klein, C.; Vogel, V.; Klaus, B.; Nadler, W.; Rosli, C.; Lutz, C.; Kulke, M.; Engelhardt, J.; Zickgraf, F. M.; Espinosa, O.; Schlesner, M.; Jiang, X. Q.; Kopp-Schneider, A.; Neuhaus, P.; Bahra, M.; Sinn, B. V.; Eils, R.; Giese, N. A.; Hackert, T.; Strobel, O.; Werner, J.; Buchler, M. W.; Weichert, W.; Trumpp, A.; Sprick, M. R., CYP3A5 mediates basal and acquired therapy resistance in different subtypes of pancreatic ductal adenocarcinoma. *Nature Medicine* **2016**, *22* (3), 278-287.
41. Ingelman-Sundberg, M.; Lauschke, V. M., Can CYP inhibition overcome chemotherapy resistance? *Trends in Pharmacological Sciences* **2020**, *41* (8), 503-506.
42. Fojo, T.; Mailankody, S.; Lo, A., Unintended Consequences of Expensive Cancer Therapeutics-The Pursuit of Marginal Indications and a Me-Too Mentality That Stifles Innovation and Creativity The John Conley Lecture. *Jama Otolaryngology-Head & Neck Surgery* **2014**, *140* (12), 1225-1236.
43. Bhamidipati, P. K.; Kantarjian, H.; Cortes, J.; Cornelison, A. M.; Jabbour, E., Management of imatinib-resistant patients with chronic myeloid leukemia. *Therapeutic Advances in Hematology* **2013**, *4* (2), 103-117.
44. Luebker, S. A.; Koepsell, S. A., Diverse mechanisms of braf inhibitor resistance in melanoma identified in clinical and preclinical studies. *Frontiers in Oncology* **2019**, *9*.
45. Antolin, A. A.; Workman, P.; Mestres, J.; Al-Lazikani, B., Polypharmacology in precision oncology: current applications and future prospects. *Current Pharmaceutical Design* **2016**, *22* (46), 6935-6945.

46. Boczkowski, J.; Poderoso, J. J.; Motterlini, R., CO-metal interaction: vital signaling from a lethal gas. *Trends in Biochemical Sciences* **2006**, *31* (11), 614-621.
47. Friedman, R., Drug resistance in cancer: molecular evolution and compensatory proliferation. *Oncotarget* **2016**, *7* (11), 11746-11755.
48. Kawahara, B.; Sen, S.; Mascharak, P. K., Reaction of carbon monoxide with cystathionine beta-synthase: implications on drug efficacies in cancer chemotherapy. *Future Medicinal Chemistry* **2020**, *12* (4), 325-337.
49. Walsh, V.; Goodman, J., From taxol to Taxol: the changing identities and ownership of an anti-cancer drug. *Medical Anthropology* **2002**, *21* (3-4), 307-36.
50. Abu Samaan, T. M.; Samec, M.; Liskova, A.; Kubatka, P.; Busselberg, D., Paclitaxel's mechanistic and clinical effects on breast cancer. *Biomolecule* **2019**, *9* (12).
51. Blumen, H.; Fitch, K.; Polkus, V., Comparison of treatment costs for breast cancer, by tumor stage and type of service. *American Health and Drug Benefit* **2016**, *9* (1), 23-31.
52. Spinks, T., Albright, H. W., Feeley, T. W., Walters, R., Burke, T. W., Aloia, T., Bruera, E., Buzdar, A., Foxhall, L., Hui, D., Summers, B., Rodriguez, A., Dubois, R., & Shine, K. I. (2012). Ensuring quality cancer care: a follow-up review of the Institute of Medicine's 10 recommendations for improving the quality of cancer care in America. *Cancer*, *118*(10), 2571–2582. <https://doi.org/10.1002/cncr.26536>

Chapter 6

Conclusion

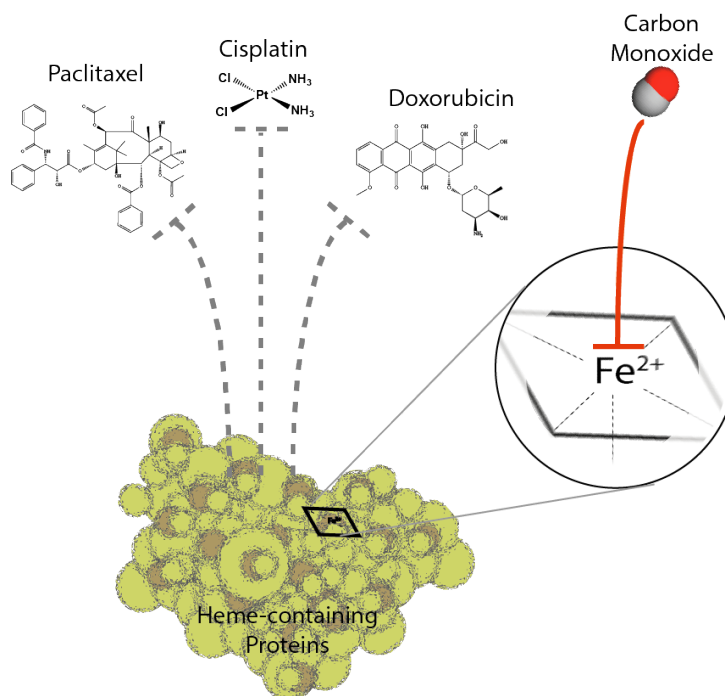


Table 6.1. Table of Content. Carbon monoxide (CO)-mediated inhibition of heme-containing enzymes towards sensitizing cancer cells to chemotherapeutics

6.1 Reimagining cancer therapy

The typical cancer drug is developed at a cost of \$1.2-1.8 billion per medicine, administered and billed to a patient at \$10,000 per month and comes to market while providing minimal patient benefit, improving survival by 2.1 months.^{1,2} It targets growth machinery processes and/or induces damage to the cancer cell, often non-specifically.³ The typical cancer drug presents as an evolutionary selection/pressure to the cancer cell, which has high plasticity and rapid growth, affording the cancer cell

the ability to quickly develop resistance to the drug.⁴ Even with the development and use of the newest, most promising, targeted inhibitors of cancer growth signaling, resistance quickly develops.^{5,6} The current cancer therapeutic strategy is expensive, minimally effective and unimaginative. A fresh approach to cancer therapy is needed.

The vast majority of deaths from cancer in the United States come not from lack of treatment, but because the treatment themselves, including recent immunotherapies for solid tumors cease to be effective to the patient and produce outcome failure-rates of 90%.⁷ The mechanisms of chemotherapeutic resistance are multisystem, but can include or more up-regulated processes including enhanced and alternative metabolism, drug degradation, and drug efflux among numerous known mechanisms.⁸ If a cancer treatment regimen does not either overwhelm or overcome these drug resistant processes, the cancer will most likely relapse. The strategy of sensitizing cancer cells, sensitizing drug resistant cancer cells to existing chemotherapeutic regimens may dramatically improve clinical outcomes.

Typical chemotherapeutics target common pathways known to be involved in carcinogenesis including constitutive growth signaling activation, angiogenesis, resistance to apoptosis, genome instability, tumor initiated inflammation and immune surveillance evasion among several processes.⁹ Rather than developing yet another small molecule inhibitor or immunotherapeutic, to which the cancer cell is robustly equipped to adapt resistance via evolutionary processes, targeting drug resistance can be likened to an “end-around” in American football, circumventing the adaptive

responses of cancer cells rather than trying to overwhelm them. Furthermore, an effective therapy that targets drug resistance mechanisms offers the prospect of repurposing clinically proven, FDA-approved and very importantly, off-patent anti-cancer drugs that are affordable and available to healthcare systems in developing and highly industrialized countries alike, a move that would improve cancer patient outcomes independent of their socioeconomic status.¹⁰

6.2 Perspective of findings

In this thesis, we have uncovered strong evidence that carbon monoxide (CO), a gasotransmitter, is a therapeutic agent for addressing molecular mechanisms of drug resistance in breast and ovarian cancer cell models. This finding has, for the first time, been supported with detailed mechanistic studies, identifying the molecular targets of CO. Its molecular targets include, but are not limited to, cystathionine β -synthase (CBS) in human breast (Chapter 2) and ovarian cancer cells (Chapter 3) and cytochrome-P450 3A4 and 2C8 (CYP3A4/2C8) in human breast cancer cells (Chapter 5). The chemical biology of CO in the cancer cell had, prior to the findings reported in this thesis, been poorly understood and almost singly attributed to cytochrome c oxidase and other potential binding partners in the mitochondria,¹¹ despite substantial evidence that CO in fact has quite low affinity for cytochrome c oxidase compared to O₂.¹² It is hoped that our findings inspire future studies into the

other mediating targets of CO in the cancer cell, many of which have been identified (Table 1.1), but have yet to be considered in the context of drug sensitization by CO.

The process of elucidating the downstream effects of CO-mediated inhibition of CBS in human breast and ovarian cancer cells has afforded tremendous insight into the diverse role CBS plays in promoting drug resistance in the cancer cell. On one hand, CBS provides indirect protection to the cancer cell from chemotherapeutic drugs by enhancing the antioxidant capacity of the cancer cell, resisting the induction of intracellular ROS by chemotherapeutics (Chapter 2). On the other hand, CBS also provides direct protection to the cancer cell from chemotherapeutic drugs by enhancing levels of intracellular, cysteine-containing species that can bind and inactivate platinum-containing chemotherapeutics (Chapter 3). Our findings show that CBS, as a therapeutic target of drug resistance, would likely improve the efficacy of therapeutic regimens utilizing multiple classes of drugs, including taxanes like paclitaxel (Chapter 2), anthracyclines like doxorubicin (Chapter 2) platinum-drugs like cisplatin (Chapter 3). Furthermore, as chemotherapeutic-induced apoptosis, independent of the therapeutic target of the chemotherapeutic, occurs via induction of ROS,^{13,14} inhibition of CBS would likely improve the efficacy of any class of drug (Figure 5.1).

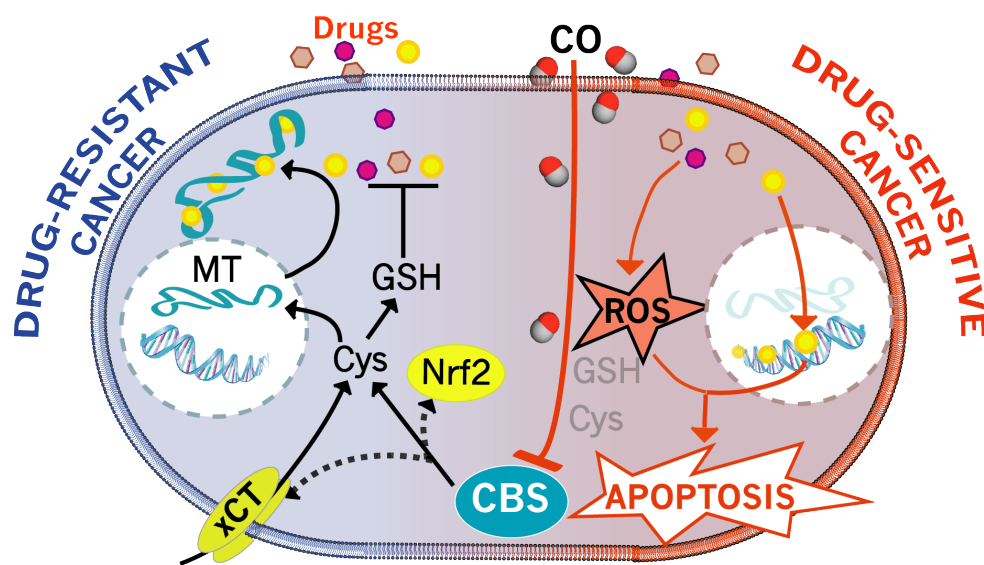


Figure 6.1 Graphical summary of CO-mediated sensitization of cancer cells to chemotherapeutics.

The second relevant target of CO identified in cancer here was CYP enzymes, namely CYP3A4/2C8 in human breast cancer cells (Chapter 5). CYPs have long been thought to be promising therapeutic targets in cancer,¹⁵ though polymorphisms in CYPs between patients hamper the affinity/efficacy of a traditional, small molecule inhibitor to inhibit CYPs with therapeutic benefit. Furthermore, the importance of CYP-mediated metabolism of endogenous and xenobiotic molecules in a healthy liver raise issues of safety and toxicity.¹⁶ For the first time, we have provided a strategy that both inhibits CYPs in the cancer cell towards therapeutic benefit and possesses high orthogonality to hepatic CYP activity. CYP-mediated inhibition of anti-cancer drugs was long hypothesized to contribute to drug resistance in cancer, though no direct evidence had existed prior to a 2016 study,¹⁷ a study mired in controversy.¹⁸

Here, we have provided what we believe is to be the first, direct evidence that CYP-inhibition can overcome chemotherapeutic resistance.

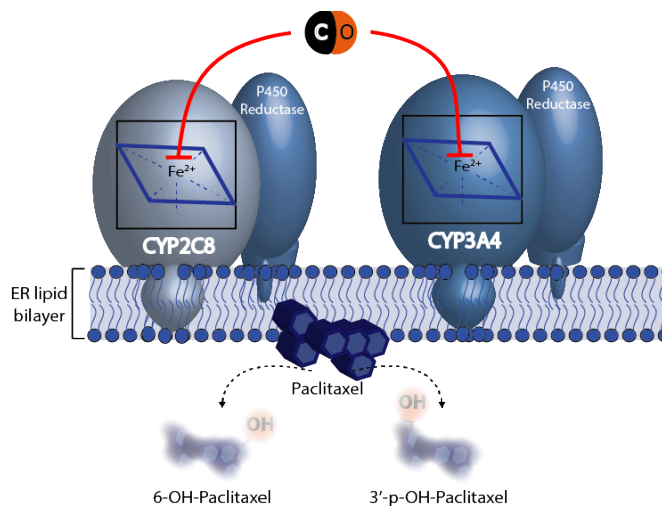


Figure 6.2 Graphical summary of CO-mediated inhibition of paclitaxel metabolism by CYP3A4/2C8.

Together, our findings in Chapters 2, 3 and 5 can be viewed through two lenses. If one can simply consider CO as a *potential* chemotherapeutic agent, this thesis can be seen as providing the necessary mechanistic studies that elucidate the chemical biology of CO, a future agent for targeting drug resistance in cancer (Figure 6.3).

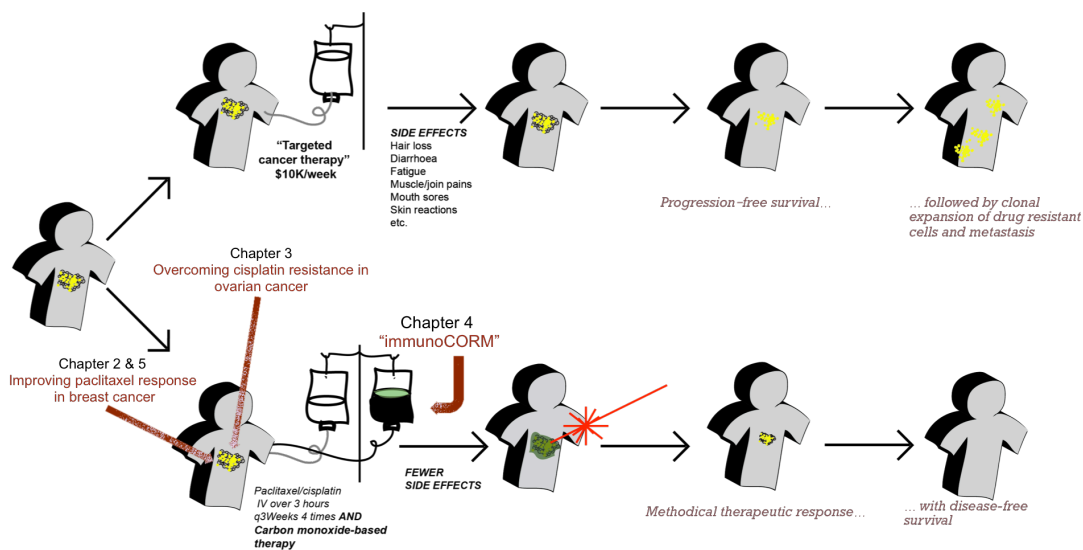


Figure 6.3. Steps towards realizing more effective chemotherapeutic regimens with carbon monoxide (CO).

If, however, one cannot see CO ever realizing its therapeutic potential, this thesis has utilized CO as a tremendous *tool* for uncovering the role that heme-containing enzymes play in promoting molecular mechanisms of drug resistance in cancer (Figure 6.4).

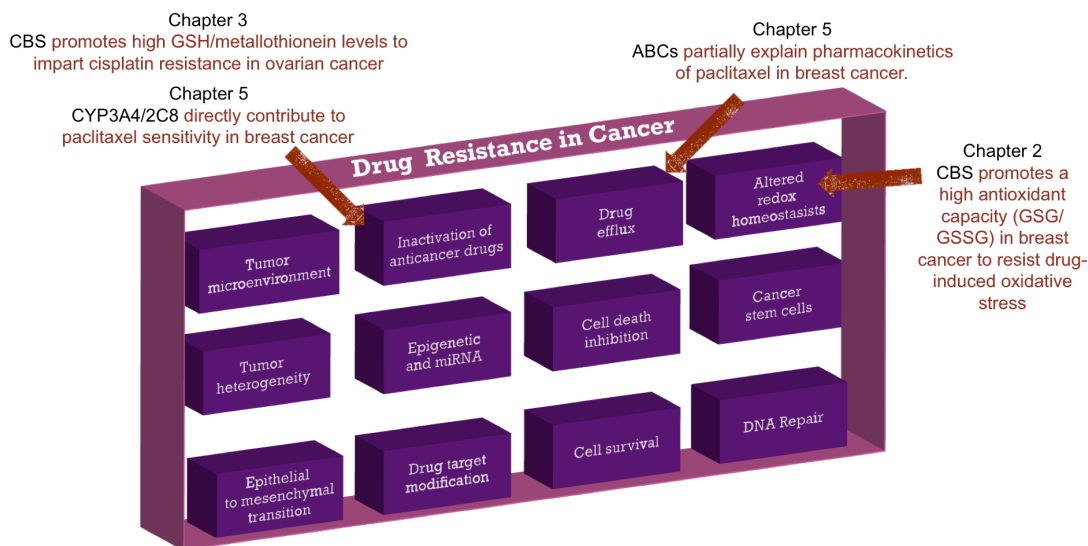


Figure 6.4. CO, a tool for studying drug resistance in cancer. Study of the chemical biology of CO in cancer revealed the role of heme-containing enzymes in molecular mechanisms of drug resistance.

The greatest technical challenge that needs to be overcome to realize the therapeutic potential of CO is achieving delivery of CO to a therapeutic site at sufficient concentrations. Our synthesis of an immunoCORM, an immunotherapeutic capable of antigen-specific delivery and controlled release of CO has been the most promising option to overcoming the technical challenge of delivering sufficient levels of CO to a therapeutic site.

6.3 Future directions

Targeting drug resistance as a therapeutic approach to cancer therapy has been proposed for several years.¹⁹ The studies reported here have provided strong validation of such a strategy, but validation is not isolated or limited to this thesis, but

has recently attracted clinical and biopharma attention. ORIC-101, a cancer drug resistance-targeting small molecule developed and patented by ORIC Pharmaceuticals, Inc. showing promise preliminary results.²⁰⁻²²

Based upon the results reported here, future studies should be performed that assess CO's ability to sensitize other established drug-resistant cancer models. Using CO will both further assess the therapeutic potential of CO and elucidate other heme-containing enzymes' roles in promoting drug resistance in these drug-resistant cancer models.

The future development of immunoCORMs will include improving the homogeneity of the product as well as applying the immunoCORM to more complex model systems, including mammalian cell co-cultures and animal models, that would further demonstrate the efficacy of antigen-mediated delivery of CO to a therapeutic target. Using diethylnitrosamine (DEN, or N-nitrosodiethylamine)-induced mouse liver cancer cell models, CO, delivered by CO-releasing, alluminosilicate nanoparticles injected directly into subcutaneous mouse xenograft tumors significantly reduced subcutaneous mouse xenograft tumors compared to tumors injected with control nanoparticles (data not shown). These promising preliminary findings from our group bode well for the delivery of CO in a complex, biological model. It would be very intriguing to assess whether immunoCORMs, synthesized and characterized as described in Chapter 4, would be capable of tumor-specific

delivery of CO in these xenograft models, or if further engineering and development would be required.

Untargeted metabolomic, quantitative proteomics and phosphoproteomics mass spectrometry are tools well suited for the continued elucidation of the chemical biology of CO. The promiscuous nature of CO towards low-valent transition metal complexes result in multiple systems being perturbed by CO. Future studies should utilize these technologies to afford greater ability to understand the multi-faceted aspects of CO signaling in the cancer cell.

It is hoped the findings from this thesis inspire similar endeavors towards overcoming resistance in cancer, for if successful, this strategy would reinvigorate the expensive and minimally effective cancer therapeutic regimens currently practiced.²

6.4 References

1. Tay-Teo, K.; Ilbawi, A.; Hill, S. R., Comparison of sales income and research and development costs for FDA-approved cancer drugs sold by originator drug companies. *Jama Network Open* **2019**, *2* (1).
2. Fojo, T.; Mailankody, S.; Lo, A., Unintended consequences of expensive cancer therapeutics-the pursuit of marginal indications and a me-too mentality that stifles innovation and creativity. The John Conley Lecture. *Jama Otolaryngology-Head & Neck Surgery* **2014**, *140* (12), 1225-1236.

3. Nurgali, K.; Jagoe, R. T.; Abalo, R., Editorial: Adverse effects of cancer chemotherapy: anything new to improve tolerance and reduce sequelae? *Frontiers in Pharmacology* **2018**, *9*.
4. Friedman, R., Drug resistance in cancer: molecular evolution and compensatory proliferation. *Oncotarget* **2016**, *7* (11), 11746-11755.
5. Bhamidipati, P. K.; Kantarjian, H.; Cortes, J.; Cornelison, A. M.; Jabbour, E., Management of imatinib-resistant patients with chronic myeloid leukemia. *Therapeutic Advances in Hematology* **2013**, *4* (2), 103-117.
6. Luebker, S. A.; Koepsell, S. A., Diverse mechanisms of braf inhibitor resistance in melanoma identified in clinical and preclinical studies. *Frontiers in Oncology* **2019**, *9*.
7. Maeda, H.; Khatami, M., Analyses of repeated failures in cancer therapy for solid tumors: poor tumor-selective drug delivery, low therapeutic efficacy and unsustainable costs. *Clinical and Translational Medicine* **2018**, *7*.
8. Housman, G.; Byler, S.; Heerboth, S.; Lapinska, K.; Longacre, M.; Snyder, N.; Sarkar, S., Drug resistance in cancer: An overview. *Cancers* **2014**, *6* (3), 1769-1792.
9. Hanahan, D.; Weinberg, R. A., Hallmarks of cancer: the next generation. *Cell* **2011**, *144* (5), 646-674.
10. Spinks, T., Albright, H. W., Feeley, T. W., Walters, R., Burke, T. W., Aloia, T., Bruera, E., Buzdar, A., Foxhall, L., Hui, D., Summers, B., Rodriguez, A., Dubois, R., & Shine, K. I. (2012). Ensuring quality cancer care: a follow-up review of the

- Institute of Medicine's 10 recommendations for improving the quality of cancer care in America. *Cancer*, *118*(10), 2571–2582. <https://doi.org/10.1002/cncr.26536>
11. Wegiel, B.; Gallo, D.; Csizmadia, E.; Harris, C.; Belcher, J.; Vercellotti, G. M.; Penacho, N.; Seth, P.; Sukhatme, V.; Ahmed, A.; Pandolfi, P. P.; Helczynski, L.; Bjartell, A.; Persson, J. L.; Otterbein, L. E., Carbon monoxide expedites metabolic exhaustion to inhibit tumor growth. *Cancer Research* **2013**, *73* (23), 7009-7021.
 12. Weber, R. E.; Vinogradov, S. N., Nonvertebrate hemoglobins: Functions and molecular adaptations. *Physiological Reviews* **2001**, *81* (2), 569-628.
 13. Kaufmann, S. H.; Earnshaw, W. C., Induction of apoptosis by cancer chemotherapy. *Experimental Cell Research* **2000**, *256* (1), 42-49.
 14. Berndtsson, M.; Hagg, M.; Panaretakis, T.; Havelka, A. M.; Shoshan, M. C.; Linder, S., Acute apoptosis by cisplatin requires induction of reactive oxygen species but is not associated with damage to nuclear DNA. *International Journal of Cancer* **2007**, *120* (1), 175-180.
 15. McFadyen, M. C. E.; Melvin, W. T.; Murray, G. I., Cytochrome P450 enzymes: Novel options for cancer therapeutics. *Molecular Cancer Therapeutics* **2004**, *3* (3), 363-371.
 16. Nebert, D. W.; Wikvall, K.; Miller, W. L., Human cytochromes P450 in health and disease. *Philosophical Transactions of the Royal Society B-Biological Sciences* **2013**, *368* (1612).

17. Noll, E. M.; Eisen, C.; Stenzinger, A.; Espinet, E.; Muckenhuber, A.; Klein, C.; Vogel, V.; Klaus, B.; Nadler, W.; Rosli, C.; Lutz, C.; Kulke, M.; Engelhardt, J.; Zickgraf, F. M.; Espinosa, O.; Schlesner, M.; Jiang, X. Q.; Kopp-Schneider, A.; Neuhaus, P.; Bahra, M.; Sinn, B. V.; Eils, R.; Giese, N. A.; Hackert, T.; Strobel, O.; Werner, J.; Buchler, M. W.; Weichert, W.; Trumpp, A.; Sprick, M. R., CYP3A5 mediates basal and acquired therapy resistance in different subtypes of pancreatic ductal adenocarcinoma. *Nature Medicine* **2016**, *22* (3), 278-287.
18. Rodriguez-Antona, C.; Ingelman-Sundberg, M., Cytochrome P450 pharmacogenetics and cancer. *Oncogene* **2006**, *25* (11), 1679-1691.
19. Leary, M.; Heerboth, S.; Lapinska, K.; Sarkar, S., Sensitization of drug resistant cancer cells: a matter of combination therapy. *Cancers* **2018**, *10* (12).
20. Elshimali, Y. I.; Wu, Y.; Khaddour, H.; Gradinaru, D.; Sukhija, H.; Chung, S. S.; Vadgama, J. V., Optimization of cancer treatment through overcoming drug resistance. *Journal of Cancer Research and Oncobiology* **2018**, *1* (2).
21. Rew, Y.; Du, X. H.; Eksterowicz, J.; Zhou, H. Y.; Jahchan, N.; Zhu, L. S.; Yan, X. L.; Kawai, H.; McGee, L. R.; Medina, J. C.; Huang, O.; Chen, C.; Zavorotinskaya, T.; Sutimantanapi, D.; Waszczuk, J.; Jackson, E.; Huang, E.; Ye, Q. P.; Fantin, V. R.; Sun, D. Q., discovery of a potent and selective steroidal glucocorticoid receptor antagonist (ORIC-101). *Journal of Medicinal Chemistry* **2018**, *61* (17), 7767-7784.

22. ORIC Pharmaceuticals. An open-label phase 1b study of ORIC-101 in combination with enzalutamide in patients with metastatic prostate cancer progressing on enzalutamide. **2019** ClinicalTrials.gov.